Conditional Degrons to Study Gene Functions During *Saccharomyces cerevisiae* Gametogenesis and Proliferation

Kumulative Dissertation

Zur

Erlangung des Doktorgrades

der Naturwissenschaften (Dr. rer. nat.)

dem Fachbereich Biologie

der Philipps-Universität Marburg

vorgelegt von

C h r i s t i a n   R e n i c k e

aus Bad Hersfeld

Marburg

September 2016

Conditional Degrons to Study Gene Functions During *Saccharomyces cerevisiae* Gametogenesis and Proliferation

Kumulative Dissertation

Zur
Erlangung des Doktorgrades
der Naturwissenschaften (Dr. rer. nat.)

dem Fachbereich Biologie
der Philipps-Universität Marburg
vorgelegt von

C h r i s t i a n   R e n i c k e

aus Bad Hersfeld

Marburg
September 2016

Die Untersuchungen zur vorliegenden Arbeit wurden von Januar 2011 bis September 2016 am Fachbereich Biologie der Philipps-Universität Marburg im Fachgebiet Molekulare Genetik durchgeführt und von Herrn PD Dr. Christof Taxis betreut.

Vom Fachbereich Biologie der Philipps-Universität Marburg als Dissertation

angenommen am:

Erstgutachter: PD Dr. Christof Taxis

Zweitgutachter: Prof. Dr. Uwe Maier

Tag der mündlichen Prüfung:

Teile dieser Arbeit sind in folgenden Artikeln veröffentlicht:

Renicke C, Schuster D, Usherenko S, Essen L-O & Taxis C (2013) A LOV2 Domain-Based Optogenetic Tool to Control Protein Degradation and Cellular Function. *Chem. Biol.* **20:** 619–26

Renicke C, Spadaccini R & Taxis C (2013) A Tobacco Etch Virus Protease with Increased Substrate Tolerance at the P1' position. *PLoS One* **8:** e67915

Unveröffentlichte Manuskripte:

Renicke C & Taxis C Development of an optogenetic tool to regulate protein stability in vivo. In *OPTOGENETICS: From Neuronal Function to Mapping & Disease Biology*, Appasani K (ed). Cambridge, UK: Cambridge University Press (Angenommenes Manuskript)

Renicke C, Allmann AK, Lutz A and Taxis C The mitotic exit network regulates spindle pole body inheritance during sporulation of budding yeast. (Manuskript im August 2016 eingereicht; unter Begutachtung)

Lutz AP, Schladebeck S, **Renicke C**, Spadaccini R, Mösch H-U & Taxis C Budding yeast HECT_2 protein Utd1 is a ubiquitin-protein ligase important for proteasome activity. (Manuskript in Vorbereitung)

Weitere Publikationen:

Renicke C & Taxis C (2016) Biophotography: concepts, applications and perspectives. *Appl. Microbiol. Biotechnol.*

Lutz AP, **Renicke C** & Taxis C (2016) Controlling Protein Activity and Degradation Using Blue Light. In *Optogenetics: Methods and Protocols*, Kianianmomeni A (ed) pp 67–78. New York, NY: Springer New York

Paul VD, Mühlenhoff U, Stümpfig M, Seebacher J, Kugler KG, **Renicke C**, Taxis C, Gavin A-C, Pierik AJ & Lill R (2015) The deca-GX 3 proteins Yae1-Lto1 function as adaptors recruiting the ABC protein Rli1 for iron-sulfur cluster insertion. *Elife* **4:** 1–23

Renicke C & Taxis C (2015) Synthetische Biologie lässt Mikroorganismen „sehen". *BIOspektrum* **21:** 380–381

Your memory is a monster; you forget - it doesn't. It simply files things away. It keeps things for you, or hides things from you - and summons them to your recall with will of its own. You think you have a memory; but it has you!

John Irving – A Prayer for Owen Meany

Zusammenfassung

Diploide *Saccharomyces cerevisiae* Zellen können widerstandsfähige Sporen bilden, um Mangelbedingungen zu überdauern. Sporulation bezeichnet eine Zelldifferenzierung, bei der meiotische Teilungen und Sporenbildung verknüpft sind. Eingeleitet wird die Sporenbildung beim Übergang in Meiose II an den Spindelpolkörpern, den Zentrosomenäquivalenten der Hefe. Eingebettet in die Kernmembran werden diese während der Meiose zweimal durch einen vorwiegend konservativen Mechanismus verdoppelt. Daraus resultieren drei Generationen von Spindelpolkörpern in Meiose II: Der erste stammt aus dem vorangegangenen Zellzyklus, der zweite wird während der meiotischen Prophase gebildet und die beiden Spindelpolkörper der dritten Generation entstehen vor Eintritt in die zweite meiotische Teilung. Zu Beginn der Meiose II formen sich an den zytoplasmatischen Plaques der Spindelpolkörper die sogenannten meiotischen Platten. Diese ermöglichen die Bildung der Prosporenmembranen, welche um die Ausstülpungen des Kerns herum wachsen und sich nach Zusammenbruch der Meiose II-Spindeln schließen. Die Sporenwand wird anschließend im Lumen der entstandenen Doppelmembran aufgebaut. Zuletzt kollabiert die Mutterzelle um die Sporen und formt den Ascus. Hefezellen sind in der Lage entsprechend der Nahrungsbedingungen Asci mit weniger als vier Sporen zu bilden indem sie weniger Proteine der meiotischen Platten produzieren. Ermöglicht wird diese Regulation durch die Polarität der Meiose II-Spindeln, durch welche meiotische Platten bevorzugt an den jüngeren Spindelpolkörpern geformt werden. Dieser Prozess stellt sicher, dass Asci mit nur zwei Sporen keine Schwesterchromatiden enthalten und trägt damit entscheidend zur Aufrechterhaltung der genetischen Vielfalt und Überlebensfähigkeit einer Population bei. Dennoch ist wenig über den zugrundeliegenden Mechanismus bekannt.

In dieser Arbeit habe ich verschiedene synthetische Methoden entwickelt, um den Einfluss des „Mitotic Exit Networks" (MEN) auf meiotische Spindelpolarität und Sporenzahlkontrolle zu erforschen. Das MEN ist ein konservierter Signaltransduktionsweg, der essentielle Funktionen während des vegetativen Wachstums erfüllt indem er die Aufteilung des Genoms mit der Zytokinese koordiniert. Außerdem kontrolliert er die Ausbildung der mitotischen Spindelpolarität während der Metaphase. Die Funktionen des MEN in der Meiose sind weitgehend unbekannt, da es an verlässlichen Methoden zur Herstellung von sporulationsspezifischen Mutanten mangelte, die nötig gewesen wären, um die für den Zellzyklus essentiellen Komponenten des MEN zu untersuchen. Zur Lösung dieses Problems

habe ich zwei verschiedene Ansätze zur Kontrolle der Proteinmengen durch konditionale Degradationssequenzen (Degrons) gewählt. Erstens wurde ein photosensitives Degron etabliert, welches auf der Fusion eines synthetischen C-terminalen Degrons an die LOV2 Photosensor-Domäne des Phototropin 1 aus *Arabidopsis thaliana* basiert. Im Dunkeln ist das Degron maskiert während konformationelle Änderungen der LOV2-Domäne unter Blaulicht zur Aktivierung des Degrons und Abbau des markierten Zielproteins führen. Zweitens wurde ein bestehendes System zur Protein-Destabilisierung weiterentwickelt, welches die Tabak-Ätz-Virus-Protease verwendet, um ein geschütztes Degron zu aktivieren. In vorangegangenen Arbeiten ermöglichte die Regulation der Biosynthese dieser Protease durch einen meiosespezifischen Promotor die Aufklärung von Proteinfunktionen während der Sporulation. Zur Entwicklung eines effizienteren Systems habe ich zwei parallele Strategien verfolgt: Durch gerichtete Evolution wurde eine Variante der Protease erzeugt, welche durch eine verringerte Substratspezifität die Verwendung potenterer Degrons zulässt. Davon unabhängig habe ich eine meiosespezifische Deaktivierung der Zielgenexpression kombiniert mit einer Steigerung der Proteaseproduktion während der Sporulation.

Dieser Ansatz konnte erfolgreich genutzt werden, um meiosespezifische Mutanten aller wesentlichen Komponenten des MEN zu erzeugen. So konnte gezeigt werden, dass dieser Signalweg die altersabhängige Entscheidung beeinflusst, an welchen Spindelpolkörpern meiotische Platten gebildet werden. Außerdem fand ich eine funktionelle Diversifizierung der MEN Komponenten während der Sporulation. Die vorgelagerte Kinase Cdc15 trägt zur Regulation der Anzahl von meiotischen Platten und der Schließung der Prosporenmembranen bei. Für die Spindelpolkörper-Auswahl zu Beginn der Meiose II sind sowohl Cdc15 als auch die nachgelagerten Komplexe aus Dbf2 bzw. Dbf20 und Mob1 notwendig. Nach den meiotischen Teilungen werden diese Komplexe für den Aufbau der Sporenwände und damit eine zuverlässige Weitergabe der haploiden Genome benötigt. Zusammengefasst zeigen diese Ergebnisse eine entwicklungsspezifische Plastizität des MEN: Das Signalnetzwerk wird nicht für das Durchlaufen der meiotischen Teilungen benötigt, verschiedene Komponenten wirken aber während bestimmter Schritte in der Sporenbildung und sichern so die erfolgreiche Weitergabe des Erbguts.

Summary

Diploid cells of *Saccharomyces cerevisiae* can form stable spores to ensure survival under poor nutritional conditions. Sporulation is a coupled developmental program of meiotic divisions and spore formation. The latter process is initiated at onset of meiosis II at the spindle pole bodies (SPBs), the yeast centrosome equivalents. The SPBs are embedded in the nuclear envelope and duplicate twice during meiosis in a mostly conservative fashion. Thus, three generations of SPBs are present in meiosis II. The first SPB inherited from mitosis, the second formed in meiotic pro-phase and the two youngest SPBs generated prior to meiosis II. At the onset of meiosis II the cytoplasmic faces of the SPBs are modified by meiotic plaques. They serve as nucleation platform for the prospore membranes, which grow around the nuclear lobes and close after meiosis II spindle breakdown. The spore wall is then formed in the lumen of the double-layered prospore membrane. Finally, the former mother cell collapses and forms the spore-containing ascus. Cells are able to adjust the spore numbers according to the available nutrients by reducing meiotic plaque protein levels to generate asci with less than four spores. This regulation is facilitated by meiosis II spindle polarity, which directs meiotic plaque formation towards the younger SPBs. Yet, the underlying mechanisms are poorly understood, although this process significantly contributes to preservation of genetic variability and population fitness by ensuring encapsulation of non-sister chromosomes in asci with only two spores.

Here, I developed different synthetic tools to study the role of the mitotic exit network (MEN) in meiotic spindle polarity and spore number control of *S. cerevisiae*. The MEN is a conserved signaling cascade essential for vegetative growth. It coordinates mitotic exit with genome segregation and cytokinesis and establishes mitotic spindly polarity in metaphase. However, the meiotic functions of this network are mainly unknown due to the lack of reliable methods for creation of meiosis-specific mutants of the mainly essential proteins of the MEN. To overcome this obstacle, I pursued two different approaches to control the abundance of a protein with sequences inducing conditional degradation (degrons). 1. I established a photo-sensitive degron module which combines the LOV2 photoreceptor domain of *Arabidopsis thaliana* phototropin 1 attached to a synthetic C-terminal degron. In the dark, this degron is sterically inaccessible. Upon blue-light illumination, structural rearrangements of the LOV2 domain lead to activation of the degron and degradation of the target protein it is fused to. 2. I improved an established system for protein destabilization, which employs tobacco etch virus (TEV) protease to activate a cryptic degron. Control of protease production by a meiosis-specific promoter has been used previously to study

protein functions during sporulation. To develop a more efficient system, I followed two strategies in parallel: by directed evolution, I created a TEV protease variant with a higher substrate tolerance, allowing usage of stronger degrons. Independently, I combined transcriptional shut-off of the target gene upon initiation of meiosis with elevated protease levels during sporulation.

The latter approach was used successfully to create meiosis-specific mutants of all core MEN components. I could demonstrate a role of the MEN in age-based selection of SPBs for meiotic plaque modification. Moreover, I found functional diversification of MEN components during sporulation. The upstream kinase Cdc15 is involved in regulation of meiotic plaque numbers and prospore membrane closure, while Cdc15 and the downstream kinase complexes consisting of Dbf2/20-Mob1 are all necessary for SPB selection at the onset of meiosis II. After the meiotic divisions, efficient genome inheritance requires Dbf2/20-Mob1 during subsequent spore wall formation. Together, these data reveal a developmental-specific plasticity of the signaling network. In contrast to mitosis, execution of meiosis does not require the MEN but faithful genome inheritance requires concerted action of different MEN components at distinct steps of spore formation.

Table of Contents

1 Introduction

1.1 Polarity in Asymmetric Cell Divisions

Polarity, a situation of biased, directed asymmetry, is fundamental process in cell biology. The establishment and maintenance of cell polarity is pivotal for many forms of cell differentiation and is most obvious in asymmetric cell division (Macara & Mili, 2008; Li, 2013; Roubinet & Cabernard, 2014). A well-studied prokaryotic example is the bacterium *Caulobacter crescentus* which divides into a surface-bound, stalked cell and one free-swimming swarmer cell relying on polar distribution of cell fate determinants (Tsokos & Laub, 2012). In higher eukaryotes, best-studied examples of cell polarity and asymmetric cell division are embryonic development and stem cell division. In the *Caenorhabditis elegans* zygote, symmetry is broken by the paternally introduced centrosome. This leads to polarization of different factors, the par (<u>par</u>titioning phenotype) proteins and the small GTPase Cdc42, along an anterior-posterior cell axis (Goldstein & Hird, 1996; Wallenfang & Seydoux, 2000; Gotta *et al*, 2001; Munro *et al*, 2004; Bienkowska & Cowan, 2012). Polarization is a prerequisite for the following oriented, asymmetric zygotic divisions and thus leads finally to formation of different cell lineages and tissues during animal development (Rose & Gönczy, 2014). Homologous factors have been shown to be critical for cell polarity establishment in many different organisms, not only during asymmetric cell division but also in neuronal polarity, tissue proliferation and cell motility (Goldstein & Macara, 2007).

To study the fundamental principles of cell polarity, the unicellular yeast *S. cerevisiae* has proven as a useful model system (Bi & Park, 2012). It is highly accessible to genetic manipulations, easy to cultivate and many well-established techniques and tools are available complemented by a large number of knowledge resources (Mager & Winderickx, 2005; Duina *et al*, 2014). *S. cerevisiae* cells divide asymmetrically by budding and spindle position has to be coordinated with the polarity axis of the cell and with cytokinesis to ensure proper genome segregation. Spindle orientation depends on the yeast centrosome equivalents, the spindle pole bodies (SPB). These are multi-layered, macromolecular structures embedded in the nuclear envelope by the central plaque. An inner plaque organizes nuclear microtubules and an outer plaque organizes cytoplasmic microtubules (Bullitt *et al*, 1997; Wigge *et al*, 1998; O'Toole *et al*, 1999; Adams & Kilmartin, 1999). This outer plaque is linked to the central plaque via the coiled-coil protein Cnm67 and contains Nud1, Spc72 and the γ-tubulin complex of Spc97, Spc98 and Tub4 (Knop & Schiebel, 1998;

Elliott *et al*, 1999; Schaerer *et al*, 2001). SPBs duplicate in a mostly conservative way in prophase, resulting in one SPB composed of mainly old and the other composed of mainly new material (Adams & Kilmartin, 1999; Menendez-Benito *et al*, 2013). The new SPB is inherited by the mother cell, while the old one is segregated to the bud. Differential SPB inheritance depends on Kar9, which exploits spindle polarity in early metaphase and orients the old SPB towards the bud. Establishment of mitotic spindle polarity is achieved by the interplay between initial symmetry breaking caused by Kar9 sumoylation, Cdk1-Clb4 phosphorylation of Kar9 and intrinsic differences between the old and the new SPB in astral microtubule organization. Cdk1-Clb5 and spindle assembly checkpoint-dependent direct phosphorylation of Kar9 by the mitotic exit network complex Dbf2-Mob1 stimulates its localization to the old SPB (Leisner *et al*, 2008; Hotz *et al*, 2012a, 2012b; Hüls *et al*, 2012; Juanes *et al*, 2013). Kar9 then mediates interaction of astral microtubules with polarized actin filaments, resulting in orientation of this SPB towards the bud neck where the microtubule plus ends are transferred to Bud6 (Yin *et al*, 2000; Beach *et al*, 2000; Liakopoulos *et al*, 2003; Hwang *et al*, 2003). Subsequently, a second, dynein-dependent mechanism translocates the old SPB into the bud (Adames & Cooper, 2000; Heil-Chapdelaine *et al*, 2000; Lee *et al*, 2003; Carvalho *et al*, 2004).

In anaphase, the spindle position checkpoint (SPOC) is a surveillance mechanism, which integrates the signals of mitotic progression with SPB position and inhibits mitotic exit and cytokinesis until the daughter cell has received its genetic material (Piatti *et al*, 2006; Scarfone & Piatti, 2015). This is accomplished by inhibition of the mitotic exit network (MEN) until passage of one SPB into the bud (Figure 1; Falk *et al*, 2016). As long as both SPBs reside in the mother cell, the upstream MEN GTPase Tem1 is inhibited by its GAP (GTPase activating protein)-complex Bfa1-Bub2 (Geymonat *et al*, 2002; Fraschini *et al*, 2006; Caydasi *et al*, 2012). This complex is held active by the mother cell-specific SPOC kinase Kin4, which prevents inhibitory phosphorylation of the complex by the polo-like kinase Cdc5 (Pereira & Schiebel, 2005; Gryaznova *et al*, 2016). Once one SPB enters the bud, Kin4 is inhibited by bud-specific Lte1 and Cdc5 inactivates Bfa1-Bub2 (Bertazzi *et al*, 2011). GTP-bound Tem1 and Cdc5 then recruit the Ste20-like kinase Cdc15 to the MEN scaffold protein Nud1 at the SPB outer plaque. Subsequently, Cdc15 recruits and activates a complex of the NDR kinase Dbf2 and its coactivator Mob1 (Asakawa *et al*, 2001; Visintin & Amon, 2001; Mohl *et al*, 2009; Valerio-Santiago & Monje-Casas, 2011; Rock & Amon, 2011; Falk *et al*, 2016). Dbf2 has a less intensively studied but partially functional redundant paralog, Dbf20 (Toyn *et al*, 1991). Activation of the Dbf2/20-Mob complexes leads to release of the

phosphatase Cdc14 from the nucleolus where it is kept inactive during the rest of the cell-cycle by Net1. Cdc14 then counteracts Cdk1 and thereby allows the cell to exit mitosis, initiate cytokinesis and reenter G1 phase (Visintin *et al*, 1998, 1999; Mohl *et al*, 2009).
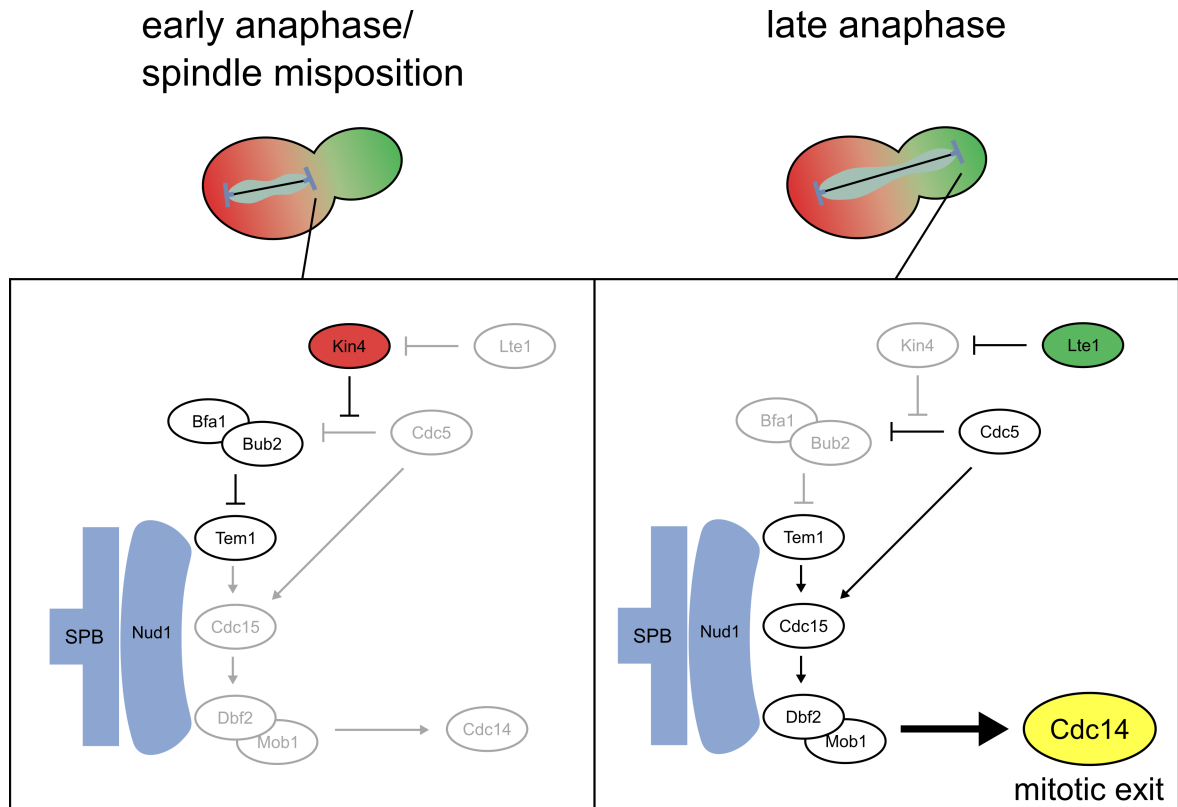

Figure 1: Coordination of mitotic exit with spindle position by the MEN. The upper part depicts the Kin4-dependent inhibitory (red) and Lte1-dependent activating (green) zones of MEN signaling in early and late anaphase. SPBs are shown in blue. The lower part shows SPOC and MEN signaling before and after entry of one SPB into the bud. **See text for details.**

Beside release of Cdc14, the MEN has additional roles during the cell cycle in directing Kar9 localization towards the old SPB in early metaphase and after mitotic exit, the MEN kinases localize to the bud neck and regulate proteins required for cytokinesis like Chs2, Cyk3, Hof1 and Inn1 (Meitinger *et al*, 2010, 2013; Hotz *et al*, 2012a; Oh *et al*, 2012).

1.2 Spindle Polarity and Spindle Pole Body Inheritance During Sporulation of *S. cerevisiae*

Diploid *S. cerevisiae* cells deprived for a fermentable carbon source as well as a nitrogen source enter the developmental program of sporulation if a non-fermentable carbon source such as acetate is available. During sporulation, the mother cell undergoes both meiotic divisions and the haploid genomes are encapsulated into spores contained in the remnants of the former mother cell called ascus (Figure 2; Neiman, 2011). This whole process is

controlled by a transcriptional cascade consisting of early-, mid- and late-sporulation transcripts. The master regulator of initiation of meiosis is the transcription factor Ime1, which is regulated on transcriptional, post-transcriptional and post-translational levels (Sherman *et al*, 1993; Shefer-Vaida *et al*, 1995; Sagee *et al*, 1998; Colomina *et al*, 1999). Ime1 activates the early-sporulation genes initiating pre-meiotic S-phase, chromosome replication and recombination (Chu *et al*, 1998). The gene product of the early gene *IME2* activates the transcription factor Ndt80 responsible for induction of the mid-sporulation genes thereby controlling progression through meiosis and initiation of spore formation (Xu *et al*, 1995; Chu & Herskowitz, 1998; Chu *et al*, 1998; Benjamin *et al*, 2003). At the end of meiosis II, the late-sporulation genes are induced, which are essential for spore wall formation as well as spore and ascus maturation (Chu *et al*, 1998).
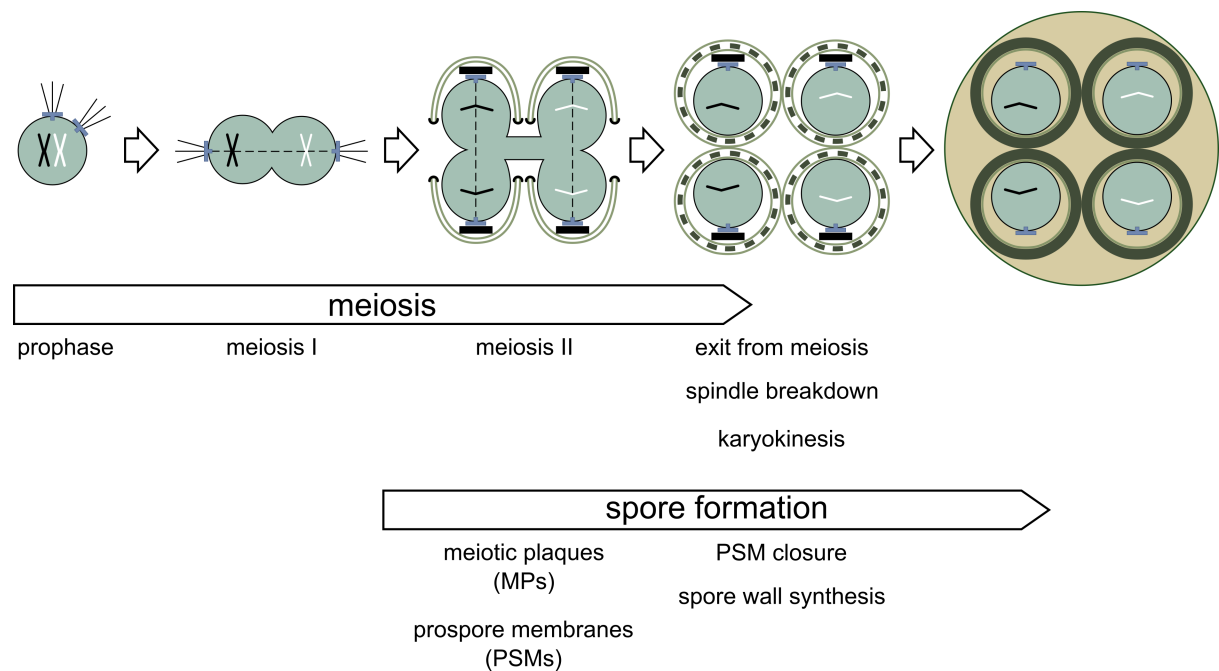

Figure 2: Sporulation of *S. cerevisiae*. The first four pictograms show the nucleus and associated structures. Homologous chromosomes are shown in black/white, SPBs in blue. Dashed lines represent meiotic spindles, solid lines astral microtubuli. MPs are represented by thick black bars, the PSMs are shown in light brown and the LEPC as black caps. The spore wall (continuous circles) and its precursors (dashed circles) are shown in dark brown. **See text for details.**

The process of spore formation is initiated at the SPBs. At transition from meiosis I to meiosis II, SPBs lose their ability to nucleate cytoplasmic microtubules. Spc72 and the γ-tubulin complex are replaced by the meiotic plaque (MP), consisting of Mpc54, Mpc70, Spo74 and Ady4 (Knop & Strasser, 2000; Nickas *et al*, 2003). The MP serves as nucleation platform and anchor for *de novo* formation of the prospore membrane (PSM), which grows by vesicle fusion around each nuclear lobe and parts of the cytoplasm (Neiman, 1998;

Nakanishi *et al*, 2006). The edge of the growing PSMs is covered by the leading edge protein coat (LEPC) consisting of Ssp1, Ady3, Irc10 and Don1 (Knop & Strasser, 2000; Nickas & Neiman, 2002; Lam *et al*, 2014). Ssp1 is necessary for localization of the other proteins to the leading edge and required to maintain the PSM opened until end of meiosis II (Moreno-Borchart *et al*, 2001; Maier *et al*, 2007; Diamond *et al*, 2009; Paulissen *et al*, 2016). After completion of meiosis II, the LEPC is removed and the PSMs close by self-fusion and subsequently the four layers (mannan, β-glucan, chitosan and dityrosine) of the spore wall are synthesized consecutively in the lumen of the PSM (Coluccio *et al*, 2004; Diamond *et al*, 2009). This thick spore wall confers high resistance against diverse environmental stresses to the spores. As a last step in sporulation the mother cell maturates to the ascus (Eastwood *et al*, 2012).

Yeast cells react on varying nutrient amounts by adjusting the number of spores per ascus (spore number control; Taxis *et al*, 2005; Gordon *et al*, 2006; Eastwood *et al*, 2012). A decreasing amount of the non-fermentable carbon source leads to a step-by-step decrease of asci containing four spores (tetrad) and an increase of asci with three (triad), two (dyad) or one (monad) spores (Davidow *et al*, 1980; Taxis *et al*, 2005). This is achieved by linkage of MP protein levels to nutrient availability; meiotic spindle polarity then directs MP formation to selected SPBs (Taxis *et al*, 2005). Meiotic spindle polarity and thus, selection of specific SPBs and their associated genomes for spore encapsulation is based on the different ages of the SPBs in meiosis II. The oldest SPB is the one, the cell inherited from mitotic growth. It gets duplicated in meiotic S-phase — the second oldest SPB forms. At the transition to meiosis II the two SPBs duplicate again producing the two youngest ones. In general, younger SPB are preferred over the older ones for modification with an MP (Taxis *et al*, 2005; Gordon *et al*, 2006). During dyad formation, this results in modification of the two youngest SPBs with MPs (Figure 3). If three spores are formed, the second oldest SPB also becomes modified by an MP. If just one spore is produced by a cell, one of the two youngest SPB will be modified by an MP (Taxis *et al*, 2005). Of the two youngest SPBs, the SPB originating from duplication of the oldest seems to be moderately preferred over the other one for assembly of an MP (Gordon *et al*, 2006). This complex selection pattern has the consequence that the two genomes of a dyad originate from two different meiosis II spindles and the resulting spores have an opposite mating type. This maximizes intra-ascus mating of the spores upon germination and preservation of heterozygosity (Taxis *et al*, 2005).
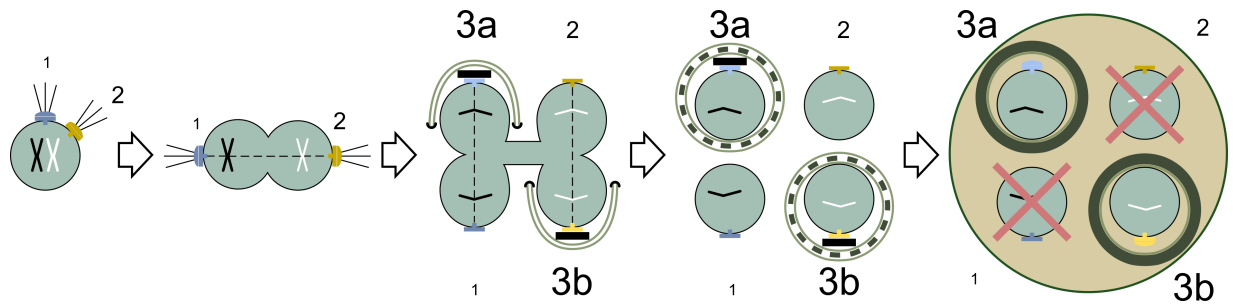
Figure 3: Non-sister dyad formation and spindle polarity during sporulation of *S. cerevisiae*. A cell initiating meiosis starts with one spindle pole body inherited from the last mitotic cell cycle (1; dark blue). In meiotic pro-phase, this SPB duplicates, leading to the second oldest SPB (2; dark yellow). Dashed lines represent meiotic spindles, solid lines astral microtubules. After meiosis I, both SPBs duplicate again, the two youngest SPBs are formed (3a and 3b; light blue and light yellow with respect to their origin). When dyads are formed, modifications of SPBs with meiotic plaques (black caps) as a prerequisite for spore formation occur preferentially at the youngest SPBs. This results in the formation of non-sister dyads since each of the youngest SPBs is associated with chromatids of distinct homologous chromosomes.

The mechanism controlling spore numbers is hardly understood. The decision how many spores are formed takes place after commitment to meiosis, a time point at the onset of meiosis I preceding meiotic plaque formation at meiosis II (Simchen, 2009; Jungbluth *et al*, 2012). After commitment to meiosis, activity of the Ras/cAMP/PKA pathway is crucial for reduction of spore numbers at low acetate concentrations. Furthermore, the potential PKA target Ady1 affects localization of MP proteins to the SPB (Deng & Saunders, 2001; Jungbluth *et al*, 2012). Intracellular CO_2/bicarbonate levels have a positive influence on spore numbers independently from the Ras/cAMP/PKA pathway (Jungbluth *et al*, 2012).

Less is known about how spindle polarity is established and maintained in meiosis. It was shown that sporulating cells with a temperature-sensitive variant of Nud1 fail in age-dependent selection of SPBs but are not affected in spore number control indicating an independent regulation of spindle polarity and spore numbers (Gordon *et al*, 2006). Furthermore, the ability to form astral microtubules in meiosis I impacts on age-dependent formation of MPs at the second oldest SPB and the youngest SPB originating from it (Gordon *et al*, 2006). It is likely that factors involved in polarity establishment and cytokinesis during vegetative growth play a role in the creation of distinct SPB identities. One candidate is the mitotic exit network since it fulfills similar functions during mitosis. During sporulation, activity of the MEN kinases is mainly restricted to meiosis II and independent of Tem1 as well as of Nud1 (Attner & Amon, 2012). Hence, no SPB localization could be observed for the remaining components. Several studies have shown that at least Cdc15 functions in PSM growth and closure as well as spore wall formation (Kamieniecki *et al*, 2005; Pablo-Hernando *et al*, 2007; Diamond *et al*, 2009; Attner & Amon, 2012). In contrast to mitosis, Dbf20 exhibits higher activity than Dbf2 and its association with Mob1 is Cdc15

dependent (Attner & Amon, 2012). Yet, direct functional characterization of the latter components suffered from the lack of methods to create reliable sporulation-specific mutants.

1.3 Conditional Mutants as a Cell Biological Tool

In reverse genetics, the most widespread initial approach to study the function of a gene product is deletion of the respective open reading frame. However, there are limits to this strategy: if a gene is essential for growth or the analyzed process or its product have multiple roles during a developmental process, constitutive mutants are pointless. These problems can be solved by conditional mutants, which show the desired defect only upon change from permissive to repressive conditions. One strategy for creating a conditional mutant is the substitution of the endogenous promoter with a promoter regulated by addition of external compounds such as galactose or tetracyclines (Gossen & Bujard, 1992; Mumberg *et al*, 1994). Other methods directly control protein activity. A prominent example is the use of temperature-sensitive mutants to study the cell cycle of *S. cerevisiae* (Hartwell *et al*, 1973). Engineered variants of some proteins can also be inhibited by chemical compounds (Bishop *et al*, 2000). A more generally applicable approach uses genetically encoded tags fused to target genes, which destabilize the protein upon application of a specific signal like heat or chemical compounds (Dohmen *et al*, 1994; Schneekloth *et al*, 2004; Nishimura *et al*, 2009). These tools rely on the ubiquitin-proteasome system (UPS), an enzymatic cascade, which finally ends with degradation of the target protein by the 26S proteasome (Ravid & Hochstrasser, 2008). The small protein ubiquitin is activated by a ubiquitin-activating enzyme (E1) and transferred to a ubiquitin-conjugating enzyme (E2). The degradation-inducing sequence (degron) is recognized by specific ubiquitin-protein ligases (E3), which mediate the transfer of ubiquitin to an accessible lysine of the target protein. Addition of further ubiquitin moieties to the previously attached ubiquitin generates a poly-ubiquitin chain, which is recognized by the 26S proteasome resulting in unfolding and degradation of the target protein. A highly conserved branch of the UPS, best studied in yeast, is the so-called Arg/N-end rule pathway. In this pathway, single N-terminal residues serve as N-degrons with varying destabilization properties (Varshavsky, 2011). These N-degrons are either directly recognized (Arg, Lys, His, Leu, Phe, Tyr, Trp and Ile) by an Arg/N-end rule specific E3 (Ubr1 in *S. cerevisiae*) or require one (Glu and Asp) or two (Gln and Asn) modifications to induce degradation. The most efficient N-degron has been shown to be Arg, however, the degron strength is not directly dependent on the number of modifications required.
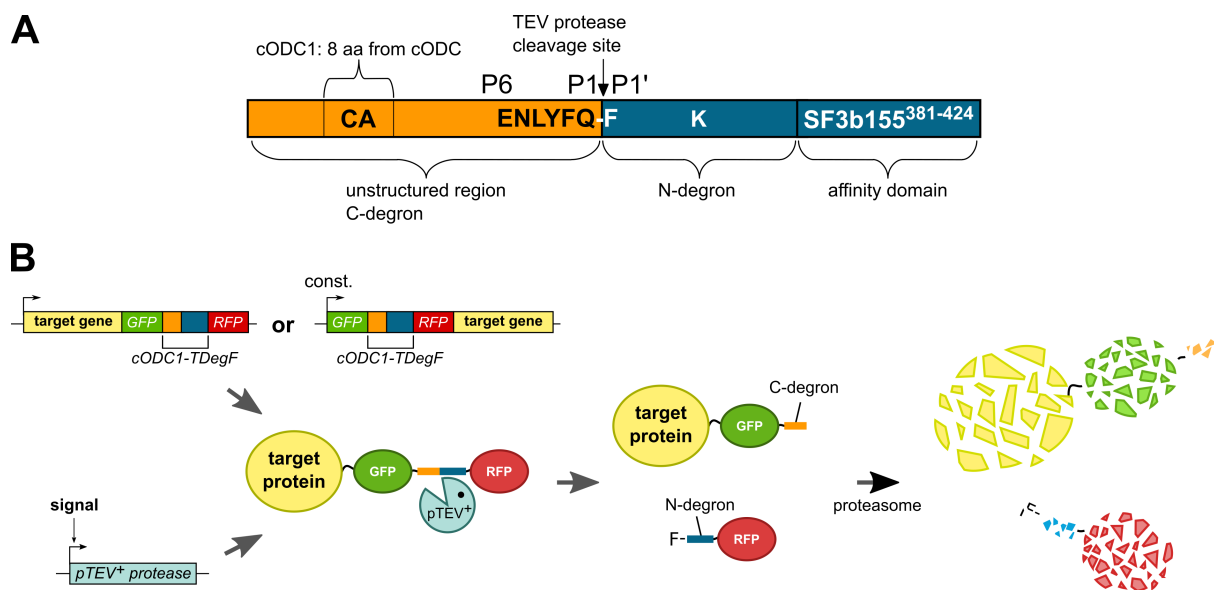
Figure 4: The TEV protease induced instability (TIPI) system. (A) Structure of the bidirectional TIPI tag. The tag consists of a C-terminal degron cODC1, followed by the TEV protease recognition sequence ENLYFQ-F; the phenylalanine residue downstream of the cleavage site constitutes an N-degron completed by an accessible lysine and the affinity domain SF3b$^{381\text{-}424}$ whose interaction domain p14 is attached to the TEV protease. **(B)** Function of the TIPI system. The sequence encoding the bidirectional TIPI tag can be fused to the 3'-end of the target gene, preserving its native promoter, or to its 5'-end, introducing a constitutively active promoter. In the example, the bidirectional TIPI tag is flanked by GFP and RFP, respectively and fused C-terminally to the target protein. Upon induction of TEV protease the tag is cleaved. This activates the degrons and mediates proteasomal degradation of attached proteins. Scheme from Jungbluth *et al*, 2010, modified.

A recently developed, versatile method for conditional control of protein stability is the tobacco etch virus (TEV) protease induced instability system (TIPI; Jungbluth *et al*, 2010; Taxis *et al*, 2009). The TIPI system employs an improved version of the highly specific and widely used protease of the tobacco etch virus fused to the p14 affinity domain (pTEV$^+$; Taxis *et al*, 2009). Its production can be controlled by a regulatable promoter or a promoter only active in distinct developmental stages. Additionally, this method uses a tag fused to a target protein and containing one or two distinct cryptic degrons. Upon TEV protease cleavage, these degrons become activated (Figure 4). The respective TEV protease recognition site (ENLYFQ-F) resides in the center of the tag. It is cleaved between the glutamine at position P1 and the phenylalanine at position P1' once the protease is produced. The phenylalanine is at the same time part of the N-terminal TIPI-degron TDegF and acts after proteolysis as an N-degron, an accessible lysine is contained in the downstream sequence. The deprotected degron and any attached protein are degraded by the 26S proteasome in an ubiquitin-dependent manner (Taxis *et al*, 2009). Furthermore, the affinity domain SF3b$^{281\text{-}424}$ is included in the tag, which recruits the pTEV$^+$ protease via interaction with the p14 domain (Taxis *et al*, 2009). The sequence upstream of the cleavage site contains the C-degron cODC1 derived from the murine ornithine decarboxylase (ODC) C-terminus (Jungbluth *et al*, 2010). It consists of an unstructured stretch of 37 amino acids

with a cysteine-alanine (CA) motif 19 amino acids upstream to the terminus. This degron is recognized directly by the proteasome without need of further modification (Takeuchi *et al*, 2008). In this set up, the two degrons inactivate each other until both are separated by TEV protease cleavage. This bi-directional tag can be fused to the N-terminus or C-terminus of target proteins but can also be inserted internally (Jungbluth *et al*, 2010). One example of developmental-specific usage of the TIPI system is control of *pTEV*[+] expression by the promoter of the early-meiotic gene *IME2* (Jungbluth *et al*, 2010, 2012). *pTEV*[+] expression upon early meiotic stages led to target protein depletion specifically during sporulation. This system was employed to study the role of genes in meiosis, which are essential for vegetative growth. Though, this approach often needed adaptation to the specific target protein by using constitutive promoters with varying strength for control of target gene expression as well as introduction of high copy numbers of the pTEV[+] encoding constructs.

Optogenetics is a rapidly emerging field that aims to employ light of various wavelengths to control protein and cellular activity. Light as signal is exceptionally fast and can be regulated precisely in both, quality and quantity. This allows frequent changes between on- and off-states. The spatial resolution is hardly achieved by other signals like chemicals or changes in temperature. Moreover, light allows for defined experimental conditions without the need of externally added compounds. Thus, light may be an ideal signal to induce protein depletion during the highly sensitive process of yeast sporulation, which is easily compromised by temperature shifts or addition of nutrients and chemicals. Different naturally occurring protein domains acting as light sensors can be employed to use light as a synthetic signal to study cell biological processes (Möglich & Moffat, 2010; Shcherbakova *et al*, 2015). Well-characterized and widely used sensor modules comprise the LOV (light oxygen voltage), BLUF (blue-light-utilizing flavin adenine dinucleotide), cryptochrome and phytochrome domains of plants and bacteria. These photoreceptors sense different wavelengths of light, ranging from the ultraviolet to the near infrared spectrum. The common feature of these domains is the transformation of the light-input into a structural output. This process relies on excitation of a chromophore, either a complexed cofactor or part of the protein itself (Shcherbakova *et al*, 2015). For example, in the LOV2 domain of phototropin 1, a flavin mononucleotide (FMN) forms a thioether bond with a cysteine sidechain of the protein leading to detachment and unfolding of a C-terminal (Jα) helix within microseconds (Harper *et al*, 2003). By exploiting the different features of these photo-sensor domains, a variety of synthetic modules were created, facilitating light control of protein activity on diverse cellular levels (Yin & Wu, 2013). The catalytic center of an

enzyme can be blocked in the dark and released by light (Wu *et al*, 2009). It is possible to control protein localization to a distinct cell compartment by light-dependent heterodimerization (Strickland *et al*, 2012). Coupling of photo-sensitive homodimerization to DNA-binding and transcriptional activation can be used to regulate gene expression (Shimizu-Sato *et al*, 2002). In addition, light-mediated indirect clustering of signal peptides can trigger signal transduction by transmembrane receptors (Bugaj *et al*, 2015). We developed a photo-sensitive degron module, which consists of a fusion between parts of the cODC1 degron to the Jα-helix of *Arabidopsis thaliana* LOV2. This degron enables direct control of protein stability by blue-light and is a reliable tool for probing gene function during meiosis (Renicke *et al*, 2013a; Renicke & Taxis, 2016). Another group created a similar degron module by combining the LOV2 domain of *Avena sativa* with a different degron sequence in zebrafish (Bonger *et al*, 2014).

1.4   Aims of this Thesis

A major focus of this study was the elucidation of molecular determinants of age-based selection of spindle pole bodies for modification with meiotic plaques. As candidates for this age-based selection the core mitotic exit network components, the kinase Cdc15, the kinase Dbf2, its paralog Dbf20 and their activator Mob1 were analyzed during sporulation of *S. cerevisiae*. To enable functional characterization of the MEN core cascade and genetic interactions of its members, methods for meiosis-specific depletion of the target proteins by conditional degrons ought to be developed. One strategy was combination of a photoreceptor domain with a well-characterized degron to enable light-induced protein destabilization. A second strategy was based on a system for degron activation upon production of and cleavage by a protease, which had already been established for meiosis-specific protein depletion. This system should be enhanced at several levels: by mutational creation of a protease variant with a broader target spectrum to allow usage of more efficient degrons as well as by combination of meiosis-specific target gene downregulation with raised protease levels. By one or several of these techniques, the single MEN components and combinations of them should be targeted allowing to assess the sporulation performance of the resulting mutants. Then, further characterization should provide information on genome inheritance, SPB selection, prospore membrane formation and closure as well as regulation of MP levels in the mutants.

2 A LOV2 Domain-Based Optogenetic Tool to Control Protein Degradation and Cellular Function.

Christian Renicke[1], Daniel Schuster[1], Svetlana Usherenko[1], Lars-Oliver Essen[2], and Christof Taxis[1,*]

[1]Department of Biology/Genetics, Philipps-Universität Marburg, Karl-von-Frisch-Strasse 8, 35043 Marburg, Germany

[2]Department of Chemistry and Biomedical Research Center, Philipps-Universität Marburg, Hans-Meerwein-Strasse, 35032 Marburg, Germany

[*]Correspondence: taxis@biologie.uni-marburg.de

Resource

A LOV2 Domain-Based Optogenetic Tool to Control Protein Degradation and Cellular Function

Christian Renicke,[1] Daniel Schuster,[1] Svetlana Usherenko,[1] Lars-Oliver Essen,[2] and Christof Taxis[1,*]

[1]Department of Biology/Genetics, Philipps-Universität Marburg, Karl-von-Frisch-Strasse 8, 35043 Marburg, Germany
[2]Department of Chemistry and Biomedical Research Center, Philipps-Universität Marburg, Hans-Meerwein-Strasse, 35032 Marburg, Germany
*Correspondence: taxis@biologie.uni-marburg.de
http://dx.doi.org/10.1016/j.chembiol.2013.03.005

SUMMARY

Light perception is indispensable for plants to respond adequately to external cues and is linked to proteolysis of key transcriptional regulators. To provide synthetic light control of protein stability, we developed a generic photosensitive degron (psd) module combining the light-reactive LOV2 domain of *Arabidopsis thaliana* phot1 with the murine ornithine decarboxylase-like degradation sequence cODC1. Functionality of the psd module was demonstrated in the model organism *Saccharomyces cerevisiae.* Generation of conditional mutants, light regulation of cyclin-dependent kinase activity, light-based patterning of cell growth, and yeast photography exemplified its versatility. In silico modeling of psd module behavior increased understanding of its characteristics. This engineered degron module transfers the principle of light-regulated degradation to nonplant organisms. It will be highly beneficial to control protein levels in biotechnological or biomedical applications and offers the potential to render a plethora of biological processes light-switchable.

INTRODUCTION

Plants are fundamentally dependent on quantitative and qualitative light perception to respond in an adequate way. Usually, they possess several photoreceptors that cover a broad range of wavelengths and intensities. In previous years, it has become more and more apparent that light regulation of plant behavior is performed by proteolysis of key regulators. The central player of this signaling cascade is the ubiquitin-protein ligase COP1 that is under negative control of several light-perceiving pathways. Active COP1 targets a vast amount of proteins for degradation by the ubiquitin-proteasome system including several transcription factors that are positive regulators of light-responsive pathways (Ito et al., 2012; Lau and Deng, 2012). Light has been recognized in recent years as an almost ideal external signal to regulate intracellular processes with unmatched spatio-temporal precision. The synthetic approach using genetically en-

coded proteins to control protein activity by light is generally referred to as optogenetics (Christie et al., 2012). So far, several light-induced expression systems have been developed that allow regulation of protein abundance (Kennedy et al., 2010; Levskaya et al., 2005; Shimizu-Sato et al., 2002; Sorokina et al., 2009), whereas light-dependent manipulation of protein stability has been largely neglected. The only available method involves intracellular formation of reactive oxygen species, which may induce unwanted side effects (Bulina et al., 2006). Until now, a synthetic tool that catches the essentials of light-regulated proteolysis and could be generally used to study it in other model organisms is not available.

A detailed reconstitution of the plant system of light-regulated degradation is very challenging, as different components act together in several pathways (Lau and Deng, 2012). However, already a simple fusion of a light-perceiving domain that regulates activity of a degradation-inducing sequence would be a very valuable tool to regulate protein stability by light. A well-studied protein domain for generation of such a synthetic, light-reactive module is the light oxygen voltage (LOV2) domain from phototropin (Christie et al., 1999; Herrou and Crosson, 2011). The LOV2 domain has been used extensively to control protein activity by light or to regulate protein-protein interactions due to its favorable features that make it suitable for usage in all kingdoms of life (Strickland et al., 2008; Wu et al., 2009; Pham et al., 2011; Strickland et al., 2012; Lungu et al., 2012). This domain consists of a flavin mononucleotide-binding core domain and the Jα-helical extension at the carboxy-terminus. Upon irradiation with blue light, a cysteine of the core domain forms a covalent adduct with the excited flavin mononucleotide (FMN). This induces a conformational change within the core followed by dissociation and unfolding of the Jα helix (Harper et al., 2003). We reasoned that this conformational change could be used to unmask a degradation-inducing sequence called degron, thereby controlling protein stability by light. One degron, compatible with such an activation mechanism, is that of murine ornithine decarboxylase (ODC). The active ODC degron induces ubiquitin-independent proteasomal degradation if attached to the carboxy-terminus of a protein. It consists of an unstructured peptide 37 amino acids long comprising a cysteine-alanine motif, which is involved in recognition by the proteasome and therefore important for degradation (Jariel-Encontre et al., 2008). This degradation mechanism is conserved in yeasts, vertebrates, and plants (DeScenzo and Minocha, 1993; Hoyt et al., 2003).
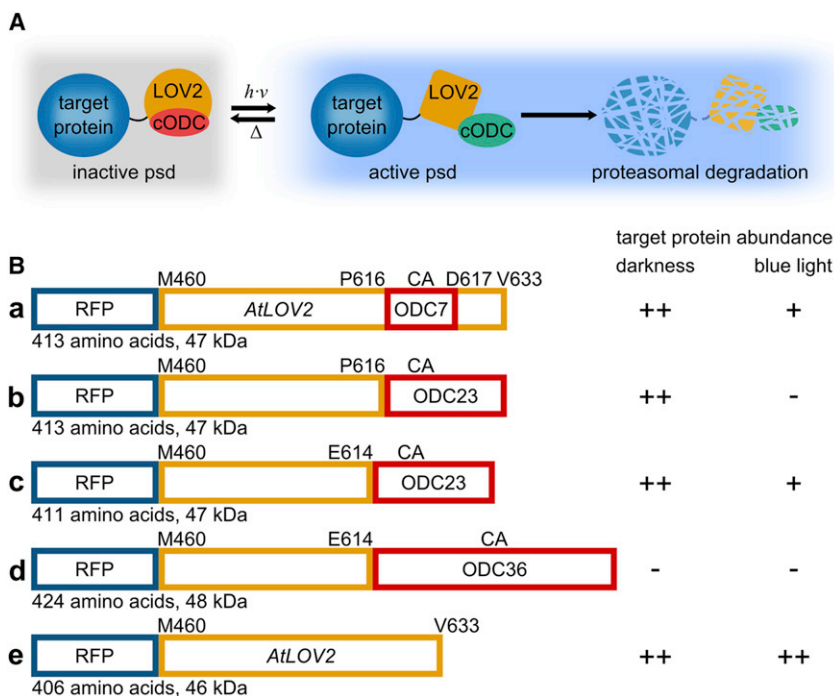
13

Figure 1. Development of a psd

(A) Schematic design of the psd module in the dark and lit states. In darkness, the cODC1 degron is inactive and the fusion protein is stable. Upon irradiation by blue light, the degron is activated and induces proteasomal degradation of the fusion protein.

(B) Realization of the psd module. Different constructs were tested for the ability to work as a psd using the target protein RFP. Construct a was derived by inserting seven amino acids from the cODC degron (MSCAQES, ODC7) between P616 and D617 of AtLOV2; construct b was derived by fusing 23 amino acids from cODC1 (MSCAQESITSLYKKAGSENLYFQ, ODC23) after P616 (psd module; the full sequence of the construct can be found in Figure S1); construct c was derived by fusing the same sequence after E614, closer to the Jα helix; and construct d was derived by using the full cODC1 degron (positive control, ODC36). The relative position of the cysteine-alanine (CA) motif to the Jα domain can be approximated from the drawing. AtLOV2 alone fused to RFP (construct e) was used as negative control. RFP fluorescence was observed by microscopy in dark and lit conditions.
See also Figure S1.

RESULTS AND DISCUSSION

Development of a Light-Reactive Degradation Domain

We constructed a conditional degron responsive to blue light by fusing the *Arabidopsis thaliana* LOV2 domain (AtLOV2) of phototropin 1 with parts of a synthetic ODC-like degron (Jungbluth et al., 2010). The degron sequence was attached to the LOV2 domain such that one requirement for activation of the ODC-like degron, an unstructured region of at least 16 amino acids in length upstream of the cysteine-alanine motif, is met only upon unfolding of the Jα helix of AtLOV2. Thus, blue-light irradiation of AtLOV2 results in activation of the ODC-like degron and leads to proteasomal degradation of the whole construct (Figure 1A). Several fusions of AtLOV2 with the degron were constructed, differing in length of the degron sequence and its attachment point to AtLOV2 (Figure 1B, constructs a–c). All fusions were placed close to the end of the Jα helix (amino acids P616 or E614) and compared in their ability to act as a light-regulatable degron with constructs d (AtLOV2 fused to full-length degron) and construct e (AtLOV2 alone) in *Saccharomyces cerevisiae*. Only construct b resulted in efficient blue light-control of protein abundance (Figure 1B). This construct was termed the photosensitive degron (psd) module, and the sequence is given in Figure S1 (available online).

Basic Characterization of the psd Module

Blue-light-induced depletion of red fluorescent protein (RFP)-psd was observed within 4 hr, whereas abundance of RFP-AtLOV2 was not affected (Figure 2A). Efficient target protein destabilization depended on the presence of the cODC1 degron and its cysteine-alanine motif; even low amounts of blue light induced depletion of the RFP-psd fusion protein (Figure S2A). Saturation was achieved at light fluxes as low as 5 μmol m^{-2} s^{-1}, as higher fluence rates did not increase the

depletion rate (data not shown). Reappearance of the target protein after light-induced depletion was tested by exposure of RFP-psd-containing cells to blue light and retransfer of the cells into darkness. The tester protein was depleted by light and partially recovered in darkness within 1 hr, whereas abundance of RFP-AtLOV2 was not affected (Figure 2B). Mutations within the LOV2 domain that inhibit FMN adduct formation (C53A; dark state mutant) or freeze the domain in the lit state (I149E) (Wu et al., 2009) inhibit light-induced destabilization or induce light-independent depletion of the psd module (Figure S2B). Moreover, we measured depletion kinetics of RFP-psd upon irradiation with blue light. We found rapid decrease of the tester protein to less than 10% of the starting levels within 2 hr (depletion half-time ± SEM, 38 ± 1 min), whereas protein amounts of the RFP control were only slightly reduced (Figure 2C; Figure S2C). This demonstrates that the performance of the psd module equals that of a conditional degron based on the same destabilization sequence (Jungbluth et al., 2010). To obtain data comparable to other degrons, we measured the half-life of RFP-psd using a cycloheximide chase experiment. We found a half-life of 157 ± 6 min (SEM) for RFP-psd in cells kept in darkness and 21 ± 1 min in cells exposed to saturating amounts of blue light (Figure 2D; Figure S2D). The >7-fold change in stability between dark and lit conditions demonstrates robustness of light-induced destabilization by the psd module. The difference between depletion half-time and half-life of RFP-psd illustrates the influence of ongoing protein synthesis: The more target protein is made, the longer it takes to deplete it. Usage of weaker promoters than *ADH1*, like *CYC1*, will be a way to obtain even faster depletion of a target protein. Another possibility is to drive expression of the construct by a regulatable promoter. In this way, target gene expression can be shut down concomitantly with destabilization of the target protein. Thus, depletion can be expected to be close to the time we found for the
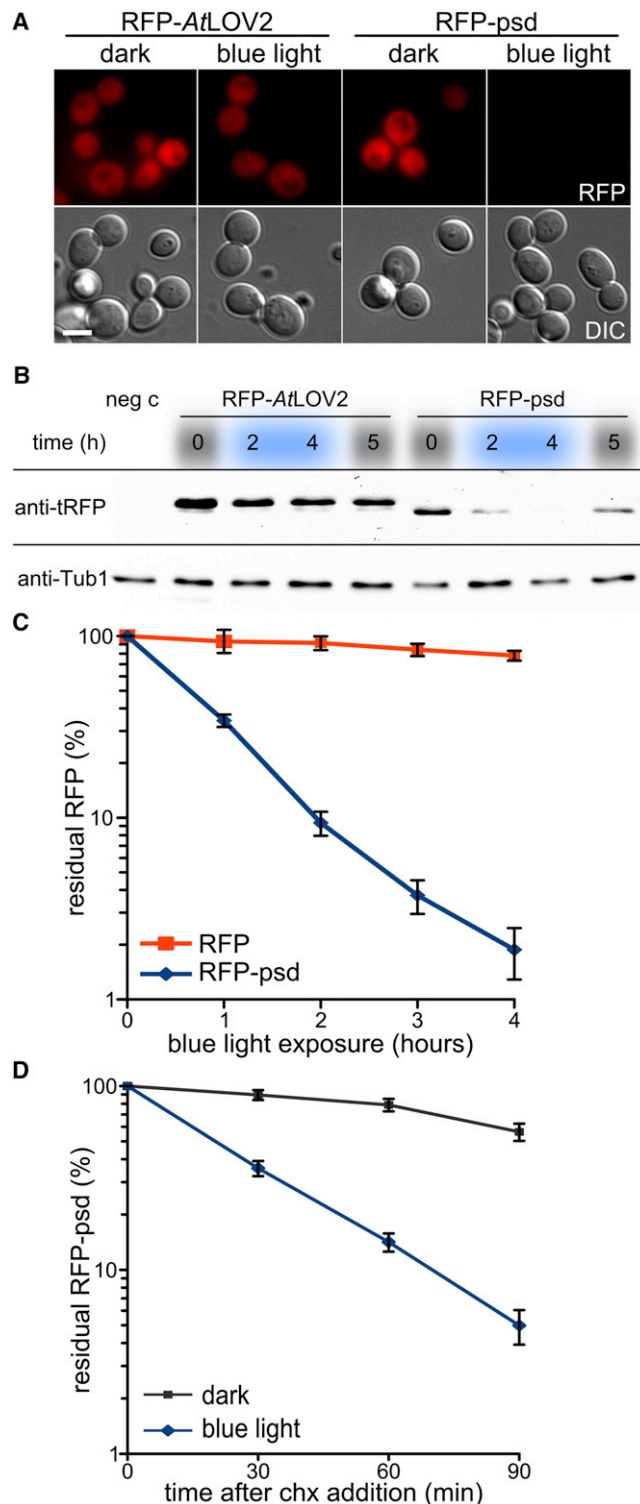
Figure 2. Light Control of Protein Stability with the psd Module

(A) Blue light activates the psd module. Fluorescence microscopy images of yeast cells expressing P_{ADH1}-RFP-AtLOV2 or P_{ADH1}-RFP-psd (plasmid based) pregrown in the dark were incubated in the absence or presence of blue light (LED lamp, 470 nm, 10 μmol m^{-2} s^{-1}) for 4 hr. Scale bar, 4 μm.

(B) Reversibility of psd-module-induced target protein depletion. Yeast cells expressing P_{ADH1}-RFP or P_{ADH1}-RFP-psd (plasmid based) were grown in liquid medium in the dark. After removal of the first sample (t = 0 hr), cells were

cycloheximide-chase experiment. For further characterization of the light-induced degron, its blue light specificity was tested. As expected, we found no significant change of target protein level in the presence of red light (Figures S2E and S2F).

Next, we assessed the possibility to visualize blue light exposure of yeast cells on a macroscopic level. Yeast cells producing high amounts of RFP-psd were grown on plates in the presence or absence of blue light. We found robust fluorescence in cells exposed to darkness and no fluorescence in cells exposed to blue light (Figure S3A). Quantification revealed that the dark/lit ratio of RFP-psd is similar in cells producing high or low amounts of RFP-psd (Figure S3B), showing that the protein synthesis rate does not influence the light response of the psd module considerably. To monitor the response of the psd module to various light intensities, a gradient of blue light was applied on cells producing RFP-psd. We observed a decrease in fluorescence upon increasing exposure to blue light. Quantification of the fluorescence reveals a direct dependency of RFP fluorescence to blue light illumination (Figure 3A; Figure S3C).

Furthermore, we were interested in obtaining a yeast strain that allows to reproduce images directly on a yeast cell lawn. We reasoned that induction of adenine auxotrophy by Ade2 depletion, which results in accumulation of a red pigment that is produced from an intermediate of the adenine biosynthesis pathway (Sharma et al., 2003), is a way to implement yeast photography. We generated conditional adenine auxotrophy by light-induced degradation of Ade2-RFP-psd (Figure S3D); usage of a gradient of blue light resulted in a gradual change of the yeast lawn color from pale to red (Figure S3E). Spatial resolution of pigment accumulation is high enough to allow photography on yeast lawns (Figure 3B). Imaging on bacterial lawns has been achieved before, which requires the addition of S-gal (3,4-cyclohexenoesculetin-β-D-galactopyranoside) to the medium to visualize the image (Levskaya et al., 2005). Using the Ade2-RFP-psd strain does not require the addition of an external compound; thus, the cells form a photosensitive screen with incorporated development of the image in vivo. Overall, the psd module allows the creation of fluorescence images or photographs based on

exposed to blue light (LED lamp, 465 nm, 30 μmol m^{-2} s^{-1}). After 4 hr of light exposure, cells were transferred to the dark. Samples taken at the indicated time points were subjected to alkaline lysis and immunoblotting. Antibodies against tRFP and Tub1 (loading control) were used for detection (negative control; neg c). Please note that even though the RFP-AtLOV2 fusion protein is seven amino acids shorter than RFP-psd, it runs slightly slower in SDS-PAGE. (C) Kinetics of psd-module-induced target protein depletion after exposure to blue light. Yeast cells expressing P_{ADH1}-RFP or P_{ADH1}-RFP-psd (plasmid based) were grown in liquid medium in the dark. After removal of the first sample (t = 0 hr), cells were exposed to blue light (LED lamp, 465 nm, 30 μmol m^{-2} s^{-1}). Curves are the means of RFP and RFP-psd protein amounts obtained from six immunoblots (representative result shown in Figure S2C). Error bars indicate SEM.

(D) Measurement of psd-module-induced target protein destabilization. Yeast cells expressing P_{ADH1}-RFP-psd (plasmid based) were grown in liquid medium in the dark. After removal of the first sample (t = 0 hr), cycloheximide (chx) was added to stop protein synthesis; cells were kept in the dark or exposed to blue light (LED lamp, 465 nm, 30 μmol m^{-2} s^{-1}) for the rest of the experiment. Curves are the means of RFP-psd protein amounts obtained from nine independent measurements. Error bars indicate SEM. The representative result is shown in Figure S2D.
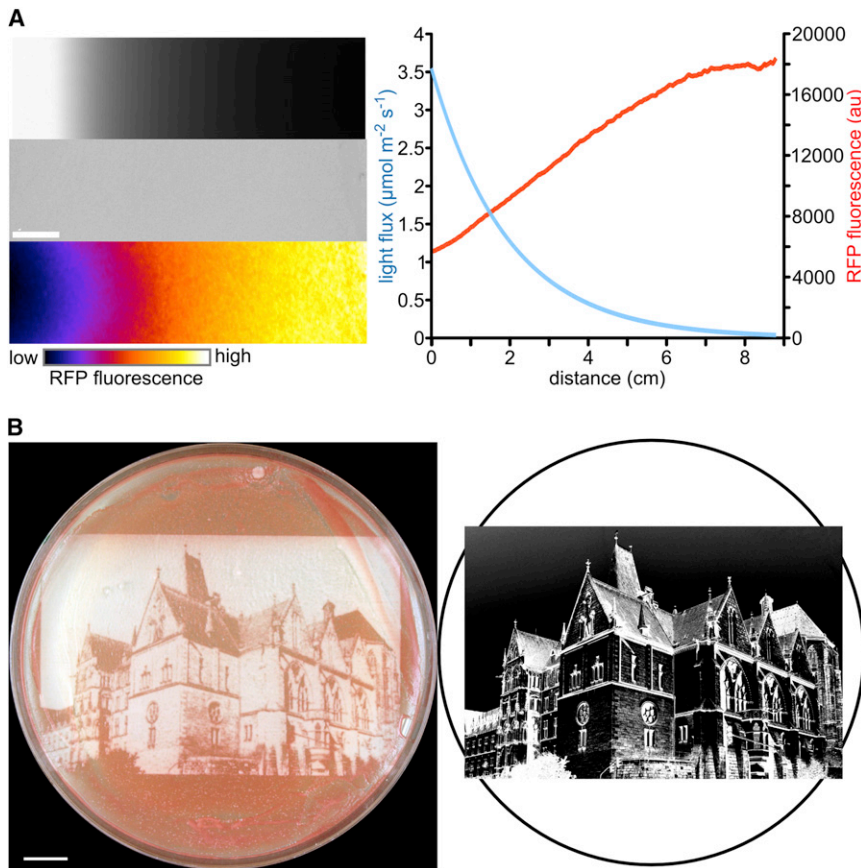
See also Figure S2.

Figure 3. Characterization of psd Module Behavior on a Macroscopic Level

(A) Input-output characteristics of the psd module in a plate assay. A neutral density gradient (uppermost image on the left) was used to generate a blue light gradient (465 nm; intensity from 0.04 to 3.54 μmol m^{-2} s^{-1}), which was applied on cells expressing P$_{TDH3}$-RFP-psd (plasmid based). Yeast cell growth is shown in the middle image on the left (bar size, 1 cm), RFP fluorescence intensity is represented as a heat map (lower left image). Background corrected fluorescence (right graph, red curve) was plotted together with calculated blue light intensity (blue curve).

(B) Yeast photography. The RFP-psd module was inserted chromosomally at the 3′ end of ADE2 (YDS91). Cells were grown for 3 days at 25°C on solid medium and irradiated by blue light (465 nm, 10 μmol m^{-2} s^{-1}) using a mask with an inverted black-and-white image of the "Alte Universität" in Marburg, Germany (right image). The resulting yeast photograph is shown on the left side. Bar size, 1 cm.

See also Figure S3.

living cells as a photosensitive agent. In principle, this gives the opportunity to store information in a community of cells in a nonpersistent way.

Cell Cycle Progression Driven by Light

To implement cell cycle control by light, we fused the psd module to dominant-active versions of two regulators of the cyclin-dependent kinase Cdc28. One is Clb2, lacking the degradation box (^{24}RLALNNVTN^{34}) sequence (Surana et al., 1993); the other is a shortened version of the cyclin B/Cdc28 inhibitor Sic1, lacking the SCF^{Cdc4}-dependent degradation sequence located within the N-terminal 105 amino acids (Berset et al., 2002). Thus, the endogenous cell-cycle-dependent regulation of Clb2 or Sic1 stability was replaced by light-dependent regulation via the psd module (Figure S4A), which should allow external control of mitosis and G1/G2 transition, respectively (Nasmyth, 1996). As expected, cells expressing the Clb2 or the Sic1 construct grew very well in the presence of blue light due to low levels of Clb2^{Δdb}-3myc-psd or ^{ΔN}Sic1-3myc-psd but accumulated these Cdc28 regulators and failed to grow in the dark (Figure 4A; Figures S4B and S4C). Analysis of cell cycle stages revealed that construct-bearing and control cells behave essentially the same during blue light exposure (Figure 4B; Figure S4D). After 5 hr in darkness, the majority of clb2^{Δdb}-3myc-psd-expressing cells exhibited a defect in metaphase to anaphase transition (Figure 4B). Cells were mostly large budded with short spindles localized at the bud neck (Figure S4D). This matches the pheno-

type reported for cells overproducing an amino-terminal truncated version of Clb2 (Ghiara et al., 1991); however, it has been reported as well that similar mutants arrest as large budded cells with elongated spindles classified as telophase (Surana et al., 1993) or mitotic exit defect (Wäsch and Cross, 2002). These differences might arise due to the usage of different strain backgrounds, Clb2 constructs, or experimental conditions, which affect the exact point at which the cells arrest in the cell cycle. Cells expressing ^{ΔN}sic1-3myc-psd were mostly large budded with multiple buds after 5 hr in darkness (Figure 4B; Figure S4D), which is the typical phenotype of cells arrested during G1/S transition due to cyclin B/Cdc28 complex inhibition (Dirick et al., 1995; Hodge and Mendenhall, 1999).

Photo-Switchable Mutants

To create conditional mutants, which are switched between permissive and restrictive conditions by light, we fused the RFP-psd module chromosomally to CDC5, CDC14, PMA1, and MCM1 and the 3myc-psd module to CDC48, UFD1, NPL4, SEC62, and SEC63. All these genes are essential for the growth of yeast (Giaever et al., 2002). The membrane protein Sec63 localizing in the endoplasmatic reticulum was included to serve as an internal control, as its C terminus faces the ER lumen. Therefore, no change in abundance is expected for this construct upon illumination with blue light. Cdc14 and Pma1 tagged with RFP-psd localized as reported for the green-fluorescent-protein-tagged proteins (Figure S5A; Huh et al., 2003), whereas for the other proteins tagged with RFP-psd, no clear localization was observed (data not shown). We found blue light-dependent growth inhibition in the cases of cdc5-RFP-psd, cdc14-RFP-psd, cdc48-3myc-psd, ufd1-3myc-psd, npl4-3myc-psd, sec62-3myc-psd, and mcm1-RFP-psd, whereas
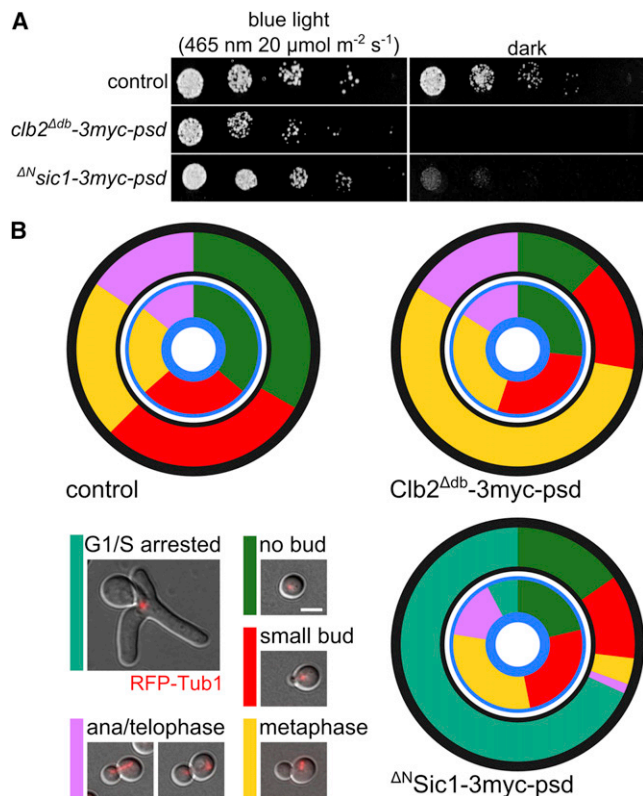
16

Figure 4. Control of Cell Cycle Events by Light

(A) Serial dilutions (1:5; first spot about 2,400 cells) of control (YDS28), *clb2*[Δdb]-*3myc-psd*, and *[ΔN]sic1-3myc-psd* (plasmid-encoded) cells were spotted on YPD plates and incubated 3 days at 25°C in absence or presence of blue light (465 nm, 20 μmol m^{-2} s^{-1}).

(B) The same yeast strains as in (A) were pregrown under blue light and then exposed to blue light (465 nm, 30 μmol m^{-2} s^{-1}) for 5 hr or kept in darkness over the same time and finally used for image acquisition. Differential inter-ference contrast and fluorescence images (RFP-Tub1) were used to catego-rize cell cycle stages according to the examples shown in the lower left. Scale bar, 3 μm. Circular graphs (outer ring: 5 hr darkness; inner ring: growth exposed to blue light) show the mean distribution of cell cycle stages obtained from four biological replicates counting at least 100 cells for each replicate. See also Figure S4.

Figure 5. Generation of Conditional Mutants Using the psd Module

(A) The gene encoding for the psd module together with RFP or 3myc was fused chromosomally to the 3' end of *CDC5* (YCT1316), *CDC14* (YCT1315), *MCM1* (YDS120), *PMA1* (YCT1338), *CDC48* (YDS175), *UFD1* (YDS187), *NPL4* (YDS191), *SEC62* (YDS174), and *SEC63* (YDS188). Serial dilutions of cells (1:5 dilutions; first spot about 2400 cells) were spotted on YPD plates and incubated three days at 25°C in absence or presence of blue light (465 nm, 20 μmol m^{-2} s^{-1}).

(B) Blue-light induced cell patterning. *sec62-RFP-psd* mutant cells (YDS82) were spread on solid medium and blue light (465 nm, 7 μmol m^{-2} s^{-1}) was applied for 3 days. The star-shaped mask (shown in the left image) was used to block light in the center of the plate. Growth of the yeast cells is shown on the right side. Bar size, 1 cm.

See also Figure S5.

pma1-RFP-psd and, as expected, *sec63-3myc-psd* cells were not affected by light (Figure 5A). Immunoblotting experiments using 3myc-psd-tagged variants showed a decrease in target protein abundance for all mutants except Sec63-3myc-psd (Fig-ure S5B). Then, we analyzed the cell cycle stages based on cell and spindle morphology for cells bearing Cdc5-3myc-psd, Cdc14-3myc-psd, and Cdc48-3myc-psd grown in darkness or under blue light. All three mutants showed distinct changes in the distribution of the cell cycle stages after blue light exposure, especially Cdc48 depletion, which resulted in an almost com-plete arrest at metaphase to anaphase transition (Figure S5C).

To investigate specificity of light-induced degradation, we measured the abundance of interaction partners upon depletion of essential proteins tagged with the psd module. A slight decrease in protein levels was observed for Kin4 and Spc72 upon loss of Cdc5, whereas no change was detectable in all other cases (Figure S5D). This indicates that, in the majority of
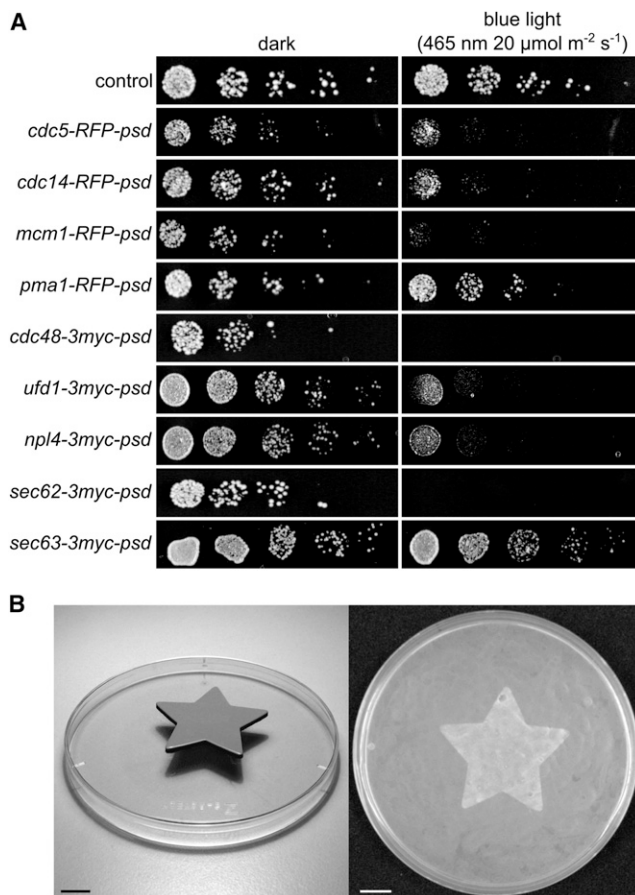
cases, destabilization of one complex subunit does not induce degradation of the other members. Furthermore, we tested whether the light sensitivity of the *sec62-RFP-psd* mutant could be used for light-based growth patterning. We spread the mutant evenly on a plate and projected a star-shaped pattern on the cell lawn. The *sec62-RFP-psd* mutant cells grew only in the area pro-tected from blue light by the mask (Figure 5B).

Simulation of psd Module Behavior

In an attempt to increase our understanding of psd module behavior, we performed in silico modeling using the computer-aided design software TinkerCell (Chandran et al., 2009). The model includes protein synthesis and takes into account conver-sion from dark to lit state and its back reaction (light conversion
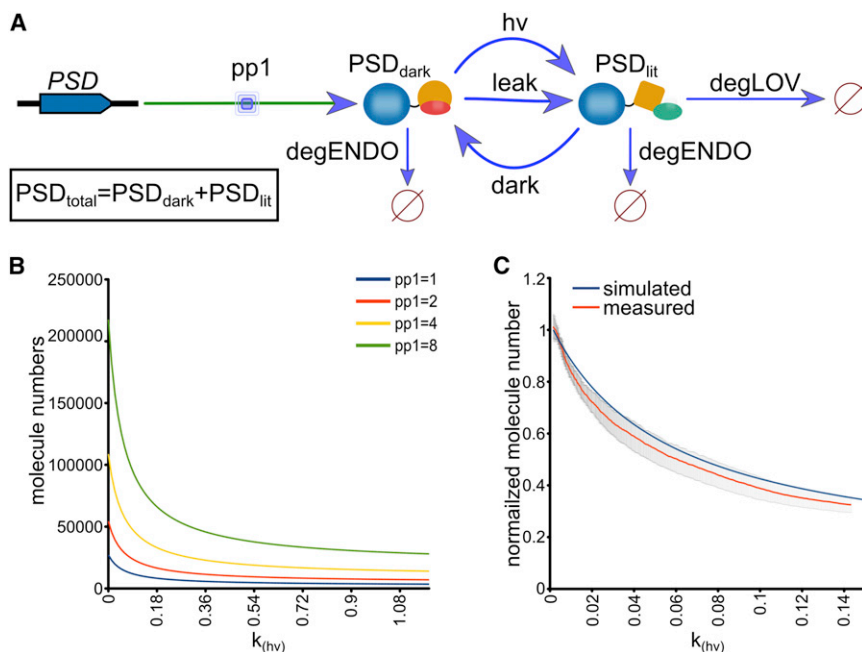
Figure 6. In Silico Modeling of psd Module Behavior

(A) Graphical representation of the TinkerCell model for light-induced degradation of the psd module. A detailed description of the model and the values used for our simulations can be found in the Experimental Procedures section. For generation of the graphs, total amounts of PSD (PSD_{dark} + PSD_{lit}) were calculated.

(B) Simulated amounts of PSD_{total} synthesized with different promoter strength (PP1 = 1; 2; 4; 8) at increasing light intensities corresponding to light fluxes from 0 to 30 μmol m^{-2} s^{-1}.

(C) Light response of the psd module. Normalized PSD_{total} amounts at different light intensities [0.04 to 3.54 μmol m^{-2} s^{-1} plotted as $k_{(hv)}$ values] simulated with TinkerCell compared to mean values of normalized fluorescence in cells exposed to a blue-light gradient (n = 3). Error bars, SD. The representative experiment is shown in Figure 3A and Figure S3C).

See also Figure S6 and Table S3.

[hv], dark conversion [leak], and reversion to the dark state [dark]), as well as endogenous and light-induced degradation (Figure 6A). To validate the model, we compared the experimentally obtained depletion half-time with the in silico data and found similar values (38 ± 1 min versus 36.5 min; Figure S6A). Then, we simulated the influence of increasing promoter strength on the protein level of the psd module (PSD_{total}) in dark (PSD_{dark}) and lit (PSD_{lit}) states at different light conditions. We found increasing amounts of PSD_{total} with increasing promoter strength (Figure 6B). However, the ratio of PSD_{total} in darkness to PSD_{total} at saturating light conditions is independent from the promoter strength, and for all conditions, a ratio of 7.8 was obtained. Experimentally, we found, for a very strong promoter, a ratio of 7.0 (P_{TDH3}-RFP-psd) and, for a promoter with intermediate strength (P_{ADH1}-RFP-psd), a ratio of 9.4 in plate assays (Figures S3A and S3B). An unpaired t test did not show a statistically significant difference in the two measurements, which suggests that the experimentally obtained data, as well as the simulation, are in agreement with an independence of the psd module response from protein synthesis rate.

Next, we simulated the response to different illumination intensities and compared it to our plate measurements (Figure 3A). We found good agreement of the simulated light response with the in vivo measurements (Figure 6C). This argues for a direct, nonlinear dependency of target protein abundance on illumination strength invoked by the features of the AtLOV2 domain [light conversion, $k_{(dark)}$, $k_{(leak)}$] and the degradation rates.

A high ratio between the number of molecules in darkness and the number of molecules under illumination is important for applicability of the psd module. To direct future developments of the photosensitive degron, its behavior was simulated using parameters that change properties of the light response or degradation characteristics. We followed psd module behavior in silico using different values for dark state recovery rate $k_{(dark)}$ and lit state conversion in darkness $k_{(leak)}$. Minimization of $k_{(leak)}$ increased

the dark/lit ratio moderately because of the lower degradation rate in darkness (Figure S6B). The dark state reversion rate $k_{(dark)}$ influences the number of target molecules in darkness but also competes with light conversion under illumination. The calculations resulted in an optimal value for $k_{(dark)}$ of 0.42 min^{-1}, which equals a dark recovery half-time of 100 s (Figure S6C) and is close to the 70 s [$k_{(dark)}$ = 0.59 min^{-1}] of AtLOV2. However, the simulation predicted a substantial impact of the psd-independent and psd-dependent degradation rates, $k_{(degENDO)}$/$k_{(degLOV)}$, on the dark/lit ratio. Slight increase of $k_{(degLOV)}$ raised the dark/lit ratio considerably, indicating a more efficient psd module (Figure S6D). In total, the in silico modeling points to the cODC-like degron as the most promising target for further improvement of the psd module.

In the present study, the psd module was used to control the stability of target proteins using light as a transducer. It complements already existing modules for control of gene expression by light (Levskaya et al., 2005; Shimizu-Sato et al., 2002; Wang et al., 2012), providing a complete toolbox to control the synthesis and stability of a selected protein. Significantly, the usage of a phytochrome/phytochrome-interacting protein-based expression system that reacts on irradiation by red and far red light (Shimizu-Sato et al., 2002; Sorokina et al., 2009) in combination with the psd module allows independent regulation of production and stability of a target protein. Thus, target protein levels can be controlled very precisely using three different light sources.

A slight drawback on general usage of the psd module for manipulation of protein stability might be that the time necessary for depletion of a target protein is longer compared to other methods for induced protein degradation (Nishimura et al., 2009), asking for further development of the psd module to alleviate this constraint. However, we demonstrated that the psd module is ready to be used for many different applications. No requirement of temperature or specialized medium has to be met, as is the case for other methods. The target proteins that

were successfully inactivated with the psd module cover diverse biological functions like cell cycle control, secretion, transcription, and biosynthesis, which demonstrates the ease with which the psd module can exert light control on a variety of cellular behaviors.

SIGNIFICANCE

A highly versatile optogenetic tool to regulate protein stability was engineered by fusing the light-reactive domain LOV2 from *Arabidopsis thaliana* with a degradation signal derived from murine ornithine decarboxylase. We demonstrated in *Saccharomyces cerevisiae* that this generic photosensitive degron (psd) module can be used to control the stability of soluble and membrane proteins with their carboxy-termini exposed to the cytosol or nucleoplasm. It allowed creation of conditional mutants, control of the cell cycle, shaping of yeast growth into any chosen pattern, or reproduction of images on a cell lawn. The psd module is smaller (20 kDa) than commonly used fluorescent proteins and responds to blue light at intensities that are orders of magnitude lower than those used for fluorescence imaging. Hence, usage of the psd module should not lead to unwanted side effects for the majority of cell biological applications. Besides, evolutionary conservation of the degradation sequence implies that the psd module is functional in other eukaryotes as well. There, high spatial resolution of light might enable applications based on the macroscopic patterning of protein activities or cell growth, which could provide an attractive alternative to template-based approaches currently used for tissue engineering (Kaji et al., 2011). In summary, the psd module reconstructs the essence of light-regulated proteolysis from plants in a simple model organism, thus offering precise light control of protein levels in biotechnological or biomedical applications.

EXPERIMENTAL PROCEDURES

Yeast Strains, Growth Conditions, and Plasmids

The *Saccharomyces cerevisiae* strains are derivatives of the S288C strain ESM356 (Pereira et al., 2001). All strains are listed with their relevant genotypes in Table S1. Standard preparations of media were used for growth (Sherman, 2002). Yeast strains with chromosomally encoded psd module fusions were constructed by chromosomal tagging using PCR products (Janke et al., 2004) obtained with pCT337 or pDS96 as template. Cells were transformed with plasmids and PCR products by the lithium acetate method (Schiestl and Gietz, 1989). Low-fluorescence medium (Taxis et al., 2006) was used to grow yeast cells in liquid cultures. Blue light irradiation of yeast cells was performed using CLF floraLED modules (470 nm; CLF Plant Climatics, Wertingen, Germany) and high-power LED stripes (465 nm; revoART, Borsdorf, Germany). Very high doses of blue light have been reported to induce slow growth in yeast (Ninnemann et al., 1970). However, growth was not influenced at fluence rates (465 nm or 470 nm, 5–30 μmol m^{-2} s^{-1}) used for our experiments (data not shown).

Plasmids were constructed by standard procedures (Ausubel et al., 1995), and details and sequences of the used vectors are available on request; yeast plasmids are listed in Table S2. Yeast cells for light-based patterning and serial dilution experiments were grown on yeast extract peptone dextrose (YPD) or synthetic complete medium (Sherman, 2002) in the presence or absence of blue light (465 nm or 470 nm, 20 μmol m^{-2} s^{-1}) at 25°C. The neutral density gradient (8.8 cm; optical density 0.04–2.0), which was used to generate graded blue light intensities, was purchased from Thorlabs (Dachau, Germany). Yeast

cells expressing P$_{TDH3}$-*RFP-psd* (plasmid based) were spread on solid medium and incubated at 30°C for 3 days to obtain the light response. Yeast cells without plasmid (ESM356-1) grown under the same conditions were used to obtain background fluorescence. A common inkjet printer was used to transfer the inverted image of the "Alte Universität" on a transparency foil, which then was used for illumination. Images were taken with a Canon Powershot A620 digital camera.

TinkerCell Simulations

The model was generated using the computer-aided design tool TinkerCell (Chandran et al., 2009). It contains a preset module for protein production (pp1), which describes gene expression, mRNA stability, and translational efficiency, as well as endogenous degradation of PSD$_{dark}$ (degENDO). We added conversion of PSD$_{dark}$ to PSD$_{lit}$ by light (hν) or dark conversion (leak). Decrease of PSD$_{lit}$ is described by dark state recovery (dark), endogenous degradation (degENDO), and light-induced degradation (degLOV). The total amount of PSD (PSD$_{total}$ = PSD$_{dark}$ + PSD$_{lit}$) was used to generate the graphs. The reactions are all first order or pseudo-first-order reactions; therefore, all conversion rates could be calculated using values from literature or our experiments (Table S3). For first-order reactions, the conversion constants can be calculated with the formula $k = \ln(2)/t_{(1/2)}$. The values for the simulations were either obtained from literature [k$_{(dark)}$ = 0.59 min^{-1}, assuming a dark state recovery half-time of 70 s; Terazima, 2011; or k$_{(leak)}$ = 0.0118 min^{-1}, assuming that 2% of the LOV2 molecules exhibit an unfolded Jα in darkness; Yao et al., 2008] or measured [k$_{(degENDO)}$ = 0.0025 min^{-1}, corresponding to a half-life of 273 min of the protein RFP-LOV2; data not shown; or k$_{(degLOV)}$ = 0.033 min^{-1}, corresponding to a half-life of 21 min for RFP-LOV2-cODC]. The light conversion rate k$_{(h\nu)}$ = 0.0404 min^{-1} (at 1 μmol m^{-2} s^{-1}) was calculated from the quantum yield of FMN (0.26 [Drepper et al., 2007] multiplied by the FMN cross-section of 4.3 × 10^{-17} cm^2 at its λ_{max} = 450 nm; Islam et al., 2003) and the number of photons (for a light flux of 1 μmol m^{-2} s^{-1}, this is 6.023 × 10^{13} cm^{-2} s^{-1}). We used the *TDH3* promoter for expression of *RFP-psd* in the light response experiment on plate; therefore, the values for expression, mRNA characteristics, and protein numbers of *TDH3* (mRNA synthesis rate, 188.1 mRNA hr^{-1}; mRNA half-life, 18 min; 89 mRNA molecules per cell, and 169,000 protein molecules per cell) were used for the initial simulations. As we found that psd module behavior is, in most aspects, independent from protein synthesis rates (Figure 6B), we kept these values for the other simulations as well.

Descriptions of microscopy, quantitative measurements, and immunoblotting are available in the Supplemental Information.

SUPPLEMENTAL INFORMATION

Supplemental Information includes six figures, three tables, and Supplemental Experimental Procedures and can be found with this article online at http://dx.doi.org/10.1016/j.chembiol.2013.03.005.

REFERENCES

Ausubel, F.M., Kingston, R.E., Seidman, F.G., Struhl, K., Moore, D.D., Brent, R., and Smith, F.A., eds. (1995). Current Protocols in Molecular Biology (New York, NY: John Wiley and Sons).

Berset, C., Griac, P., Tempel, R., La Rue, J., Wittenberg, C., and Lanker, S. (2002). Transferable domain in the G(1) cyclin Cln2 sufficient to switch degradation of Sic1 from the E3 ubiquitin ligase SCF(Cdc4) to SCF(Grr1). Mol. Cell. Biol. *22*, 4463–4476.

Bulina, M.E., Chudakov, D.M., Britanova, O.V., Yanushevich, Y.G., Staroverov, D.B., Chepurnykh, T.V., Merzlyak, E.M., Shkrob, M.A., Lukyanov, S., and Lukyanov, K.A. (2006). A genetically encoded photosensitizer. Nat. Biotechnol. *24*, 95–99.

Chandran, D., Bergmann, F.T., and Sauro, H.M. (2009). TinkerCell: modular CAD tool for synthetic biology. J. Biol. Eng. *3*, 19.

Christie, J.M., Salomon, M., Nozue, K., Wada, M., and Briggs, W.R. (1999). LOV (light, oxygen, or voltage) domains of the blue-light photoreceptor phototropin (nph1): binding sites for the chromophore flavin mononucleotide. Proc. Natl. Acad. Sci. USA *96*, 8779–8783.

Christie, J.M., Gawthorne, J., Young, G., Fraser, N.J., and Roe, A.J. (2012). LOV to BLUF: flavoprotein contributions to the optogenetic toolkit. Mol. Plant *5*, 533–544.

DeScenzo, R.A., and Minocha, S.C. (1993). Modulation of cellular polyamines in tobacco by transfer and expression of mouse ornithine decarboxylase cDNA. Plant Mol. Biol. *22*, 113–127.

Dirick, L., Böhm, T., and Nasmyth, K. (1995). Roles and regulation of Cln-Cdc28 kinases at the start of the cell cycle of Saccharomyces cerevisiae. EMBO J. *14*, 4803–4813.

Drepper, T., Eggert, T., Circolone, F., Heck, A., Krauss, U., Guterl, J.K., Wendorff, M., Losi, A., Gärtner, W., and Jaeger, K.E. (2007). Reporter proteins for in vivo fluorescence without oxygen. Nat. Biotechnol. *25*, 443–445.

Ghiara, J.B., Richardson, H.E., Sugimoto, K., Henze, M., Lew, D.J., Wittenberg, C., and Reed, S.I. (1991). A cyclin B homolog in S. cerevisiae: chronic activation of the Cdc28 protein kinase by cyclin prevents exit from mitosis. Cell *65*, 163–174.

Giaever, G., Chu, A.M., Ni, L., Connelly, C., Riles, L., Véronneau, S., Dow, S., Lucau-Danila, A., Anderson, K., André, B., et al. (2002). Functional profiling of the Saccharomyces cerevisiae genome. Nature *418*, 387–391.

Harper, S.M., Neil, L.C., and Gardner, K.H. (2003). Structural basis of a phototropin light switch. Science *301*, 1541–1544.

Herrou, J., and Crosson, S. (2011). Function, structure and mechanism of bacterial photosensory LOV proteins. Nat. Rev. Microbiol. *9*, 713–723.

Hodge, A., and Mendenhall, M. (1999). The cyclin-dependent kinase inhibitory domain of the yeast Sic1 protein is contained within the C-terminal 70 amino acids. Mol. Gen. Genet. *262*, 55–64.

Hoyt, M.A., Zhang, M., and Coffino, P. (2003). Ubiquitin-independent mechanisms of mouse ornithine decarboxylase degradation are conserved between mammalian and fungal cells. J. Biol. Chem. *278*, 12135–12143.

Huh, W.K., Falvo, J.V., Gerke, L.C., Carroll, A.S., Howson, R.W., Weissman, J.S., and O'Shea, E.K. (2003). Global analysis of protein localization in budding yeast. Nature *425*, 686–691.

Islam, S.D.M., Penzkofer, A., and Hegemann, P. (2003). Quantum yield of triplet formation of riboflavin in aqueous solution and of flavin mononucleotide bound to the LOV1 domain of Phot1 from Chlamydomonas reinhardtii. Chem. Phys. *291*, 97–114.

Ito, S., Song, Y.H., and Imaizumi, T. (2012). LOV domain-containing F-box proteins: light-dependent protein degradation modules in Arabidopsis. Mol. Plant *5*, 573–582.

Janke, C., Magiera, M.M., Rathfelder, N., Taxis, C., Reber, S., Maekawa, H., Moreno-Borchart, A., Doenges, G., Schwob, E., Schiebel, E., and Knop, M. (2004). A versatile toolbox for PCR-based tagging of yeast genes: new fluorescent proteins, more markers and promoter substitution cassettes. Yeast *21*, 947–962.

Jariel-Encontre, I., Bossis, G., and Piechaczyk, M. (2008). Ubiquitin-independent degradation of proteins by the proteasome. Biochim. Biophys. Acta *1786*, 153–177.

Jungbluth, M., Renicke, C., and Taxis, C. (2010). Targeted protein depletion in Saccharomyces cerevisiae by activation of a bidirectional degron. BMC Syst. Biol. *4*, 176.

Kaji, H., Camci-Unal, G., Langer, R., and Khademhosseini, A. (2011). Engineering systems for the generation of patterned co-cultures for controlling cell-cell interactions. Biochim. Biophys. Acta *1810*, 239–250.

Kennedy, M.J., Hughes, R.M., Peteya, L.A., Schwartz, J.W., Ehlers, M.D., and Tucker, C.L. (2010). Rapid blue-light-mediated induction of protein interactions in living cells. Nat. Methods *7*, 973–975.

Lau, O.S., and Deng, X.W. (2012). The photomorphogenic repressors COP1 and DET1: 20 years later. Trends Plant Sci. *17*, 584–593.

Levskaya, A., Chevalier, A.A., Tabor, J.J., Simpson, Z.B., Lavery, L.A., Levy, M., Davidson, E.A., Scouras, A., Ellington, A.D., Marcotte, E.M., and Voigt, C.A. (2005). Synthetic biology: engineering Escherichia coli to see light. Nature *438*, 441–442.

Lungu, O.I., Hallett, R.A., Choi, E.J., Aiken, M.J., Hahn, K.M., and Kuhlman, B. (2012). Designing photoswitchable peptides using the AsLOV2 domain. Chem. Biol. *19*, 507–517.

Nasmyth, K. (1996). At the heart of the budding yeast cell cycle. Trends Genet. *12*, 405–412.

Ninnemann, H., Butler, W.L., and Epel, B.L. (1970). Inhibition of respiration in yeast by light. Biochim. Biophys. Acta *205*, 499–506.

Nishimura, K., Fukagawa, T., Takisawa, H., Kakimoto, T., and Kanemaki, M. (2009). An auxin-based degron system for the rapid depletion of proteins in nonplant cells. Nat. Methods *6*, 917–922.

Pereira, G., Tanaka, T.U., Nasmyth, K., and Schiebel, E. (2001). Modes of spindle pole body inheritance and segregation of the Bfa1p-Bub2p checkpoint protein complex. EMBO J. *20*, 6359–6370.

Pham, E., Mills, E., and Truong, K. (2011). A synthetic photoactivated protein to generate local or global Ca(2+) signals. Chem. Biol. *18*, 880–890.

Schiestl, R.H., and Gietz, R.D. (1989). High efficiency transformation of intact yeast cells using single stranded nucleic acids as a carrier. Curr. Genet. *16*, 339–346.

Sharma, K.G., Kaur, R., and Bachhawat, A.K. (2003). The glutathione-mediated detoxification pathway in yeast: an analysis using the red pigment that accumulates in certain adenine biosynthetic mutants of yeasts reveals the involvement of novel genes. Arch. Microbiol. *180*, 108–117.

Sherman, F. (2002). Getting started with yeast. Methods Enzymol. *350*, 3–41.

Shimizu-Sato, S., Huq, E., Tepperman, J.M., and Quail, P.H. (2002). A light-switchable gene promoter system. Nat. Biotechnol. *20*, 1041–1044.

Sorokina, O., Kapus, A., Terecskei, K., Dixon, L.E., Kozma-Bognar, L., Nagy, F., and Millar, A.J. (2009). A switchable light-input, light-output system modelled and constructed in yeast. J. Biol. Eng. *3*, 15.

Strickland, D., Moffat, K., and Sosnick, T.R. (2008). Light-activated DNA binding in a designed allosteric protein. Proc. Natl. Acad. Sci. USA *105*, 10709–10714.

Strickland, D., Lin, Y., Wagner, E., Hope, C.M., Zayner, J., Antoniou, C., Sosnick, T.R., Weiss, E.L., and Glotzer, M. (2012). TULIPs: tunable, light-controlled interacting protein tags for cell biology. Nat. Methods *9*, 379–384.

Surana, U., Amon, A., Dowzer, C., McGrew, J., Byers, B., and Nasmyth, K. (1993). Destruction of the CDC28/CLB mitotic kinase is not required for the metaphase to anaphase transition in budding yeast. EMBO J. *12*, 1969–1978.

Taxis, C., Maeder, C., Reber, S., Rathfelder, N., Miura, K., Greger, K., Stelzer, E.H., and Knop, M. (2006). Dynamic organization of the actin cytoskeleton during meiosis and spore formation in budding yeast. Traffic *7*, 1628–1642.

Terazima, M. (2011). Studies of photo-induced protein reactions by spectrally silent reaction dynamics detection methods: applications to the photoreaction of the LOV2 domain of phototropin from Arabidopsis thaliana. Biochim. Biophys. Acta *1814*, 1093–1105.

Wang, X., Chen, X., and Yang, Y. (2012). Spatiotemporal control of gene expression by a light-switchable transgene system. Nat. Methods *9*, 266–269.

Wäsch, R., and Cross, F.R. (2002). APC-dependent proteolysis of the mitotic cyclin Clb2 is essential for mitotic exit. Nature *418*, 556–562.

Wu, Y.I., Frey, D., Lungu, O.I., Jaehrig, A., Schlichting, I., Kuhlman, B., and Hahn, K.M. (2009). A genetically encoded photoactivatable Rac controls the motility of living cells. Nature *461*, 104–108.

Yao, X., Rosen, M.K., and Gardner, K.H. (2008). Estimation of the available free energy in a LOV2-J alpha photoswitch. Nat. Chem. Biol. *4*, 491–497.

Supplemental Information

A LOV2 Domain-Based Optogenetic Tool

to Control Protein Degradation

and Cellular Function

Christian Renicke, Daniel Schuster, Svetlana Usherenko, Lars-Oliver Essen, and Christof Taxis

1

LQMRKGIDLATTLERIEKNFVITDPRLPDNPIIFASDSFLELTEYSREEILGRNCRFLQGPETDLTTVKKIR
NAIDNQTEVTVQLINYTKSGKKFWNIFHLQPMRDQKGEVQYFIGVQLDGSKHVEPVRNVIEETAVKEGEDLV
KKTAVNIDEAVRELPMSCAQESITSLYKKAGSENLYFQ

Figure S1, Related to Figure 1

Amino acid sequence of the psd-module (*At*LOV2-cODC1; size 20 kDa). The sequence of the Jα helix is highlighted in blue, that of the cODC1 degron in orange. The cysteine-alanine motif is shown in bold letters. The cysteine residue, which was mutated to alanine to verify proteasomal degradation of the psd-module, is underlined.
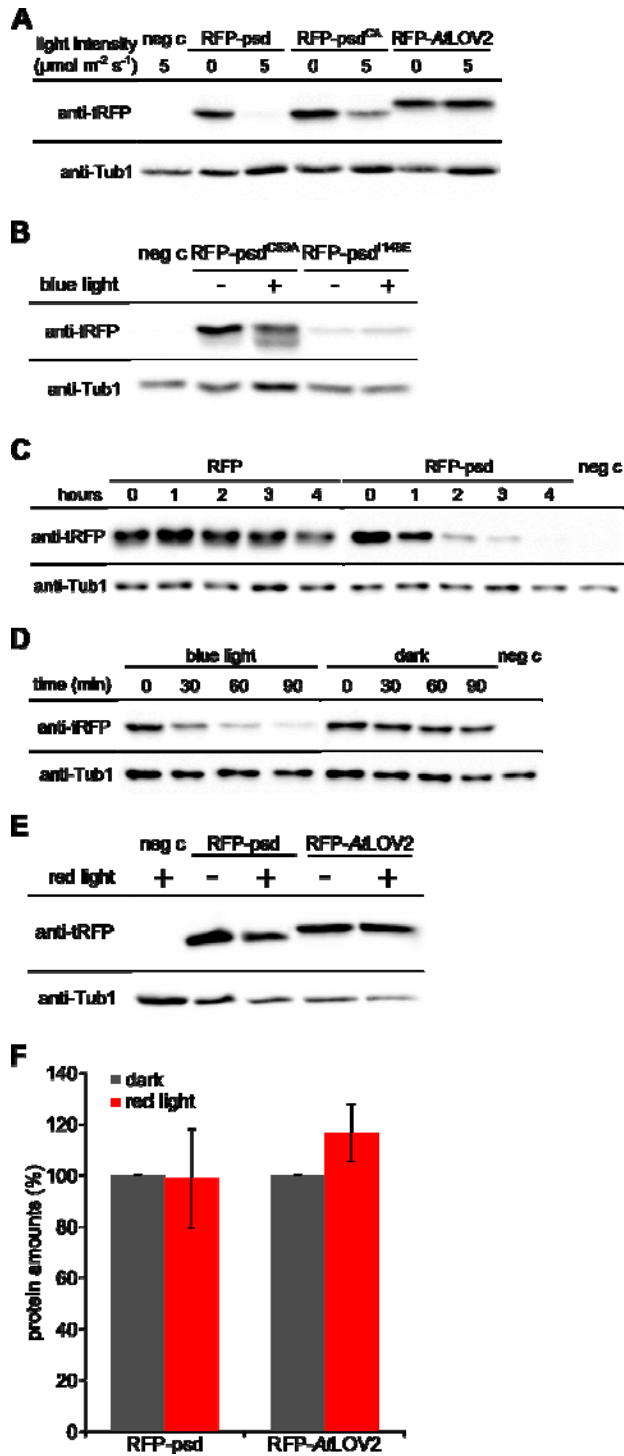
Figure S2, Related to Figure 2

(**A**) Abundance of RFP-psd after exposure of the cells with distinct amounts of blue light. Yeast cells expressing P_{ADH1}-*RFP-psd,* P_{ADH1}-*RFP-psd*^{CA}*, and* P_{ADH1}-*RFP-AtLOV2*

(plasmid based) were grown overnight on solid media in the absence or presence of blue light (LED lamp, 470 nm, intensity as indicated in the figure). Equal amounts of cells were taken from the plate and lysed by alkaline lysis. Conditions for immunoblotting as described for **Figure 2B**. Please note that RFP-*At*LOV2 is seven amino acids shorter than RFP-psd, but due to the different amino acid composition of the very C-terminus it runs slightly slower in SDS-PAGE.

(**B**) Dark and lit state mutants of the LOV2 domain render the psd-module insensitive to light exposure. Yeast cells in logarithmic growth phase expressing the dark state mutant P_{ADH1}-RFP-AtLOV2^{C53A}-cODC1 and the lit state mutant P_{ADH1}-RFP-AtLOV2^{I149E}-cODC1 (plasmid based) were exposed for four hours to blue light (LED lamp, 465 nm, 30 µmol m^{-2} s^{-1}) or kept in the dark. Numbering of the mutated residues started at the beginning of *At*LOV2 domain. Equal amounts of cells were lysed by alkaline lysis and total protein extracts used for immunoblotting (as in **Figure 2B)**.

(**C**) Kinetics of psd-module induced target protein depletion after exposure to blue light. Yeast cells expressing P_{ADH1}-*RFP* or P_{ADH1}-*RFP-psd* (plasmid based) were grown in liquid medium in the dark. After removal of the first sample (t=0 hours), cells were exposed to blue light (LED lamp, 465 nm, 30 µmol m^{-2} s^{-1}). Samples were taken at the indicated time points, subjected to alkaline lysis and immunoblotting. Antibodies against tRFP and Tub1 (loading control) were used for detection (negative control; neg c). Please note that RFP (26 kDa) and RFP-psd (47 kDa) do not have the same molecular weight, but are shown next to each other to facilitate comparison.

(**D**) Measurement of psd-module induced target protein destabilization. Yeast cells expressing P_{ADH1}-*RFP-psd* (plasmid based) were grown in liquid medium in the dark. After removal of the first sample (t=0 hours), cycloheximide was added to stop protein synthesis; cells were kept in the dark or exposed to blue light (LED lamp, 465 nm, 30 µmol m^{-2} s^{-1}) for the rest of the experiment. Other experimental conditions as in **Figure 2B**.

(**E**) Stability of RFP-psd is not influenced by red light. Yeast cells expressing P_{ADH1}-*RFP-AtLOV2* and P_{ADH1}-*RFP-psd* (plasmid based) were grown in the presence or absence of red light (675 nm, 7 µmol m^{-2} s^{-1}). Other experimental conditions as in **Figure 2B**.

(**F**) Quantification of the results shown in (**E**). The graph shows the mean protein amount obtained from four biological replicates; error bars, standard error of the mean.

4
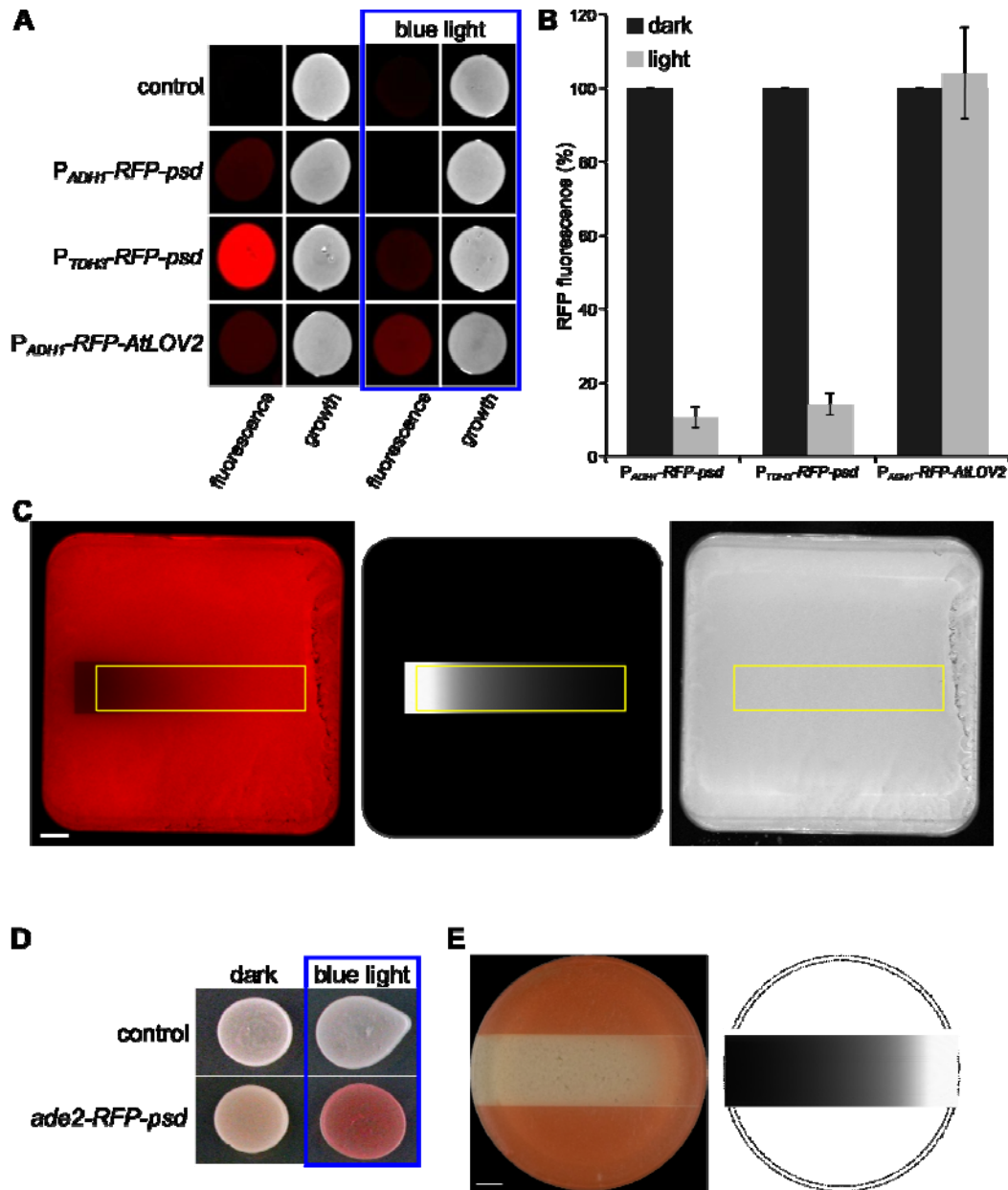
Figure S3, Related to Figure 3

(**A**) Observation of RFP-psd abundance on macroscopic level. Yeast cells grown in a patch expressing P$_{ADH1}$-*RFP-psd,* P$_{TDH3}$-*RFP-psd,* and P$_{ADH1}$-*RFP-AtLOV2* (plasmid based) were kept in the absence or presence of blue light (470 nm, 20 µmol m^{-2} s^{-1}) for 8 hours. Digital images of the yeast patches and the fluorescence were taken using a fluorescence image analyzer.

(**B**) Quantification of the results shown in (**A**). The mean RFP fluorescence of eight

biological replicates is shown; error bars, standard error of the mean.

(**C**) RFP fluorescence image (left side) of the experiment used for light-dose response shown in **Figure 3A**. The area for quantification is indicated by the yellow box. The neutral density gradient used during illumination is shown in the middle, yeast growth on the plate is shown on the right. Bar size 1 cm.

(**D**) Yeast cells missing the enzyme phosphoribosylaminoimidazole carboxylase (Ade2) are defective in adenine biosynthesis and accumulate the intermediate 5'-phosphoribosyl-5-aminoimidazole (AIR) in the cells, which is toxic for yeast. Detoxification requires oxidation of AIR by P450 monooxygenases as well as transport into the vacuole and results in pigment accumulation as indicated by red colony morphology. The *RFP-psd* module was inserted chromosomally at the 3' end of *ADE2*. Growth of the cells for three days at 25 °C in patches with blue light (465 nm, 20 µmol m^{-2} s^{-1}) illumination resulted in formation of the red pigment, whereas control cells stayed pale. Images of the patches were taken with a digital camera.

(**E**) Experimental conditions as in **Figure 3B**. A neutral density gradient (right image) was used to generate graded blue light intensities for illumination of Ade2-RFP-psd cells growing in a lawn. Bar size 1 cm.

6
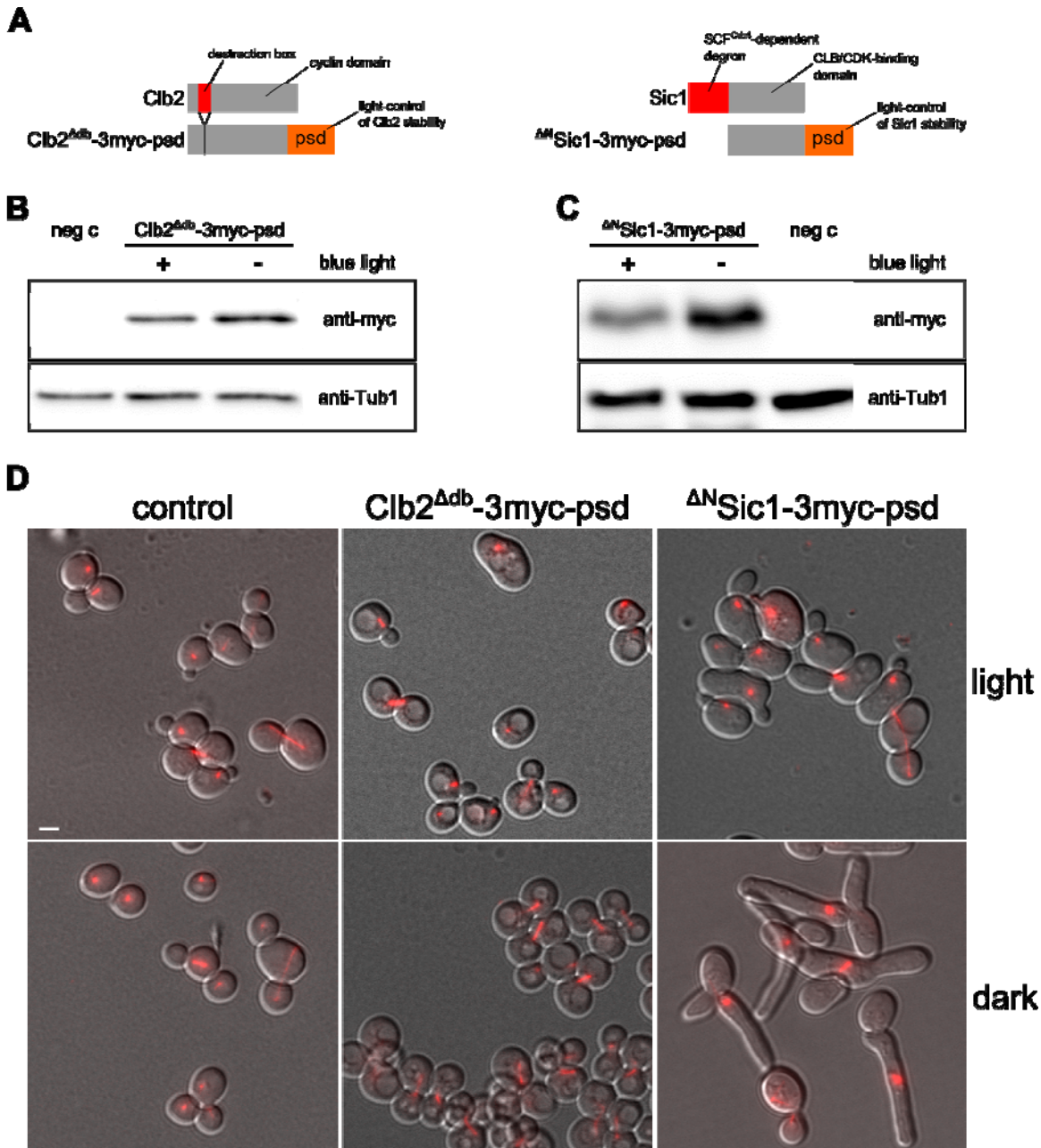
Figure S4, Related to Figure 4

Control of cell cycle events by light.

(**A**) The scheme illustrates the modifications within *CLB2* and *SIC1* to obtain optogenetic variants of these cell cycle regulators.

(**B**) Clb2$^{\Delta db}$ -3myc-psd accumulates in cells kept in the dark. Cells expressing *clb2$^{\Delta db}$-3myc-psd* (plasmid based) were pre-grown in liquid medium exposed to blue light (465 nm, 30 µmol m^{-2} s^{-1}), followed by an incubation period of 4 hours under blue light or in

7

darkness, before samples were taken and subjected to immunoblotting using anti-myc and anti-tubulin antibody.

(**C**) $^{\Delta N}$Sic1-3myc-psd accumulates in cells kept in the dark. Cells expressing $^{\Delta N}sic1$-$3myc$-psd were treated as described in (**B**)**.**

(**D**) Microscopy images used to obtain data shown in **Figure 4B.** Examples of control cells, Clb2$^{\Delta db}$-3myc-psd, and $^{\Delta N}$Sic1-3myc-psd cells kept under blue light or in the dark for five hours. Overlays are DIC images and maximum projections of RFP-Tub1 images (shown in red), scale bar, 3 µm.

8

A

RFP | DIC

Cdc14-RFP-psd

Pma1-RFP-psd

B

neg c | Cdc5-3myc-psd | Cdc14-3myc-psd | Cdc48-3myc-psd | Mcm1-3myc-psd | Pma1-3myc-psd | Sec62-3myc-psd

0 4 | 0 4 | 0 4 | 0 4 | 0 4 | 0 4 | hours

anti-tRFP

anti-Tub1

neg c | Ufd1-3myc-psd | Npl4-3myc-psd | Sec63-3myc-psd

0 4 | 0 4 | 0 4 | hours

anti-tRFP

anti-Tub1

C

cell cycle species (%)

100
80
60
40
20
0

- + | - + | - + | - + | blue light
control | Cdc48-3myc-psd | Cdc14-3myc-psd | Cdc5-3myc-psd

anaphase/telophase
RFP-Tub1
metaphase
small bud
no bud

D

Cdc5-3myc-psd Spc72-6HA | Cdc5-3myc-psd Kin4-6HA | Sec62-3myc-psd Sec63-6HA | Sec62-3myc-psd Sec66-6HA | Mcm1-3myc-psd Snf5-6HA | Mcm1-3myc-psd Snf6-6HA | Cdc48-3myc-psd Ufd1-6HA | Cdc48-3myc-psd Npl4-6HA | neg c

0 4 | 0 4 | 0 4 | 0 4 | 0 4 | 0 4 | 0 4 | 0 4 | hours
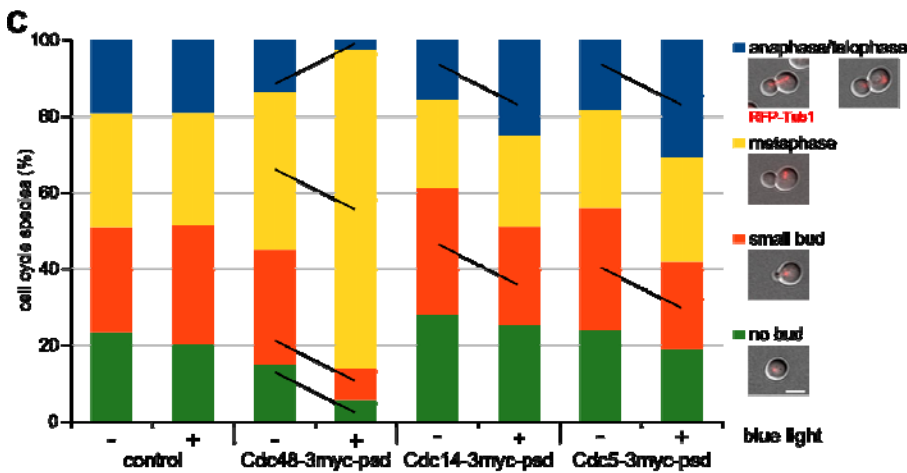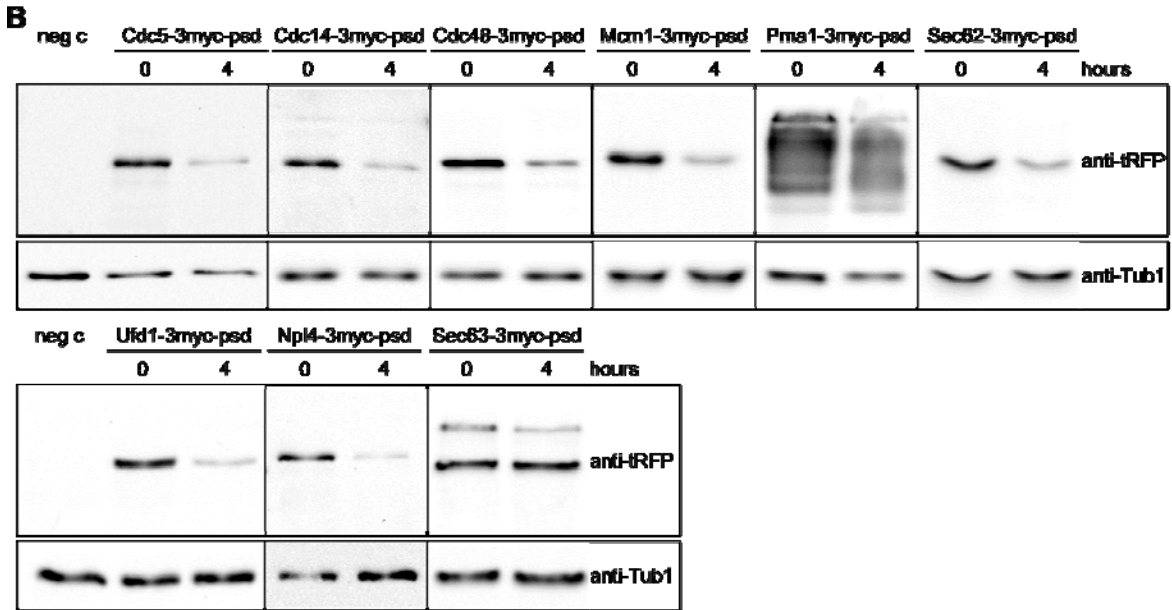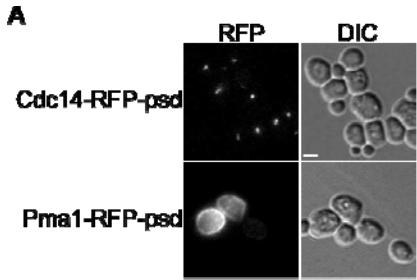
anti-myc

anti-HA

anti-Tub1

9

29

Figure S5, Related to Figure 5

Creation of conditional mutants using the psd-module. The kinase Cdc5 and the phosphatase Cdc14 are essential for the exit of mitosis. The AAA-ATPase Cdc48 and its complex partners Npl4 and Ufd1 are involved in ubiquitin-mediated protein degradation, the transcription factor Mcm1 in expression of genes during transition from G1 to G2, the plasma membrane H^+-ATPase Pma1 in pH homeostasis, and the membrane proteins Sec62 and Sec63 in protein translocation into the endoplasmic reticulum.

(**A**) Localization of essential proteins tagged with RFP-psd. Fluorescence microscopy images of the tagged proteins. RFP (left) and differential interference contrast (DIC; right) images are shown. Cdc14 and Pma1 show a clear localization in the nucleolus and at the plasma membrane, respectively. Scale bar: 3 μm.

(**B**) Immunodetection analysis of 3myc-psd tagged proteins. Samples were taken at 0 hours of cells grown in the dark and after 4 hours of blue-light exposure. The yeast strains YDS28 (control), YCR134 (Cdc5-3myc-psd), YDS177 (Cdc14-3myc-psd), YDS175 (Cdc48-3myc-psd), YDS171 (Mcm1-3myc-psd), YDS170 (Pma1-3myc-psd), YDS174 (Sec62-3myc-psd), YDS187 (Ufd1-3myc-psd), YDS191 (Npl4-3myc-psd), and YDS188 (Sec63-3myc-psd) were used to obtain the immunoblots. Conditions as in **Figure 2B**. Please note that we show all the proteins at the same level to facilitate comparison between them, although they have different molecular weights.

(**C**) Cdc48-3myc-psd, Cdc14-3myc-psd, and Cdc5-3myc-psd cells show an increase of distinct cell cycle stages if exposed to blue light. The yeast strains YDS28 (control), YDS175 (Cdc48-3myc-psd), YDS177 (Cdc14-3myc-psd), and YDS176 (Cdc5-3myc-psd) were pre-grown in the dark, exposed to blue light (465 nm, 30 μmol m^{-2} s^{-1}) for four hours or kept in dark for the same time period. DIC and fluorescence images (RFP-Tub1) were used to categorize cell cycle stages according to the examples shown on the right side of the figure. The graph shows the mean distribution of cell cycle stages obtained from four biological replicates counting at least 100 cells for each replicate. Statistically significant changes (pairwise t-tests) between dark and lit conditions are indicated by a line. Scale bar: 3 μm.

(**D**) Generally, the psd-module does not induce depletion of interaction partners. Immunodetection analysis of 3myc-psd tagged proteins and 6HA tagged proteins that are subunits of a complex. Samples were taken at 0 hours of cells grown in the dark and after

10

4 hours of blue-light exposure (465 nm, 30 µmol m^{-2} s^{-1}). The yeast strains YCR134 (Cdc5-3myc-psd/Spc72-6HA), YCR135 (Cdc5-3myc-psd/Kin4-6HA), YCR137 (Sec62-3myc-psd/Sec63-6HA), YCR136 (Sec62-3myc-psd/Sec63-6HA), YCR144 (Mcm1-3myc-psd/Snf5-6HA), YCR143 (Mcm1-3myc-psd/Snf6-6HA), YCR155 (Cdc48-3myc-psd/Ufd1-6HA), YCR149 (Cdc48-3myc-psd/Npl4-6HA), and YDS28 (control, neg c) were used to obtain the immunoblots. Conditions as in **Figure 2B**. Please note that we show all the proteins at the same level to facilitate comparison between them, although they have different molecular weights.
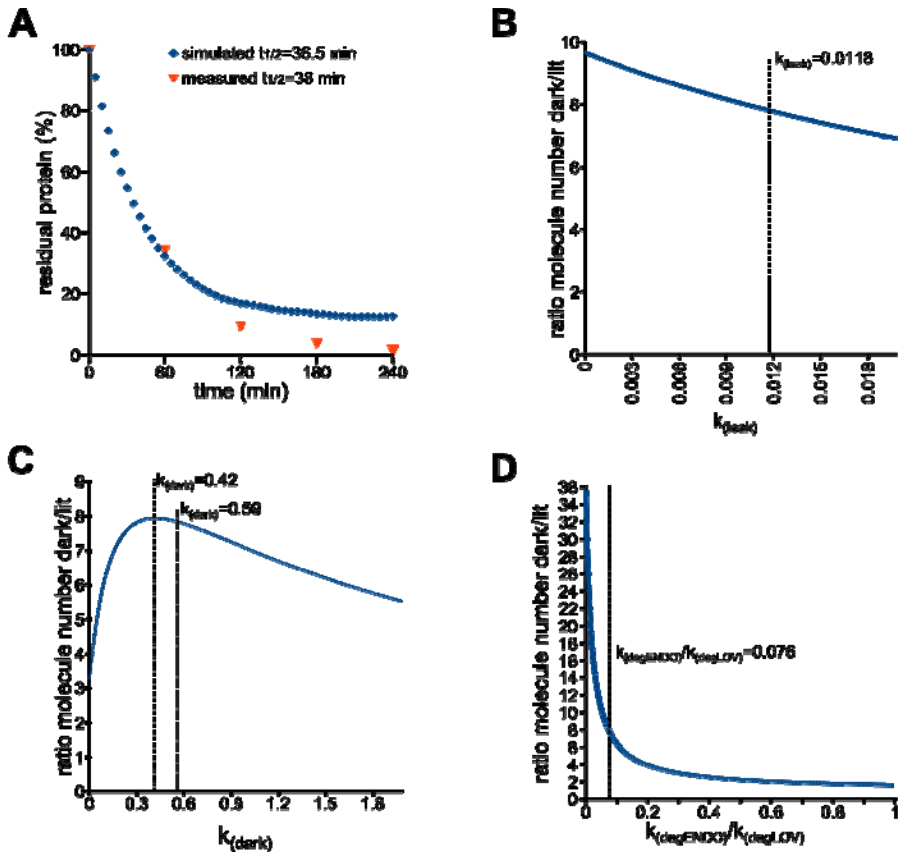
11

Figure S6, Related to Figure 6

(**A**) Predicted kinetics of protein depletion using the PSD module (blue diamonds) match experimentally obtained values (red triangles). Experimental data were taken from **Figure 2C**. Simulation of PSD amounts was performed at saturating light levels ($k_{(hv)}$ = 1.2 min^{-1} corresponding to a light flux of 30 µmol m^{-2} s^{-1}) over time.

(**B**) The lit state conversion rate in darkness $k_{(leak)}$ influences the molecule number in darkness. The graph shows the PSD$_{total}$ dark/lit ratio at $k_{(leak)}$ values varied from 0 to 0.0198 min^{-1}; the $k_{(leak)}$=0.0118 of AtLOV2 is indicated by a dashed line.

(**C**) The dark state recovery rate $k_{(dark)}$ influences the dark/lit ratio of molecule numbers. The curve was obtained from a simulation varying $k_{(dark)}$ from 0 to 2 min^{-1}. The maximum ratio (7.95) at $k_{(dark)}$=0.42 min^{-1} is indicated by a pointed line, the dark recovery rate of AtLOV2 ($k_{(dark)}$=0.59 min^{-1}) results in a ratio of 7.8 (indicated by a dashed line).

(**D**) Decreasing the $k_{(degENDO)}/k_{(degLOV)}$ ratio makes the psd-module more efficient. PSD$_{total}$ dark/lit ratio plotted against $k_{(degENDO)}/k_{(degLOV)}$. The graph was obtained from a simulation of changes in $k_{(degENDO)}$ from 0 to 0.033 min^{-1}. The $k_{(degENDO)}/k_{(degLOV)}$ ratio of 0.076 of the psd-

12

module is indicated by a dashed line.

Tables

Table S1. Yeast Strains, Related to Experimental Procedures

Name	Genotype	Source
ESM356-1	*MATa ura3-53 leu2Δ1 his3Δ200 trp1Δ63*	Pereira et al., 2001
YDS28	ESM356-1 P*HIS3*-mCherry-TUB1::TRP1	Jungbluth et al., 2010
YCT1315	ESM365-1 *cdc14-RFP-AtLOV2-cODC1::kanMX*	this study
YDS177	YDS28 *cdc14-3myc-AtLOV2-cODC1::kanMX*	this study
YCT1316	ESM365-1 *cdc5-RFP-AtLOV2-cODC1::kanMX*	this study
YDS176	YDS28 *cdc5-3myc-AtLOV2-cODC1::kanMX*	this study
YDS175	YDS28 *cdc48-3myc-AtLOV2-cODC1::kanMX*	this study
YCT1338	ESM365-1 *pma1-RFP-AtLOV2-cODC1::kanMX*	this study
YDS170	YDS28 *pma1-3myc-AtLOV2-cODC1::kanMX*	this study
YDS174	YDS28 *sec62-3myc-AtLOV2-cODC1::kanMX*	this study
YDS171	YDS28 *mcm1-3myc-AtLOV2-cODC1::kanMX*	this study
YDS187	YDS28 *ufd1-3myc-AtLOV2-cODC1::kanMX*	this study
YDS188	YDS28 *sec63-3myc-AtLOV2-cODC1::kanMX*	this study
YDS191	YDS28 *npl4-3myc-AtLOV2-cODC1::kanMX*	this study
YDS91	ESM365-1 *ade2-RFP-AtLOV2-cODC1::kanMX*	this study
YCR134	YDS28 *cdc5-3myc-AtLOV2-cODC1::kanMX SPC72-6HA::HIS3MX6*	this study
YCR135	YDS28 *cdc5-3myc-AtLOV2-cODC1::kanMX KIN4-6HA::HIS3MX6*	this study
YCR136	YDS28 *sec62-3myc-AtLOV2-cODC1::kanMX SEC66-6HA::HIS3MX6*	this study
YCR137	YDS28 *sec62-3myc-AtLOV2-cODC1::kanMX SEC63-6HA::HIS3MX6*	this study
YCR143	YDS28 *mcm1-3myc-AtLOV2-cODC1::kanMX SNF6-6HA::HIS3MX6*	this study
YCR144	YDS28 *mcm1-3myc-AtLOV2-cODC1::kanMX SNF5-6HA::HIS3MX6*	this study
YCR149	YDS28 *cdc48-3myc-AtLOV2-cODC1::kanMX NPL4-6HA::HIS3MX6*	this study
YCR155	YDS28 *cdc48-3myc-AtLOV2-cODC1::kanMX UFD1-6HA::HIS3MX6*	this study

13

Table S2. Plasmids, Related to Experimental Procedures

Name	Genotype	Source
pRS315	*LEU2 ARS209/CEN2 ori bla*	Sikorski and Hieter, 1989
pCT320	pRS315 P$_{ADH1}$-*tagRFP*	this work
pCT322	pRS315 P$_{ADH1}$-*tagRFP-AtLOV2*	this work
pCT334	pRS315 P$_{ADH1}$-*tagRFP-AtLOV2-cODC1*	this work
pDS87	pRS315 P$_{ADH1}$-*tagRFP-AtLOV2-cODC1*^{CA}	this work
pDS90	pRS315 P$_{TDH3}$-*tagRFP-AtLOV2-cODC1*	this work
pCT337	*tagRFP-AtLOV2-cODC1::kanMX ori bla*	this work
pDS96	*3myc-AtLOV2-cODC1::kanMX ori bla*	this work
pDS97	pRS315 P$_{ADH1}$-^{ΔN}*sic1-3myc-AtLOV2-cODC1*	this work
pDS101	pRS315 P$_{CLB2}$-*clb2*^{Δdb}-*3myc-AtLOV2-cODC1*	this work
pDS118	pRS315 P$_{ADH1}$-*tagRFP-AtLOV2*^{C53A}-*cODC1*	this work
pDS119	pRS315 P$_{ADH1}$-*tagRFP-AtLOV2*^{I149E}-*cODC1*	this work

Table S3. Values Used for In Silico Simulations, Related to Figure 6 and Figure S6

Name	Value	Source
dark state recovery $k_{(dark)}$	0.59 min^{-1}	Terazima, 2011
conversion of PSD_{dark} to PSD_{lit} in darkness $k_{(leak)}$	0.0118 min^{-1}	Yao et al., 2008
endogenous degradation rate $k_{(degENDO)}$	0.0025 min^{-1}	This study
light-induced degradation $k_{(degLOV)}$	0.033 min^{-1}	This study
light conversion rate $k_{(hv)}$ at 1 µmol m^{-2} s^{-1}	0.0404 min^{-1}	This study
quantum yield FMN	0.26	Drepper et al., 2007
FMN cross section at λ_{max} (450 nm)	4.3*10^{-17} cm^2	Islam et al., 2003
TDH3 mRNA synthesis rate	188.1 hr^{-1}	Holstege et al., 1998
TDH3 mRNA half-life	18 min	Holstege et al., 1998
TDH3 mRNA molecules/cell	89	Holstege et al., 1998
Tdh3 protein molecules/cell	169 000	Ghaemmaghami et al., 2003

Experimental Procedures

Microscopy and Image Processing

Live-cell imaging of yeast cells was performed as described (Jungbluth et al., 2010) using a Zeiss Axiovert 200 equipped with a Hamamatsu camera, DAPI, EGFP and rhodamine filter sets and a 63x Plan Apochromat oil lens (NA 1.4). DIC images were collected in a single plane, fluorescence images in a single plane or as z-stack with 0.5 µm intervals using the image acquisition software Volocity 5.03 (Perkin Elmer). The software ImageJ was used for image processing and fluorescence quantification (Collins, 2007).

Immunoblotting, Quantitative Measurements, and Statistics

Immunoblotting experiments with samples obtained from yeast were performed as described (Jungbluth et al., 2010).

Measurements to characterize the psd-module in yeast cells were performed with at least four biological replicates measured on two different days. The figures show representative results (immunoblotting, growth test, fluorescence measurements of cells grown on solid medium, and microscopy images) or mean results (**Figure 2C, 2D, 3A** upper right panel**, 4B, 6C, Figure S2F, S3B, S5C**). Error bars show the standard error of the mean (s.e.m.) or standard deviation (indicated in figure legends). Statistical analysis (pairwise t-test) was done with the QuickCalcs online calculator (www.graphpad.com/quickcalcs/index.cfm).

The fluorescence of yeast cells grown on solid media was measured using the fluorescence image analyzer Fujifilm LAS-4000 equipped with a 16-bit CCD-camera, white light (to image growth of yeast cells), green light-emitting LEDs (emission maximum 520 nm) and an emission filter set (575 nm-DF20) suitable for RFP observation. The cells were incubated before imaging in the presence or absence of blue light as described in the figure legends. Linear fluorescence profiles of yeast cell lawns were obtained by the use of the program ImageJ. A rectangular area (**Figure S3C**; 88×19 mm) in the center of the plate was selected and mean gray values were quantified using the "plot profile" option.

Supplemental References

Collins, T.J. (2007). ImageJ for microscopy. Biotechniques 43, 25-30.

Ghaemmaghami, S., Huh, W.K., Bower, K., Howson, R.W., Belle, A., Dephoure, N., O'Shea, E.K., and Weissman, J.S. (2003). Global analysis of protein expression in yeast. Nature 425, 737-741.

16

Holstege, F.C., Jennings, E.G., Wyrick, J.J., Lee, T.I., Hengartner, C.J., Green, M.R., Golub, T.R., Lander, E.S., and Young, R.A. (1998). Dissecting the regulatory circuitry of a eukaryotic genome. Cell 95, 717-728.

Sikorski, R.S., and Hieter, P. (1989). A system of shuttle vectors and yeast host strains designed for efficient manipulation of DNA in Saccharomyces cerevisiae. Genetics 122, 19-27.

17

3 Development of an optogenetic tool to regulate protein stability in vivo.

Christian Renicke[1], and Christof Taxis[1,2]

[1]Department of Biology/Genetics, Philipps-Universität Marburg, Karl-von-Frisch-Strasse 8, 35043 Marburg, Germany

[2]Department of Chemistry/Biochemistry, Philipps-Universität Marburg, Hans-Meerwein-Strasse 4, 35043 Marburg, Germany

Development of an optogenetic tool to regulate protein stability *in vivo*

Christian Renicke[1] and Christof Taxis[1, 2]

1. Introduction

The introduction of the green fluorescent protein as a genetically encoded marker for the observation of physiological events in living organisms revolutionized life-sciences (1, 2). Recently, the biologist's toolbox was expanded by another branch in which light is used to precisely manipulate cellular functions via genetically expressed photoactuators. Both approaches, aiming at either observation or regulation of cellular processes, are referred to as optogenetics (3, 4). The second strategy requires a bifunctional protein which comprises a sensor-domain for photo-reception and an effector-domain facilitating a specific output. Light as signal has certain advantages compared to e.g. small molecule approaches to regulate cell behavior or protein activities. Mainly, these are the unmatched temporal and spatial control as well as precise regulation of quantity and quality of light. However, many biological systems rely on and react to light as an important environmental cue. This has to be considered for experimental design of an optogenetic approach.

In recent years, many different tools have been developed using light to influence protein activity by either regulating synthesis, localization, activity or stability, which has been described in depth by several reviews (5-7). These tools fall into two broad classes: The first consists of naturally occurring photoactuators that need minimal adjustments to be used in heterologous systems like the channelrhodopsins that revolutionized neuronal studies at all levels; from single cell measurements in isolated neurons up to behavioral studies in whole animals (8). Although such photoactuators might be directly transferable into the experimental organism of choice, generation of improved variants by knowledge-based site-specific mutagenesis or directed evolution is a way to improve applicability of these tools. This offers researchers the opportunity to use an experimental setup that is optimized for their needs (9). The second class are synthetic, modular photoactuators that provide a novel cellular function by controlling the activity of an effector-domain with a photoreceptor. In general, an in-depth understanding of the light-induced changes in the photoreceptor and the regulation mechanism of the effector domain is necessary to succeed in such an approach. This has been very successfully utilized

to achieve site-specific regulation of protein activities like a small GTPase or actin filament formation (10, 11).

Some generalizable trends became evident that have been employed effectively for several approaches. One example is the development of tools for light-regulation of transcription, which took advantage of the characterization of proteins that change their association with a photoreceptor in dependence of its signaling state (12-18). Another way to control protein abundance generically is to regulate the degradation of a target protein. Light-control of protein stability has been established by regulating the activity of a degradation sequence with a photoreceptor domain (19, 20) or by uncaging of a small chemical compound (21). In all three methods, the ubiquitin-proteasome system, which is the main proteolytic machinery in eukaryotes (22), is used for proteolysis of the target protein. Thus, these methods are restricted to target proteins that reside in the nucleus or the cytosol of an eukaryotic cell.

The LOV2 domains of *Arabidopsis thaliana* and *Avena sativa* phototropin1 have been used to regulate function of an effector domain in several optogenetic tools (7, 23). This is somewhat similar to its original role in plant phototropism, in which the domain regulates the activity of an adjacent kinase domain in the protein phototropin1 (24). The family of LOV2 domains are well studied photoreceptors; they use a flavin mononucleotide (FMN) cofactor as primary light-sensing molecule. After excitation of FMN by blue-light, a covalent bond is formed between the carbon atom at position 4a of FMN and the sulphur of a cysteine residue. This adduct formation induces conformational rearrangements in the LOV2 domain that lead to the unfolding of a C-terminal helix, the so called Jα helix (23). The structural change at the C-terminus of the LOV2 domain upon excitation with blue-light has been used to regulate accessibility and activity of synthetic degrons. The LOV2 domain of *A. sativa* phototropin1 and a degradation sequence consisiting of four amino acids was used to generate the so called blue-light inducible degradation construct which has been shown to mediate light-control of protein stability in mammalian cell culture and zebrafish embryos (19). In another implementation, the degron is a synthetic variant of the C-terminal degron of murine ornithine decarboxylase (ODC), which is called cODC1 (25) linked to the LOV2 domain of *A. thaliana* phototropin1 (Figure 1A and (20)). The ODC degron belongs to the few known degrons that induce proteasomal degradation independent of ubiquitylation, a common prerequisite for proteins to be degraded by the proteasome. It has been shown to be useful for *in vivo*

destabilization of proteins in budding yeast, tobacco plants, and mammalian cell culture or to study protein degradation *in vitro* (26-30).

A

A. thaliana phototropin1 LOV2   **cODC1[23]**

M[460]RKGIDLATT[...]NIDEAVRELP[616]**MSCAQESITSLYKKAGSENLYFQ**   photo-sensitive degron (psd) module
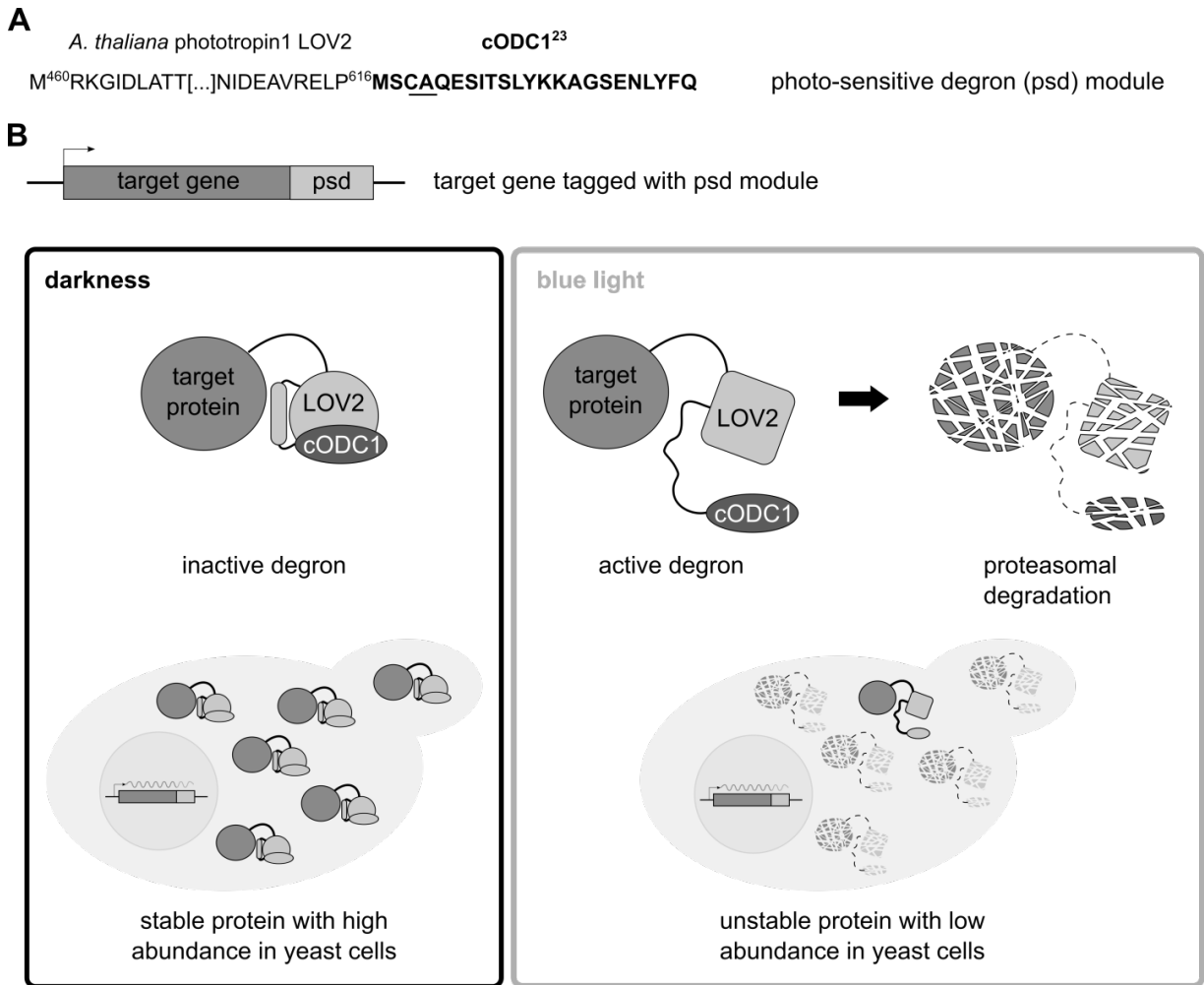
B

Figure 1: The photo-sensitive degron (psd) module. A) The psd module consists of the *A. thaliana* phototropin1 LOV2 domain (amino acids 460 to 616) with a C-terminal extension of 23 amino acids from the synthetic degron cODC1 (letters in bold) containing the crucial CA motif (underlined). This degron was derived from the murine ornithine decarboxylase C-terminal degradation sequence. B) Activation mechanism of the psd module exemplified in the yeast *Saccharomyces cerevisiae*. The gene encoding the psd module can be used to extend the target gene at the 3'-end. This leads to the formation of a fusion protein that is stable in darkness. Exposure of the yeast cells with blue-light leads to a structural change in the LOV2 core domain and unfolding of a C-terminal α helix, which exposes and activates the cODC1 degron. This induces proteasomal degradation of the target. Subsequently, target protein levels drop until a new equilibrium between ongoing biosynthesis and degradation has been reached.

To induce degradation, two requirements have to be met for ODC derived degrons: a stretch of 37 amino acids without secondary structure has to be present at the very C-terminus of the protein and a cysteine-alanine motif must reside roughly in the center of the sequence. The cysteine residue has been shown to be required for

proteasome association and the lack of secondary structure is important for induction of proteolysis (31-33). Thus, it can be assumed that light-induced unfolding of the Jα helix is not only necessary for exposure but also for activation of the degron (Figure 1B).

The photosensitive degron module has been developed and characterized in the yeast *Saccharomyces cerevisiae*. There, it was applied successfully to regulate growth, secretion, cell cycle events and enzymatic activity by blue-light and recently, it was shown to work in the nematode *Caenorhabditis elegans* as well (20, 34).

In this chapter, we discuss practical aspects of using the psd module in yeast, point-out problems that might arise and strategies to circumvent these obstacles. Furthermore, we provide guidelines for usage of the psd module variants with different destabilization characteristics and we describe typical applications and experimental designs, e.g. target protein inactivation by light during the developmental program of sporulation and observation of target protein depletion by live-cell imaging.

2. Methodology

2.1. Yeast strains, plasmids and growth conditions

No specialized yeast strain is necessary to control protein stability by light. The psd module can be inserted at a chromosomal locus at the 3' end of a gene by standard procedures or the desired fusion gene may be created on plasmid (20, 35). The latter approach might require a yeast strain lacking the target gene but in turn provides the opportunity to uncouple target gene expression from intrinsic regulation by substitution of the original promoter. No specialized requirements are necessary for medium composition. We used all kinds of standard solid medium for plate assays (36). Clear plastic cell culture flasks with a ventilated cap were used to grow cells in liquid cultures. In this case, coloring of a medium might be an issue due to absorption of relevant wavelengths resulting in decreased light penetration. Therefore, low fluorescence medium was used to grow yeast cells in shaking cultures (37). It might be noteworthy that low fluorescent medium is quite similar to synthetic complete medium, however the latter contains riboflavins that are used as essential cofactor by the LOV2 domain. In yeast strains or under growth conditions in which riboflavins are limiting due to reduced biosynthesis, addition of flavinmononucleotide to the medium might be a way to ensure availability of the cofactor.

2.2. Illumination conditions

Common light emitting diodes (LED), either high-power blue-light LEDs or RGB LEDs, connected to a dimmer were used to illuminate yeast cells. In general, the light-intensity was adjusted to a photon flux of 30 µmol m^{-2} s^{-1} at the level of the cells with an optometer (e.g. P2000, equipped with light-detector D-9306-2, Gigahertz-Optik, Türkenfeld, Germany). Lightproof boxes with LEDs mounted to the lid were used to expose the cells to specific illumination conditions. The interior of the boxes was lined with reflective film to increase light-yield. For live-cell and time-lapse microscopy experiments, a single blue-light LED was placed in the transmitted light path to allow specific illumination of the sample. During recording of fluorescence images, the LED was switched off. A light-flux of up to 30 µmol m^{-2} s^{-1} does not influence the growth rate of wild type cells, even very light-sensitive *yap1Δ* mutant cells were still proliferating under these conditions. Moreover, the presence of a psd-module construct did not result in decreased growth rate under these conditions (20, 37).

2.3. Detection of target proteins in yeast cells

Standard techniques were applied to quantify the target protein content in yeast cells (38). Target protein abundance in yeast cultures was analyzed by immunoblotting. Whole cell extracts were prepared by alkaline lysis and trichloroacetic acid precipitation (39). SDS-PAGE and blotting was performed following standard procedures (40, 41). Fluorescence microscopy was used for single-cell measurements of target protein levels modified with a fluorescent protein and the psd module (20), whereas quantification at population scale was done by fluorimeter measurements (37).

3. Results and Discussion

3.1. Regulation of protein abundance by light

Control of protein levels by light requires the fusion of the psd module to the carboxy-terminus of the target, which has to reside in the nucleus or the cytosol to be accessible for proteasomal degradation. In addition, successful regulation depends on the intrinsic stability of the target protein. Regulation of protein abundance with the psd module works best for stable proteins with a long half-life. If a protein has a very short half-life, it may not be further destabilized by the psd module. For such proteins it might be more advisable to control the gene expression of the target by light (42).

The half-lives of the diverse psd module variants that are available range from 6 to 20 minutes at destabilizing conditions (20, 37 and Table 1). The half-lives of most yeast proteins have been measured (43), which might help in finding the most promising method for initial experiments.

In yeast, a target gene can be expanded conveniently at the 3'-end by homologous recombination with PCR generated cassettes (35), a technique suitable for generation of chromosomally integrated gene fusions with the psd module as well (20). Furthermore, this does not interfere with the naturally evolved regulation of target gene-expression, which preserves the normal response to changes in the environment. An alternative is the usage of a strain with a deletion of the target gene complemented with a plasmid bearing the psd module-modified target gene. In such a construct, it might be worth to exchange the promoter of the target gene with a regulatable promoter like P_{GAL1} or the variants P_{GALL} or P_{GALS} that have reduced expression strength (35). Such dual control allows transcriptional repression concomitantly with protein destabilization, however it requires a switch in growth medium in case a *GAL1* promoter variant is used to regulate the expression of the target gene.
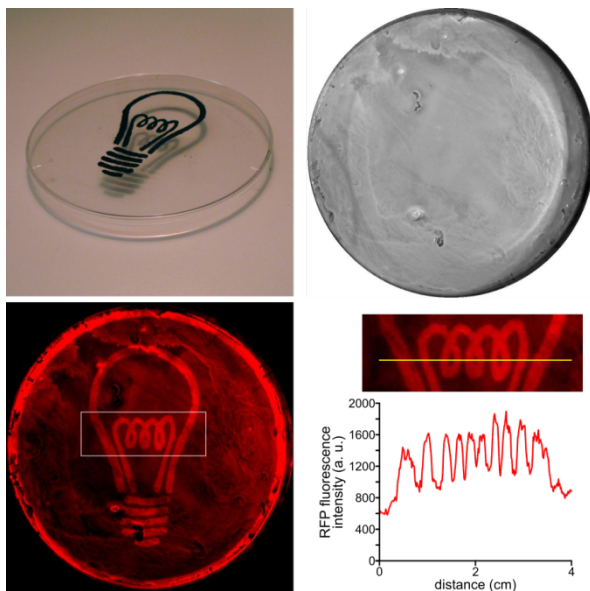

Figure 2: Construction of a light-sensor using the psd-module. Yeast cells expressing P_{TDH3}-*RFP-psd* (plasmid based) were spread on solid medium and incubated at 30 °C for 24 hours. Blue-light (465 nm, 10 µmol m^{-2} s^{-1}) was applied on parts of the plate using a mask (upper left panel). Please note that the rim of the plate was not illuminated due to the usage of a hood to block lateral light. RFP fluorescence (lower left image) and yeast cell growth (upper right image) were imaged with a fluorescence image analyzer and a digital camera, respectively. The graph (lower right panel) shows the line plot of fluorescence (measured along the yellow line) after background subtraction. The magnified area is indicated in the fluorescence image. Background fluorescence was obtained from cell-free areas.

Light exhibits unique advantages compared to other signals that may be applied to switch conditional mutants to the inactive state. One advantage is spatial control of illumination, which can be used to regulate the abundance of a target very precisely (Figure 2).

Such spatial control has also been used for light-regulation of enzymatic activity to implement yeast photography (20), which shows convincingly that enzymatic activity can be regulated with high spatial precision. This is not only achievable on a macroscopic scale, even experiments on the microscopic level could benefit from selective-illumination approaches: a specific protein might be inactivated in a fraction of the cells, whereas both, light-exposed and undisturbed cells are observed at the same time. The proof-of-principle for such an experimental setup has been achieved with a chemical biology method for the regulation of protein stability (21).

3.3. Application of the psd module to generate conditional mutants

Regulation of protein abundance by light is a powerful approach to create conditional mutants. The psd module has been used to exert light-control over proteins with diverse cellular functions. Among others, the abundance of the Polo-like kinase Cdc5, the phosphatase Cdc14, the AAA-ATPase Cdc48, the iron-sulfur cluster biogenesis factor Yae1 or Sec62, a subunit of the translocon necessary for import into the endoplasmic reticulum has been regulated by light (20, 44). Indirectly, reversed regulation has been achieved with constitutively active variants of cyclin-dependent kinase regulators modified with the psd module in an otherwise wild type background. In this case, accumulation of the modified regulators in darkness leads to a block in cell cycle progression at a distinct step in each case (20). The psd module can be employed to create conditional mutants by inactivating proteins during vegetative growth. Moreover, it is also a useful tool to investigate a developmental process. In yeast, the differentiation program of sporulation is coupled to the meiotic cell divisions; it is induced by starvation conditions and leads to the generation of up to four spores containing haploid genomes from a diploid mother cell (45). Usage of a conditional mutant to inactivate a protein during meiosis has the advantage that perturbation of the vegetative growth phase is minimized and inactivation is reversible. With the psd module, inactivation of the target protein is induced by blue-light exposure after the entry into meiosis has been initiated in most cells (Figure 3A and B).
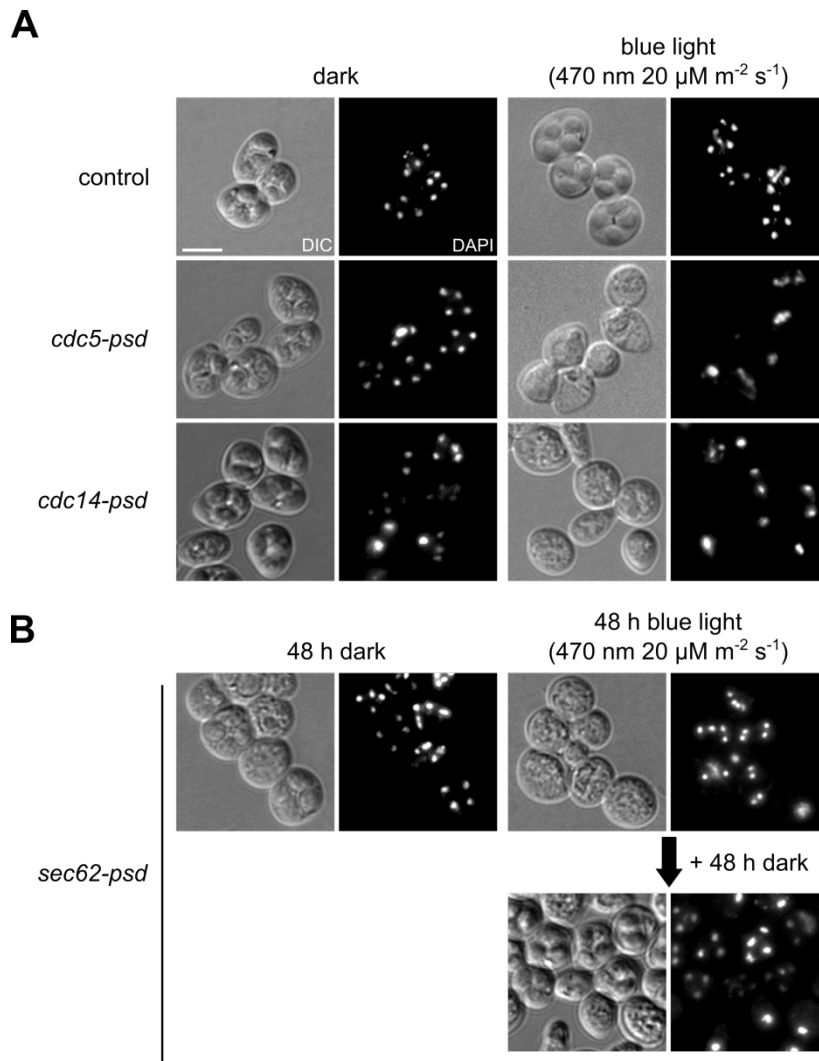
Figure 3: Generation of conditional mutants with the psd module. A) Depletion of Cdc5-RFP-psd and Cdc14-RFP-psd by blue light after induction of sporulation leads to block of spore formation. Diploid yeast cells (genotypes indicated in the figure) were subjected to sporulation conditions at 25 °C for two days in absence or presence of blue light (470 nm, 20 µmol m^{-2} s^{-1}) Images show cells in differential interference contrast and HOECHST 33342 stained DNA in the DAPI channel. Scale bar: 5 µm. B) Depletion of Sec62-RFP-psd leads to a reversible block in sporulation. Cells were exposed for 48 h to sporulation conditions as described in A and then subjected to additional 48 h of incubation in darkness.

Light-induced depletion of Cdc5-psd, Cdc14-psd, and Sec62-psd during meiosis suggested that target protein activity is lost quickly after induction of the sporulation program, resulting in specific defects in progression through different phases of the meiotic divisions or spore formation. Inactivation of the Polo-like kinase Cdc5 resulted in cells that were mostly arrested during early phases of meiosis I, inactivation of Cdc14 blocked cells at the metaphase to anaphase transition of meiosis I, whereas cells with reduced Sec62 levels finished most likely both meiotic

divisions but were unable form refractive spores (Figure 3A and B and our unpublished observations). Interestingly, the cells which were arrested in sporulation due to Sec62 depletion were able to complete the developmental program when placed into darkness after 48 h blue-light incubation (Figure 3B). This behavior demonstrated nicely the reversibility of target protein depletion by protein biosynthesis. Similarly, reappearance of a target has been observed previously by following a fluorescent protein modified with the psd module (20).

3.4. Detection of target proteins modified with the psd module

During regulation of protein stability with the photo-sensitive degron, it is important to follow the abundance of the target protein before and after the transition from permissive to restrictive conditions. Commonly available methods can be used to record the changes over time, like fluorescence microscopy (Figure 4), fluorimeter measurements and immunoblotting (20, 37). Although not tested by us, methods like flow cytometry or mass spectrometry are also applicable for this purpose (46, 47). For fluorescence-based approaches, the target protein has to be modified with a fluorescent tag in addition to the psd module. In yeast, modification can be done by choosing an appropriate cassette plasmid that contains the gene for the fluorescent protein of choice N-terminally fused to the psd module (20). Modification of a target with such an approach has been used to observe the disappearance of the target protein *in vivo* after illuminating the cells with blue-light (Figure 4).
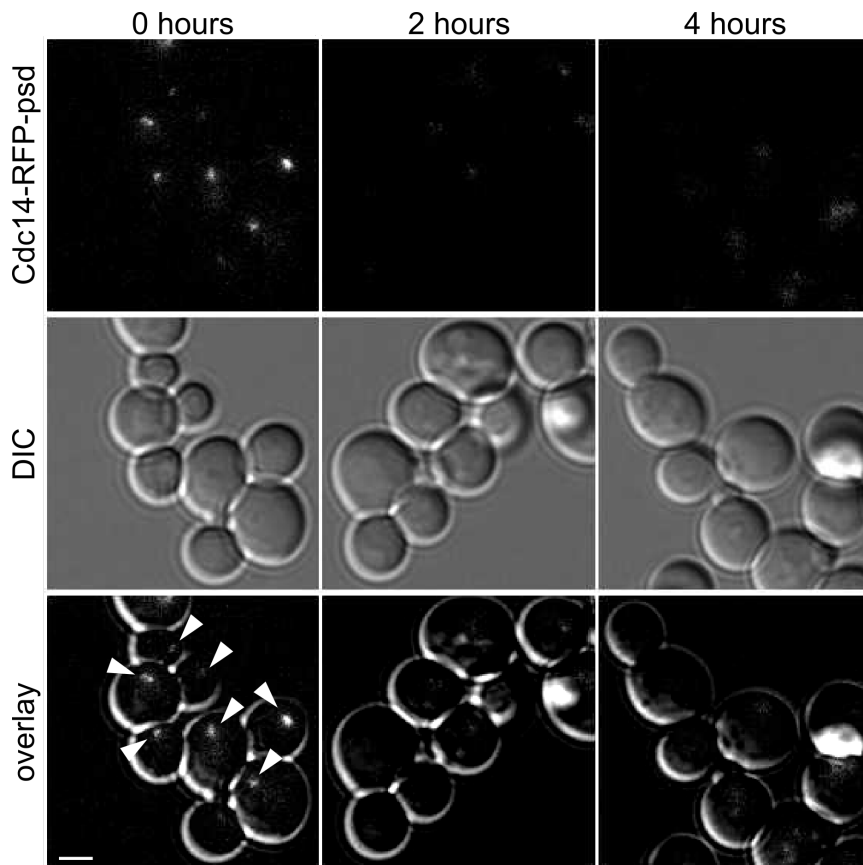
Figure 4: Live-cell microscopy of Cdc14-RFP-psd. Images of cells containing Cdc14-RFP-psd were recorded before and after illuminating the cells with blue-light (465 nm; 30 µmol m^{-2} s^{-1}) for the times indicated in the figure (scale bar 2 µm). The fluorescence signals show the typical nucleolar localization of Cdc14 at the beginning of the experiment (marked by arrowheads in the overlay of fluorescence and DIC channel), which disappear already after two hours of blue-light exposure.

Fluorimeter measurements or immunoblotting may require more time and several steps of sample preparation but offer advantages regarding signal-to-noise ratio, specificity or sensitivity. In case of immunoblotting, the target protein is modified with a smaller tag. The decision for one of these methods can be made largely on the available equipment and the specific experimental requirements.

3.2. Variants of the psd module

A mutagenesis-based approach was done to create improved variants of the psd-module (37). Firstly, mutations were tested in the setting of the psd module, which have been described in the literature to improve the switching behavior of homologous LOV2 domains. Secondly, we made mutants by random mutagenesis and selected variants with interesting characteristics. Finally, we combined both approaches and merged promising mutations into one construct (Figure 5). Our efforts resulted in variants with improved switching behavior, which is in case of the

psd module the abundance of the target protein in cells kept in darkness divided by its abundance in blue-light illuminated cells. In addition, we identified variants with a threefold decrease in half-life under destabilizing conditions. However, the latter variants showed decreased stability in darkness as well. An overview of selected psd module variants is given in table 1.
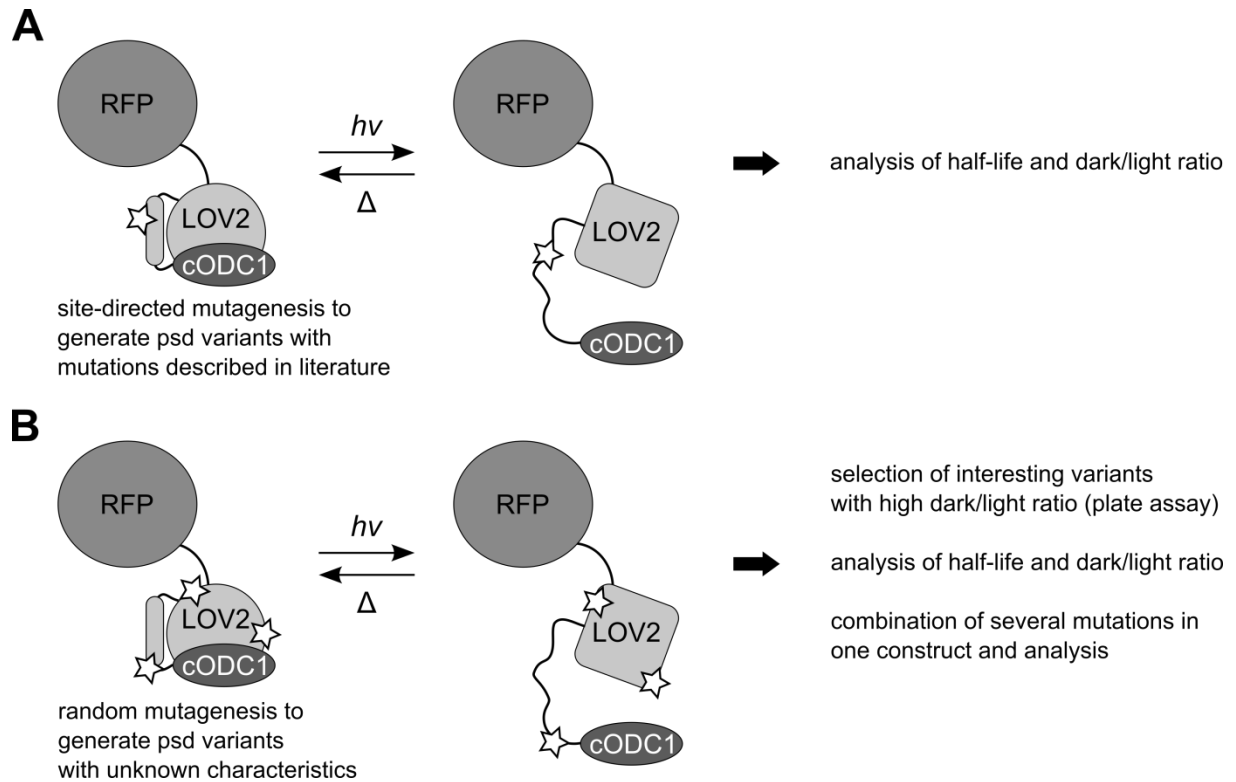

Figure 5: Mutagenesis strategies to improve the psd module. A) Site-directed mutagenesis was used to generate variants of the psd module containing mutations that have been shown to change the signaling characteristics of homologous LOV2 domains. These variants were then tested for their dark/light switching behavior and their half-lives in cells kept in darkness or exposed to blue-light. B) Random mutagenesis was used to generate a library of psd module variants. Fluorescence measurements were used to quantify abundance of the red fluorescent protein that is fused to the psd module in cells grown in darkness and in cells exposed to blue-light. Interesting clones were analyzed as described in **A**. Site-directed mutagenesis was used to combine promising mutations in one construct followed by further characterization.

The diversification of psd module characteristics has consequences for its usage: the choice of psd module variants is depending on the characteristics of the target protein. It is probably best to modify a target protein that is highly abundant and is required in high levels to sustain its specific cellular function with the original psd module or one of the variants with high switching ratio (K121M N128Y G138A and K92R E132A E155G). The latter two variants showed reduced half-lives at restrictive conditions (37), which was crucial to obtain a yeast strain in which the cyclin-dependent kinase Cdc28 could be inactivated by light (Figure 6).
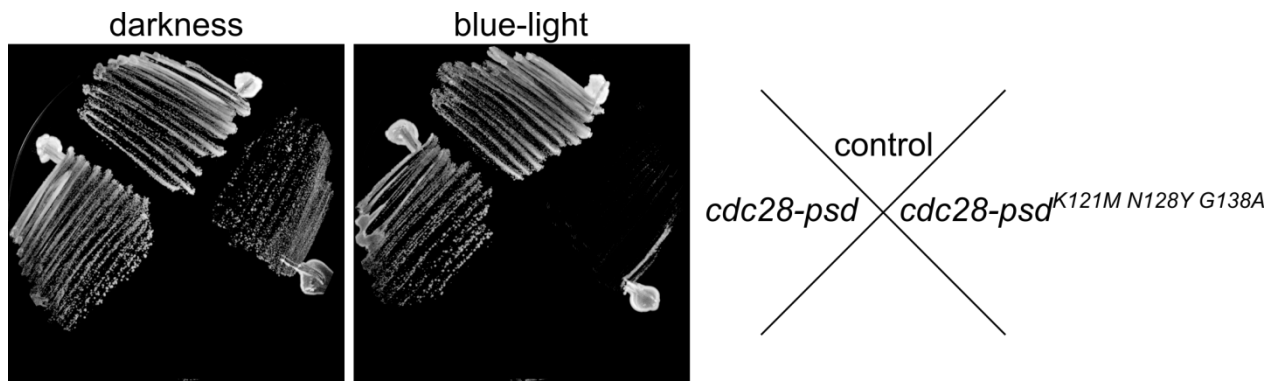
darkness   blue-light

control
cdc28-psd ✕ *cdc28-psd*[K121M N128Y G138A]

Figure 6: Inactivation of the yeast cyclin-dependent kinase Cdc28 by blue-light. Yeast strains with cdc28-psd variants (as indicated in the figure) and an isogenic control strain were streaked on solid YPD medium and incubated for two days in darkness or exposed to blue-light (465 nm, 30 µmol m^{-2} s^{-1}) at 30 °C.

Target proteins that are required only in low amounts need a psd module variant that leads to minimal levels at restrictive conditions. Examples are variants with half-lives of 10 minutes and below (K92R E132A E139N N148D E155G and K121M N128Y) in blue-light illuminated cells (37). The abundance of a specific yeast protein has been measured by different approaches (46, 48-50), the results of these efforts might be helpful in deciding which psd module variant is appropriate for successfully creating the desired mutant; alternatively, several psd module variants can be tested for a specific target.

4. Concluding remarks

Light-regulation of protein stability has high potential as an easy-to-implement tool that can be used to great effect. Light as signal provides outstanding features, especially spatial precision and modulation of illumination strength. It has been shown that this can be used to gradually tune the activity of an enzyme in yeast (20). Such tunability offers novel experimental design to e.g. gain information about network behavior after reducing the amounts of single nodes or to determine cellular thresholds for a protein's function. Importantly, the psd module induces changes in protein levels fairly fast, which allows to record dynamic behavior of a system in a reasonable time. One way to improve the method would be to combine it with light-repressible transcription (51) or light-activated gene silencing (13) to control protein abundance twofold through biosynthesis as well as stability. Variants of the psd module that react to different wavelengths would also be of advantage. However, currently no photoreceptors with a compatible activation mechanism are known that are excited by longer wavelengths. Such variants could be used in analogy to the

multi-colored family of fluorescent proteins; target proteins modified with psd modules that respond to different excitation-wavelengths could be used to destabilize several proteins in the same cell at distinct time points.

Overall, photoactuators from the optogenetic toolbox offer ample opportunities to influence cells on molecular level and to interfere with regulatory processes in a merely non-invasive way. Regulation of protein abundance by light with the photo-sensitive degron is a valuable addition to this package that complements the existing tools. While light has been used for centuries to observe biological systems using microscopy, recent years have shown that it is also a versatile signal to control cellular events in a precise way.

Table 1: Characteristics of psd module variants[1]

name	Half-life in darkness (min)		Half-life in 30 µmol m^{-2} s^{-1} blue-light (min)		dark/light switching ratio
Wild type psd module	123	±21	20	±1	11
K92R E132A E155G	102	±41	12	±0.4	22
K121M N128Y G138A	92	±28	13	±1	22
K92R E132A E139N N148D E155G	66	±10	10	±0.4	16
K121M N128Y	44	±8	9	±0.3	14

[1]The measurements have been published previously by Usherenko and colleagues (37).

5. References

1. Chudakov DM, Matz MV, Lukyanov S, Lukyanov KA. Fluorescent proteins and their applications in imaging living cells and tissues. Physiol Rev. 2010;90(3):1103-63. Epub 2010/07/29.

2. Tsien RY. The green fluorescent protein. Annu Rev Biochem. 1998;67:509-44. Epub 1998/10/06.

3. Deisseroth K, Feng G, Majewska AK, Miesenbock G, Ting A, Schnitzer MJ. Next-generation optical technologies for illuminating genetically targeted brain circuits. The Journal of neuroscience : the official journal of the Society for Neuroscience. 2006;26(41):10380-6. Epub 2006/10/13.

4. Miesenbock G. The optogenetic catechism. Science. 2009;326(5951):395-9. Epub 2009/10/17.

5. Gautier A, Gauron C, Volovitch M, Bensimon D, Jullien L, Vriz S. How to control proteins with light in living systems. Nat Chem Biol. 2014;10(7):533-41. Epub 2014/06/18.

6. Zhang K, Cui B. Optogenetic control of intracellular signaling pathways. Trends in biotechnology. 2015;33(2):92-100. Epub 2014/12/23.

7. Ziegler T, Moglich A. Photoreceptor engineering. Frontiers in molecular biosciences. 2015;2:30. Epub 2015/07/03.

8. Hausser M. Optogenetics: the age of light. Nat Methods. 2014;11(10):1012-4. Epub 2014/09/30.

9. Lin JY. A user's guide to channelrhodopsin variants: features, limitations and future developments. Experimental physiology. 2011;96(1):19-25. Epub 2010/07/14.

10. Baarlink C, Wang H, Grosse R. Nuclear actin network assembly by formins regulates the SRF coactivator MAL. Science. 2013;340(6134):864-7. Epub 2013/04/06.

11. Wu YI, Frey D, Lungu OI, Jaehrig A, Schlichting I, Kuhlman B, et al. A genetically encoded photoactivatable Rac controls the motility of living cells. Nature. 2009;461(7260):104-8. Epub 2009/08/21.

12. Kim B, Lin MZ. Optobiology: optical control of biological processes via protein engineering. Biochemical Society transactions. 2013;41(5):1183-8. Epub 2013/09/26.

13. Konermann S, Brigham MD, Trevino AE, Hsu PD, Heidenreich M, Cong L, et al. Optical control of mammalian endogenous transcription and epigenetic states. Nature. 2013;500(7463):472-6. Epub 2013/07/24.

14. Levskaya A, Chevalier AA, Tabor JJ, Simpson ZB, Lavery LA, Levy M, et al. Synthetic biology: engineering Escherichia coli to see light. Nature. 2005;438(7067):441-2. Epub 2005/11/25.

15. Ohlendorf R, Vidavski RR, Eldar A, Moffat K, Moglich A. From dusk till dawn: one-plasmid systems for light-regulated gene expression. J Mol Biol. 2012;416(4):534-42. Epub 2012/01/17.

16. Polstein LR, Gersbach CA. Light-inducible spatiotemporal control of gene activation by customizable zinc finger transcription factors. Journal of the American Chemical Society. 2012;134(40):16480-3. Epub 2012/09/12.

17. Shimizu-Sato S, Huq E, Tepperman JM, Quail PH. A light-switchable gene promoter system. Nat Biotechnol. 2002;20(10):1041-4. Epub 2002/09/10.

18. Wang X, Chen X, Yang Y. Spatiotemporal control of gene expression by a light-switchable transgene system. Nat Methods. 2012;9(3):266-9. Epub 2012/02/14.

19. Bonger KM, Rakhit R, Payumo AY, Chen JK, Wandless TJ. General method for regulating protein stability with light. ACS chemical biology. 2014;9(1):111-5. Epub 2013/11/05.

20. Renicke C, Schuster D, Usherenko S, Essen LO, Taxis C. A LOV2 domain-based optogenetic tool to control protein degradation and cellular function. Chem Biol. 2013;20(4):619-26. Epub 2013/04/23.

21. Delacour Q, Li C, Plamont MA, Billon-Denis E, Aujard I, Le Saux T, et al. Light-Activated Proteolysis for the Spatiotemporal Control of Proteins. ACS chemical biology. 2015;10(7):1643-7. Epub 2015/05/06.

22. Goldberg AL. Functions of the proteasome: from protein degradation and immune surveillance to cancer therapy. Biochemical Society transactions. 2007;35(Pt 1):12-7. Epub 2007/01/11.

23. Pudasaini A, El-Arab KK, Zoltowski BD. LOV-based optogenetic devices: light-driven modules to impart photoregulated control of cellular signaling. Frontiers in molecular biosciences. 2015;2:18. Epub 2015/05/20.

24. Harper SM, Christie JM, Gardner KH. Disruption of the LOV-Jalpha helix interaction activates phototropin kinase activity. Biochemistry. 2004;43(51):16184-92. Epub 2004/12/22.

25. Jungbluth M, Renicke C, Taxis C. Targeted protein depletion in Saccharomyces cerevisiae by activation of a bidirectional degron. BMC Syst Biol. 2010;4:176. Epub 2010/12/31.

26. Ghoda L, van Daalen Wetters T, Macrae M, Ascherman D, Coffino P. Prevention of rapid intracellular degradation of ODC by a carboxyl-terminal truncation. Science. 1989;243(4897):1493-5. Epub 1989/03/17.

27. Loetscher P, Pratt G, Rechsteiner M. The C terminus of mouse ornithine decarboxylase confers rapid degradation on dihydrofolate reductase. Support for the pest hypothesis. J Biol Chem. 1991;266(17):11213-20. Epub 1991/06/15.

28. DeScenzo RA, Minocha SC. Modulation of cellular polyamines in tobacco by transfer and expression of mouse ornithine decarboxylase cDNA. Plant Mol Biol. 1993;22(1):113-27. Epub 1993/04/01.

29. Hoyt MA, Zhang M, Coffino P. Ubiquitin-independent mechanisms of mouse ornithine decarboxylase degradation are conserved between mammalian and fungal cells. J Biol Chem. 2003;278(14):12135-43. Epub 2003/02/04.

30. Matsuzawa S, Cuddy M, Fukushima T, Reed JC. Method for targeting protein destruction by using a ubiquitin-independent, proteasome-mediated degradation pathway. Proc Natl Acad Sci U S A. 2005;102(42):14982-7. Epub 2005/10/13.

31. Ravid T, Hochstrasser M. Diversity of degradation signals in the ubiquitin-proteasome system. Nature reviews Molecular cell biology. 2008;9(9):679-90. Epub 2008/08/14.

32. Takeuchi J, Chen H, Coffino P. Proteasome substrate degradation requires association plus extended peptide. EMBO J. 2007;26(1):123-31. Epub 2006/12/16.

33. Takeuchi J, Chen H, Hoyt MA, Coffino P. Structural elements of the ubiquitin-independent proteasome degron of ornithine decarboxylase. Biochem J. 2008;410(2):401-7. Epub 2007/11/06.

34. Hermann A, Liewald JF, Gottschalk A. A photosensitive degron enables acute light-induced protein degradation in the nervous system. Curr Biol. 2015;25(17):R749-50. Epub 2015/09/02.

35. Janke C, Magiera MM, Rathfelder N, Taxis C, Reber S, Maekawa H, et al. A versatile toolbox for PCR-based tagging of yeast genes: new fluorescent proteins, more markers and promoter substitution cassettes. Yeast. 2004;21(11):947-62. Epub 2004/08/31.

36. Guide to yeast genetics and molecular biology. Methods Enzymol. 1991;194:1-863. Epub 1991/01/01.

37. Usherenko S, Stibbe H, Musco M, Essen LO, Kostina EA, Taxis C. Photo-sensitive degron variants for tuning protein stability by light. BMC Syst Biol. 2014;8:128. Epub 2014/11/19.

38. Ausubel FM, Kingston, R.E., Seidman, F.G., Struhl, K., Moore, D.D., Brent, R., and Smith, F.A., editor. Current Protocols in Molecular Biology. New York, USA: John Wiley and Sons; 1995.

39. Yaffe MP, Schatz G. Two nuclear mutations that block mitochondrial protein import in yeast. Proc Natl Acad Sci U S A. 1984;81(15):4819-23. Epub 1984/08/01.

40. Laemmli UK. Cleavage of structural proteins during the assembly of the head of bacteriophage T4. Nature. 1970;227(5259):680-5. Epub 1970/08/15.

41. Towbin H, Staehelin T, Gordon J. Electrophoretic transfer of proteins from polyacrylamide gels to nitrocellulose sheets: procedure and some applications. Proc Natl Acad Sci U S A. 1979;76(9):4350-4. Epub 1979/09/01.

42. Pathak GP, Strickland D, Vrana JD, Tucker CL. Benchmarking of optical dimerizer systems. ACS synthetic biology. 2014;3(11):832-8. Epub 2014/10/29.

43. Belle A, Tanay A, Bitincka L, Shamir R, O'Shea EK. Quantification of protein half-lives in the budding yeast proteome. Proc Natl Acad Sci U S A. 2006;103(35):13004-9. Epub 2006/08/19.

44. Paul VD, Muhlenhoff U, Stumpfig M, Seebacher J, Kugler KG, Renicke C, et al. The deca-GX3 proteins Yae1-Lto1 function as adaptors recruiting the ABC protein Rli1 for iron-sulfur cluster insertion. eLife. 2015;4:e08231. Epub 2015/07/17.

45. Neiman AM. Ascospore formation in the yeast Saccharomyces cerevisiae. Microbiol Mol Biol Rev. 2005;69(4):565-84. Epub 2005/12/13.

46. Newman JR, Ghaemmaghami S, Ihmels J, Breslow DK, Noble M, DeRisi JL, et al. Single-cell proteomic analysis of S. cerevisiae reveals the architecture of biological noise. Nature. 2006;441(7095):840-6. Epub 2006/05/16.

47. Selevsek N, Chang CY, Gillet LC, Navarro P, Bernhardt OM, Reiter L, et al. Reproducible and consistent quantification of the Saccharomyces cerevisiae proteome by SWATH-mass spectrometry. Molecular & cellular proteomics : MCP. 2015;14(3):739-49. Epub 2015/01/07.

48. Chong YT, Koh JL, Friesen H, Duffy SK, Cox MJ, Moses A, et al. Yeast Proteome Dynamics from Single Cell Imaging and Automated Analysis. Cell. 2015;161(6):1413-24. Epub 2015/06/06.

49. Ghaemmaghami S, Huh WK, Bower K, Howson RW, Belle A, Dephoure N, et al. Global analysis of protein expression in yeast. Nature. 2003;425(6959):737-41. Epub 2003/10/17.

50. Kulak NA, Pichler G, Paron I, Nagaraj N, Mann M. Minimal, encapsulated proteomic-sample processing applied to copy-number estimation in eukaryotic cells. Nat Methods. 2014;11(3):319-24. Epub 2014/02/04.

51. Sorokina O, Kapus A, Terecskei K, Dixon LE, Kozma-Bognar L, Nagy F, et al. A switchable light-input, light-output system modelled and constructed in yeast. Journal of biological engineering. 2009;3:15. Epub 2009/09/19.

4 A Tobacco Etch Virus Protease with Increased Substrate Tolerance at the P1' position.

Christian Renicke[1], Roberta Spadaccini[2], and Christof Taxis[1]*

[1]Department of Biology/Genetics, Philipps-Universität Marburg, Karl-von-Frisch-Strasse 8, 35043 Marburg, Germany

[2]Dipartimento di Scienze e tecnologie, Universita' degli studi del Sannio, Benevento, Italy

*Correspondence: taxis@biologie.uni-marburg.de

A Tobacco Etch Virus Protease with Increased Substrate Tolerance at the P1' position

Christian Renicke[1], Roberta Spadaccini[2], Christof Taxis[1]*

1 Department of Biology/Genetics, Philipps-Universität Marburg, Marburg, Germany, **2** Dipartimento di Scienze e tecnologie, Universita' degli studi del Sannio, Benevento, Italy

Abstract

Site-specific proteases are important tools for *in vitro* and *in vivo* cleavage of proteins. They are widely used for diverse applications, like protein purification, assessment of protein–protein interactions or regulation of protein localization, abundance or activity. Here, we report the development of a procedure to select protease variants with altered specificity based on the well-established *Saccharomyces cerevisiae* adenine auxotrophy-dependent red/white colony assay. We applied this method on the tobacco etch virus (TEV) protease to obtain a protease variant with altered substrate specificity at the P1' Position. *In vivo* experiments with tester substrates showed that the mutated TEV protease still efficiently recognizes the sequence ENLYFQ, but has almost lost all bias for the amino acid at the P1' Position. Thus, we generated a site-specific protease for synthetic approaches requiring *in vivo* generation of proteins or peptides with a specific N-terminal amino acid.

Competing interests: The authors have declared that no competing interests exist.

* E-mail: taxis@biologie.uni-marburg.de

Introduction

The tobacco etch virus (TEV) protease is an important enzyme for life science research. Its high specificity and robustness make it ideal for diverse applications. It is used *in vitro* for protein purification and *in vivo* to test for protein–protein interactions, for induced proteolysis and to generate conditional mutants [1-6]. The biological function of the protease is to proteolyse the viral polyprotein into single proteins during tobacco etch virus biogenesis. The canonical recognition sequence of the protease is given as ENLYFQ-G/S, although with low stringency at several positions [7]. Especially glycine or serine at the seventh position (P1' position) of the recognition sequence can be replaced by another amino acid (except proline), after which at least partial substrate proteolysis has been observed [8].

This tolerance at the P1' position is crucial for one of the *in vivo* techniques based on the TEV protease, the TEV protease induced protein instability (TIPI) system. There, the protease is used to cleave a tag called cODC1-TDegF, which is fused to the target protein. This results in the activation of two degradation sequences (degrons) which induce proteasomal degradation of the degrons and the target [9]. After proteolysis, the degron called TDegF releases an N-degron, which is a destabilizing amino acid exposed at the amino-terminus of a

protein [5]. In *Saccharomyces cerevisiae*, 12 of the 20 fundamental amino acids are classified as destabilizing if exposed at the amino-terminus of a protein. They are either directly recognized by the ubiquitin-protein ligase Ubr1 (primary destabilizing amino acids arginine, phenylalanine, leucine, isoleucine, histidine, tyrosine, tryptophan, lysine) or after one or two enzymatic modifications (secondary destabilizing amino acids aspartate, glutamate and tertiary destabilizing amino acids glutamine, asparagine). An accessible lysine residue results in polyubiquitylation of the substrate and subsequently in degradation by the 26S proteasome [10]. Recently, it was found that some amino acids originally considered as stabilizing residues become destabilizing upon acetylation at the α-amino group of their N-terminal residues (methionine, alanine, valine, serine, threonine, cysteine). However, this modification of the N-terminal amino acid takes place only if the second amino acid is not a basic one. Acetylated amino acids are recognized and polyubiquitylated by the ubiquitin-protein ligase Doa10 resulting in proteasomal degradation [11].

The second degron activated by TEV protease proteolysis of the cODC1-TDegF tag is the C-degron cODC1, which is a synthetic degron based on the features of the C-terminal degron of murine ornithine decarboxylase (cODC). Two features are essential for the activity of the synthetic degron: a 37 amino acid-long unstructured peptide at the very carboxy-

terminus of a protein and a cysteine-alanine motif, which has to be present roughly in the middle of this unstructured region. This degron is directly recognized and degraded by the proteasome, without the involvement of polyubiquitylation [12]. The cODC1 degron was fused N-terminally to the TDegF degron to engineer a degradation tag with two degrons that protect each other from proteasomal degradation. This bidirectional degradation tag can be placed internally or at either terminus of the target protein. Proteasomal degradation is activated in either case by a single cleavage step by the TEV protease [9].

Overall, three characteristics are important for TIPI: TEV protease production which depends mainly on the expression strength of the promoter chosen for protease production; substrate proteolysis by the TEV protease, which is influenced by protease-substrate interaction and recognition of the cleavage sequence, and the destabilization strength of the activated degron (Figure 1A). During the initial development of the method, the proteolysis rate of the substrate by the TEV protease has been increased by fusing the interacting domains of p14 and SF3B155$^{381-424}$ to the protease and the substrate, respectively. Furthermore, shortening of the protease removed a TEV protease recognition sequence present at the C-terminus that reduces activity of the full length protease by competitive inhibition [5,13]. This engineered variant of the TEV protease has been named pTEV+ protease. A systematic test of all amino acids at the P1' position of the recognition sequence has not been undertaken in the context of the TIPI system for the shortened TEV protease, although this position influences both the proteolysis rate and the strength of the N-degron. Work in bacteria has shown that arginine, which is the strongest N-degron [14], decreases substrate proteolysis by the TEV protease considerably if present at the P1' position [8]. Recently, random mutagenesis followed by a screen was performed to find a TEV protease variant with efficient proteolysis of the recognition sequence ENLYFQ-D [15], which is cleaved by the TEV protease *in vitro* and *in vivo* with intermediate to high efficiency, depending on the experimental conditions [5,8]. The TEV protease variant obtained by this screen was found to be less active against the recognition sequence ENLYFQ-S and showed slightly increased activity towards ENLYFQ-D [15].

A powerful genetic technique, which could be used to screen in yeast for TEV protease variants with specific properties, is the adenine auxotrophy-based red/white colony assay. Generation of a red pigment in the yeast vacuole can be observed visually in yeast colonies in this assay if the N-succinyl-5-aminoimidazole-4-carboxamide ribotide synthetase (Ade1) or the phosphoribosylaminoimidazole carboxylase (Ade2) is not functional. This screen has been used among many other purposes to identify genetic interactions, study chromosome stability, or examine protein function [16-18]. In most cases, assays used a procedure that indicated the presence of the *ADE1* or *ADE2* gene. However, we reasoned that it should be possible to use this assay in the context of the TIPI system to visualize protein stability, as it has been done for another degron as well [19].

Here, we report a detailed analysis of the influence of different amino acids at the P1' position of the recognition sequence on the processivity of a shortened TEV protease variant. Furthermore, we describe the development of an Ade2-based assay that can be used to search for protease mutants with changed substrate preference or for conditions that influence substrate proteolysis. Combining this procedure with random mutagenesis, we obtained a TEV protease variant with increased *in vivo* processivity of recognition sequences containing large, branched and positively charged amino acids at the P1' position. This TEV protease mutant showed almost no P1' position preference within the context of the TIPI system and might be a valuable tool for other experiments requiring site-directed proteolysis as well.

Results

In vivo proteolysis of substrates with different recognition sequences by the pTEV+ protease

First, we wanted to know to which extent different amino acids at the P1' position of the recognition sequence influence proteolytic activity of the pTEV+ protease, which has higher processivity due to removal of the last 8 amino acids and increased substrate affinity by the p14-SF3B155$^{381-424}$ domains. We expressed tester substrates (cyan fluorescent protein (CFP)-TDegX-red fluorescent protein(RFP); X = amino acid at the P1' position) containing all 20 fundamental amino acids at the P1' position in yeast cells and followed their proteolysis after induction of pTEV+ protease synthesis using the galactose-inducible *GAL1* promoter. We observed that only proline was not processed at all, presence of the other amino acids at this position led to complete or partial proteolysis. Such incomplete proteolysis was found for the constructs with arginine, isoleucine, leucine, lysine, or valine at the P1' position. In these cases full length CFP-TDegX-RFP was detected four hours after induction of pTEV+ protease production, whereas no full length tester substrate was observable for the other constructs. In general, a higher degree of proteolysis was obtained with smaller amino acids at the P1' position compared to larger amino acids, aromatic to aliphatic and negatively to positively charged ones (Figure 1B). The pattern we found is in good agreement with the data obtained with full-length TEV protease without a domain to increase substrate affinity [8].

To measure the combined effect of proteolytic efficiency and destabilization strength, we quantified the stability of the RFP part of the tester substrates after induction of pTEV+ protease production. This revealed that amino acids that are classified as stabilizing according to the "classical" view [10] showed only a slight decrease of RFP fluorescence. A similar decrease was also observed for the uncleavable CFP-TDegP-RFP substrate (Figure 1C), which suggests declined tester substrate synthesis at later time points. Due to the presence of histidine at the P2' position, no acetylation and subsequent destabilization via the Doa10 pathway is expected for these amino acids. Exposure of a destabilizing residue at the N-terminus resulted in complete depletion of X-RFP in most cases. To measure differences between the constructs, we calculated depletion efficiencies
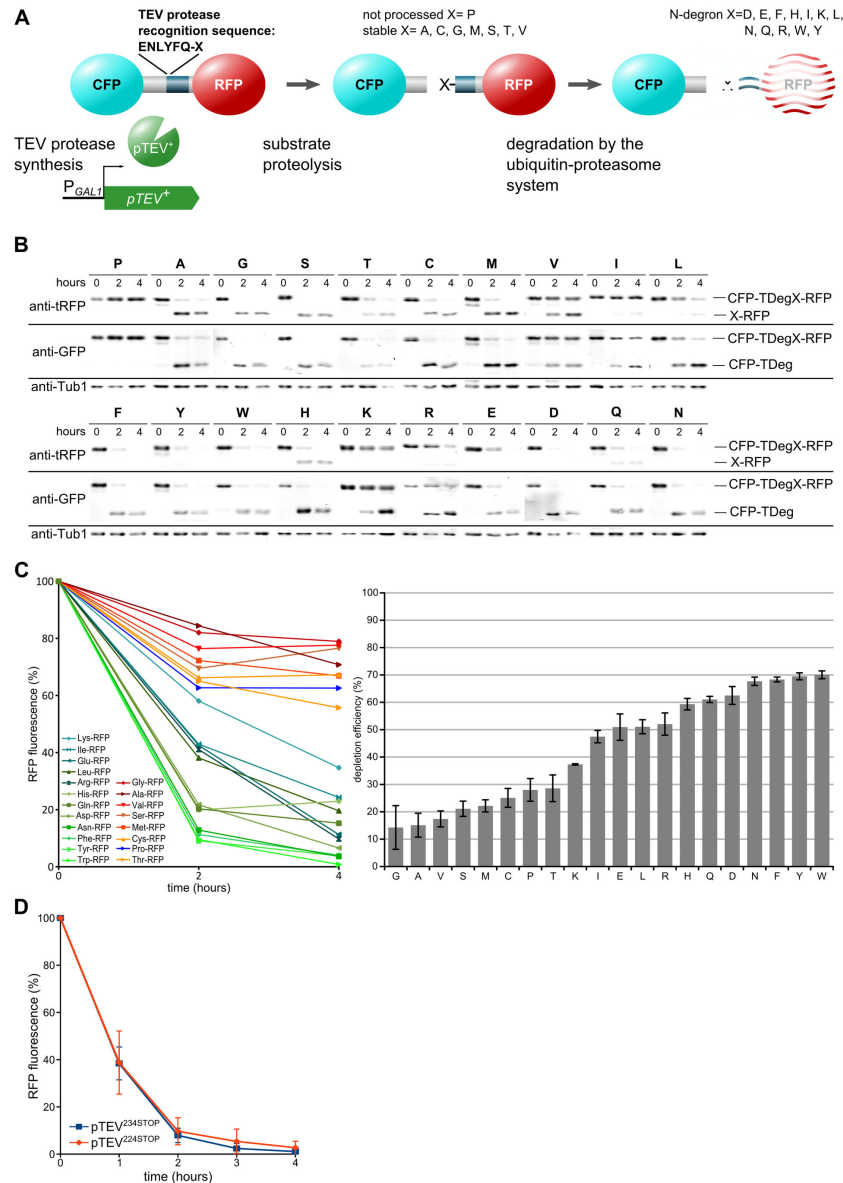
Figure 1. Activation of the N-degron is rate limiting during substrate depletion by the TIPI system. A) TIPI efficiency is influenced by three factors, synthesis of the TEV protease by the galactose-inducible *GAL1* promoter, proteolysis of the recognition sequence, and degradation of the target protein by the ubiquitin-proteasome system. A reporter protein consisting of two fluorescent proteins (cyan and red) fused together by the TDegX sequence containing the TEV protease recognition sequence (X= amino acid at position P1') and the N-degron sequence. Please note that we follow the original classification of stabilizing and destabilizing residues without considering N-degrons that are produced by N-acetylation. In our constructs, histidine follows X, which prevents acetylation of X in case of Met, Ala, Ser, Cys, Thr, and Val. **B)** *In vivo* analysis of the P1' specificity of the pTEV+ protease. Processing of the tester constructs CFP-TDegX-RFP (plasmid based) was observed after induction of pTEV+ protease production (P*GAL1*-*pTEV*+ in strain YCT1169) by addition of galactose (2% final concentration). Total cell extracts were fractionated by SDS-polyacrylamide electrophoresis, followed by immunoblotting with antibodies directed against GFP, tRFP and Tub1 (loading control). **C)** Quantification of X-RFP depletion. RFP fluorescence (same constructs as in B) was measured by a fluorimeter after induction of pTEV+ protease synthesis (left graph) and the depletion efficiency of the different substrates was calculated (right graph). Curves are mean values of at least four measurements, normalized to initial RFP fluorescence. Depletion efficiency is represented by the area above each curve (error bars: SEM). **D)** C-terminal truncation of the TEV protease at position 224 does not influence its activity. The abundance of the tester substrate CFP-TDegF-RFP was followed over time after expression of different *pTEV protease* variants by fluorimeter measurements (conditions as in C). The plasmid pDS7 was used to express the substrate in yeast strains YCT1243 and YCT1244; error bars represent standard deviation; each construct was measured at least five times.
doi: 10.1371/journal.pone.0067915.g001

60

that reflect how fast a substrate is processed and degraded. For most destabilizing amino acids at the P1' position, depletion efficiencies between 60 and 70% were reached (Figure 1C). Remarkably, the tertiary N-degron asparagine at the P1' position was found to be among the residues with highest depletion efficiency (Figure 1C), although the transformation of this amino acid into an N-degron requires two additional modifications after TEV protease cleavage [10]. Furthermore, we observed that constructs with lysine, isoleucine, leucine, glutamate, and arginine at the P1' position, which were processed by the pTEV+ protease with low efficiency (Figure 1B), exhibited depletion efficiencies around 50% or below (Figure 1C). The correlation between TEV protease cleavage and depletion efficiency as well as the high depletion efficiency of asparagine suggest that the rate-limiting step during substrate depletion is proteolysis by the TEV protease. Moreover, our analysis showed that the strongest N-degron (arginine) at the P1' position is severely disfavored for cleavage by the TEV protease. Next, we tested whether further shortening of the TEV protease (stop codon at position 224 of the TEV protease sequence compared to stop codon at position 234) would increase processivity of the protease. However, we found no difference between the two proteases towards TDegF containing substrates (Figure 1D) as well as substrates with TDegR and TDegP (data not shown).

Screen for a TEV protease variant with improved recognition of arginine at the P1' position

To increase the proteolysis rate of a TEV protease recognition sequence with arginine at the P1' position, we set up a screening procedure which allowed us to select for a TEV protease with efficient proteolysis of the recognition sequence ENLYFQ-R. We fused two variants of the bidirectional degron green fluorescent protein (GFP)-cODC1-TDegX-RFP (X=F, R) to the Ade2 enzyme which is necessary to produce adenine (Figure 2A). Upon induction of pTEV+ protease synthesis in these strains, the cells containing the phenylalanine construct showed an adenine auxotrophy phenotype. The cells were red on adenine-containing medium and unable to grow on adenine-free medium, whereas control cells or cells bearing the arginine construct were adenine prototroph (Figure 2B). This demonstrates that only efficient proteolysis of the degron construct induces depletion of the modified Ade2 and evokes the adenine auxotrophy phenotype. This clear Ade⁻ phenotype in cells bearing the TDegF construct indicated that screening for a TEV protease that efficiently processes the recognition sequence ENLYFQ-R might be possible.

We used PCR-based random mutagenesis and homologous recombination in yeast to generate a pool of plasmids containing *pTEV+ protease* mutants in the *ade2-GFP-cODC1-TDegR-RFP* strain. The plasmids of transformants which showed a red colony phenotype on TEV protease production-inducing galactose plates were rescued from yeast into *Escherichia coli*, retransformed and tested with a patch assay as well as immunoblotting for efficient Ade2 depletion (Figure 2C and data not shown). Plasmids of confirmed transformants were sequenced and used as template for further rounds of mutagenesis, in total about 1200 clones were screened. All of

the tested *pTEV+ protease* alleles, obtained from the last round, encoded for a protein with a single amino acid exchange. In these mutants, the arginine at position 345, which corresponds to R203 in the TEV protease sequence, was changed to glycine. The *ade2-GFP-cODC1-TDegR-RFP* strain transformed with a plasmid containing the R345G mutant was subjected to a serial dilution growth assay. The strain showed adenine auxotrophy upon production of the mutated protease, as expected (Figure 2D). This demonstrated that the chosen strategy to obtain a pTEV protease with efficient proteolysis of the recognition sequence ENLYFQ-R was successful. Subsequently, we will refer to this mutant version as pTEV2 protease.

P1'-dependent substrate selectivity of the pTEV2 protease

To test whether the pTEV2 protease has an altered substrate preference, we assessed the efficiency of proteolysis of all 20 fundamental amino acids at the position P1'. Again, we used the CFP-TDegX-RFP constructs to follow proteolysis. We found that all recognition sequences with amino acids other than proline at the P1' position were processed efficiently, most constructs were completely processed two hours after induction of pTEV2 synthesis. Substrates with aspartate, glutamate, isoleucine, threonine, and valine showed residual amounts of the full length tester construct after two hours, arginine and phenylalanine also after four hours (Figure 3A). In comparison to the results obtained with the pTEV+ protease, constructs with arginine, isoleucine, leucine, lysine or valine at the P1' position were cleaved more efficiently by the pTEV2 protease, indicating that the pTEV2 protease has lost almost all preference for the amino acid at the P1' position. The arginine-containing construct was moderately better cleaved by the pTEV2 protease, whereas the cleavage of the phenylalanine-containing construct was somewhat decreased (Figure 3B). Overall, we found that exchange of a single amino acid in the TEV protease resulted in improved proteolysis of substrates with aliphatic or positively charged amino acids at the P1' position of the TEV recognition sequence *in vivo*.

Moreover, we were interested to follow the fate of the X-RFP part upon production of the pTEV2 protease. We measured the RFP fluorescence of all 20 constructs and found no change in behavior for tester substrates bearing proline or stabilizing amino acids at the P1' position. However, several constructs containing destabilizing residues were depleted much faster upon induction of pTEV2 protease synthesis; their depletion rates were now much more similar to each other. Tyrosine or asparagine at the P1' position induced fastest depletion, whereas substrates with glutamate or isoleucine were slowest. Constructs with the other destabilizing amino acids induced efficient depletion within two to three hours, especially leucine, lysine and arginine were improved considerably (Figure 3C). Our measurements with the CFP-TDegX-RFP substrates revealed that the pTEV2 protease allows generation of some N-degrons with much higher efficiency.

Structural analysis of Ubr1 has revealed that a leucine instead of a histidine at the P2' position is favored for recognition of type 1 substrates by the UBR box present in
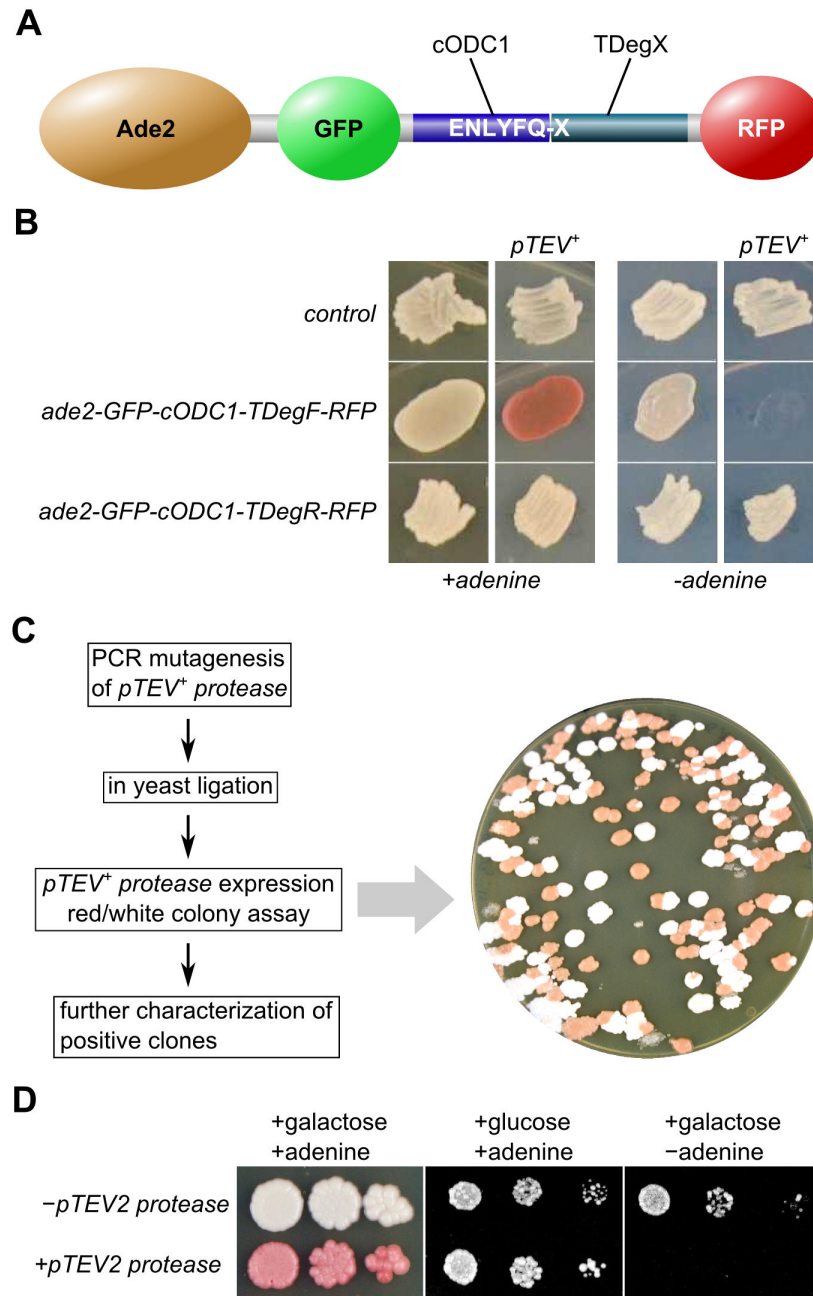
Figure 2. Generation of a TEV protease that cleaves efficiently the recognition sequence ENLYFQ-R. A) Scheme of the construct used for the screening procedure: The bidirectional degron module GFP-cODC1-TDegX-RFP (X = F or R) was fused to the phosphoribosylaminoimidazole carboxylase Ade2. Cleavage by the TEV protease leads to activation of the C-degron cODC1 and the N-degron TDegX resulting in proteasomal degradation of Ade2-GFP-cODC1 as well as TDegX-RFP. **B**) Test for adenine biosynthesis in cells bearing different degron constructs fused chromosomally to *ADE2*. The yeast strains (ESM356-1, YCT1266, and YCR8) were grown in patches on solid media (YPD, YP+galactose, yeast nitrogen base + 2% glucose, and yeast nitrogen base + 2% galactose; from left to right). **C**) Scheme illustrating the mutagenesis and selection procedure to obtain a TEV protease which efficiently processes the recognition sequence ENLYFQ-R (left side). The plate is an example to show the difference in color of clones with efficient proteolysis of ENLYFQ-R (red colonies) and clones with insufficient proteolysis (white colonies). Please note that the high degree of red colonies was obtained because the R345G mutant was generated already in the first round of mutagenesis and enriched in subsequent rounds. **D**) Expression of *pTEV2 protease* (plasmid-based, R345G mutant) using the *GAL1* promoter induces the adenine auxotrophy phenotype in *ade2-GFP-cODC1-TDegR-RFP* cells (YCR6). Serial dilutions (1:10) were grown on solid media as in B.

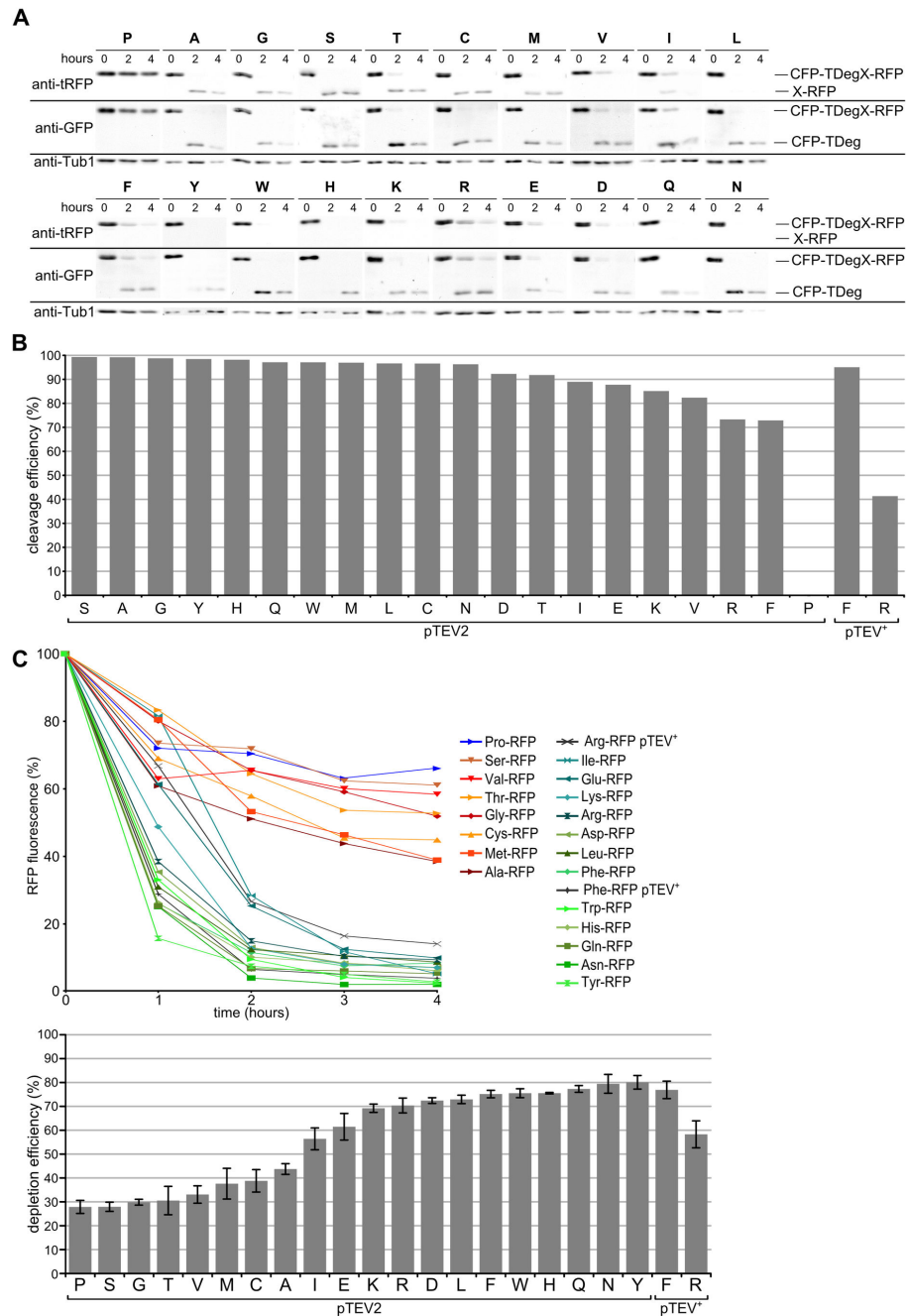doi: 10.1371/journal.pone.0067915.g002

62

Figure 3. *In vivo* analysis of the P1' Specificity of the pTEV2 protease. A) Processing of the tester constructs CFP-TDegX-RFP (plasmid encoded) was observed after induction of pTEV2 protease production (P_{GAL1}-*pTEV2* in yeast strain YCR56). Conditions as in Figure 1B. **B**) Quantification of the P1' Specificity of the pTEV2 protease. Decrease of full length tester construct after two hours was normalized to initial values and relative efficiency normalized to proline was calculated (cleavage efficiency = ($[X]_{2h}/[Pro]_{2h}$×100-100) ×(−1)), assuming that the recognition sequence with proline at the P1' Position is not cleaved at all. For each construct two immunoblotting experiments were quantified. Values for constructs with Arg and Phe at the P1' Position cleaved by the pTEV+ protease obtained at the same time are shown as reference. Yeast strains YCR56 (pTEV2 protease production) or YCT1169 (pTEV+ protease production) harboring plasmid-based constructs were used for the measurements. **C**) Quantification of X-RFP depletion. The RFP fluorescence was analyzed by fluorimeter measurements after induction of pTEV2 protease synthesis (upper graph, conditions as in Figure 1C) and the depletion efficiency was calculated (error bars: SEM of at least three experiments). Same constructs as in B. The difference between the arginine construct cleaved by pTEV2 and pTEV+ protease is very significant (unpaired t test; p = 0.007).
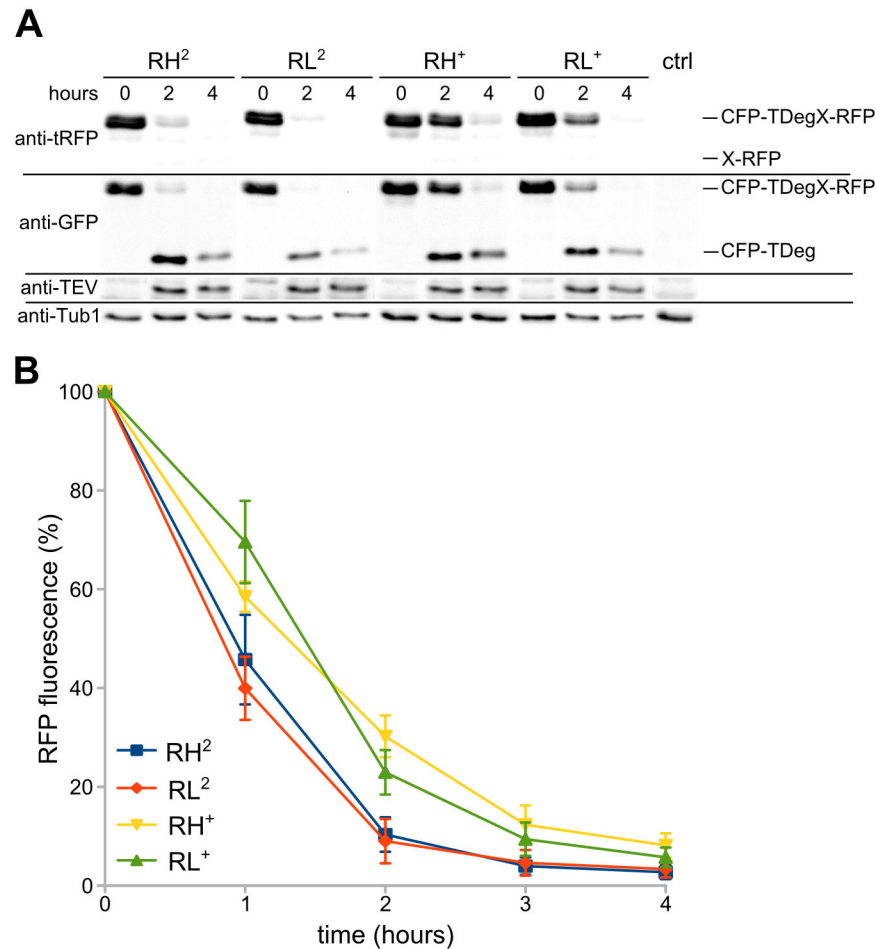
doi: 10.1371/journal.pone.0067915.g003

Figure 4. Influence of the P2' residue on substrate degradation. A) Analysis of tester construct proteolysis and depletion as well as TEV protease production by immunoblotting. Tester constructs (plasmid based): CFP-TDegXY-RFP, XY=RH, RL, X corresponds to the P1' position, Y to the P2' position; proteases: pTEV+ (yeast strain YCT1169), pTEV2 (YCR56). Conditions as in Figure 1B; antibodies directed against tRFP, GFP, TEV, and Tub1 (loading control) were used to obtain the immunoblot. **B)** The RFP fluorescence of the tester constructs CFP-TDegXY-RFP was followed over time after induction of TEV protease synthesis by fluorimeter measurements (three measurements for each construct; error bars indicate the standard error of the mean; same constructs as in A).

Ubr1 [20]. Therefore, we assessed whether we could further improve depletion efficiency of the construct with arginine at the P1' position by a change of the P2' position. The TEV protease recognition sequence in the CFP-TDegR-RFP tester substrate was changed from ENLYFQ-R**H** to ENLYFQ-R**L** and substrate behavior after induction of protease production was measured. First, we analyzed proteolysis of the RH and RL constructs by both proteases, but did not find a striking difference. Furthermore, the experiment showed that increased proteolysis of the RH and RL constructs by the pTEV2 protease is not due to increased protease production, as protein levels were comparable for both proteases (Figure 4A). Then, we measured depletion of the RFP part of the construct. Again, we did not observe a significant change in depletion of the RL-containing constructs upon proteolysis of the substrates

by the pTEV+ or pTEV2 protease (Figure 4B). These results strengthen the view that proteolysis by the TEV protease is the rate limiting step during substrate degradation by the TIPI system. The only exceptions might be substrates with glutamate or isoleucine at the P1' position, which are cleaved better by the pTEV2 protease than arginine or phenylalanine-containing substrates (Figure 3B), but which showed a lower depletion efficiency (Figure 3C). Indeed, glutamate and isoleucine have been categorized as the weakest N-degrons [14].

Predicted structural impact of the R203G mutation

Finally, we were interested to know whether the R203G mutation has a structural impact on the TEV protease that could explain the changes in substrate preferences. We
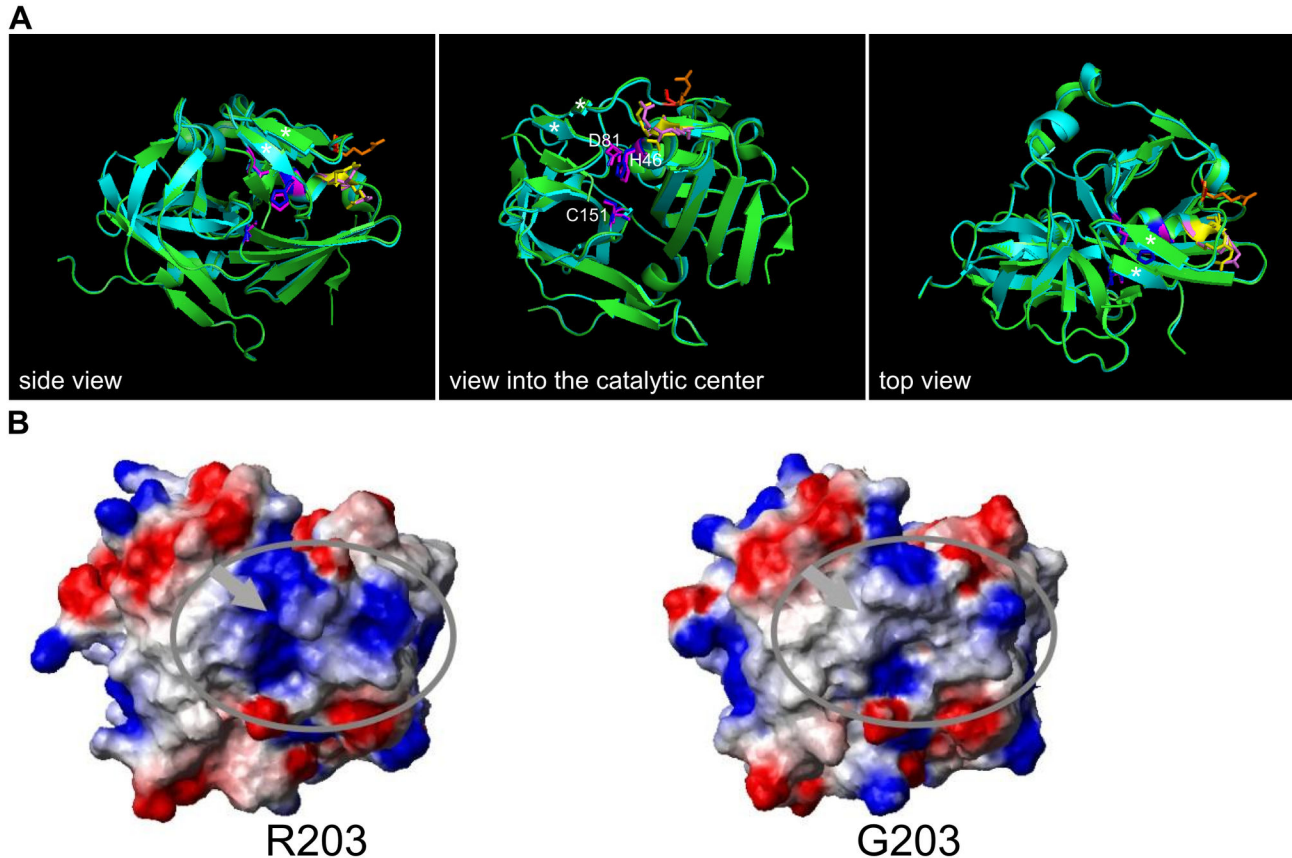
64

Figure 5. Structural comparison of the TEV protease with the R203G mutant. A) Ribbon structure of the TEV protease (green) was overlaid with the mutant (dark cyan). The structure of the R203G mutant, which corresponds to R345G in the pTEV+ protease, was obtained by homology modeling using an x-ray structure of the TEV protease as template. Views from three different sides are shown. The residues of the catalytic triad H46, D81, and C151 are indicated (TEV protease: blue; mutant: magenta). The two arginine residues close to the catalytic center (R49, R50) are shown in yellow (TEV protease) and light magenta (G203 mutant). The R203 residue is shown in orange, the G203 in red. The two β-sheets, which are mentioned in the text that close the catalytic center are marked by asterisks. **B**) Surface charge distribution of the TEV protease compared to the R203G mutant. Surface charges were calculated using the software package MolMol. Positive charge is represented by blue color, negative charge by red color.
doi: 10.1371/journal.pone.0067915.g005

generated a homology model of the R203G mutant using the published structure of the TEV protease [21]. This revealed no obvious difference within the structure. The mutated residue R203 is located quite far from the catalytic center; it is part of a loop near the C-terminus connecting two beta-sheets with the core of the protease. These two beta-sheets are part of a lid-like structure which is closing the catalytic grove. Subsequently, we performed molecular docking of peptides containing different recognition sequences with the TEV protease and the R203G mutant, but no striking differences were observed concerning binding of the peptides or hydrogen bond formation to residues forming the catalytic center (data not shown). However, we noticed that two arginines (R49, R50) are located between the catalytic center and R203 (Figure 5A). Together, these three residues might create a positively charged surface patch, whereas the R203G mutant would decrease the charge in this area. Indeed, electrostatic surface

calculations predicted that the positive charge is reduced in the mutant in this area (Figure 5B), which might allow easier access of a substrate with a positively charged amino acid at the P1' position to the catalytic center.

Discussion

Here, we studied in detail the usability of the TEV protease as a tool to generate N-degrons for protein destabilization. We found that substrates with the aromatic amino acids phenylalanine, tyrosine and tryptophan or the tertiary N-degron glutamine at the P1' position of the recognition sequence show quickest depletion kinetics among the 20 tested substrates. Furthermore, we present a screening procedure depending on the destabilization of Ade2. This allowed us to select a TEV protease variant that showed, within the context of the TIPI system, a higher *in vivo* processivity of branched aliphatic and

Ubiquitin fusion technique, pulse chase measurement:
R > K D N F W L > Q H Y > E I > P C A M V G S T

Ubiquitin fusion technique, fluorescent timer-based measurement:
R > K > D > Q > N > F > W > L > H > E > Y > P > I > C > A > M > V > G > S > T

TIPI system, fluorescence-based measurement:
Y > N > Q > H > W > F > L > D > R > K > E > I > A > C > M > V > T > G > S > P

primary, secondary, tertiary destabilizing residue
stabilising residue according to classical classification

Figure 6. Comparison of the apparent N-degron strength generated and measured by different methods. Apparent N-degron strength ordered from high to low destabilizing activity. Pulse chase data were obtained by Bachmaier et al., 1989, fluorescent timer-based measurements by Khmaelinski et al., 2012, fluorescence-based measurements during this study. A color code indicates whether an amino acid is a primary (dark cyan), secondary (blue) or tertiary (red) destabilizing residue at the amino-terminus of a protein, or if it is stabilizing (gold) in the absence of N-acetylation.
doi: 10.1371/journal.pone.0067915.g006

positively charged amino acids at position P1'. Structural analysis suggested that better accessibility of the active site might be responsible for the increased substrate tolerance of the mutated TEV protease. This TEV protease variant might be useful to generate peptides or proteins carrying specific amino acids at the N-terminus by site-specific proteolysis.

It is interesting to compare the apparent strength of N-degrons generated by the TIPI system or the ubiquitin fusion technique [22]. The same amino acids seem to destabilize quite differently (Figure 6), depending on the method used to measure the half life and the way the N-degron is generated. A possible explanation is that in one or both of the methods the rate-limiting step is not the recognition of the N-degron but its generation. Such a view is supported by the observation that Ubr1 binds peptides having arginine or phenylalanine at the N-terminus with the same affinity *in vitro* [23] as well as by our observation that changing the amino acid at the P2' position to leucine, which increases the affinity of the active N-degron with Ubr1, does not enhance tester protein depletion. Moreover, the differences in depletion efficiency we found for the tester substrates with destabilizing amino acids activated by the pTEV2 protease were not very pronounced and can be explained at least in part by differences in cleavage efficiency. This is best seen for the amino acids glutamate and glutamine. No matter if the ubiquitin fusion technique or the TIPI system is used, glutamine always appears to be the stronger N-degron over glutamate (Figure 6), although glutamine needs to be converted to glutamate before arginylation creates the species recognized by Ubr1. The TIPI system makes it possible to detect the relation between cleavage and degradation efficiency, as the uncleaved species is stable, whereas the ubiquitin fusion technique destabilizes the uncleaved species via the ubiquitin fusion degradation pathway [24].

Notably, shortening of the TEV protease and addition of the p14-SF3B155[381-424] interaction domains did not change the specificity of the TEV protease. The activity gain observed in the variant with shortened C-terminus originates most likely from release of auto-inhibition due to absence of the very C-terminal located TEV protease recognition sequence [13]. But, the increased processivity of the variant with the interaction domains can be assumed to stem from prolonged protease-substrate interaction. The finding that both changes do not influence the selectivity of the TEV protease towards its substrate strengthen the view that size and structure of the catalytic center govern substrate preference of the TEV protease [25].

Unclear is how many amino acids after the autolysis-site 219 have to be present for full activity of the protease. The amino acids from 221 to 235 have intrinsic flexibility and were not found in the x-ray structures [13,21], but at least a few of these residues are essential for TEV protease activity. Removing the C-terminus up to position 219 leads to almost complete loss of proteolytic activity [26,27], whereas truncation after position 224 resulted in a fully active protease *in vivo*. Although highly flexible, these residues might be important for the correct folding of two beta-strands near the C-terminus that form a kind of lid which closes the catalytic center.

Our screen resulted in a pTEV protease variant that is almost insensitive to changes at the P1' position of the recognition sequence within the context of the TIPI system. Our analysis revealed that for the TIPI system, a TEV protease recognition site with tyrosine or glutamine at position P1' induces depletion of the substrate with highest efficiency. However, the latter residue might not be ideal in all circumstances; glutamine is a tertiary N-degron that requires the efficient execution of two additional enzymatic reactions before the N-degron is recognized by Ubr1. These steps might not always be executed efficiently during a developmental process or in all cell types.

Even though the pTEV2 protease has an extended substrate tolerance, we did not find negative effects of high pTEV2 protease production in yeast. Additionally, the modified

Table 1. Yeast strains used in this study.

Name	Genotype	Source
ESM356-1	*MATa ura3-53 leu2Δ1 his3Δ200 trp1Δ63*	[35]
YCT1169	ESM356 *ura3::P$_{GAL1}$-p14^{D122Y}-TEV^{234STOP}::kanMX*	[5]
YCT1243	ESM356 *ura3::P$_{GAL1}$-p14^{D122Y}-myc-TEV^{234STOP}::kanMX*	This study
YCT1244	ESM356 *ura3::P$_{GAL1}$-p14^{D122Y}-myc-TEV^{224STOP}::kanMX*	[9]
YCR56	ESM356 *ura3::P$_{GAL1}$-p14^{D122Y}-TEV$^{R203G\ 234STOP}$::kanMX*	This study
YCT1266	YCT1169 *ADE2-GFP-cODC1-TDegF-mKate::hphNT1*	This study
YCR8	YCT1169 *ADE2-GFP-cODC1-TDegR-mKate::hphNT1*	This study
YCR6	ESM356 *ADE2-GFP-cODC1-TDegR-mKate::hphNT1*	This study

protease might not only be useful for *in vivo* applications, also *in vitro* applications might benefit from it. Due to the substrate extension, peptides or proteins with a defined N-terminal amino acid might be produced in higher yields and/or using less TEV protease.

Recently, a random mutagenesis-based approach has been undertaken to increase the processivity of the TEV protease towards the recognition sequence ENLYFQ-D, which is cleaved in bacterial cells with moderate efficiency. In this study, three related TEV protease mutants with up to 14 amino acid exchanges were found. These enzymes displayed enhanced activity towards the non-native substrate combined with decreased proteolysis of the canonical recognition sequence ENLYFQ-S [15]. Most of the mutations are quite far from the catalytic center, which suggests that the substrate selectivity of the TEV protease can be influenced by small changes in the whole protein. Interestingly, one of the mutations, which is present in two of the mutants, is near the catalytic center (R50K) and quite close to the arginine 203, which was mutated to a glycine in case of the pTEV2 protease. Although the amino acids present at the P1' position in the two screens are quite different (aspartate versus arginine), it is tempting to speculate that the electrostatic surface in this region of the protease has an important influence on substrate selectivity. Indeed, bioinformatic analysis of the chymotrypsin family of serine proteases, which is related to the family of 3C cysteine proteases the TEV protease belongs to [28], has shown that substrate specificity is conferred by the catalytic cleft and neighboring surface loops that are thought to stabilize the specific fold of the substrate binding pocket [29].

The selection procedure we developed allows in principle to customize substrate selection by any protease that can be expressed in yeast without toxic effects. Several other selection procedures have been developed in bacteria or yeast previously [15,25,30-33]. Compared to these selection procedures, the Ade2-based assay offers two *in vivo* selection methods (growth/non-growth on adenine-free medium or appearance of red color on adenine-containing medium), which allows a certain flexibility in the set-up of the screen. Importantly, no toxic compound has to be added to the cells, as it is the case for yeast methods based on uracil auxotrophy/5-FOA resistance [34]. Yet, the selection procedures using Ura3 and Ade2 could also be combined to screen for two different selection criteria simultaneously. In principle, the screening procedure can also be reversed to search for protease inhibitors or protease-inhibiting peptides. It might be feasible to exchange the TEV protease with another viral protease and use the adenine-based screening to search in yeast cells for compounds that decrease protease activity.

Materials and Methods

Yeast strains, growth conditions and plasmids

The *Saccharomyces cerevisiae* strains are derivatives of the S288C strain ESM356 [35]. All strains are listed with their relevant genotypes in Table **1**. Standard preparations of media were used for growth [36]; low-fluorescence medium [37] was used to grow yeast cells for fluorimeter measurements. Yeast strains with chromosomally encoded *ADE2-GFP-cODC1-TDegF-RFP* and *ADE2-GFP-cODC1-TDegR-RFP* were constructed using PCR products [38] obtained with pCT314 and pCR20 as template, respectively. Yeast transformations with plasmids and PCR products were performed using the lithium acetate method [39].

Plasmids were constructed by standard procedures [40], details and sequences of the used vectors are available on request; plasmids are listed in Table **2**. Serial dilution experiments were performed as described [9] with minimal or complex medium supplemented with glucose or galactose. The expression of the pTEV protease variants is repressed on glucose and induced on galactose containing medium. Images were taken with a Canon Powershot A620 digital camera.

Immunoblotting and calculation of pTEV2 protease cleavage efficiency

Immunoblotting experiments were performed as described using antibodies directed against GFP (Santa Cruz biotechnology, Santa Cruz, USA), tRFP (Biocat, Heidelberg, Germany), TEV protease (a kind gift of M. Ehrmann, (University of DuisburgEssen), tubulin (a kind gift of M. Knop, University of Heidelberg), and HRPO-coupled antibodies directed against mouse or rabbit IgG (Santa Cruz biotechnology, Santa Cruz, USA). The pTEV2 protease cleavage efficiency for the different amino acids at the P1' position was measured using immunoblots. The amount of full-length tester substrate was measured for each construct at the different time points and normalized to initial amounts (=100%). These values were normalized to proline (=no cleavage) to generate the graph.

Quantitative fluorescence measurements

The RFP fluorescence was measured in yeast as follows. Cells were grown in liquid low fluorescence medium supplemented with 2% raffinose until the logarithmic growth phase was reached. Galactose (2% final concentration) was added to the cultures after removal of the first sample (t=0 hours) to induce protease production. Equal amounts of cells were taken at the indicated time points, treated with sodium azide (10 mM final concentration), and stored on ice until the end of the assay. Finally, samples were transferred to a black, flat-bottom 96-well microtiter plate (Greiner Bio-One, Germany) and the RFP fluorescence was measured with a microplate

Table 2. Plasmids used in this study.

Name	Features	Source
pRS414	*TRP1 ARS/CEN*	[41]
pDS7	P$_{ADH1}$-*yeCFP-TDegF-mKATE* in pRS414	[5]
pDS18	P$_{ADH1}$-*yeCFP-TDegM-mKATE* in pRS414	[5]
pDS21-L	P$_{ADH1}$-*yeCFP-TDegL-mKATE* in pRS414	This study
pDS21-N	P$_{ADH1}$-*yeCFP-TDegN-mKATE* in pRS414	This study
pDS21-P	P$_{ADH1}$-*yeCFP-TDegP-mKATE* in pRS414	This study
pDS21-E	P$_{ADH1}$-*yeCFP-TDegE-mKATE* in pRS414	This study
pDS21-K	P$_{ADH1}$-*yeCFP-TDegK-mKATE* in pRS414	This study
pDS21-T	P$_{ADH1}$-*yeCFP-TDegT-mKATE* in pRS414	This study
pDS21-S	P$_{ADH1}$-*yeCFP-TDegS-mKATE* in pRS414	This study
pDS21-G	P$_{ADH1}$-*yeCFP-TDegG-mKATE* in pRS414	This study
pDS21-Y	P$_{ADH1}$-*yeCFP-TDegY-mKATE* in pRS414	This study
pDS21-C	P$_{ADH1}$-*yeCFP-TDegC-mKATE* in pRS414	This study
pDS21-I	P$_{ADH1}$-*yeCFP-TDegI-mKATE* in pRS414	This study
pDS21-R	P$_{ADH1}$-*yeCFP-TDegR-mKATE* in pRS414	This study
pDS21-W	P$_{ADH1}$-*yeCFP-TDegW-mKATE* in pRS414	This study
pDS21-D	P$_{ADH1}$-*yeCFP-TDegD-mKATE* in pRS414	This study
pDS31	P$_{ADH1}$-*yeCFP-TDegH-mKATE* in pRS414	This study
pDS33	P$_{ADH1}$-*yeCFP-TDegV-mKATE* in pRS414	This study
pDS30	P$_{ADH1}$-*yeCFP-TDegA-mKATE* in pRS414	This study
pDS32	P$_{ADH1}$-*yeCFP-TDegQ-mKATE* in pRS414	This study
pCR41	P$_{ADH1}$-*yeCFP-TDegRL-mKATE* in pRS414	This study
pRS313	*HIS3 ARS/CEN*	[41]
pCT310	P$_{GAL1}$-*YFP-p14^{D122Y}-TEV^{234STOP}* in pRS313	This study
pRS41N	*natNT2 ARS/CEN*	[42]
pCR30X2	P$_{GAL1}$-*GFP-p14^{D122Y}-TEV$^{R203G\ 234STOP}$* in pRS41N	This study
pFA6a-hphNT1	*hphNT1*	[38]
pCT314	*GFP-cODC1-TDegF-mKate::hphNT1* in pFA6a-hphNT1	[9]
pCR20	*GFP-cODC1-TDegR-mKate::hphNT1* in pFA6a-hphNT1	This study
pDS15	*ura3::kanMX::*P$_{GAL1}$-*p14^{D122Y}-myc-TEV^{234STOP}* in pRS306K	[9]
pDS28	*ura3::kanMX::*P$_{GAL1}$-*p14^{D122Y}-myc-TEV^{224STOP}* in pRS306K	This study
pCR40	*ura3::kanMX::*P$_{GAL1}$-*p14^{D122Y}-TEV$^{R203G\ 234STOP}$* in pRS306K	This study
pCR29	P$_{GAL1}$-*GFP-p14^{D122Y}-TEV^{234STOP}* in pRS41N	This study
pCR39X20	P$_{GAL1}$-*GFP-p14^{D122Y}-TEV^{234STOP}* in pGREG566	This study
pGREG566	P$_{GAL1}$-*GFP::HIS3 kanMX URA3 ARS/CEN*	[43]

reader (Safire, TECAN, Crailsheim, Germany). Excitation conditions: 10 flashes of light with a wavelength of 555 nm; fluorescence was observed at a wavelength of 585 nm. Depletion efficiency was obtained from the mean curve by calculating the area above each curve. A depletion efficiency of 100% would be correlating to a curve with 0% RFP fluorescence at all time points, a depletion efficiency of 0% would be a curve with 100% RFP fluorescence at all time points. The higher the value for the depletion efficiency, the faster the construct is depleted from the cell.

References

Generation of pTEV⁺ protease variants and red/white colony assay

Random mutagenesis of the pTEV⁺ protease was performed by standard procedure [40]. The mutagenic PCR was performed with taq polymerase in the presence of different manganese chloride concentrations (0 mM, 0.62 mM, and 1.25 mM) and a two-fold excess of dCTP and dTTP. In the first two rounds of mutagenesis, the plasmid pCT310 was used as template and the oligos p14end_for (TGTACTATAATGCCAACAGGG) and rec2-seq (GCGTGACATAACTAATTACATG) for PCR. Homologous recombination in yeast was used to clone the mutagenized PCR product into the *TEV protease* expression vector pCR29. A third round of mutagenesis was performed using the best performing clone of the first two screens (plasmid pCR30X2) as template and the oligos rec1_p14_tev (GAATTCGATATCAAGCTTATCGATACCGTCGACAATGGCGATGCAAGCGGCC) and rec2_p14_TEV234stop (GCGTGACATAACTAATTACATGACTCGAGGTCGACCTTACAATTGAGTCGCTTCC). Again, homologous recombination was used to clone the PCR product into plasmid pGREG566 [43] to obtain the *pTEV2 protease* expressing plasmid pCR39X20. The yeast transformants of each screening round were grown on non-inducing, selective medium (yeast extract peptone dextrose (YPD) containing 100 µg/ml Nourseothricin (pCR29) or 200 µg/ml Geneticin (pGREG566)). After two days at 30 °C, transformants were replicated on yeast extract peptone (YP) +galactose plates and incubated for two more days at 30 °C to induce the red colony phenotype. Development of dark-red colonies required additional incubation of the plates at 4 °C for several days. In total, about 1200 clones were screened in the red/white colony assay. After each round of mutagenesis, plasmids of positive clones were rescued in *E. coli*, retransformed into the yeast strain YCR6 and tested by a patch assay (as shown in Figure 2B) and immunoblotting for efficient Ade2-GFP-cODC1-TDegR-RFP depletion. Plasmids of confirmed positive clones were selected for sequencing. Positive clones obtained in the last round of mutagenesis were tested in a serial dilution growth test (Figure 2D).

Author Contributions

Conceived and designed the experiments: CR RS CT. Performed the experiments: CR RS CT. Analyzed the data: CR RS CT. Contributed reagents/materials/analysis tools: CR CT. Wrote the manuscript: CR RS CT.

1. Waugh DS (2011) An overview of enzymatic reagents for the removal of affinity tags. Protein Expr Purif 80: 283-293. doi:10.1016/j.pep. 2011.08.005. PubMed: 21871965.

2. Henrichs T, Mikhaleva N, Conz C, Deuerling E, Boyd D et al. (2005) Target-directed proteolysis at the ribosome. Proc Natl Acad Sci U S A 102: 4246-4251. doi:10.1073/pnas.0408520102. PubMed: 15784745.

3. Gavin AC, Bösche M, Krause R, Grandi P, Marzioch M et al. (2002) Functional organization of the yeast proteome by systematic analysis of protein complexes. Nature 415: 141-147. PubMed: 11805826.

4. Pauli A, Althoff F, Oliveira RA, Heidmann S, Schuldiner O et al. (2008) Cell-type-specific TEV protease cleavage reveals cohesin functions in Drosophila neurons. Dev Cell 14: 239-251. doi:10.1016/j.devcel. 2007.12.009. PubMed: 18267092.

5. Taxis C, Stier G, Spadaccini R, Knop M (2009) Efficient protein depletion by genetically controlled deprotection of a dormant N-degron. Mol Syst Biol 5: 267. PubMed: 19401679.

6. Wehr MC, Laage R, Bolz U, Fischer TM, Grünewald S et al. (2006) Monitoring regulated protein-protein interactions using split TEV. Nat Methods 3: 985-993. doi:10.1038/nmeth967. PubMed: 17072307.

7. Adams MJ, Antoniw JF, Beaudoin F (2005) Overview and analysis of the polyprotein cleavage sites in the family Potyviridae. Mol Plant Pathol 6: 471-487. doi:10.1111/j.1364-3703.2005.00296.x. PubMed: 20565672.

8. Kapust RB, Tözsér J, Copeland TD, Waugh DS (2002) The P1' specificity of tobacco etch virus protease. Biochem Biophys Res Commun 294: 949-955. doi:10.1016/S0006-291X(02)00574-0. PubMed: 12074568.

9. Jungbluth M, Renicke C, Taxis C (2010) Targeted protein depletion in Saccharomyces cerevisiae by activation of a bidirectional degron. BMC Syst Biol 4: 176. doi:10.1186/1752-0509-4-176. PubMed: 21190544.

10. Varshavsky A (2011) The N-end rule pathway and regulation by proteolysis. Protein Sci 20: 1298-1345. doi:10.1002/pro.666. PubMed: 21633985.

11. Hwang CS, Shemorry A, Varshavsky A (2010) N-terminal acetylation of cellular proteins creates specific degradation signals. Science 327: 973-977. doi:10.1126/science.1183147. PubMed: 20110468.

12. Hoyt MA, Coffino P (2004) Ubiquitin-free routes into the proteasome. Cell Mol Life Sci 61: 1596-1600. PubMed: 15224184.

13. Nunn CM, Jeeves M, Cliff MJ, Urquhart GT, George RR et al. (2005) Crystal structure of tobacco etch virus protease shows the protein C terminus bound within the active site. J Mol Biol 350: 145-155. doi: 10.1016/j.jmb.2005.04.013. PubMed: 15919091.

14. Bachmair A, Finley D, Varshavsky A (1986) In vivo half-life of a protein is a function of its amino-terminal residue. Science 234: 179-186. doi: 10.1126/science.3018930. PubMed: 3018930.

15. Verhoeven KD, Altstadt OC, Savinov SN (2012) Intracellular detection and evolution of site-specific proteases using a genetic selection system. Appl Biochem Biotechnol 166: 1340-1354. doi:10.1007/s12010-011-9522-6. PubMed: 22270548.

16. McGrew JT, Xiao ZX, Fitzgerald-Hayes M (1989) Saccharomyces cerevisiae mutants defective in chromosome segregation. Yeast 5: 271-284. doi:10.1002/yea.320050407. PubMed: 2675488.

17. Flaman JM, Frebourg T, Moreau V, Charbonnier F, Martin C et al. (1995) A simple p53 functional assay for screening cell lines, blood, and tumors. Proc Natl Acad Sci U S A 92: 3963-3967. doi:10.1073/pnas.92.9.3963. PubMed: 7732013.

18. Barbour L, Xiao W (2006) Synthetic lethal screen. Methods Mol Biol 313: 161-169. PubMed: 16118433.

19. Renicke C, Schuster D, Usherenko S, Essen LO, Taxis C (2013) A LOV2 domain-based optogenetic tool to control protein degradation and cellular function. Chem Biol 20: 619-626. doi:10.1016/j.chembiol. 2013.03.005. PubMed: 23601651.

20. Choi WS, Jeong BC, Joo YJ, Lee MR, Kim J et al. (2010) Structural basis for the recognition of N-end rule substrates by the UBR box of ubiquitin ligases. Nat Struct Mol Biol 17: 1175-1181. doi:10.1038/nsmb. 1907. PubMed: 20835240.

21. Phan J, Zdanov A, Evdokimov AG, Tropea JE, Peters HK 3rd et al. (2002) Structural basis for the substrate specificity of tobacco etch virus protease. J Biol Chem 277: 50564-50572. doi:10.1074/jbc.M207224200. PubMed: 12377789.

22. Varshavsky A (2005) Ubiquitin fusion technique and related methods. Methods Enzymol 399: 777-799. doi:10.1016/S0076-6879(05)99051-4. PubMed: 16338395.

23. Xia Z, Webster A, Du F, Piatkov K, Ghislain M et al. (2008) Substrate-binding sites of UBR1, the ubiquitin ligase of the N-end rule pathway. J Biol Chem 283: 24011-24028. doi:10.1074/jbc.M802583200. PubMed: 18566452.

24. Johnson ES, Ma PC, Ota IM, Varshavsky A (1995) A proteolytic pathway that recognizes ubiquitin as a degradation signal. J Biol Chem 270: 17442-17456. doi:10.1074/jbc.270.29.17442. PubMed: 7615550.

25. Sun P, Austin BP, Tözsér J, Waugh DS (2010) Structural determinants of tobacco vein mottling virus protease substrate specificity. Protein Sci 19: 2240-2251. doi:10.1002/pro.506. PubMed: 20862670.

26. Parks TD, Howard ED, Wolpert TJ, Arp DJ, Dougherty WG (1995) Expression and purification of a recombinant tobacco etch virus NIa proteinase: biochemical analyses of the full-length and a naturally occurring truncated proteinase form. Virology 210: 194-201. doi: 10.1006/viro.1995.1331. PubMed: 7793070.

27. Kapust RB, Tözsér J, Fox JD, Anderson DE, Cherry S et al. (2001) Tobacco etch virus protease: mechanism of autolysis and rational design of stable mutants with wild-type catalytic proficiency. Protein Eng 14: 993-1000. doi:10.1093/protein/14.12.993. PubMed: 11809930.

28. Gorbalenya AE, Donchenko AP, Blinov VM, Koonin EV (1989) Cysteine proteases of positive strand RNA viruses and chymotrypsin-like serine proteases. A distinct protein superfamily with a common structural fold. FEBS Lett 243: 103-114. doi:10.1016/0014-5793(89)80109-7. PubMed: 2645167.

29. Süel GM, Lockless SW, Wall MA, Ranganathan R (2003) Evolutionarily conserved networks of residues mediate allosteric communication in proteins. Nat Struct Biol 10: 59-69. doi:10.1038/nsb881. PubMed: 12483203.

30. Cottier V, Barberis A, Lüthi U (2006) Novel yeast cell-based assay to screen for inhibitors of human cytomegalovirus protease in a high-throughput format. Antimicrob Agents Chemother 50: 565-571. doi: 10.1128/AAC.50.2.565-571.2006. PubMed: 16436711.

31. Kim SY, Park KW, Lee YJ, Back SH, Goo JH et al. (2000) In vivo determination of substrate specificity of hepatitis C virus NS3 protease: genetic assay for site-specific proteolysis. Anal Biochem 284: 42-48. doi:10.1006/abio.2000.4662. PubMed: 10933854.

32. O'Loughlin TL, Greene DN, Matsumura I (2006) Diversification and specialization of HIV protease function during in vitro evolution. Mol Biol Evol 23: 764-772. doi:10.1093/molbev/msj098. PubMed: 16423863.

33. Sices HJ, Kristie TM (1998) A genetic screen for the isolation and characterization of site-specific proteases. Proc Natl Acad Sci U S A 95: 2828-2833. doi:10.1073/pnas.95.6.2828. PubMed: 9501175.

34. Dünkler A, Müller J, Johnsson N (2012) Detecting protein-protein interactions with the Split-Ubiquitin sensor. Methods Mol Biol 786: 115-130. doi:10.1007/978-1-61779-292-2_7. PubMed: 21938623.

35. Pereira G, Tanaka TU, Nasmyth K, Schiebel E (2001) Modes of spindle pole body inheritance and segregation of the Bfa1p-Bub2p checkpoint protein complex. EMBO J 20: 6359-6370. doi:10.1093/emboj/20.22.6359. PubMed: 11707407.

36. Sherman F (2002) Getting started with yeast. Methods Enzymol 350: 3-41. doi:10.1016/S0076-6879(02)50954-X. PubMed: 12073320.

37. Taxis C, Maeder C, Reber S, Rathfelder N, Miura K et al. (2006) Dynamic organization of the actin cytoskeleton during meiosis and spore formation in budding yeast. Traffic 7: 1628-1642. doi:10.1111/j. 1600-0854.2006.00496.x. PubMed: 17118118.

38. Janke C, Magiera MM, Rathfelder N, Taxis C, Reber S et al. (2004) A versatile toolbox for PCR-based tagging of yeast genes: new fluorescent proteins, more markers and promoter substitution cassettes. Yeast 21: 947-962. doi:10.1002/yea.1142. PubMed: 15334558.

39. Schiestl RH, Gietz RD (1989) High efficiency transformation of intact yeast cells using single stranded nucleic acids as a carrier. Curr Genet 16: 339-346. doi:10.1007/BF00340712. PubMed: 2692852.

40. Ausubel FM, Kingston RE, Seidman FG, Struhl K, Moore DD, Brent R, Smith FA, editors (1995) Current Protocols in Molecular Biology. New York, USA: John Wiley and Sons.

41. Sikorski RS, Hieter P (1989) A system of shuttle vectors and yeast host strains designed for efficient manipulation of DNA in Saccharomyces cerevisiae. Genetics 122: 19-27. PubMed: 2659436.

42. Taxis C, Knop M (2006) System of centromeric, episomal, and integrative vectors based on drug resistance markers for Saccharomyces cerevisiae. BioTechniques 40: 73-78. doi: 10.2144/000112040. PubMed: 16454043.

43. Jansen G, Wu C, Schade B, Thomas DY, Whiteway M (2005) Drag&Drop cloning in yeast. Gene 344: 43-51. doi:10.1016/j.gene. 2004.10.016. PubMed: 15656971.

69

5 The mitotic exit network regulates spindle pole body inheritance during sporulation of budding yeast.

Christian Renicke[1], Ann-Katrin Allmann[1], Anne Pia Lutz[1], and Christof Taxis[1, 2*]

[1]Department of Biology/Genetics, Philipps-Universität Marburg, Karl-von-Frisch-Strasse 8, 35043 Marburg, Germany

[2]Department of Chemistry/Biochemistry, Philipps-Universität Marburg, Hans-Meerwein-Strasse 4, 35043 Marburg, Germany

[*]Corresponding author

Email address: taxis@biologie.uni-marburg.de; phone number: (+49)6421-2823046; fax number: (+49)6421-2823032

Manuscript under review.

The mitotic exit network regulates spindle pole body selection during sporulation of budding yeast

Christian Renicke[1], Ann-Katrin Allmann[1], Anne Pia Lutz[1], and Christof Taxis[1, 2*]

[1]Department of Biology/Genetics, Philipps-Universität Marburg, Karl-von-Frisch-Strasse 8, 35043 Marburg, Germany

[2]Department of Chemistry/Biochemistry, Philipps-Universität Marburg, Hans-Meerwein-Strasse 4, 35043 Marburg, Germany

[*]Corresponding author

Email address: taxis@biologie.uni-marburg.de; phone number: (+49)6421-2823046; fax number: (+49)6421-2823032

Keywords: conditional degron/differential centrosome inheritance/meiotic plaque formation/meiosis/spindle polarity

Running title: The MEN controls meiotic SPB inheritance

Character count (excluding reference section): 64,504

Abstract

Age-based inheritance of centrosomes in eukaryotic cells is associated with faithful chromosome distribution during asymmetric cell divisions. During *Saccharomyces cerevisiae* ascospore formation, such an inheritance mechanism regulates encapsulation of selected haploid genomes into spores. Here, we present evidence for involvement of the mitotic exit network (MEN) in this process and functional diversification of MEN components during sporulation. The kinase Cdc15 as well as the kinase complexes Dbf2/20-Mob1 are necessary for age-based selection of spindle pole bodies (yeast centrosome equivalents) at the onset of meiosis II. After the meiotic divisions, efficient genome inheritance requires Dbf2/20-Mob1 during a late step in spore maturation, most likely at a later step than the previously reported function of Cdc15 in cytokinesis. In conclusion, the meiotic functions of the MEN are far more complex than previously thought. In contrast to the mitotic roles of the pathway, execution of meiosis does not rely on the MEN, whereas faithful genome inheritance requires MEN signaling at several steps during spore formation, reminiscent of mitotic MEN functions in spindle polarity establishment, mitotic exit and cytokinesis.

Introduction

Differential inheritance of centrosomes or corresponding structures can be observed in many organisms ranging from simple, unicellular fungi to mammals (Pereira *et al*, 2001; Yamashita *et al*, 2007; Wang *et al*, 2009; Conduit & Raff, 2010; Januschke *et al*, 2011; Izumi & Kaneko, 2012; Salzmann *et al*, 2014). The underlying spindle polarity is based on distinct functional qualities of the spindle poles and important for high fidelity of genome inheritance during asymmetric cell divisions (Miller & Rose, 1998; Piel *et al*, 2000; Beach *et al*, 2000; Liakopoulos *et al*, 2003; Rebollo *et al*, 2007; Rusan & Peifer, 2007; Wang *et al*, 2009; Januschke *et al*, 2013; Lerit & Rusan, 2013). One of the best-studied model organisms for spindle polarity is the yeast *Saccharomyces cerevisiae*. Cells of *S. cerevisiae* divide asymmetrically by budding. Alignment of the mitotic spindle with the mother-daughter axis requires coordinated interactions of astral microtubules (aMT) with polarized actin cables at the bud neck and the bud cortex (Shaw *et al*, 1997; Beach *et al*, 2000; Sheeman *et al*, 2003; Liakopoulos *et al*, 2003). The intrinsic result of spindle polarity in *S. cerevisiae* is an age-based inheritance mechanism of the spindle pole bodies (SPB), the sole microtubule organizing centers equivalent to centrosomes of higher eukaryotes. The predominantly conservative SPB duplication between G1 and S phase results in an older SPB and a younger SPB, which consists mostly of newly synthesized proteins (Adams & Kilmartin, 1999; Menendez-Benito *et al*, 2013). This younger SPB is retained in the mother cell whereas the old SPB migrates into the bud (Pereira *et al*, 2001).

During gametogenesis of *S. cerevisiae*, which is called sporulation, the situation is even more complex due to the higher number of genomes that have to be faithfully distributed. In this developmental program, spore formation is coupled to the meiotic cell divisions resulting in the formation of four haploid genomes encapsulated by spore walls and contained within the remnants of the former mother cell, then called ascus (Esposito & Klapholz, 1981). During the meiotic divisions, SPBs are duplicated twice, which results in four SPBs of three different generations: one old, one of intermediate age, and two young SPBs. The meiotic divisions show no obvious asymmetry; yet, establishment of meiotic spindle polarity has been demonstrated by an age-based hierarchy of SPB inheritance during spore formation (Taxis *et al*, 2005). Sporulation is initiated in cells deprived for a fermentable carbon source as

well as a nitrogen source in the presence of a non-fermentable carbon source such as acetate (Freese *et al*, 1982). Timing and progression of meiosis and spore formation is controlled by a transcriptional cascade; early, middle, mid-late and late gene expression events can be distinguished (Kawaguchi *et al*, 1992; Chu *et al*, 1998). Initiation of spore formation takes place at the cytoplasmic faces of SPBs, which are modified by meiotic plaques (MP) at the onset of meiosis II (Davidow *et al*, 1980; Knop & Strasser, 2000; Nickas *et al*, 2003). These structures are composed of the essential components Mpc54, Mpc70/Spo21, Spo74 as well as the auxiliary, stabilizing factor Ady4 and substitute the γ-tubulin complex and its receptor Spc72 responsible for aMT nucleation (Knop & Schiebel, 1998; Knop & Strasser, 2000; Nickas *et al*, 2003).

The meiotic plaque serves as nucleation platform and anchor for *de novo* formation of the prospore membranes (PSM), which derive from fusion of secretory vesicles and grow around the nuclear lobes including parts of the cytoplasm (Neiman, 1998; Nakanishi *et al*, 2006; Mathieson *et al*, 2010). A protein coat consisting of Ssp1, Ady3, Irc10 and Don1 covers the leading edge of the growing PSM (Knop & Strasser, 2000; Nickas & Neiman, 2002; Lam *et al*, 2014). The protein Ssp1 is essential for formation of the PSM; it is required for localization of the other proteins to the leading edge and to maintain the opening of the PSM until end of meiosis II (Moreno-Borchart *et al*, 2001). The cytokinetic event of PSM closure occurs after spindle breakdown and depends on the removal of Ssp1 from the leading edge (Maier *et al*, 2007; Diamond *et al*, 2009; Paulissen *et al*, 2016). Finally, the four spore wall layers (mannan, β-glucan, chitosan and dityrosine) are synthesized within the lumen of the PSM, resulting in protection of spores against harsh environmental conditions, whereas the remnants of the mother cell mature to form the ascus (Coluccio *et al*, 2004, 2008; Eastwood *et al*, 2012).

Spindle polarity plays an essential role for spore number control. This means that sporulating *S. cerevisiae* cells regulate the number of MPs and thus, spores in response to the available nutrients. Reduction of e.g. acetate leads to a decrease in MP protein levels, which results in modification of selected SPBs with an MP and the formation of less than four spores per cell (Davidow *et al*, 1980; Nickas *et al*, 2004; Taxis *et al*, 2005; Gordon *et al*, 2006). In this case, SPB inheritance is not random but linked to the age of the SPB: the two young SPBs are preferred over the older

ones and the oldest SPB has the least chance to be incorporated into a spore. This mechanism maximizes intra-ascus mating by the inheritance of non-sister genomes originating from the two different meiosis II spindles. Thus, beneficial heterozygosities are preserved, which provide fitness advantages at population level (Taxis *et al*, 2005).

How meiotic cells are able to discriminate between the different SPBs and generate a signal for MP formation is still an open question. Once the process is initiated, MP components self-organize into the mature MP, which is thought to be a crystal-like structure reminiscent of the central plaque of the SPB (Bullitt *et al*, 1997; Taxis *et al*, 2005). The current model is that the crystal-like structure develops rapidly due to a positive feedback mechanism until saturation is reached. MP formation happens in a consecutive fashion with a delay at older SPBs (Taxis *et al*, 2005). Besides this stepwise MP formation, age-based selection of SPBs relies on the outer plaque proteins Nud1 as well as Spc72; potentially, these proteins link presence of aMT to differences between the SPBs (Gordon *et al*, 2006).

During vegetative growth of *S. cerevisiae*, several factors and pathways are involved in establishment and maintenance of cell and spindle polarity. Among them is the mitotic exit network (MEN), an equivalent to the metazoan hippo tumor suppressor pathway (Hergovich & Hemmings, 2012). In mitosis, the essential function of the MEN takes place in late anaphase by integration of temporal cues of mitotic progression with spatial signals of spindle positioning to control the release of Cdc14 to the cytoplasm (Shou *et al*, 1999; Visintin *et al*, 1999; Bardin *et al*, 2000; Adames *et al*, 2001; Hu *et al*, 2001). The main role of the phosphatase Cdc14 is to counteract Cdk1 activity, thereby allowing the cell to exit mitosis and to reenter G1 phase (Jaspersen *et al*, 1998; Visintin *et al*, 1998; Mohl *et al*, 2009). However, the MEN fulfills functions also before and after mitotic exit: during metaphase, it is required for establishment of spindle polarity by targeting Kar9 localization to aMTs nucleated at the old SPB; after exit from mitosis, it acts directly on several proteins at the bud neck to promote cytokinesis (Meitinger *et al*, 2010, 2013; Hotz *et al*, 2012a, 2012b).

The core MEN consists of the small GTPase Tem1, the PAK-like kinase Cdc15, the downstream NDR (nuclear Dbf2-related) kinases Dbf2 and Dbf20, Mob1 and the SPB outer plaque protein Nud1. Thereby, Mob1 forms complexes with the paralogs Dbf2 and Dbf20 and acts as a coactivator; Nud1 serves as signaling scaffold

(Gruneberg *et al*, 2000; Lee *et al*, 2001; Mah *et al*, 2001; Visintin & Amon, 2001; Rock *et al*, 2013). Until late anaphase, Tem1 is kept in its inactive GDP-bound form by the bipartite GAP (GTPase activating protein) Bfa1-Bub2 (Geymonat *et al*, 2002; Fraschini *et al*, 2006; Caydasi *et al*, 2012). To activate the MEN, the polo-like kinase Cdc5 inhibits the GAP activity of Bfa1-Bub2 by phosphorylation, a function which is antagonized by the spindle position checkpoint kinase Kin4 (Hu *et al*, 2001; Hu & Elledge, 2002; Geymonat *et al*, 2003; Park *et al*, 2004; Pereira & Schiebel, 2005; Maekawa *et al*, 2007; Kim *et al*, 2012). As the daughter cell-directed SPB enters the bud, Kin4 is inhibited by Lte1, which localizes bud-specific (Geymonat *et al*, 2009; Bertazzi *et al*, 2011; Falk *et al*, 2011). This triggers activation of Tem1 and Cdc5 at the daughter-localized SPB and leads to SPB recruitment of Cdc15, which activates the Dbf2-Mob1 kinase complex resulting in sustained release of Cdc14 from the nucleolus to the cytoplasm (Asakawa *et al*, 2001; Visintin & Amon, 2001; Mohl *et al*, 2009; Valerio-Santiago & Monje-Casas, 2011; Rock & Amon, 2011; Gryaznova *et al*, 2016; Falk *et al*, 2016).

During sporulation, MEN activity has been detected mostly during the second meiotic division (Attner & Amon, 2012). Phenotypic analyses on Cdc15 mutants showed participation in PSM formation, exit from meiosis II and cytokinesis (Kamieniecki *et al*, 2005; Pablo-Hernando *et al*, 2007; Diamond *et al*, 2009; Attner & Amon, 2012). Furthermore, several mechanistic differences between mitotic and meiotic cell divisions exist: Firstly, the requirement for Nud1 and SPB localization is lost (Attner & Amon, 2012). Secondly, the GTPase Tem1 and its GAP complex Bfa1-Bub2 are dispensable for activation of the kinases Cdc15 and Dbf2/20-Mob1 and spore formation (Gordon *et al*, 2006; Attner & Amon, 2012). Thirdly, Dbf20 is the predominantly active NDR kinase and needs Cdc15 activity to associate with the Mob1 coactivator (Attner & Amon, 2012).

Here, we report multiple meiotic roles of the MEN in regulation of SPB inheritance, meiotic plaque numbers and cytokinesis during sporulation of *S. cerevisiae*. At the transition from meiosis I to meiosis II, Cdc15 exhibits an inhibitory function on MP formation, while the terminal Dbf2-Mob1 and Dbf20-Mob1 kinase complexes are involved in establishment of meiotic spindle polarity. After meiosis II, Cdc15 functions independently in PSM closure, whereas Dbf2-Mob1 and Dbf20-Mob1 are necessary for efficient spore maturation.

Results

Enhancement of a system for sporulation-specific protein depletion

Most of the proteins of the MEN fulfill essential roles in vegetative growth of *S. cerevisiae*. Therefore, a reliable and generic system to create loss-of-function mutants of essential proteins during meiosis was necessary. We decided to use the meiosis-specific variant of the tobacco etch virus (TEV) protease induced protein instability system (TIPI) that involves activation of a degradation-inducing sequence (degron) by a TEV protease with enhanced processivity (pTEV$^+$) to downregulate MEN components specifically during sporulation (Taxis *et al*, 2009; Jungbluth *et al*, 2010, 2012). However, we changed the existing method in two points: we replaced the constitutive promoters (P$_{ADH1}$ or P$_{CYC1}$) with a promoter that is active only during vegetative growth (P$_{MCD1}$; Klein *et al*, 1999; Clyne *et al*, 2003) and exchanged the *CYC1* terminator of the pTEV$^+$ construct by the *DIT1* terminator. This terminator confers about fourfold higher expression levels of a tester construct than the *CYC1* terminator in logarithmically growing cells and is enhanced under diverse starvation conditions (Yamanishi *et al*, 2013; Ito *et al*, 2013). We envisioned that these changes should lead to robust downregulation of target proteins specifically during meiosis; the chromosomal tagging construct P$_{MCD1}$-*GFP-TDegF-3HA* was termed *sid*-tag (<u>s</u>porulation-<u>i</u>nduced <u>d</u>epletion) (Figure 1A). To check the effect of the terminator exchange in combination with the meiosis-specific *IME2* promoter, we compared meiotic expression of a P$_{IME2}$-*GFP-pTEV*$^+$ construct with terminator sequences of either *CYC1* or *DIT1*. Indeed, the expression of the P$_{IME2}$-*GFP-pTEV*$^+$-T$_{DIT1}$ construct was two- to threefold higher than that of the P$_{IME2}$-*GFP-pTEV*$^+$-T$_{CYC1}$ construct (Figure 1B). A P$_{IME2}$-*pTEV*$^+$-T$_{DIT1}$ construct was integrated at two chromosomal loci (*HIS3* and *TRP1*) to ensure efficient meiotic production of the pTEV$^+$ protease.

The essential MEN kinase Cdc15 was used as target to benchmark the modified system during sporulation and vegetative growth. Remarkably, Cdc15 was efficiently depleted shortly after induction of meiosis (Figure 1C). Compared to a logarithmically growing culture, protein levels were already reduced in the pre-sporulation culture (0 h). Similar observations have been made before with the *MCD1* promoter; it may be that the number of M-phase cells is reduced in cultures growing in medium containing the poor carbon source acetate (Klein *et al*, 1999). As expected, Cdc15 depletion resulted in a massive sporulation phenotype; cells were able to perform the

meiotic divisions but did not form spore-containing asci (Figure 1D). Instead, cells arrested with either two or four nuclei or contained no distinct nuclei. This observation was in agreement with earlier studies, which suggested a role for Cdc15 in exit of meiosis II, prospore membrane growth and closure as well as spore wall maturation (Kamieniecki *et al*, 2005; Pablo-Hernando *et al*, 2007; Diamond *et al*, 2009; Attner & Amon, 2012). In contrast, chromosomal fusion of the *sid*-tag to *CDC15* did not impair vegetative growth or localization of sid-Cdc15 to the spindle pole body (SPB) in mitotic anaphase (Figure 1E). These results imply that the modifications of the meiosis-specific TIPI system increased the usability of the method.

Dbf2-Mob1 and Dbf20-Mob1 are required for efficient spore formation

To gather information about a putative function of the Dbf2-Mob1 and Dbf20-Mob1 complexes during sporulation, we first sought to examine the meiotic localization of Dbf2 and Dbf20 fused to GFP. In line with previous results on Cdc15 and Mob1 localization and the lack of Nud1 requirement for meiotic MEN activity (Attner & Amon, 2012), we did not observe specific localization of Dbf2 and Dbf20 during the course of sporulation (Supplementary Figure S1).

We then investigated the role of the Dbf2-Mob1 and Dbf20-Mob1 complexes during sporulation by creation of depletion mutants for the single proteins (Dbf2↓, Dbf20↓ and Mob1↓) or different combinations (Dbf2↓ Dbf20↓, Dbf2↓ Mob1↓, Dbf20↓ Mob1↓ and Dbf2↓ Dbf20↓ Mob1↓). The efficiency of protein depletion and *pTEV*[+] expression was checked by Western blot analysis during the initial time points of sporulation for the single mutants. This revealed a considerable decrease for all targets within the first four hours (Supplementary Figure S2A). During vegetative growth, no negative effect was observed in any of the strains (Supplementary Figure S2B and C). Subsequently, we used these strains to assess spore formation and spore number control. In short, a reduction of spore numbers compared to the control strain was observable for the Mob1↓ mutant, all double mutants and the triple mutant (Figure 2A, Supplementary Figure S3). This reduction was most pronounced at the highest acetate concentration that we tested (1 %); the mutants displayed a decrease in the number of tetrads and an increase of dyads and monads. At 0.1 % acetate, the control strain formed mostly triads and dyads; the Dbf2↓ Mob1↓ and Dbf2↓ Dbf20↓ Mob1↓ strains showed clear reduction of these species coupled with increased numbers of monads and cells with no detectable nuclei. At 0.01 % acetate, the Dbf2↓

Mob1↓ and Dbf20↓ Mob1↓double mutants as well as the Dbf2↓ Dbf20↓ Mob1↓ triple mutant showed a decrease in asci with more than one spores and an increase of cells without stained nuclei in comparison with the control. While most mutants showed an impact on spore numbers, they still reacted to lowered acetate concentration by a decrease in sporulation efficiency (Figure 2B). In summary, the results indicate a redundant role of the MEN kinases Dbf2 and Dbf20 in spore formation and imply additional Cdc15 targets during sporulation. Surprisingly, the Dbf2↓ Dbf20↓ double mutant and the Mob1↓ mutant showed no significant difference to the control strain in sporulation efficiency, whereas the triple mutant did. In conclusion, our data suggest some independent functions of Dbf2/20 on the one hand and Mob1 on the other hand.

The reduction of spore numbers in the mutants could be evoked by decreased levels of MP proteins. Therefore, we measured the levels of Mpc54-9Myc, Mpc70-9Myc and Spo74-9Myc during sporulation in the Mob1↓, Dbf2↓ Dbf20↓ and the Dbf2↓ Dbf20↓ Mob1↓ mutants. This revealed no significant changes of the MP protein amounts in the terminal MEN kinase mutants as well as in the Cdc15↓ mutant (Supplementary Figure S4). Thus, we could exclude reduction of MP protein levels as reason for impaired spore formation.

The MEN influences meiotic genome inheritance and SPB selection

Next, we investigated genome inheritance during yeast meiosis in a subset of MEN mutants. In dyads, the preference for the young SPBs for modification with a MP leads to nearly exclusive packaging of genomes from different meiosis II spindles. This results in the formation of non-sister dyads, containing homologous and not sister chromosomes in the two spores (Davidow *et al*, 1980; Okamoto & Iino, 1981; Nickas *et al*, 2004; Taxis *et al*, 2005; Gordon *et al*, 2006). To investigate whether genome inheritance was disturbed in the MEN mutants, we used a yeast strain that allows assessment of sister-chromosome segregation (Gordon *et al*, 2006). This diploid strain harbors a centromere-linked gene encoding for RFP on one copy of chromosome V and one for GFP on the other. Both genes are expressed only after prospore membrane closure. The two different fluorescent proteins permit discrimination of non-sister and sister dyads, depending on the fluorescent label distribution within the spores of a dyad (Figure 3A). Due to the complete lack of spores in the Cdc15↓ mutant, we performed this experiment with the Mob1↓ single

mutant, the Dbf2↓ Dbf20↓ double mutant and the Dbf2↓ Dbf20↓ Mob1↓ triple mutant. We observed a fraction of sister-dyads below 5 % in the control strain comparable to the results of an earlier study (Gordon *et al*, 2006). Both, the Mob1↓ and the Dbf2↓ Dbf20↓ strains produced significantly more sister-dyads, while the Dbf2↓ Dbf20↓ Mob1↓ mutant exhibited a further increased fraction of sister-dyads. Additionally, the assay allowed detection of chromosome segregation defects indicated by spores with either both or no fluorophores. Yet, no increase of cells with missegregated chromosomes was found in the mutant strains (Supplementary Figure S5). Thus, inactivation of the terminal MEN kinase modules interferes with faithful genome inheritance but not chromosome segregation. As in the sporulation assay, the data suggest that Dbf2/20 and Mob1 act to some extent separately from each other, as the triple mutant showed an additive effect compared to the Mob1↓ single and Dbf2↓ Dbf20↓ double mutants.

The observed phenotype could be due to a defect in age-based inheritance of SPBs caused by a changed pattern of MP formation. To test this possibility, we used a strain with the moderately slow maturating tagRFP-T (maturation half-time: ~100 min; Shaner *et al*, 2008) as fluorescent timer fused to the integral SPB component Spc42 together with Mpc54-YFP as MP marker. This allowed correlation of SPB age with MP formation. Due to the maturation kinetics of tagRFP-T, three modification patterns were distinguished in cells with two mature MPs: modification of the two third generation SPBs, modification of a first or second generation and one third generation SPB and modification of the first and second generation SPBs.

For a completely random selection, the expected fractions would be 16.7 % for modification of only the third generation SPBs, 16.7 % for selected first and second generation SPBs, while selection of one first or second generation SPB together with one third generation SPB would occur in 66.7 % of the cells. However, selection of SPBs for modification with MPs has been shown to be highly regulated; the two third generation SPBs are by far preferred over the older ones. In unperturbed cells with two meiotic plaques, about 95 % of the cells modify the two youngest SPBs with MPs (Taxis *et al*, 2005; Gordon *et al*, 2006). We found similar values for the control strain in our experiments (Figure 3B). Strikingly, all four tested mutants exhibited significantly lower percentages of cells with meiotic plaques at the youngest SPBs. In the Mob1↓ mutant, 25 % of the cells showed modification of one older and one

younger SPB, in the Dbf2↓ Dbf20↓ double mutant 17 % and in the Dbf2↓ Dbf20↓ Mob1↓ triple mutant 18 % of cells displayed this pattern. This phenotype was even more severe in the Cdc15↓ mutant (30 %) accompanied by MP formation at the oldest SPBs in 17 % of the cells, a situation rarely found in the other strains. In summary, the results demonstrate a role for the MEN in SPB selection during sporulation. Moreover, our data imply additional Cdc15 targets beside Dbf2, Dbf20 and Mob1.

Multiple roles of the MEN at different steps of spore formation

To investigate the influence of Cdc15, Dbf2, Dbf20 and Mob1 on numbers of mature MPs, we performed fluorescence microscopy and followed the number of bright Mpc54-YFP signals during a sporulation time course. In accordance with a previous study that used Mpc70 as marker for meiotic plaques (Pablo-Hernando *et al*, 2007), we found robust localization of Mpc54 at SPBs in the Cdc15↓ strain, but no formation of refractive spores (Figure 4A). This could be explained by previously described defects in exit from meiosis II and PSM closure (Kamieniecki *et al*, 2005; Pablo-Hernando *et al*, 2007; Diamond *et al*, 2009). Remarkably, Cdc15 depletion led to a drastic increase in the number of cells with four mature MPs. In contrast, the kinetics of MP formation and number of MPs formed were comparable in cells deficient for the terminal MEN components and the control strain (Figure 4B). Most cells formed two or three meiotic plaques due to exposure of the cells to low acetate conditions. However, the majority of cells depleted for Mob1, Dbf2 and Dbf20 or Dbf2, Dbf20 and Mob1 failed in formation of refractive spores; at the end of the time course only about 20 % of the cells contained spores compared to around 60 % in the control (Figure 4B). This suggests that Cdc15 functions partially via Dbf2, Dbf20 and Mob1 in cytokinesis. Additionally, Cdc15 is required for control of MP numbers independently from Dbf2, Dbf20 and Mob1.

To follow PSM formation directly, we used a strain with the leading edge protein Don1 fused to GFP. Again, the Cdc15↓ mutant strain formed no refractive spores but accumulated cells with faint Don1-GFP signals staining whole PSMs (Supplementary Figure S6). This localization pattern has been attributed to cells that are about to close the PSM (Taxis *et al*, 2006; Maier *et al*, 2007). In contrast, PSM numbers were not affected by Cdc15 depletion regarding slightly more asynchronous cultures between the experiments. During similar experiments with the Mob1↓, Dbf2↓ Dbf20↓

and Dbf2↓ Dbf20↓ Mob1↓ mutants under conditions favoring low spore numbers, we observed a comparable development of PSMs in all strains. Unlike control cells, just a minority of mutant cells formed refractive spores during the experiment, whereas the number of cells without Don1-GFP signals increased at the last time points (Figure 5). Thus, cells with reduced activity of the Dbf2-Mob1 or Dbf20-Mob1 complexes are probably defective at an early step in spore maturation rather than PSM closure.

A negative role of Nud1 in spore formation

The temperature-sensitive *nud1-2* allele induces a severe defect in SPB inheritance (Gordon *et al*, 2006). However, pronounced defects in SPB selection and genome inheritance were already found at permissive temperatures. Therefore, we investigated Nud1 function by using a sporulation-induced depletion mutant. The protein was fully functional during vegetative growth and quickly depleted upon induction of sporulation (Supplementary Figure S7A, B, and C). Surprisingly, in contrast to the *nud1-2* allele, depletion of Nud1 induced higher spore numbers per ascus accompanied by a modest increase of unsporulated cells (Figure 6A, Supplementary Figure S7D). We considered that SPB-associated Nud1 might be inaccessible for degradation resulting in depletion of only cytoplasmic Nud1, whereas a small fraction of SPB-associated Nud1 might be sufficient for its function. Hence, we applied the depletion system on the SPB protein Cnm67, which links Nud1 to the central plaque (Schaerer *et al*, 2001). No side effects were found during vegetative growth and sporulation-induced depletion kinetics of Cnm67 were comparable to those of Nud1 (Supplementary Figure S7A, B, and C). Depletion of Cnm67 completely blocked spore formation with most cells mono-nucleated or without nuclei (Supplementary Figure S7E). Successful Cnm67 depletion makes it less likely that residual Nud1 fractions at the SPB are causing the observed phenotype in Nud1↓ cells. Subsequently, we performed a genome inheritance assay with the Nud1↓ strain and found a nearly random distribution of sister and non-sister dyads as reported for the *nud1-2* allele (Figure 6B; Gordon *et al*, 2006). Furthermore, we observed an increase of cells with missegregated chromosomes V (Figure 6C). Thus, Nud1 seems to fulfill a negative role during spore formation but is necessary for efficient establishment of meiotic spindle polarity and chromosome segregation.

Both, Cnm67 and Nud1 possess putative phosphorylation consensus sites for either Cdc15 ([S/T]X[R/K]) or Dbf2/20-Mob1 (RXXS) and have been shown to be hyperphosphorylated in a cell cycle-dependent manner (Gruneberg *et al*, 2000; Schaerer *et al*, 2001; Mah *et al*, 2005; Mok *et al*, 2010; Keck *et al*, 2011). We analyzed Nud1 and Cnm67 during sporulation in the Cdc15↓, Mob1↓, Dbf2↓ Dbf20↓ and Dbf2↓ Dbf20↓ Mob1↓ mutants by Western blotting (Supplementary Figure S8). Only the Mob1↓ strain showed differences to the control; Nud1 abundance was increased at 0 h and during sporulation. Interestingly, a similar increase in Nud1 levels was not observed in the triple mutant. These results make it unlikely that the altered sporulation behavior of the MEN mutants is caused by changes in Nud1 or Cnm67 levels. Though, due to the limitations of a standard SDS-PAGE, we cannot rule out that e.g. posttranslational modifications of Nud1 or Cnm67 may alter affinity for meiotic plaque proteins.

A major function of Nud1 is the nucleation of aMT together with the γ-tubulin complex receptor Spc72 (Knop & Schiebel, 1998; Gruneberg *et al*, 2000). As Spc72 has an influence on meiotic SPB selection (Gordon *et al*, 2006), we investigated aMT association to SPBs during anaphase I using Bik1-3GFP as marker, which is a microtubule plus end tracking protein (Markus & Lee, 2011; Su *et al*, 2011; Hanson *et al*, 2016). In most cells with an anaphase I spindle both SPBs were occupied with aMTs (Figure 6D). A smaller fraction of cells showed aMTs only at the older SPB, whereas cells with aMTs at the second oldest SPB as well as cells without aMTs were rarely found.

Hyperactivation of the MEN during sporulation

To obtain further insights in MEN signaling during sporulation, we used a Cdc15 gain-of-function mutant; in mitosis, expression of a truncated allele of *CDC15* (*CDC15ΔC*, corresponding to amino acids 1 to 750) leads to hyperactivation of the MEN cascade (Bardin *et al*, 2003; Rock & Amon, 2011). We used this allele under control of the meiosis-specific *SPO74* promoter and added a photo-sensitive degron module to minimize Cdc15ΔC levels during vegetative growth by blue-light dependent destabilization of the hyperactive kinase (Renicke *et al*, 2013). Considerable amounts of the construct accumulated specifically during meiosis and were sufficient to complement the Cdc15↓ phenotype (Supplementary Figure S9A and B). Presence of Cdc15ΔC during meiosis in addition to the endogenous wild-type

protein led to a decrease in spore formation and sporulation efficiency (Figure 7A). Compared to control cells, levels of the meiotic plaque protein Mpc54 were increased, the amounts of Spo74 were reduced whereas Mpc70 was unaffected (Figure 7B; Supplementary Figure S9C). Additionally, we observed a decrease of Nud1 levels while no changes were found for Cnm67 (Figure 7C; Supplementary Figure S9D). A genome inheritance assay revealed no effect of Cdc15ΔC (Supplementary Figure S9E). Thus, hyperactivation of the MEN during sporulation impinges on spore formation, most likely through limitation of Spo74, but does not cause aberrant SPB inheritance.

The MEN regulators Cdc5 and Kin4 in meiosis

Previously, it has been shown that during sporulation Tem1 and its GAP complex Bfa1-Bub2 are dispensable for MEN activation (Kamieniecki *et al*, 2005; Gordon *et al*, 2006). We thought that the mitotic antagonists Cdc5 and Kin4 were promising candidates as meiotic regulators of the MEN (D'Aquino *et al*, 2005; Pereira & Schiebel, 2005; Maekawa *et al*, 2007; Gryaznova *et al*, 2016; Falk *et al*, 2016). Cdc5 has been shown *in vivo* to act directly on Cdc15 and to be required for Cdc14 release also in meiosis II while Kin4 was able to phosphorylate Cdc15 *in vitro* (Lee & Amon, 2003; Clyne *et al*, 2003; Ptacek *et al*, 2005; Sourirajan & Lichten, 2008; Attner *et al*, 2013). Due to its functions prior meiosis II (Lee & Amon, 2003; Clyne *et al*, 2003; Sourirajan & Lichten, 2008; Jungbluth *et al*, 2010; Attner *et al*, 2013; Li *et al*, 2015), functional characterization of Cdc5 in late steps of meiosis is challenging. Hence, we focused on localization analysis of an YFP marked variant. During mitosis, Cdc5-YFP localized as previously described (Supplementary Figure S10A; Shirayama *et al*, 1998; Song *et al*, 2000; Park *et al*, 2004). During sporulation, colocalization with Spc42-RFP and Don1-CFP allowed discrimination between cells prior to meiotic divisions, in meiosis I, in meiosis II, cells with prospores as well as those with refractive spores. No distinct signals were observed in cells in G1 phase and pre-meiotic S-phase, while Cdc5 was found in the nucleus and at the SPBs from meiosis I until late meiosis II; afterwards, the distinct signals disappeared (Figure 8A). Localization of Cdc5 to the nucleus and SPBs from meiosis I to early meiosis II was reported previously and corresponds to its early MEN-independent meiotic functions (Lee *et al*, 2003; Clyne *et al*, 2003; Sourirajan & Lichten, 2008; Shirk *et al*, 2011; Attner *et al*, 2013). Additionally, we looked at cells with less than four distinct Don1-

CFP signals at SPBs or leading edges of PSMs. Cdc5-YFP signals were frequently observed at all four SPBs disregarding the number of Don1-CFP signals (Figure 8B). Thus, it is rather unlikely that Cdc5 is a direct meiotic activator of the MEN with respect to SPB selection.

The kinase Kin4 displayed no specific localization during sporulation, whereas the localization during vegetative growth was found to be as reported in the literature (Supplementary Figure S10B and C; D'Aquino *et al*, 2005; Pereira & Schiebel, 2005). We generated a *sid-KIN4* mutant strain that allowed efficient depletion of the protein during sporulation; the tag had no impact on mitotic function of Kin4 (Supplementary Figure S11A, B, and C). Remarkably, the Kin4 depletion caused severe reduction of spore numbers accompanied by a pronounced increase in cells with no nuclei, which resulted in a drastic decrease in sporulation efficiency (Figure 8C; Supplementary Figure S11D). This shows that Kin4 is necessary for efficient spore formation, although no meiotic function for the canonical Kin4 target Bfa1-Bub2 was found (Kamieniecki *et al*, 2005; Gordon *et al*, 2006), which suggests another meiotic target involved in spore formation. Assays to investigate sister dyad formation and chromosome segregation revealed no changes for this mutant (Figure 8D and E). Thus, participation of Kin4 in MEN regulation of SPB selection and cytokinesis is rather unlikely.

Discussion

During sporulation of diploid *S. cerevisiae* cells, spindle polarity results in preferential inheritance of newly formed SPBs if less than four spores are formed (Gordon *et al*, 2006). The decision how many and which SPBs and their associated genomes will be incorporated into spores takes place at the onset of meiosis II by formation of meiotic plaques at selected SPBs (Knop & Strasser, 2000; Taxis *et al*, 2005). Our results demonstrate that the MEN functions in this regulatory step in two ways: Cdc15, Dbf2, Dbf20 and Mob1 work together in age-based selection of SPBs for modification with meiotic plaques. Independently, Cdc15 is involved in control of MP numbers. Finally, we observed further functional diversification during PSM closure and spore maturation.

Parallels between mitotic and meiotic functions of the mitotic exit network

In mitosis, the MEN is required for establishment of spindle polarity (Hotz *et al*, 2012a, 2012b), exit from mitosis and cytokinesis and its activation mechanism is tightly linked to the SPB by its scaffold protein Nud1 (reviewed in Juanes & Piatti, 2016). During the developmental program of sporulation, a rewiring of the MEN takes place. Activity of the MEN kinases is independent of SPB localization, Dbf20 is more abundant and exhibits higher activity than Dbf2 and its association with Mob1 is Cdc15-dependent (Attner & Amon, 2012). Similar to mitosis, the MEN is involved in anaphase II release of Cdc14, in exit of meiosis II and cytokinesis (Kamieniecki *et al*, 2005; Pablo-Hernando *et al*, 2007; Diamond *et al*, 2009; Attner & Amon, 2012).

This study provides evidence that Dbf2/20-Mob1 are involved in spore formation. In contrast to Cdc15 inactivation, depletion of the terminal MEN kinases did not result in complete failure of sporulation, but in random spore abortion. This implies that Cdc15 does not rely exclusively on Dbf2/20-Mob1. The sporulation assays confirmed that Dbf2 and Dbf20 act redundantly, whereas Mob1 might have Dbf2/20-independent functions during sporulation. Moreover, Don1 localization experiments suggest two roles of the MEN after exit of meiosis II. Accumulation of faint Don1-GFP on whole PSMs in Cdc15↓ cells indicates a defect in PSM closure, most likely due to a failure in removal of Ssp1 from the leading edge of the PSM (Maier *et al*, 2007; Diamond *et al*, 2009; Paulissen *et al*, 2016). Disappearance of Don1-GFP signals from the PSMs with subsequent spore maturation defects in cells depleted for Dbf2, Dbf20 and Mob1 points to a defect in spore wall assembly (Coluccio *et al*, 2004).

Another independent function of Cdc15 was found in regulation of MP numbers. MP protein levels were unchanged, yet, MP numbers were drastically increased in the Cdc15↓ strain. This is reminiscent of the phenotype found for an *ADY1* deletion mutant. There, MP levels were not affected but MP numbers were strongly reduced (Deng & Saunders, 2001; Jungbluth *et al*, 2012). Although opposing in their effects, both mutants seem to impact on the ability of MP components to form a mature MP.

Establishment of mitotic spindle polarity depends on regulation of Kar9 localization by the MEN towards the old SPB (Leisner *et al*, 2008; Hotz *et al*, 2012a, 2012b). Our results indicate that also meiotic spindle polarity is regulated by the MEN. However, it is unlikely that Kar9 is involved in this process since it is not required for faithful SPB selection (Gordon *et al*, 2006). Although Cdc15 and Dbf2/20-Mob1 are not found at the SPBs (Supplementary Figure S1; Attner & Amon, 2012), they contribute to the

selection of the younger SPBs for MP formation. This function correlates with a subtle increase in activity of Dbf2/20-Mob1 at the transition from meiosis I to meiosis II reported by a previous study (Attner & Amon, 2012). Thus, similar to mitosis, low activity might be sufficient for MEN function in SPB selection, whereas high activity seems to be required for cytokinesis after meiosis II (Visintin & Amon, 2001; Bardin *et al*, 2003; Hotz *et al*, 2012a, 2012b).

SPB selection was clearly affected in all MEN mutants that we tested, however Cdc15 depletion resulted in the strongest phenotype. This could imply a functional separation between Cdc15 and Dbf2/20-Mob1, similarly to the distinct phenotypes in late sporulation. Yet, we cannot rule out that potential differences in depletion efficiencies had an impact on our experiments, especially for earlier meiotic functions. The effects on SPB selection of Dbf2/20-Mob1 mutants were lower than that of Nud1 mutants (Figure 7B; Gordon *et al*, 2006). Strikingly, Cdc15 depletion caused similar randomization of SPB selection as Nud1-2 inactivation (Figure 3B; Gordon *et al*, 2006), which could place Cdc15 as upstream regulator of this process.

Surprisingly, we found a positive effect of Nud1 depletion on spore numbers conversely to that of the *nud1-2* allele (Gordon *et al*, 2006), pointing to an inhibitory function of Nud1 on MP formation. We cannot fully explain the phenotypic differences of the two mutants. Similar to meiosis-specific Nud1 depletion, it can be assumed that Nud1-2 dissociates from the SPB at restrictive temperature as shown in vegetatively growing cells (Gruneberg *et al*, 2000). However, the timing of Nud1 inactivation as well as experimental conditions were different, which could account for the dissimilar sporulation results. Remarkably, effects on genome inheritance were comparable for both mutants (Figure 7B; Gordon *et al*, 2006). Although, it has been published by different groups that Nud1 localizes to the SPB during meiosis II, the number of SPBs with Nud1 signals varied in these reports (Knop & Strasser, 2000; Nickas *et al*, 2004; Attner & Amon, 2012). Thus, an inhibitory function of Nud1 on MP formation cannot be excluded by the available experimental data.

A negative effect of Nud1 on spore formation might also explain the unexpected phenotypic enhancement observed in most experiments for the Mob1↓ mutant compared to the Dbf2↓ Dbf20↓ double mutant, as Nud1 levels were increased in cells depleted for Mob1. Functional connection of Mob1 to Mps1 that is involved in SPB

homeostasis might provide an explanation for these findings (Winey *et al*, 1991; Luca & Winey, 1998; Elserafy *et al*, 2014; Burns *et al*, 2015).

Regulation of the MEN during sporulation

An interesting question is the intrinsic activation mechanism of the MEN. Lack of the GTPase Tem1 as well as its GAP Bfa1-Bub2, essential for signal integration and MEN function in mitosis, have no obvious effect on sporulation (Gordon *et al*, 2006; Attner & Amon, 2012). The main mitotic Tem1 function is localization of Cdc15 to the SPB, consequently Nud1-dependent SPB association is dispensable for meiotic MEN activity (Visintin & Amon, 2001; Rock & Amon, 2011; Attner & Amon, 2012). Recently, a mechanism for activation of the core mammalian Hippo-pathway consisting of Mst2, Lats1 and hMob1 has been proposed in which hMob1 acts as scaffold for the kinases (Ni *et al*, 2015). There, the Cdc15 ortholog Mst2 autophosphorylates multiple residues within its linker region to allow hMob1 docking. This leads to a conformational change allowing recruitment of the NDR kinase Lats1 and formation of a ternary complex, which then permits direct activation of Lats1 by Mst2. The high conservation of Hippo signaling provokes the question of a similar activation mechanism in budding yeast meiosis. Like Mst2, Cdc15 is capable of autophosphorylation and is required for Dbf2/20-Mob1 interaction (Jaspersen *et al*, 1998; Asakawa *et al*, 2001; Ptacek *et al*, 2005; Attner & Amon, 2012). Moreover, the Nud1 independent activation of Dbf2/20-Mob1 (Attner & Amon, 2012) suggests a comparable mechanism for the MEN in meiosis.

Known upstream regulators of the MEN during mitosis are the kinases Cdc5 and Kin4 (D'Aquino *et al*, 2005; Pereira & Schiebel, 2005; Maekawa *et al*, 2007; Gryaznova *et al*, 2016; Falk *et al*, 2016). We observed SPB and nuclear localization of the Polo-like kinase Cdc5 during the meiotic divisions until prospores became visible. A comparable localization pattern was correlated with Cdc5 functions during meiotic SPB duplication (Attner *et al*, 2013). Analysis of Cdc5, Spc42, and Don1 localization did not reveal a connection between SPB localization of Cdc5 with the number of PSMs. Thus, it is unlikely that Cdc5 localization is directly linked to MEN-dependent SPB selection. The data on depletion of the mitotic Cdc5 antagonist Kin4 indicate that this kinase is required for efficient sporulation but not for SPB selection and genome inheritance. Differences between Kin4 and MEN mutants in the latter

assays and the dispensability of Bfa1-Bub2 for spore formation (Gordon *et al*, 2006) suggest that Kin4 acts in a different pathway.

Is meiotic SPB selection regulated by a dynamic process?

Two opposing processes could occur at the transition from anaphase I to metaphase II: removal of aMTs and formation of MPs. Differences in aMT nucleation between the old and the new SPB have been observed in mitosis and impact on mitotic spindle polarity (Juanes *et al*, 2013). During meiosis, a short time window might exist in which the two older SPBs still possess aMTs while the new SPBs do not (Figure 6D). A necessity to remove aMT before MP formation would explain the slight delay in MP maturation at older SPBs (Taxis *et al*, 2005). Limiting amounts of MP components and a positive feedback loop in MP maturation then might result in the observed SPB selection patterns. Nud1 or Cdc15 inactivation impinge on this process to a similar extend (Figure 6B; Gordon *et al*, 2006); Nud1 directly functions in aMT nucleation (Knop & Schiebel, 1998; Gruneberg *et al*, 2000). Whether Cdc15 impacts on aMT dynamics during meiosis or is part of another pathway remains an open question.

Material & Methods

Yeast strains and plasmids.

All yeast strains used in this study are derivatives of SK1 strains YKS32 (Knop & Strasser, 2000) and LH177 (Huang *et al*, 2005) and their relevant genotypes are described in Supplementary Table S1. PCR-based manipulation of target genes at the chromosomal locus was performed as previously described (Janke *et al*, 2004; Taxis & Knop, 2012). Yeast transformation was done by the lithium acetate method (Schiestl & Gietz, 1989). Correct integration of the PCR products was tested by PCR on chromosomal DNA and if applicable by immunodetection of the fusion proteins. Genetic manipulations were introduced into haploid strains; diploids were obtained by mating of respective haploids. Alternatively, diploids were obtained by tetrad dissection of heterozygous strains and subsequent mating of haploids. For creation of YCR329, the P_{IME2}-$pTEV^+$-T_{DIT1}::*kanMX4* cassette of pCR107 was amplified with primers containing homologous sequences for *HIS3* or *TRP1.* For creation of YCR370, the *kanMX4* resistance markers of YAB12 and a *MATα* haploid of YCT716 were substituted by the PCR-amplified *hphNT1* cassette of pFA6a-hphNT1.

Standard protocols were used for yeast cultivation (Sherman, 2002). In general, strains with stable integrations were grown on YPD, selection for antibiotics resistances was performed on YPD (1 % yeast extract, 2 % peptone, 2 % glucose) supplemented with 100 µg/l ClonNAT, 200 µg/l G418 or 300 µg/l HygromycinB, selection for auxotrophy markers was done on synthetic complete (SC) medium with 2 % glucose lacking uracil, leucine, histidine, tryptophan or lysine. Growth assays were performed with 1:5 serial dilutions using an initial OD_{600} of 0.008. For fluorescence microscopy of vegetatively growing cells, low fluorescence medium (LFM) with 2 % glucose was used (Usherenko et al, 2014).

Plasmids were constructed by standard methods (Ausubel et al, 2001) and are listed with their respective genotypes in Supplementary Table S2. Yeast codon-optimized yomNeonGreen (Shaner et al, 2013) was synthesized by GeneArt (Life technologies, Carlsbad, USA). To create pCR93, pmTurquoise2-C1 (Goedhart et al, 2012) was used as template to create three cassettes with overlapping linker sequences by PCR; these fragments were then joined and cloned into the T_{ADH1}-containing backbone of pYM12 by Gibson assembly (Gibson et al, 2009). For creation of pCR87 and pCR124 from pKT178-yomTagRFP-T and pKT146-yomTagRFP-T (Lee et al, 2013) the open reading frames of the genes were changed by site-directed mutagenesis within a linker sequence to make the plasmids compatible with S3-primers (Janke et al, 2004). pCR118 was created by ligation of a PCR product containing the first 2250 base pairs of $CDC15$ into pDS89, subsequent site-directed mutagenesis of the psd coding region to yield the psd^{E139N} variant (Usherenko et al, 2014) and finally replacement of the $ADH1$ promoter by the one of $SPO74$ from pCR6.

Sporulation experiments

Synchronous sporulation in liquid culture was performed as described before (Taxis et al, 2005). For the plasmid-based experiments of sporulation-specific expression of $CDC15\Delta C$-psd^{E139N}, the glycerol step was skipped and SC instead of YP medium was used; liquid pre-cultures were grown in ventilated, clear cell culture flasks and illuminated by blue light LEDs (465 nm) with a photon flux of 30 µmol m^{-2} s^{-1}; cells were incubated in the dark during sporulation. For live-cell microscopy, cells were attached to poly-L-lysine coated glass-bottom dishes (MatTek Corporation, Ashland, USA) 4 h after induction of sporulation, washed twice with 0.01 % potassium acetate

(KOAc) and covered with 0.1 % KOAc or water. Total sporulation was checked after 2 days.

To assess spore numbers, sporulation on solid medium with 1 %, 0.1 % and 0.01 % KOAc and DNA staining with Hoechst 33342 were performed as previously described (Jungbluth *et al*, 2012). Experiments on sister dyad formation were done in the same way skipping cell fixation and DNA staining.

Microscopy

Microscopy was performed with an Axiovert 200M inverse microscope (Zeiss, Oberkochen, Germany) equipped with a 1394 ORCA ERA CCD camera (Hamamatsu Photonics, Hamamatsu City, Japan), filter sets for DAPI, cyanGFP, EGFP, YFP and rhodamine (Chroma Technology, Bellows Falls, USA) and a Zeiss 63x Plan Apochromat oil lens (NA 1.4). Single-plane bright field or phase contrast images of the cells and z-stacks (0.5 µm or 0.3 µm z-spacing) in the appropriate fluorescence channels were recorded using the image acquisition software Volocity 5.3 (PerkinElmer, Waltham, USA). 2×2 binning was used for time course experiments. Images were exported as 16-bit TIFFs and further processed and evaluated in ImageJ (Schneider *et al*, 2012). For analysis of protein localization, image stacks (0.3 µm z-spacing) of the fluorescent channels were deconvolved: first, point spread functions for each channel were computed by the ImageJ plugin PSF Generator using the Richards & Wolf model (Kirshner *et al*, 2013); image deconvolution was then performed on the z-stacks by the ImageJ plugin DeconvolutionLab with 25 iterations of the Richardson-Lucy algorithm (Vonesch & Unser, 2008). Composites for evaluations were prepared using maximum projections of the fluorescence channels and bicubic image scaling. No image manipulations other than adjustment of histogram and background subtraction were applied. SPB distances were measured in ImageJ by the "3D Distance Tool" (https://imagej.nih.gov/ij/macros/tools/3D_Distance_Tool.txt) with stacks of 0.3 µm spaced images covering whole cells.

Immunoblotting

Samples from liquid cultures were treated by alkaline lysis with subsequent TCA precipitation and subjected to immunoblotting as previously described (Jungbluth *et al*, 2010). For quantification of meiotic plaque proteins and Nud1 and Cnm67, protein

samples of the time course (4-10 h, samples taken every hour) were pooled before subjecting them to SDS-PAGE. Proteins were detected by primary antibodies specific for either hemagglutinin (HA; Sigma-Aldrich, St. Louis, USA), Myc (Cell Signaling Technology, Danvers, USA), TEV protease (a kind gift of M. Ehrmann, University of Duisburg-Essen, Germany) or Tub1 (loading control; Abcam, Cambridge, UK), HRPO-coupled secondary antibodies against mouse or rabbit IgG (Dianova, Hamburg, Germany; Santa Cruz Biotechnology, Santa Cruz, USA) with a Chemostar professional imaging device (INTAS, Göttingen, Germany). Representative images were prepared by inverting grey values and adjusting brightness and contrast. Quantification of the signals was done using 16-bit images and ImageJ. Protein levels were corrected for tubulin signals and normalized to the respective controls.

Quantitative fluorescence measurements

Sodium azide was immediately added to samples from liquid cultures to a final concentration of 10 mM and samples were stored on ice until the end of the experiment. Then, samples were transferred into a black, flat-bottom 96-well microplate and fluorescence intensity was recorded with a plate reader (Synergy Mx, BioTek, Winooski, USA); wavelengths were set to 485 nm excitation and 525 nm emission. A control strain (YKS32 with pRS426) was used to subtract background fluorescence.

Data evaluation and statistical tests

Data evaluation and visualization was performed in R (R Core Team, 2015). Fractions of different cell species were calculated in percent of total cells. Stacked bar plots were created with mean values. Box plots show the median, first and third quartiles, notches span maximum 1.5-fold of interquartile range, data points outside this range are shown as separate points. Numbers of independent biological replicates are stated in the figure descriptions ("n").

Sporulation efficiency as a simplified measure of sporulation performance was calculated by the following formula:

$$sporulation\ efficiency = \frac{cell\ fraction_{monads} + 2 \times cell\ fraction_{dyads} + 3 \times cell\ fraction_{triads} + 4 \times cell\ fraction_{tetrads}}{4}$$

Weighted changes in the fractions of cell species for Figure 3 were computed for each experiment as followed:

$$weighted\ change_{cell\ species} = log_2 \frac{cell\ fraction_{mutant}}{cell\ fraction_{control}} \times |cell\ fraction_{mutant} - cell\ fraction_{control}|$$

Median values of the different cell species per strain were used to create a heat map for every acetate concentration.

Tests for statistical significance of differences were performed according to data type and structure: Fisher's exact test was used for categorical data with more than two categories. Categorical data with only two categories were transformed to continuous relative values. Shapiro-Wilk test was applied to check for normality. Accordingly, a Welch two-sample t-test or the exact Wilcoxon-Mann-Whitney test of the "coin" R-package (Hothorn *et al*, 2008) was used to check for statistical significant differences. For testing differences in meiotic plaque protein levels and initial amounts of Nud1 and Cnm67, two-sided one-sample t-tests against 100 % were performed.

Acknowledgements

Author contributions

CR and CT designed the experiments. CR, A-KA and APL performed the experiments. CR, A-KA and CT analyzed and interpreted the data. CR and CT prepared the manuscript. All authors read and approved the manuscript.

Conflict of Interest

The authors declare that they have no competing interests.

References

Adames NR, Oberle JR & Cooper JA (2001) The surveillance mechanism of the spindle position checkpoint in yeast. *J Cell Biol* **153:** 159–68

Adams IR & Kilmartin J V (1999) Localization of core spindle pole body (SPB) components during SPB duplication in Saccharomyces cerevisiae. *J Cell Biol* **145:** 809–23

Asakawa K, Yoshida S, Otake F & Toh-e A (2001) A novel functional domain of

Cdc15 kinase is required for its interaction with Tem1 GTPase in Saccharomyces cerevisiae. *Genetics* **157:** 1437–50

Attner MA & Amon A (2012) Control of the mitotic exit network during meiosis. *Mol Biol Cell* **23:** 3122–32

Attner MA, Miller MP, Ee L, Elkin SK & Amon A (2013) Polo kinase Cdc5 is a central regulator of meiosis I. *Proc Natl Acad Sci U S A* **110:** 14278–83

Bardin AJ, Boselli MG & Amon A (2003) Mitotic exit regulation through distinct domains within the protein kinase Cdc15. *Mol Cell Biol* **23:** 5018–30

Bardin AJ, Visintin R & Amon A (2000) A mechanism for coupling exit from mitosis to partitioning of the nucleus. *Cell* **102:** 21–31

Beach DL, Thibodeaux J, Maddox P, Yeh E & Bloom K (2000) The role of the proteins Kar9 and Myo2 in orienting the mitotic spindle of budding yeast. *Curr Biol* **10:** 1497–506

Bertazzi DT, Kurtulmus B & Pereira G (2011) The cortical protein Lte1 promotes mitotic exit by inhibiting the spindle position checkpoint kinase Kin4. *J Cell Biol* **193:** 1033–48

Bullitt E, Rout MP, Kilmartin J V & Akey CW (1997) The yeast spindle pole body is assembled around a central crystal of Spc42p. *Cell* **89:** 1077–86

Burns S, Avena JS, Unruh JR, Yu Z, Smith SE, Slaughter BD, Winey M & Jaspersen SL (2015) Structured illumination with particle averaging reveals novel roles for yeast centrosome components during duplication. *Elife* **4:** e08586

Caydasi AK, Lohel M, Grünert G, Dittrich P, Pereira G & Ibrahim B (2012) A dynamical model of the spindle position checkpoint. *Mol Syst Biol* **8:** 582

Chu S, DeRisi J, Eisen M, Mulholland J, Botstein D, Brown PO & Herskowitz I (1998) The transcriptional program of sporulation in budding yeast. *Science* **282:** 699–705

Clyne RK, Katis VL, Jessop L, Benjamin KR, Herskowitz I, Lichten M & Nasmyth K (2003) Polo-like kinase Cdc5 promotes chiasmata formation and cosegregation of sister centromeres at meiosis I. *Nat Cell Biol* **5:** 480–5

Coluccio A, Bogengruber E, Conrad MN, Dresser ME, Briza P & Neiman AM (2004) Morphogenetic pathway of spore wall assembly in Saccharomyces cerevisiae. *Eukaryot Cell* **3:** 1464–75

Coluccio AE, Rodriguez RK, Kernan MJ & Neiman AM (2008) The yeast spore wall enables spores to survive passage through the digestive tract of Drosophila. *PLoS One* **3:** e2873

Conduit PT & Raff JW (2010) Cnn dynamics drive centrosome size asymmetry to ensure daughter centriole retention in Drosophila neuroblasts. *Curr Biol* **20:** 2187–92

D'Aquino KE, Monje-Casas F, Paulson J, Reiser V, Charles GM, Lai L, Shokat KM & Amon A (2005) The protein kinase Kin4 inhibits exit from mitosis in response to spindle position defects. *Mol Cell* **19:** 223–34

Davidow LS, Goetsch L & Byers B (1980) Preferential Occurrence of Nonsister Spores in Two-Spored Asci of SACCHAROMYCES CEREVISIAE: Evidence for Regulation of Spore-Wall Formation by the Spindle Pole Body. *Genetics* **94:**

581–95

Deng C & Saunders WS (2001) ADY1, a novel gene required for prospore membrane formation at selected spindle poles in Saccharomyces cerevisiae. *Mol Biol Cell* **12:** 2646–59

Diamond AE, Park J-S, Inoue I, Tachikawa H & Neiman AM (2009) The anaphase promoting complex targeting subunit Ama1 links meiotic exit to cytokinesis during sporulation in Saccharomyces cerevisiae. *Mol Biol Cell* **20:** 134–45

Eastwood MD, Cheung SWT, Lee KY, Moffat J & Meneghini MD (2012) Developmentally programmed nuclear destruction during yeast gametogenesis. *Dev Cell* **23:** 35–44

Elserafy M, Šarić M, Neuner A, Lin T, Zhang W, Seybold C, Sivashanmugam L & Schiebel E (2014) Molecular mechanisms that restrict yeast centrosome duplication to one event per cell cycle. *Curr Biol* **24:** 1456–66

Esposito RE & Klapholz S (1981) Meiosis and ascospore development. *Cold Spring Harb Monogr Arch* **11:** 211–287

Falk JE, Chan LY & Amon A (2011) Lte1 promotes mitotic exit by controlling the localization of the spindle position checkpoint kinase Kin4. *Proc Natl Acad Sci U S A* **108:** 12584–90

Falk JE, Tsuchiya D, Verdaasdonk J, Lacefield S, Bloom K & Amon A (2016) Spatial signals link exit from mitosis to spindle position. *Elife* **5:** e14036

Fraschini R, D'Ambrosio C, Venturetti M, Lucchini G & Piatti S (2006) Disappearance of the budding yeast Bub2-Bfa1 complex from the mother-bound spindle pole contributes to mitotic exit. *J Cell Biol* **172:** 335–46

Freese EB, Chu MI & Freese E (1982) Initiation of yeast sporulation of partial carbon, nitrogen, or phosphate deprivation. *J Bacteriol* **149:** 840–51

Geymonat M, Spanos A, de Bettignies G & Sedgwick SG (2009) Lte1 contributes to Bfa1 localization rather than stimulating nucleotide exchange by Tem1. *J Cell Biol* **187:** 497–511

Geymonat M, Spanos A, Smith SJM, Wheatley E, Rittinger K, Johnston LH & Sedgwick SG (2002) Control of mitotic exit in budding yeast. In vitro regulation of Tem1 GTPase by Bub2 and Bfa1. *J Biol Chem* **277:** 28439–45

Geymonat M, Spanos A, Walker PA, Johnston LH & Sedgwick SG (2003) In vitro regulation of budding yeast Bfa1/Bub2 GAP activity by Cdc5. *J Biol Chem* **278:** 14591–14594

Gibson DG, Young L, Chuang R-Y, Venter JC, Hutchison CA & Smith HO (2009) Enzymatic assembly of DNA molecules up to several hundred kilobases. *Nat Methods* **6:** 343–5

Goedhart J, von Stetten D, Noirclerc-Savoye M, Lelimousin M, Joosen L, Hink MA, van Weeren L, Gadella TWJ & Royant A (2012) Structure-guided evolution of cyan fluorescent proteins towards a quantum yield of 93%. *Nat Commun* **3:** 751

Gordon O, Taxis C, Keller PJ, Benjak A, Stelzer EHK, Simchen G & Knop M (2006) Nud1p, the yeast homolog of Centriolin, regulates spindle pole body inheritance in meiosis. *EMBO J* **25:** 3856–68

Gruneberg U, Campbell K, Simpson C, Grindlay J & Schiebel E (2000) Nud1p links

astral microtubule organization and the control of exit from mitosis. *EMBO J* **19:** 6475–88

Gryaznova Y, Koca Caydasi A, Malengo G, Sourjik V & Pereira G (2016) A FRET-based study reveals site-specific regulation of spindle position checkpoint proteins at yeast centrosomes. *Elife* **5:** e14029

Hanson MG, Aiken J, Sietsema D V, Sept D, Bates EA, Niswander L & Moore JK (2016) Novel α-tubulin mutation disrupts neural development and tubulin proteostasis. *Dev Biol* **409:** 406–19

Hergovich A & Hemmings BA (2012) Hippo signalling in the G2/M cell cycle phase: lessons learned from the yeast MEN and SIN pathways. *Semin Cell Dev Biol* **23:** 794–802

Hothorn T, Hornik K, Wiel MA van de & Zeileis A (2008) Implementing a Class of Permutation Tests: The coin Package. *J Stat Softw* **28:** 1–23

Hotz M, Leisner C, Chen D, Manatschal C, Wegleiter T, Ouellet J, Lindstrom D, Gottschling DE, Vogel J & Barral Y (2012a) Spindle Pole Bodies Exploit the Mitotic Exit Network in Metaphase to Drive Their Age-Dependent Segregation. *Cell* **148:** 958–972

Hotz M, Lengefeld J & Barral Y (2012b) The MEN mediates the effects of the spindle assembly checkpoint on Kar9-dependent spindle pole body inheritance in budding yeast. *Cell Cycle* **11:** 3109–16

Hu F & Elledge SJ (2002) Bub2 is a cell cycle regulated phospho-protein controlled by multiple checkpoints. *Cell Cycle* **1:** 351–355

Hu F, Wang Y, Liu D, Li Y, Qin J & Elledge SJ (2001) Regulation of the Bub2/Bfa1 GAP complex by Cdc5 and cell cycle checkpoints. *Cell* **107:** 655–65

Huang LS, Doherty HK & Herskowitz I (2005) The Smk1p MAP kinase negatively regulates Gsc2p, a 1,3-beta-glucan synthase, during spore wall morphogenesis in Saccharomyces cerevisiae. *Proc Natl Acad Sci U S A* **102:** 12431–6

Ito Y, Yamanishi M, Ikeuchi A, Imamura C, Tokuhiro K, Kitagawa T & Matsuyama T (2013) Characterization of five terminator regions that increase the protein yield of a transgene in Saccharomyces cerevisiae. *J Biotechnol* **168:** 486–92

Izumi H & Kaneko Y (2012) Evidence of asymmetric cell division and centrosome inheritance in human neuroblastoma cells. *Proc Natl Acad Sci U S A* **109:** 18048–53

Janke C, Magiera MM, Rathfelder N, Taxis C, Reber S, Maekawa H, Moreno-Borchart A, Doenges G, Schwob E, Schiebel E & Knop M (2004) A versatile toolbox for PCR-based tagging of yeast genes: new fluorescent proteins, more markers and promoter substitution cassettes. *Yeast* **21:** 947–62

Januschke J, Llamazares S, Reina J & Gonzalez C (2011) Drosophila neuroblasts retain the daughter centrosome. *Nat Commun* **2:** 243

Januschke J, Reina J, Llamazares S, Bertran T, Rossi F, Roig J & Gonzalez C (2013) Centrobin controls mother-daughter centriole asymmetry in Drosophila neuroblasts. *Nat Cell Biol* **15:** 241–8

Jaspersen SL, Charles JF, Tinker-Kulberg RL & Morgan DO (1998) A late mitotic regulatory network controlling cyclin destruction in Saccharomyces cerevisiae. *Mol Biol Cell* **9:** 2803–17

Juanes MA & Piatti S (2016) The final cut: cell polarity meets cytokinesis at the bud neck in S. cerevisiae. *Cell Mol Life Sci*: 1–22

Juanes MA, Twyman H, Tunnacliffe E, Guo Z, ten Hoopen R & Segal M (2013) Spindle pole body history intrinsically links pole identity with asymmetric fate in budding yeast. *Curr Biol* **23:** 1310–9

Jungbluth M, Mösch H-U & Taxis C (2012) Acetate regulation of spore formation is under the control of the Ras/cyclic AMP/protein kinase A pathway and carbon dioxide in Saccharomyces cerevisiae. *Eukaryot Cell* **11:** 1021–32

Jungbluth M, Renicke C & Taxis C (2010) Targeted protein depletion in Saccharomyces cerevisiae by activation of a bidirectional degron. *BMC Syst Biol* **4:** 176

Kamieniecki RJ, Liu L & Dawson DS (2005) FEAR but not MEN genes are required for exit from meiosis I. *Cell Cycle* **4:** 1093–8

Kawaguchi H, Yoshida M & Yamashita I (1992) Nutritional Regulation of Meiosis-specific Gene Expression in Saccharomyces cerevisiae. *Biosci Biotechnol Biochem* **56:** 289–297

Keck JM, Jones MH, Wong CCL, Binkley J, Chen D, Jaspersen SL, Holinger EP, Xu T, Niepel M, Rout MP, Vogel J, Sidow A, Yates JR & Winey M (2011) A cell cycle phosphoproteome of the yeast centrosome. *Science* **332:** 1557–61

Kim J, Luo G, Bahk YY & Song K (2012) Cdc5-dependent asymmetric localization of bfa1 fine-tunes timely mitotic exit. *PLoS Genet* **8:** e1002450

Kirshner H, Aguet F, Sage D & Unser M (2013) 3-D PSF fitting for fluorescence microscopy: implementation and localization application. *J Microsc* **249:** 13–25

Klein F, Mahr P, Galova M, Buonomo SB, Michaelis C, Nairz K & Nasmyth K (1999) A central role for cohesins in sister chromatid cohesion, formation of axial elements, and recombination during yeast meiosis. *Cell* **98:** 91–103

Knop M & Schiebel E (1998) Receptors determine the cellular localization of a gamma-tubulin complex and thereby the site of microtubule formation. *EMBO J* **17:** 3952–67

Knop M & Strasser K (2000) Role of the spindle pole body of yeast in mediating assembly of the prospore membrane during meiosis. *EMBO J* **19:** 3657–67

Lam C, Santore E, Lavoie E, Needleman L, Fiacco N, Kim C & Neiman AM (2014) A visual screen of protein localization during sporulation identifies new components of prospore membrane-associated complexes in budding yeast. *Eukaryot Cell* **13:** 383–91

Lee BH & Amon A (2003) Role of Polo-like kinase CDC5 in programming meiosis I chromosome segregation. *Science* **300:** 482–6

Lee S, Lim WA & Thorn KS (2013) Improved blue, green, and red fluorescent protein tagging vectors for S. cerevisiae. *PLoS One* **8:** e67902

Lee SE, Frenz LM, Wells NJ, Johnson AL & Johnston LH (2001) Order of function of the budding-yeast mitotic exit-network proteins Tem1, Cdc15, Mob1, Dbf2, and Cdc5. *Curr Biol* **11:** 784–8

Lee W-L, Oberle JR & Cooper J a (2003) The role of the lissencephaly protein Pac1 during nuclear migration in budding yeast. *J Cell Biol* **160:** 355–64

Leisner C, Kammerer D, Denoth A, Britschi M, Barral Y & Liakopoulos D (2008) Regulation of Mitotic Spindle Asymmetry by SUMO and the Spindle-Assembly Checkpoint in Yeast. *Curr Biol* **18:** 1249–1255

Lerit DA & Rusan NM (2013) PLP inhibits the activity of interphase centrosomes to ensure their proper segregation in stem cells. *J Cell Biol* **202:** 1013–22

Li P, Shao Y, Jin H & Yu H-G (2015) Ndj1, a telomere-associated protein, regulates centrosome separation in budding yeast meiosis. *J Cell Biol* **209:** 247–59

Liakopoulos D, Kusch J, Grava S, Vogel J & Barral Y (2003) Asymmetric loading of Kar9 onto spindle poles and microtubules ensures proper spindle alignment. *Cell* **112:** 561–74

Luca FC & Winey M (1998) MOB1, an essential yeast gene required for completion of mitosis and maintenance of ploidy. *Mol Biol Cell* **9:** 29–46

Maekawa H, Priest C, Lechner J, Pereira G & Schiebel E (2007) The yeast centrosome translates the positional information of the anaphase spindle into a cell cycle signal. *J Cell Biol* **179:** 423–36

Mah AS, Elia AEH, Devgan G, Ptacek J, Schutkowski M, Snyder M, Yaffe MB & Deshaies RJ (2005) Substrate specificity analysis of protein kinase complex Dbf2-Mob1 by peptide library and proteome array screening. *BMC Biochem* **6:** 22

Mah AS, Jang J & Deshaies RJ (2001) Protein kinase Cdc15 activates the Dbf2-Mob1 kinase complex. *Proc Natl Acad Sci U S A* **98:** 7325–30

Maier P, Rathfelder N, Finkbeiner MG, Taxis C, Mazza M, Le Panse S, Haguenauer-Tsapis R & Knop M (2007) Cytokinesis in yeast meiosis depends on the regulated removal of Ssp1p from the prospore membrane. *EMBO J* **26:** 1843–52

Markus SM & Lee W-L (2011) Regulated offloading of cytoplasmic dynein from microtubule plus ends to the cortex. *Dev Cell* **20:** 639–51

Mathieson EM, Schwartz C & Neiman AM (2010) Membrane assembly modulates the stability of the meiotic spindle-pole body. *J Cell Sci* **123:** 2481–90

Meitinger F, Palani S, Hub B & Pereira G (2013) Dual function of the NDR-kinase Dbf2 in the regulation of the F-BAR protein Hof1 during cytokinesis. *Mol Biol Cell* **24:** 1290–304

Meitinger F, Petrova B, Lombardi IM, Bertazzi DT, Hub B, Zentgraf H & Pereira G (2010) Targeted localization of Inn1, Cyk3 and Chs2 by the mitotic-exit network regulates cytokinesis in budding yeast. *J Cell Sci* **123:** 1851–61

Menendez-Benito V, van Deventer SJ, Jimenez-Garcia V, Roy-Luzarraga M, van Leeuwen F & Neefjes J (2013) Spatiotemporal analysis of organelle and macromolecular complex inheritance. *Proc Natl Acad Sci U S A* **110:** 175–80

Miller RK & Rose MD (1998) Kar9p is a novel cortical protein required for cytoplasmic microtubule orientation in yeast. *J Cell Biol* **140:** 377–90

Mohl DA, Huddleston MJ, Collingwood TS, Annan RS & Deshaies RJ (2009) Dbf2-Mob1 drives relocalization of protein phosphatase Cdc14 to the cytoplasm during exit from mitosis. *J Cell Biol* **184:** 527–39

Mok J, Kim PM, Lam HYK, Piccirillo S, Zhou X, Jeschke GR, Sheridan DL, Parker SA, Desai V, Jwa M, Cameroni E, Niu H, Good M, Remenyi A, Ma J-LN, Sheu Y-

J, Sassi HE, Sopko R, Chan CSM, De Virgilio C, et al (2010) Deciphering protein kinase specificity through large-scale analysis of yeast phosphorylation site motifs. *Sci Signal* **3:** ra12

Moreno-Borchart AC, Strasser K, Finkbeiner MG, Shevchenko A, Shevchenko A & Knop M (2001) Prospore membrane formation linked to the leading edge protein (LEP) coat assembly. *EMBO J* **20:** 6946–57

Nakanishi H, Morishita M, Schwartz CL, Coluccio A, Engebrecht J & Neiman AM (2006) Phospholipase D and the SNARE Sso1p are necessary for vesicle fusion during sporulation in yeast. *J Cell Sci* **119:** 1406–15

Neiman AM (1998) Prospore membrane formation defines a developmentally regulated branch of the secretory pathway in yeast. *J Cell Biol* **140:** 29–37

Ni L, Zheng Y, Hara M, Pan D & Luo X (2015) Structural basis for Mob1-dependent activation of the core Mst-Lats kinase cascade in Hippo signaling. *Genes Dev* **29:** 1416–31

Nickas ME, Diamond AE, Yang M-J & Neiman AM (2004) Regulation of spindle pole function by an intermediary metabolite. *Mol Biol Cell* **15:** 2606–16

Nickas ME & Neiman AM (2002) Ady3p links spindle pole body function to spore wall synthesis in Saccharomyces cerevisiae. *Genetics* **160:** 1439–50

Nickas ME, Schwartz C & Neiman AM (2003) Ady4p and Spo74p are components of the meiotic spindle pole body that promote growth of the prospore membrane in Saccharomyces cerevisiae. *Eukaryot Cell* **2:** 431–45

Okamoto S & Iino T (1981) Selective abortion of two nonsister nuclei in a developing ascus of the hfd-1 mutant in Saccharomyces cerevisiae. *Genetics* **99:** 197–209

Pablo-Hernando ME, Arnaiz-Pita Y, Nakanishi H, Dawson D, del Rey F, Neiman AM & Vázquez de Aldana CR (2007) Cdc15 is required for spore morphogenesis independently of Cdc14 in Saccharomyces cerevisiae. *Genetics* **177:** 281–93

Park J-E, Park CJ, Sakchaisri K, Karpova T, Asano S, McNally J, Sunwoo Y, Leem S-H & Lee KS (2004) Novel functional dissection of the localization-specific roles of budding yeast polo kinase Cdc5p. *Mol Cell Biol* **24:** 9873–86

Paulissen SM, Slubowski CJ, Roesner JM & Huang LS (2016) Timely closure of the prospore membrane requires SPS1 and SPO77 in Saccharomyces cerevisiae. *Genetics***:** 143–148

Pereira G & Schiebel E (2005) Kin4 kinase delays mitotic exit in response to spindle alignment defects. *Mol Cell* **19:** 209–21

Pereira G, Tanaka TU, Nasmyth K & Schiebel E (2001) Modes of spindle pole body inheritance and segregation of the Bfa1p-Bub2p checkpoint protein complex. *EMBO J* **20:** 6359–70

Piel M, Meyer P, Khodjakov A, Rieder CL & Bornens M (2000) The respective contributions of the mother and daughter centrioles to centrosome activity and behavior in vertebrate cells. *J Cell Biol* **149:** 317–30

Ptacek J, Devgan G, Michaud G, Zhu H, Zhu X, Fasolo J, Guo H, Jona G, Breitkreutz A, Sopko R, McCartney RR, Schmidt MC, Rachidi N, Lee S-J, Mah AS, Meng L, Stark MJR, Stern DF, De Virgilio C, Tyers M, et al (2005) Global analysis of protein phosphorylation in yeast. *Nature* **438:** 679–84

R Core Team (2015) R: A Language and Environment for Statistical Computing.

Rebollo E, Sampaio P, Januschke J, Llamazares S, Varmark H & González C (2007) Functionally unequal centrosomes drive spindle orientation in asymmetrically dividing Drosophila neural stem cells. *Dev Cell* **12:** 467–74

Renicke C, Schuster D, Usherenko S, Essen L-O & Taxis C (2013) A LOV2 domain-based optogenetic tool to control protein degradation and cellular function. *Chem Biol* **20:** 619–26

Rock JM & Amon A (2011) Cdc15 integrates Tem1 GTPase-mediated spatial signals with Polo kinase-mediated temporal cues to activate mitotic exit. *Genes Dev* **25:** 1943–54

Rock JM, Lim D, Stach L, Ogrodowicz RW, Keck JM, Jones MH, Wong CCL, Yates JR, Winey M, Smerdon SJ, Yaffe MB & Amon A (2013) Activation of the yeast Hippo pathway by phosphorylation-dependent assembly of signaling complexes. *Science* **340:** 871–5

Rusan NM & Peifer M (2007) A role for a novel centrosome cycle in asymmetric cell division. *J Cell Biol* **177:** 13–20

Salzmann V, Chen C, Chiang C-YA, Tiyaboonchai A, Mayer M & Yamashita YM (2014) Centrosome-dependent asymmetric inheritance of the midbody ring in Drosophila germline stem cell division. *Mol Biol Cell* **25:** 267–75

Schaerer F, Morgan G, Winey M & Philippsen P (2001) Cnm67p is a spacer protein of the Saccharomyces cerevisiae spindle pole body outer plaque. *Mol Biol Cell* **12:** 2519–33

Schiestl RH & Gietz RD (1989) High efficiency transformation of intact yeast cells using single stranded nucleic acids as a carrier. *Curr Genet* **16:** 339–46

Schneider CA, Rasband WS & Eliceiri KW (2012) NIH Image to ImageJ: 25 years of image analysis. *Nat Methods* **9:** 671–5

Shaner NC, Lambert GG, Chammas A, Ni Y, Cranfill PJ, Baird MA, Sell BR, Allen JR, Day RN, Israelsson M, Davidson MW & Wang J (2013) A bright monomeric green fluorescent protein derived from Branchiostoma lanceolatum. *Nat Methods* **10:** 407–9

Shaner NC, Lin MZ, McKeown MR, Steinbach P a, Hazelwood KL, Davidson MW & Tsien RY (2008) Improving the photostability of bright monomeric orange and red fluorescent proteins. *Nat Methods* **5:** 545–51

Shaw SL, Yeh E, Maddox P, Salmon ED & Bloom K (1997) Astral microtubule dynamics in yeast: a microtubule-based searching mechanism for spindle orientation and nuclear migration into the bud. *J Cell Biol* **139:** 985–94

Sheeman B, Carvalho P, Sagot I, Geiser J, Kho D, Hoyt MA & Pellman D (2003) Determinants of S. cerevisiae dynein localization and activation: Implications for the mechanism of spindle positioning. *Curr Biol* **13:** 364–372

Sherman F (2002) Getting started with yeast. *Methods Enzymol* **41:** 3–41

Shirayama M, Zachariae W, Ciosk R & Nasmyth K (1998) The Polo-like kinase Cdc5p and the WD-repeat protein Cdc20p/fizzy are regulators and substrates of the anaphase promoting complex in Saccharomyces cerevisiae. *EMBO J* **17:** 1336–49

Shirk K, Jin H, Giddings TH, Winey M & Yu H-G (2011) The Aurora kinase Ipl1 is necessary for spindle pole body cohesion during budding yeast meiosis. *J Cell Sci* **124:** 2891–6

Shou W, Seol JH, Shevchenko A, Baskerville C, Moazed D, Chen ZWS, Jang J, Charbonneau H & Deshaies RJ (1999) Exit from mitosis is triggered by Tem1-dependent release of the protein phosphatase Cdc14 from nucleolar RENT complex. *Cell* **97:** 233–44

Song S, Grenfell TZ, Garfield S, Erikson RL & Lee KS (2000) Essential function of the polo box of Cdc5 in subcellular localization and induction of cytokinetic structures. *Mol Cell Biol* **20:** 286–98

Sourirajan A & Lichten M (2008) Polo-like kinase Cdc5 drives exit from pachytene during budding yeast meiosis. *Genes Dev* **22:** 2627–32

Su X, Qiu W, Gupta ML, Pereira-Leal JB, Reck-Peterson SL & Pellman D (2011) Mechanisms underlying the dual-mode regulation of microtubule dynamics by Kip3/kinesin-8. *Mol Cell* **43:** 751–63

Taxis C, Keller P, Kavagiou Z, Jensen LJ, Colombelli J, Bork P, Stelzer EHK & Knop M (2005) Spore number control and breeding in Saccharomyces cerevisiae: a key role for a self-organizing system. *J Cell Biol* **171:** 627–40

Taxis C & Knop M (2012) Ubiquitin Family Modifiers and the Proteasome: Reviews and Protocols. In, Dohmen JR & Scheffner M (eds) pp 611–626. Totowa, NJ: Humana Press

Taxis C, Maeder C, Reber S, Rathfelder N, Miura K, Greger K, Stelzer EHK & Knop M (2006) Dynamic organization of the actin cytoskeleton during meiosis and spore formation in budding yeast. *Traffic* **7:** 1628–42

Taxis C, Stier G, Spadaccini R & Knop M (2009) Efficient protein depletion by genetically controlled deprotection of a dormant N-degron. *Mol Syst Biol* **5:** 267

Usherenko S, Stibbe H, Muscò M, Essen L-O, Kostina EA & Taxis C (2014) Photo-sensitive degron variants for tuning protein stability by light. *BMC Syst Biol* **8:** 128

Valerio-Santiago M & Monje-Casas F (2011) Tem1 localization to the spindle pole bodies is essential for mitotic exit and impairs spindle checkpoint function. *J Cell Biol* **192:** 599–614

Visintin R & Amon A (2001) Regulation of the mitotic exit protein kinases Cdc15 and Dbf2. *Mol Biol Cell* **12:** 2961–74

Visintin R, Craig K, Hwang ES, Prinz S, Tyers M & Amon A (1998) The phosphatase Cdc14 triggers mitotic exit by reversal of Cdk-dependent phosphorylation. *Mol Cell* **2:** 709–18

Visintin R, Hwang ES & Amon A (1999) Cfi1 prevents premature exit from mitosis by anchoring Cdc14 phosphatase in the nucleolus. *Nature* **398:** 818–23

Vonesch C & Unser M (2008) A fast thresholded landweber algorithm for wavelet-regularized multidimensional deconvolution. *IEEE Trans Image Process* **17:** 539–49

Wang X, Tsai J-W, Imai JH, Lian W-N, Vallee RB & Shi S-H (2009) Asymmetric centrosome inheritance maintains neural progenitors in the neocortex. *Nature* **461:** 947–55

Winey M, Goetsch L, Baum P & Byers B (1991) MPS1 and MPS2: novel yeast genes defining distinct steps of spindle pole body duplication. *J Cell Biol* **114:** 745–54

Yamanishi M, Ito Y, Kintaka R, Imamura C, Katahira S, Ikeuchi A, Moriya H & Matsuyama T (2013) A genome-wide activity assessment of terminator regions in Saccharomyces cerevisiae provides a ″terminatome″ toolbox. *ACS Synth Biol* **2:** 337–47

Yamashita YM, Mahowald AP, Perlin JR & Fuller MT (2007) Asymmetric inheritance of mother versus daughter centrosome in stem cell division. *Science* **315:** 518–21
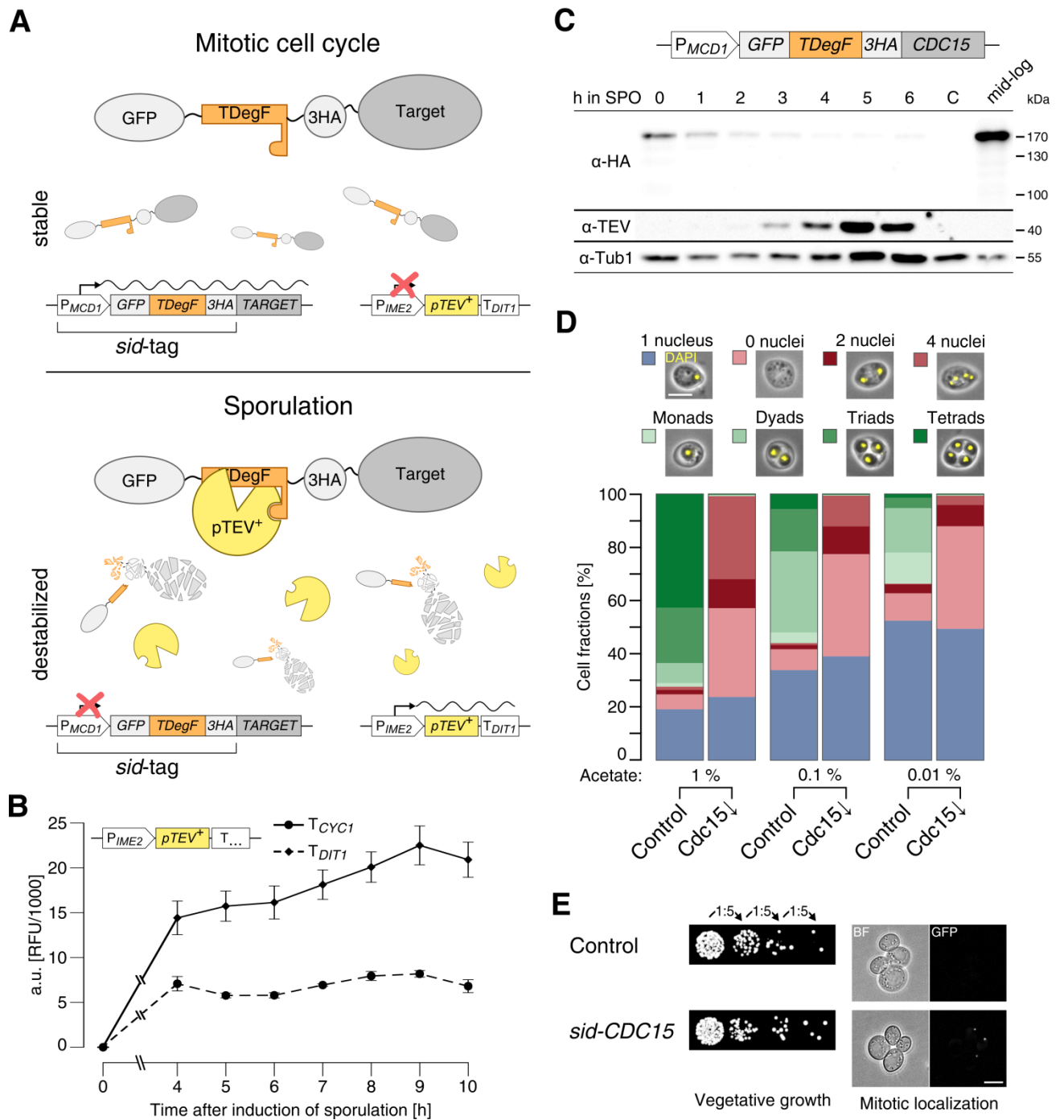
Figure 1 – Enhanced sporulation-induced protein depletion

A – Principle of sporulation-induced protein depletion (sid). The *sid*-tag is fused to the 5'-end of the target gene and substitutes the original promoter with the mitosis-specific *MCD1* promoter and the *GFP-TDegF* (TEV protease dependent degron)-*3HA*-tag. At one or more chromosomal loci, a functional cassette of meiosis-specific *IME2* promoter, *pTEV*[+] gene and *DIT1* terminator is integrated. During vegetative growth, the target gene is expressed and stable. Upon switch to sporulation conditions, the *MCD1* promoter is downregulated and pTEV[+] is produced after

initiation of meiosis. TEV cleavage of TDegF leads to activation of an N-degron and degradation of the target protein by the ubiquitin-proteasome system.

B – Terminator dependency of GFP-pTEV$^+$ production during sporulation. Diploid yeast cells with high-copy plasmids bearing either P_{IME2}-GFP-pTEV$^+$-T_{CYC1} or P_{IME2}-GFP-pTEV$^+$-T_{DIT1} were subjected to sporulation conditions. Expression of the constructs was followed by fluorimeter measurements, an empty vector control allowed background subtraction (T_{CYC1}: n = 2, T_{DIT1}: n = 9, means ± SEM).

C – Sporulation-induced depletion of Cdc15. Diploid *sid-CDC15* cells with four integrated copies of P_{IME2}-pTEV$^+$-T_{DIT1} were subjected to sporulation in. Samples for immunoblotting were taken at the indicated time points as well as during mid-log growth phase, a strain without *sid*-tag served as negative control. Anti-HA, anti-TEV, and anti-Tub1 (loading control) antibodies were used for detection.

D – Sporulation of the Cdc15 depletion mutant. The Cdc15 depletion strain (Cdc15↓) was sporulated together with a control strain on solid sporulation medium with 1 %, 0.1 % and 0.01 % acetate. Cells were classified according to their morphology and number of nuclei. Bar plot shows average results of at least 6 biological replicates. Scale bar: 5 µm.

E – Characterization of the *sid-CDC15* strain during vegetative growth. *sid-CDC15* cells were subjected to a serial dilution growth assay (left) as well as fluorescence microscopy for mitotic localization using (scale bar: 5 µm).
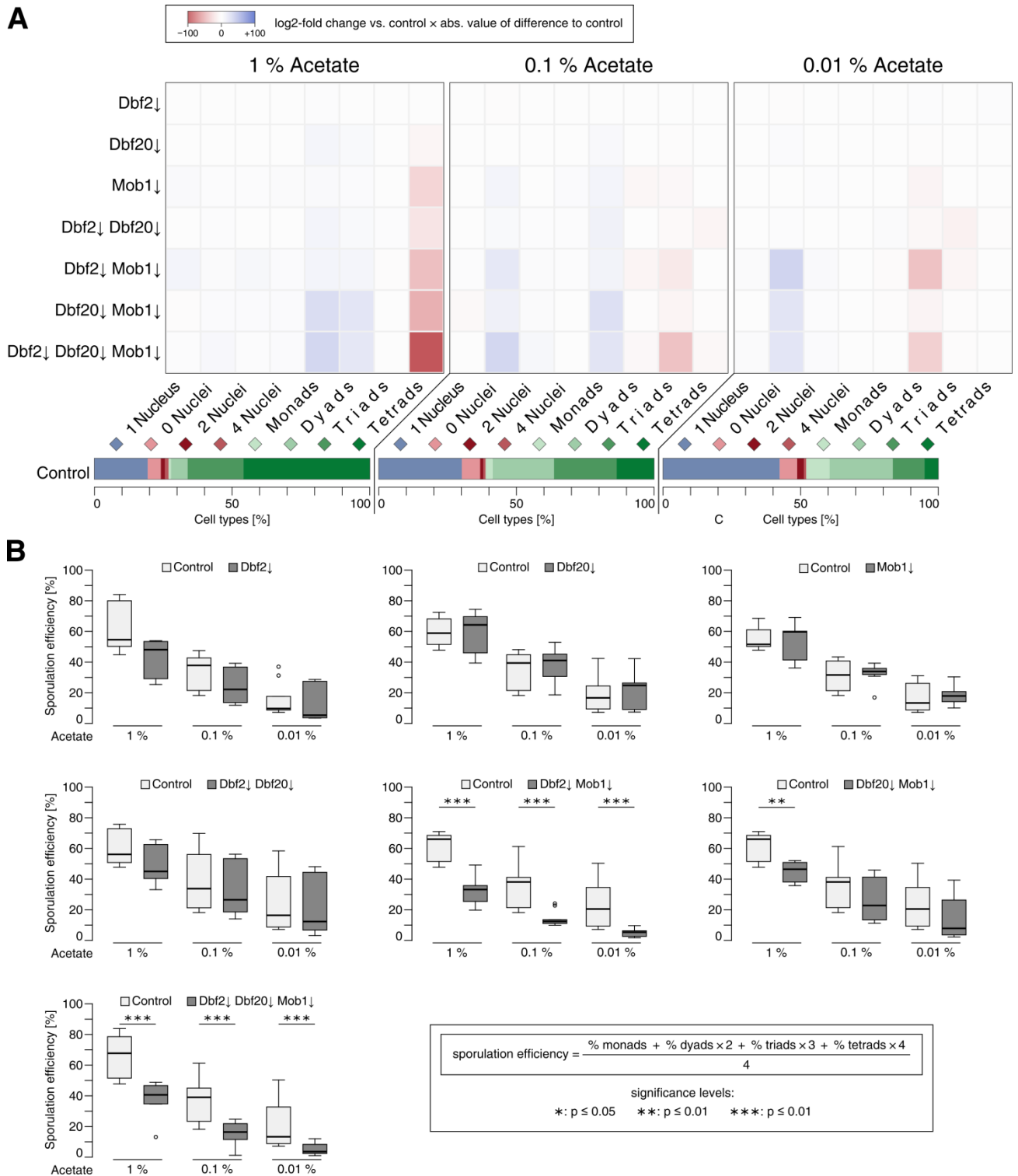
Figure 2 –Dbf2-Mob1 and Dbf20-Mob1 are required for efficient sporulation.

A – Impaired spore formation in strains with deficiencies in MEN kinase complexes. Depletion mutants for the indicated proteins were sporulated together with a control strain as described for Figure 1D. Cells were classified according to numbers of spores and nuclei. For each cell category and experiment, log2-fold changes relative to the control strain were calculated and multiplied with the absolute

value of the difference to the control. Median values for the biological replicates (n ≥ 6) of the single strains were computed and these values were then translated into a heat map with negative changes colored blue and positive changes red. As reference, reference sporulation profiles of the control are shown below (means of all experiments).

B – MEN kinase mutants show reduced sporulation efficiency. Sporulation efficiencies were calculated for the experiments described in **A**. Statistical significance of the differences was checked by Wilcoxon-Mann-Whitney tests against controls (n ≥ 6).
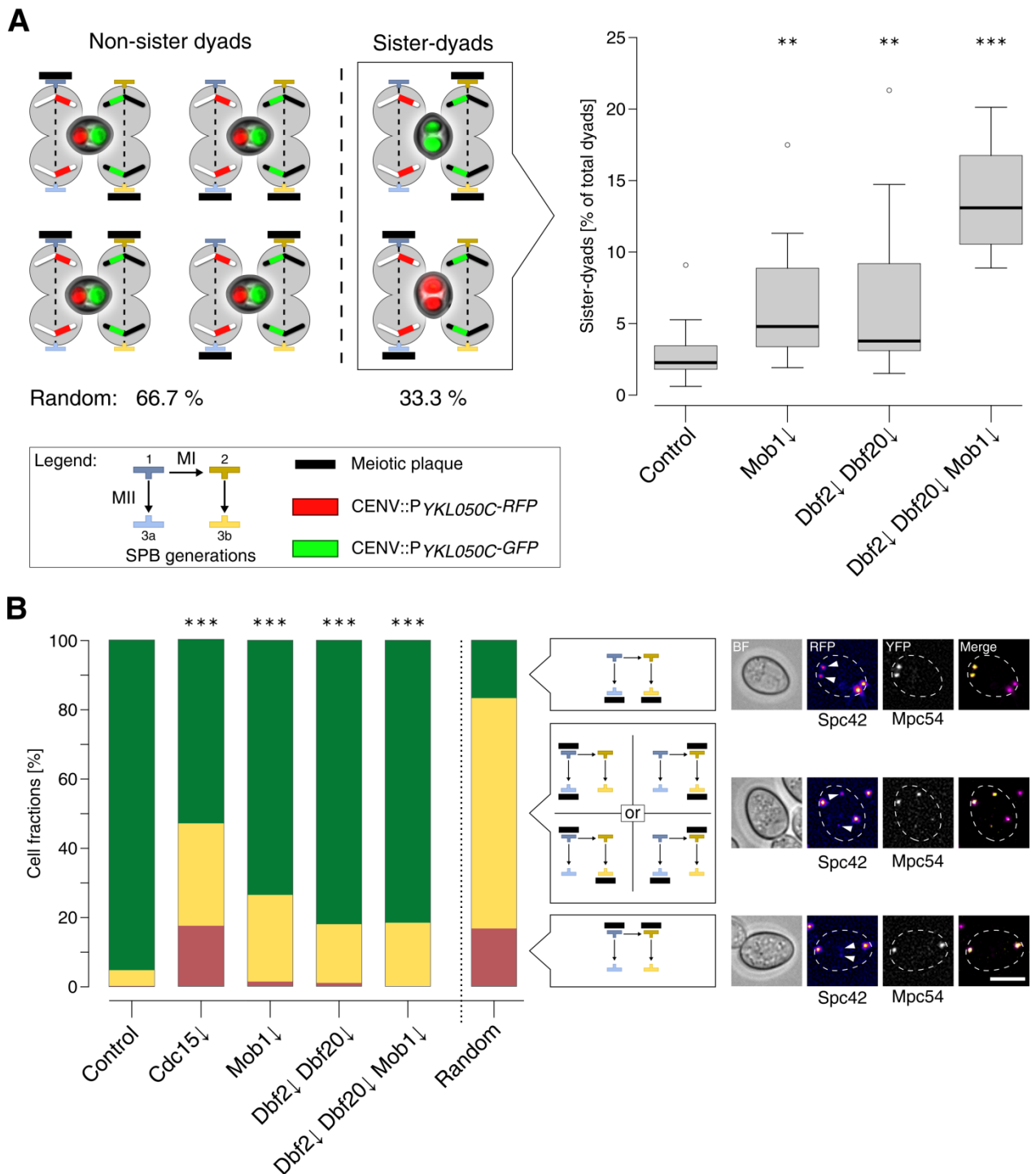
Figure 3 – The MEN is required for efficient genome inheritance during meiosis.

A – Faithful chromosome inheritance depends on the MEN. Indicated mutants were created in a strain background heterozygous for the spore-autonomous markers CENV::P$_{YKL050C}$-RFP and CENV::P$_{YKL050C}$-GFP, which allows discrimination between sister and non-sister chromosome inheritance by fluorescence microscopy. Left part of the panel depicts the different possibilities of SPB modification with two meiotic plaques and images of the resulting dyads together with the theoretical

probabilities for sister and non-sister dyad distribution in case of random SPB selection. For the graph on the right, strains were sporulated on solid sporulation medium with 0.1 % acetate and different dyad types were evaluated. Statistical significance of differences was tested by Wilcoxon-Mann-Whitney tests (n ≥ 12; ∗∗: p ≤ 0.01, ∗∗∗: p ≤ 0.001).

B – MEN kinases are involved in age-based SPB selection during meiosis. Live-cell microscopy images of cells with Spc42-tagRFP-T (marker for SPB age) and MPC54-YFP (MP marker). Cells with two bright Mpc54-YFP signals were classified according to the SPB generations the MPs resided; three classes could be clearly distinguished: MPs at the youngest SPBs (green), the oldest SPBs (red) and at one younger and one older SPB (yellow). Differences to the control were all highly significant (Fisher's exact test, p ≤ 0.001, Control: 1137 cells, Cdc15↓: 132 cells, Mob1↓: 379 cells, Dbf2↓ Dbf20↓: 430 cells, Dbf2↓ Dbf20↓ Mob1↓: 349 cells from at least 4 independent biological replicates). The right bar depicts distribution of cell types for a theoretical random situation. Example images show cells in brightfield channel (BF), Spc42-RFP signals in false colors (arrow heads mark the youngest SPBs), Mpc54-YFP signals and merges of the two fluorescence channels, cell outlines are shown as broken white lines (scale bar: 5 µm).
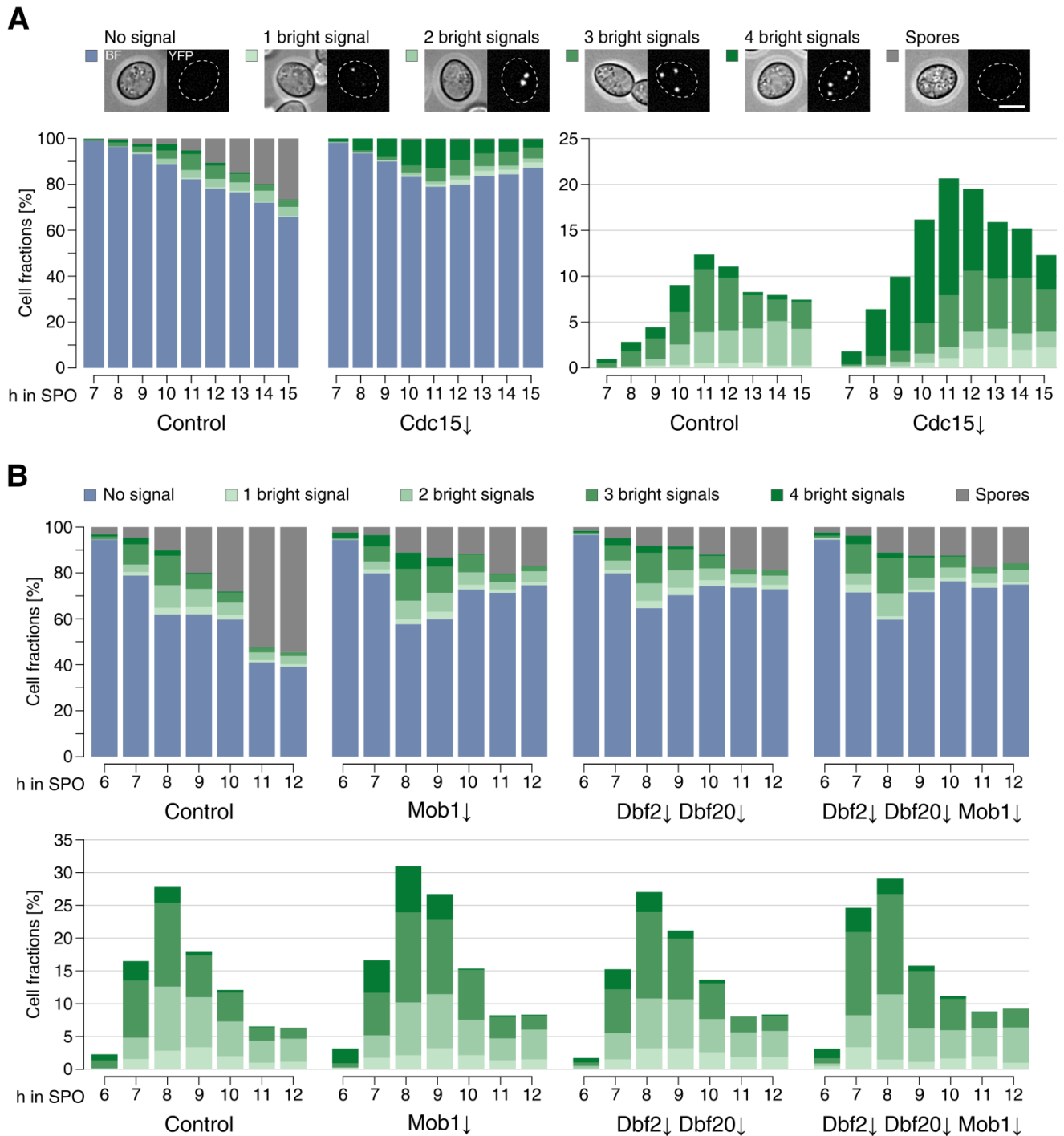
Figure 4 – Functional separation of Cdc15 and the Dbf2-Mob1 and Dbf20-Mob1 complexes.

A – Cdc15 is restricts meiotic plaque numbers and is essential for completion of sporulation. Meiotic plaque and spore formation was observed in Cdc15↓ cells compared to control cells. Conditions as in Figure 3B. Cells were classified according to the number of punctuate bright Mpc54-YFP signals and presence of refractive spores. On the left stacked bar plots of all cell classes are shown, on the right only

the fractions of cells with Mpc54-YFP signals (n = 5). Examples show cells brightfield as well as YFP signals (scale bar: 5 µm).

B – Dbf2, Dbf20 and Mob1 are involved in a late step of sporulation. Meiotic plaque formation was followed over time in the indicated mutants. The upper panel shows plots of all cell classes while the lower panel shows only the fractions of cells with meiotic plaques (Control, Mob1↓ and Dbf2↓ Dbf20↓: n = 4; Dbf2↓ Dbf20↓ Mob1↓: n = 2; scale bar: 5 µm).
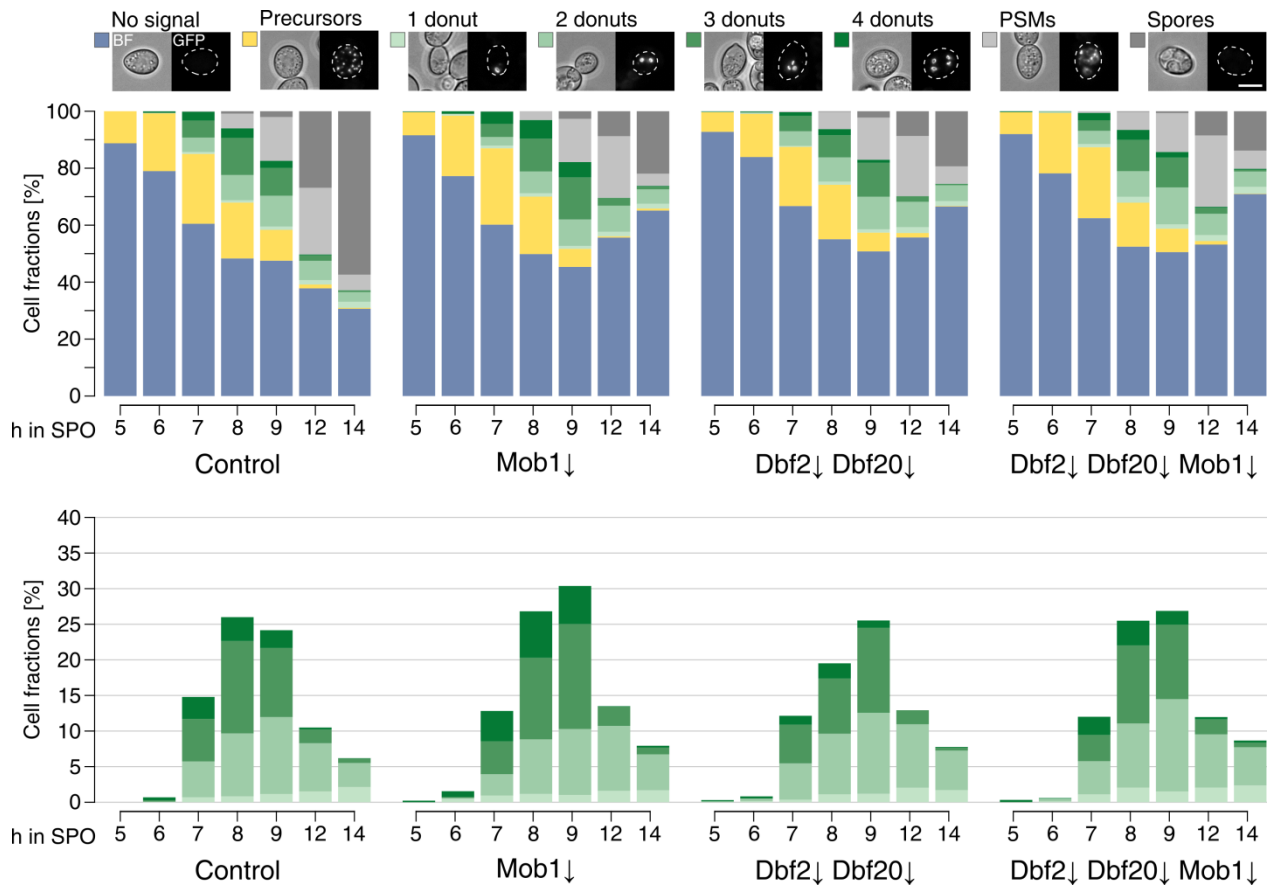
Figure 5 – Mob1↓, Dbf2↓ and Dbf20↓ mutants show a defect at a step that is post-meiotic and prior to spore wall formation. PSM formation in Mob1↓, Dbf2↓ Dbf20↓, Dbf2↓ Dbf20↓ Mob1↓ mutants and a control strain during a sporulation time course under conditions favoring low spore numbers. Don1-GFP was used as marker for the leading edge of PSMs. By correlation of fluorescent and brightfield images cells prior to meiosis I (no distinct Don1-GFP signals; blue), prior to meiosis II (Don1-GFP at precursor vesicles; yellow), in meiosis II with one to four donuts (Don1-GFP signals at the leading edges of PSMs; light to dark green), cells at/after closure of the PSMs (Don1-GFP signals at whole PSMs; light grey) and cells with refractive spores (dark grey) could be distinguished. Left panel shows fractions of all cell classes, right panel only cells with donuts (n = 4; scale bar: 5 μm).
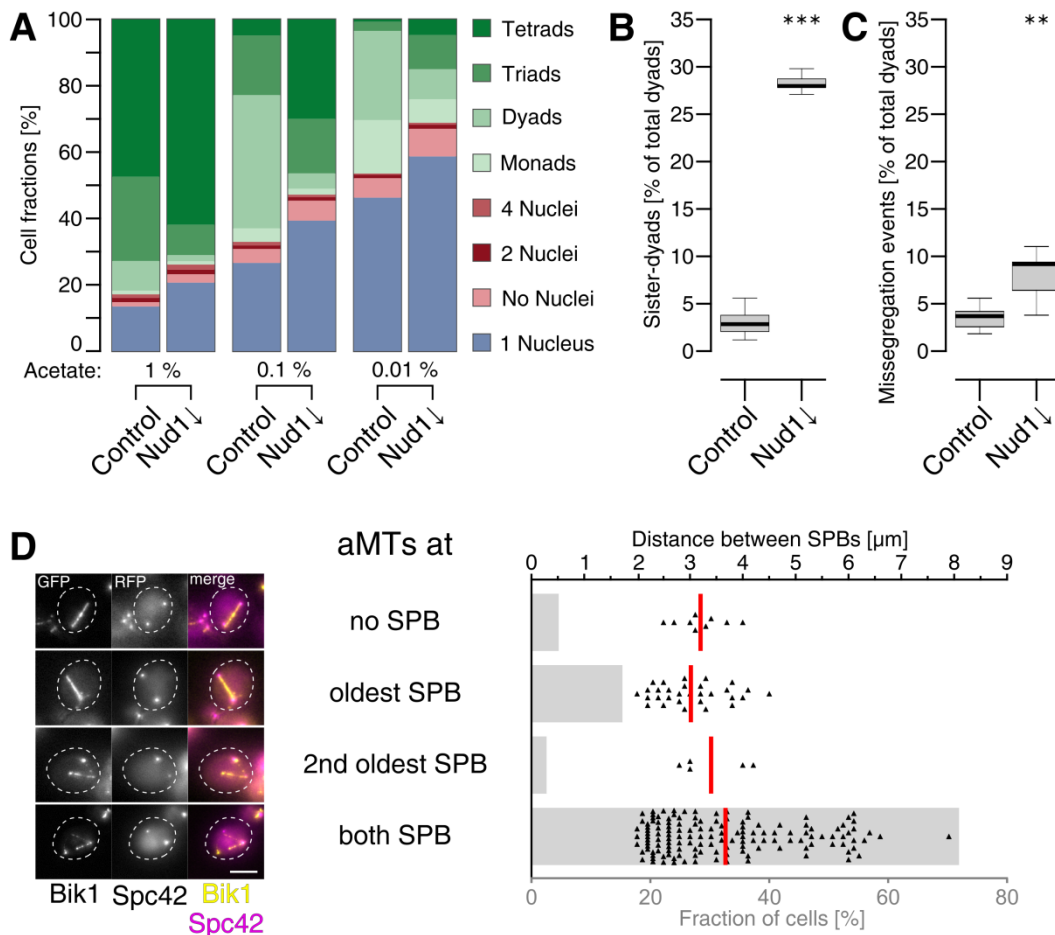
Figure 6 – Dual role of the SPB component Nud1 during sporulation

A – Spore numbers are positively affected by Nud1 depletion. Sporulation on solid medium with indicated acetate concentrations was performed with a Nud1↓ and a control strain. Cell types were evaluated in respect to numbers of nuclei and spores (n ≥ 4).

B – Nud1 is essential for SPB selection. An experiment analogous to the one described for Figure 3A was performed with a Nud1↓ and a control strain. Dyads with one spore of each color (non-sister dyads) and with both spores containing the same fluorophore (sister-dyads) were counted. Statistical significance of differences was tested by a Welch two-sample t-test (n ≥ 8; ∗∗∗: p ≤ 0.001).

C – Chromosome segregation defects in the Nud1↓ mutant. Dyads of the same experiment as in **B** were evaluated regarding chromosome segregation defects (two-colored or non-colored spores). Statistical significance of the difference was checked by a Wilcoxon-Mann-Whitney test (n ≥ 8; ∗∗: p ≤ 0.01).

D – SPB age-dependent nucleation of aMTs during anaphase I. Cells bearing the spindle and aMT marker Bik1-4GFP as well as Spc42-tdTomato were subjected to sporulation. Fluorescence images of cells in anaphase I (SPB distance ≥ 2 µm) were classified according to aMT presence at no SPB, at the oldest SPB, at the second oldest SPB or both. Example images for each category are shown on the left (scale bar 5 µm); the graph shows fractions of the different classes as grey bars (lower axis). The SPB distance (upper axis) is indicated for each cell (total 206 cells; red bars represent median values).
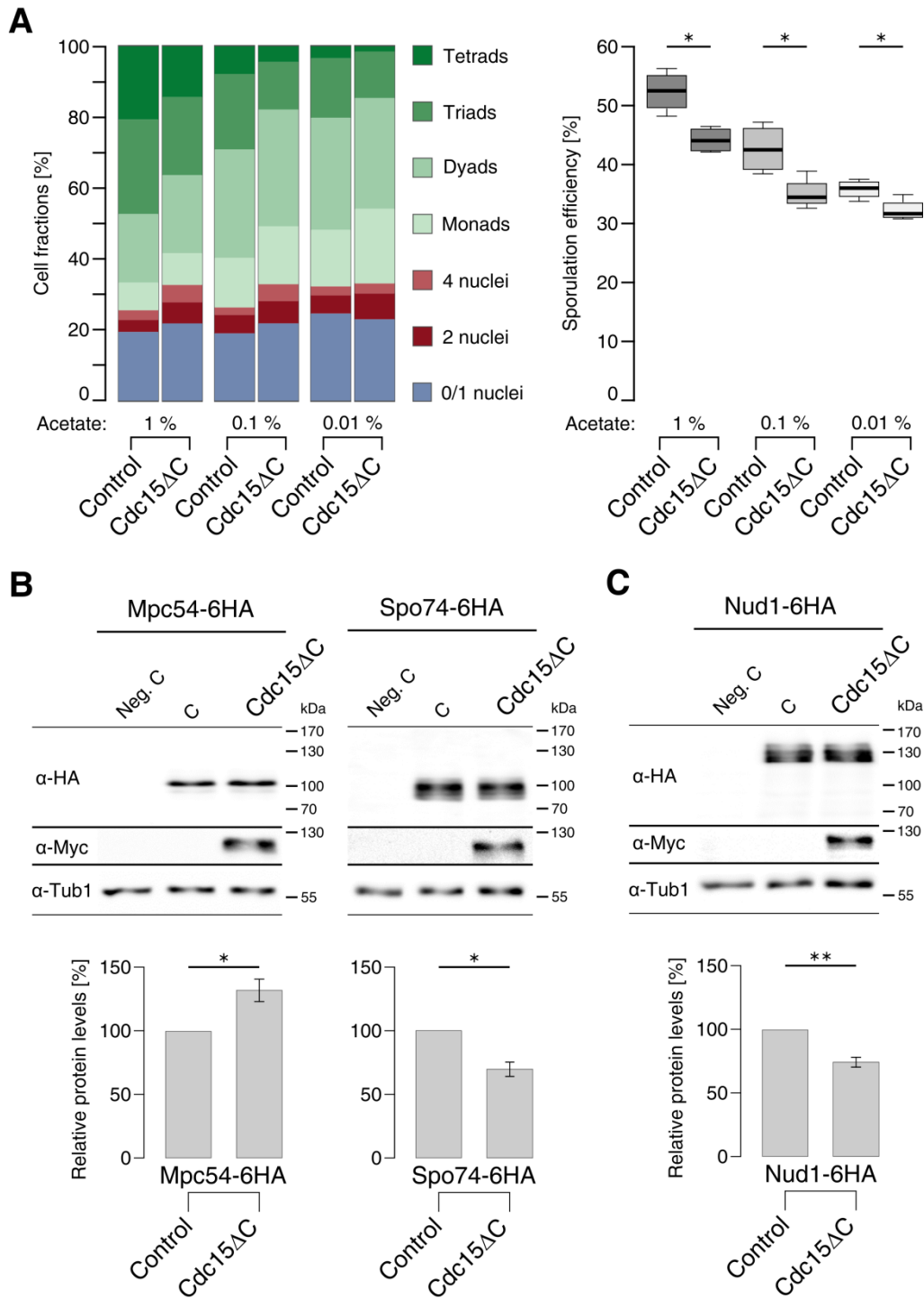
Figure 7 – Hyperactivation of MEN interferes with spore formation and regulation of protein levels of Nud1 and meiotic plaque components.

A – Meiosis-specific production of Cdc15ΔC results in slightly reduced spore numbers. Sporulation of a diploid strain transformed with either an empty vector (Control) or a plasmid bearing a truncated *CDC15* construct (Cdc15ΔC) under control of the mid-sporulation-specific promoter of *SPO74*. Sporulation was performed as described for Figure 1D. Left panel shows the means of the different cell classes,

114

right panel sporulation efficiencies (n ≥ 4; ∗: p ≤ 0.05 in a Wilcoxon-Mann-Whitney test).

B – Aberrant meiotic plaque protein levels in response to Cdc15ΔC. Strains with the meiotic plaque components Mpc54, Mpc70 and Spo74 tagged with 6HA were transformed with the same plasmids as in **A** and subjected to sporulation in liquid medium (1 % acetate). Samples collected at 4 h, 5 h, 6 h, 7 h, 8 h, 9 h and 10 h post-induction were pooled and subjected to western blot analysis. Anti-HA antibody was used to detect the meiotic plaque proteins; anti-Myc antibody visualized production of the Cdc15ΔC construct, anti-Tub1 antibody served as loading control. Upper panel: Western blot signals. Lower panel: quantified meiotic plaque protein levels corrected for Tub1 and normalized to the respective controls (n = 4; means ± SEM; ∗: p ≤ 0.05 in a one-sample t-test).
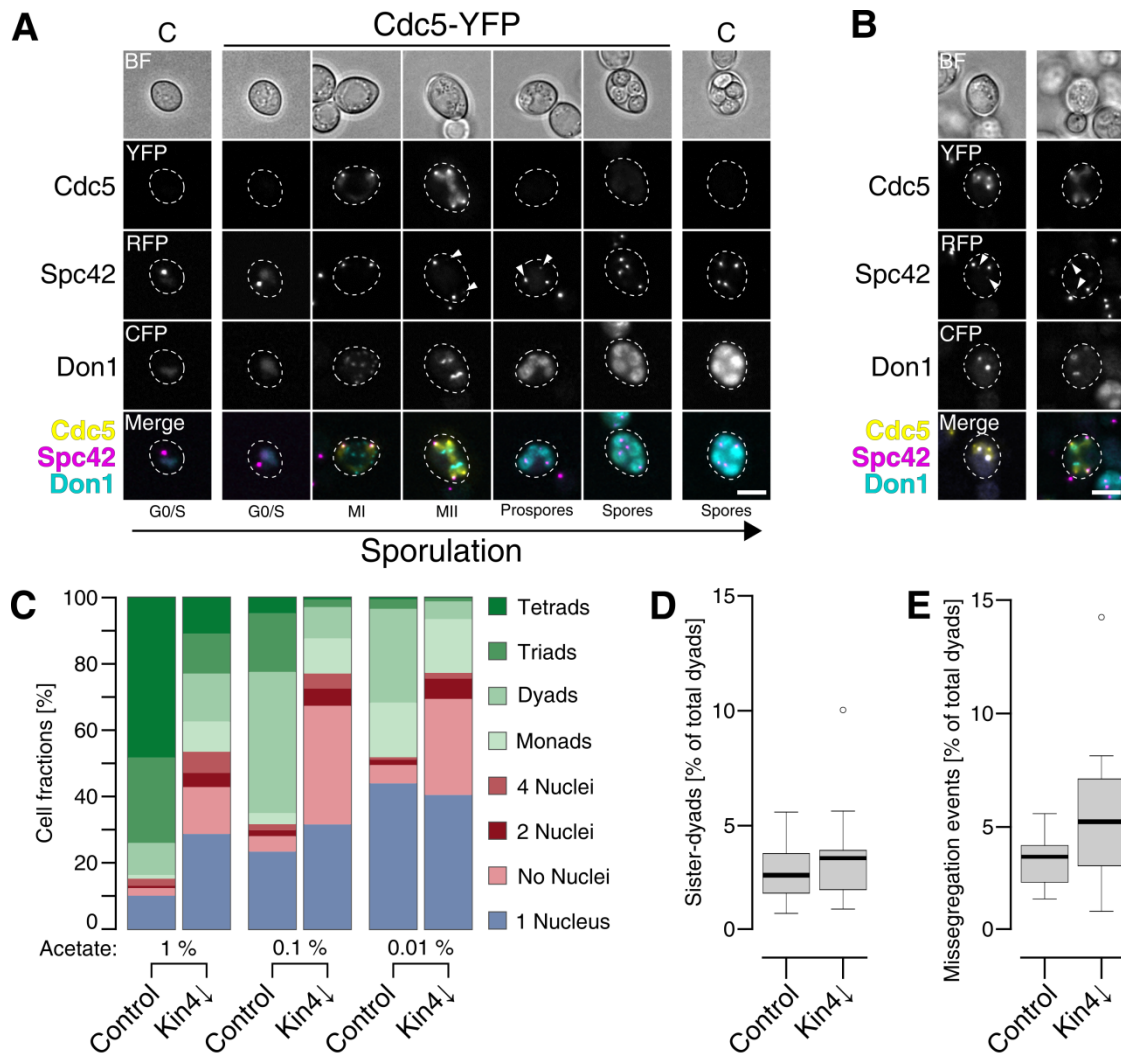
Figure 8 – Analysis of the MEN upstream regulators Cdc5 and Kin4 during sporulation.

A – Localization of Cdc5 during meiosis. Live-cell imaging was performed with a strain bearing Cdc5-YFP, Spc42-RFP and Don1-CFP under sporulation conditions. Correlation between Spc42-RFP, Don1-CFP and brightfield images enabled assignment of cells to five different stages: G0/S phase, meiosis I, meiosis II and post-meiotic stages with or without refractive spores (scale bar: 5 μm).

B – Cdc5 localization in cells with less than four PSMs. Representative images of cells with less than four distinct Don1-CFP signals. Meiosis II cells at an early stage (left panel) and late stage (right panel) are shown (scale bar: 5 μm).

C – Impaired spore formation in a Kin4↓ strain. Sporulation of a Kin4↓ strain was compared to a control strain as described for Figure 1D (n ≥ 6).

D – Sister dyad formation is not affected by Kin4-depletion. The experiment was performed with a Kin4↓ and a control strain as described for Figure 3A. Dyads with one spore of each color (non-sister dyads) and with both spores containing the same fluorophore (sister-dyads) were counted. No statistically significant differences to the control were found (Wilcoxon-Mann-Whitney; n ≥ 11).

E – Kin4 depletion does not affect chromosome segregation. Dyads of the same experiment as in **D** were evaluated regarding chromosome segregation defects (two-colored or non-colored spores). Differences to the control were not statistically significant (Wilcoxon-Mann-Whitney test; n ≥ 11).

Supplementary material

The mitotic exit network regulates spindle pole body selection during sporulation of budding yeast

Christian Renicke[1], Ann-Katrin Allmann[1], Anne Pia Lutz[1], and Christof Taxis[1, 2*]

[1]Department of Biology/Genetics, Philipps-Universität Marburg, Karl-von-Frisch-Strasse 8, 35043 Marburg, Germany

[2]Department of Chemistry/Biochemistry, Philipps-Universität Marburg, Hans-Meerwein-Strasse 4, 35043 Marburg, Germany

*Corresponding author

Email address: taxis@biologie.uni-marburg.de; phone number: (+49)6421-2823046; fax number: (+49)6421-2823032

Content:

Supplementary Figure S1 – Live-cell imaging of Dbf2-GFP and Dbf20-GFP localization during sporulation. Strains with an *RFP-TUB1* fusion integrated at the *TRP1* locus and either no further modification (Control), *DBF2-GFP* (YAL47) or *DBF20-GFP* were subjected to sporulation conditions and images were taken hourly from 4 h to 9 h. Cells were classified to the different sporulation stages according to spindle and cell morphology. Images of cells in mitotic anaphase are included as reference (left panels). Cell outlines are indicated as broken lines. Scale bars: 5 µm (please note the smaller scale in the mitotic images).
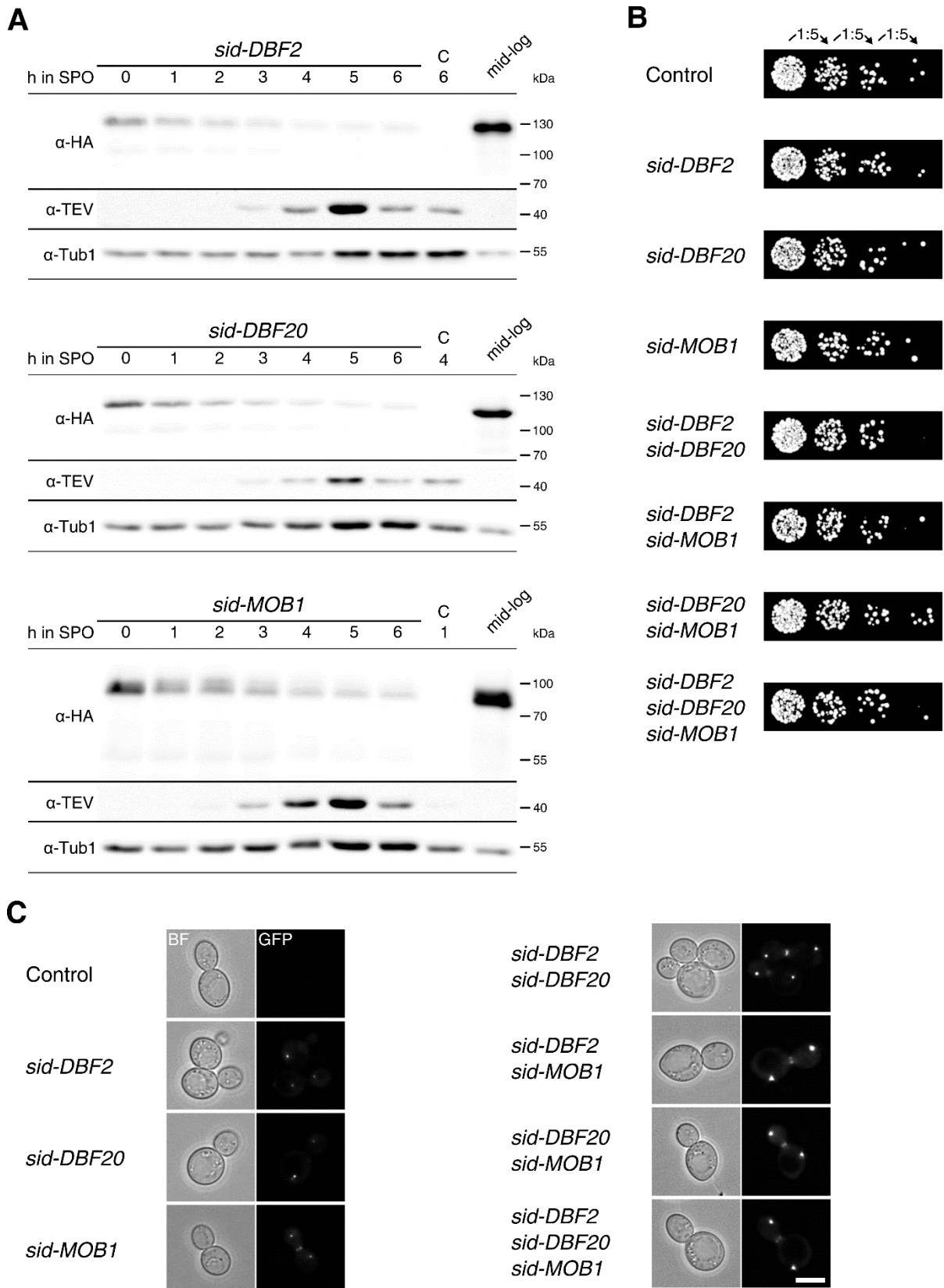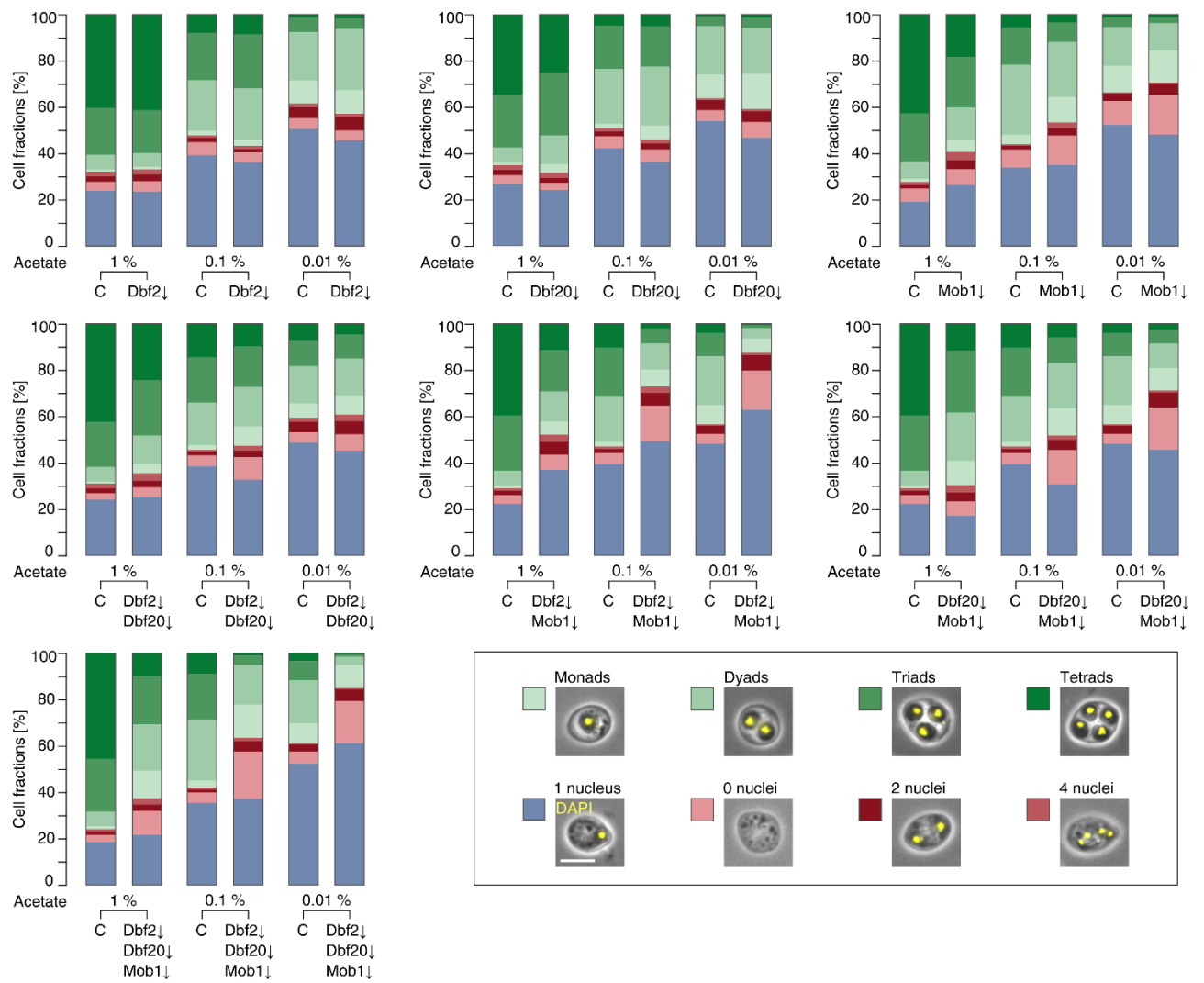
Supplementary Figure S2 – Sporulation-specific protein depletion and vegetative characterization of *sid-DBF2*, *sid-DBF20* and *sid-MOB1*.

A – Meiotic depletion of Dbf2, Dbf20 and Mob1. Depletion strains for Dbf2, Dbf20 and Mob1 were subjected to sporulation in liquid medium with 1 % acetate. Samples were collected hourly from 0 h to 6 h. Additionally, samples from mid-log cultures in

YPD were taken. Samples of different time points from a strain with only the P_{IME2}-$pTEV^+$-T_{DIT1} construct were used as control (C). Fusion proteins were detected by anti-HA antibodies, TEV protease production was monitored by anti-TEV antibody and anti-Tub1 signals served as loading controls.

B – Vegetative growth of strains with different combinations of *sid-DBF2, sid-DBF20* and *sid-MOB1*. Serial 1:5 dilutions of indicated mutants and the same control as in **A** were spotted on YPD plates and images were taken after two days incubation at 30 °C.

C – Mitotic localization of the fusion proteins. Cultures of the same strains as in **B** were grown to mid-log phase in LFM with 2 % glucose and images were taken in brightfield (BF) and GFP channels. Scale bar: 5 µm.

Supplementary Figure S3 – Sporulation profiles for the different Dbf2↓, Dbf20↓ and Mob1↓ strains. The indicated mutants were sporulated together with a control strain with only P_{IME2}-$pTEV^+$-T_{DIT1} (C) on solid sporulation medium with three different acetate concentrations (1 %, 0.1 % and 0.01 %). Cells were classified according to morphology and number of nuclei. Stacked bars represent the means of at least six independent biological replicates. Scale bar: 5 µm.
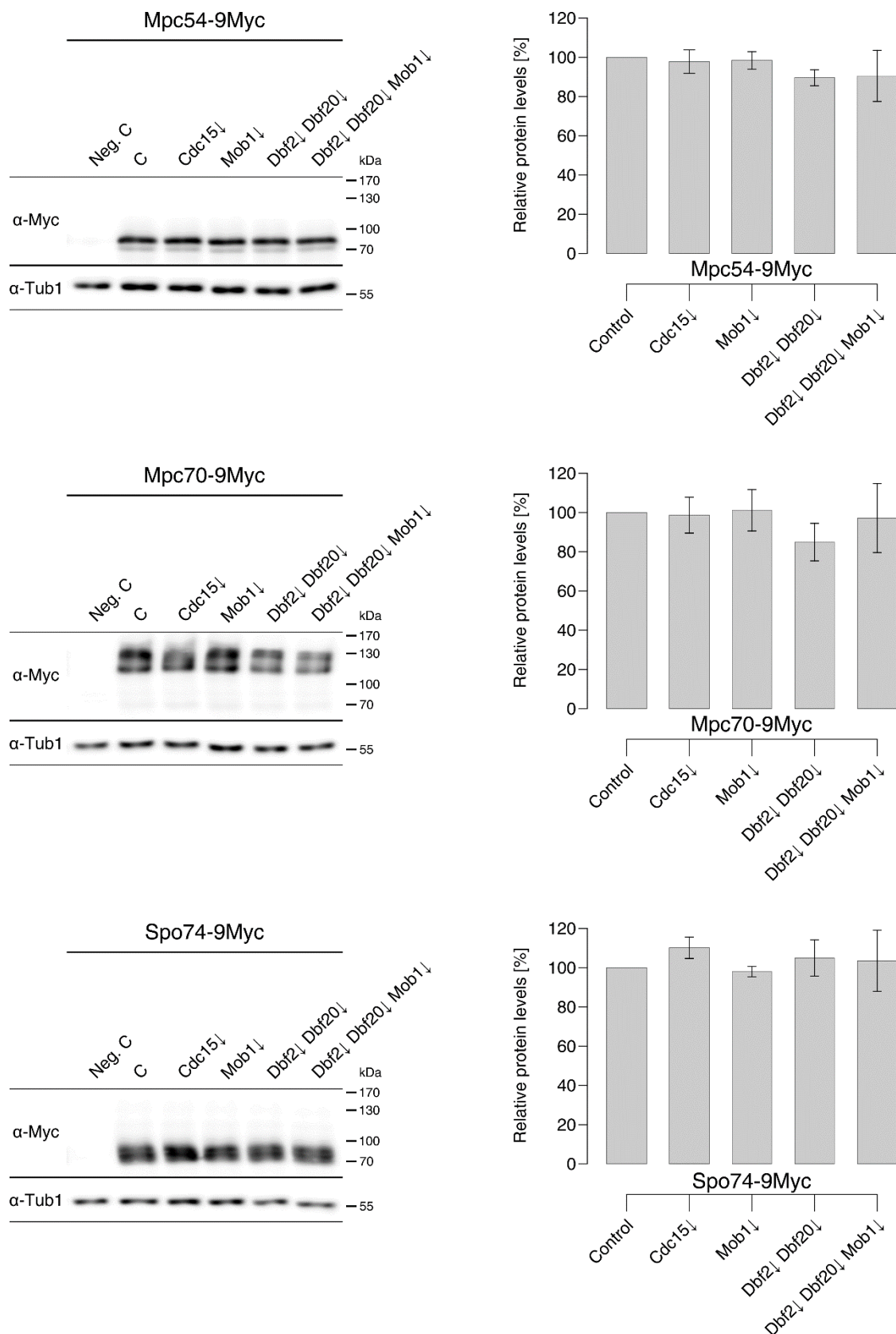
Supplementary Figure S4 – Meiotic plaque protein levels in the Cdc15↓, Mob1↓, Dbf2↓ Dbf20↓ and Dbf2↓ Dbf20↓ Mob1↓ mutants. *MPC54*, *MPC70* and *SPO74* were endogenously tagged with *9Myc* in the Mob1↓, the Dbf2↓ Dbf20↓ and the Dbf2↓ Dbf20↓ Mob1↓ strains as well as in a control strain (C). Strains were then subjected to sporulation in liquid medium (1 % acetate) and samples were taken every hour

from 5 h to 10 h after induction of sporulation. Western blot analysis was performed with pooled samples. A strain without modifications was used as negative control (neg. C). Meiotic plaque proteins were detected using anti-Myc antibody and signals of an anti-Tub1 antibody served as loading control. The left panel shows the Western blot signals, the right panel quantifications of protein amounts corrected for Tub1 and normalized to the control (means of four biological replicates ± SEM).
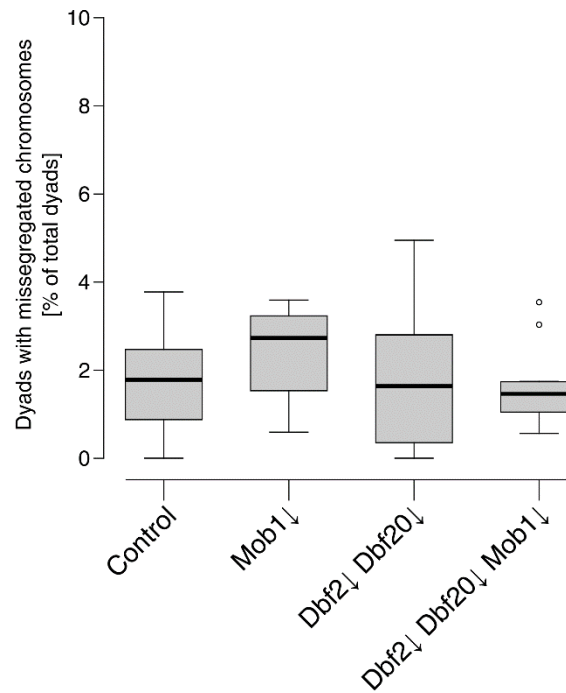
Supplementary Figure S5 – Chromosome segregation in dyads of the Mob1↓, Dbf2↓ Dbf20↓ and Dbf2↓ Dbf20↓ Mob1↓ strains. The experiments shown in Figure 3A were evaluated with regard to chromosome V missegregation events. Dyads with either one red and one green or both red or green colored spores were classified as faithful segregation events while dyads with one or two spores without or with both fluorophores were counted as missegregation events and fractions of total dyad number was visualized (n ≥ 12).
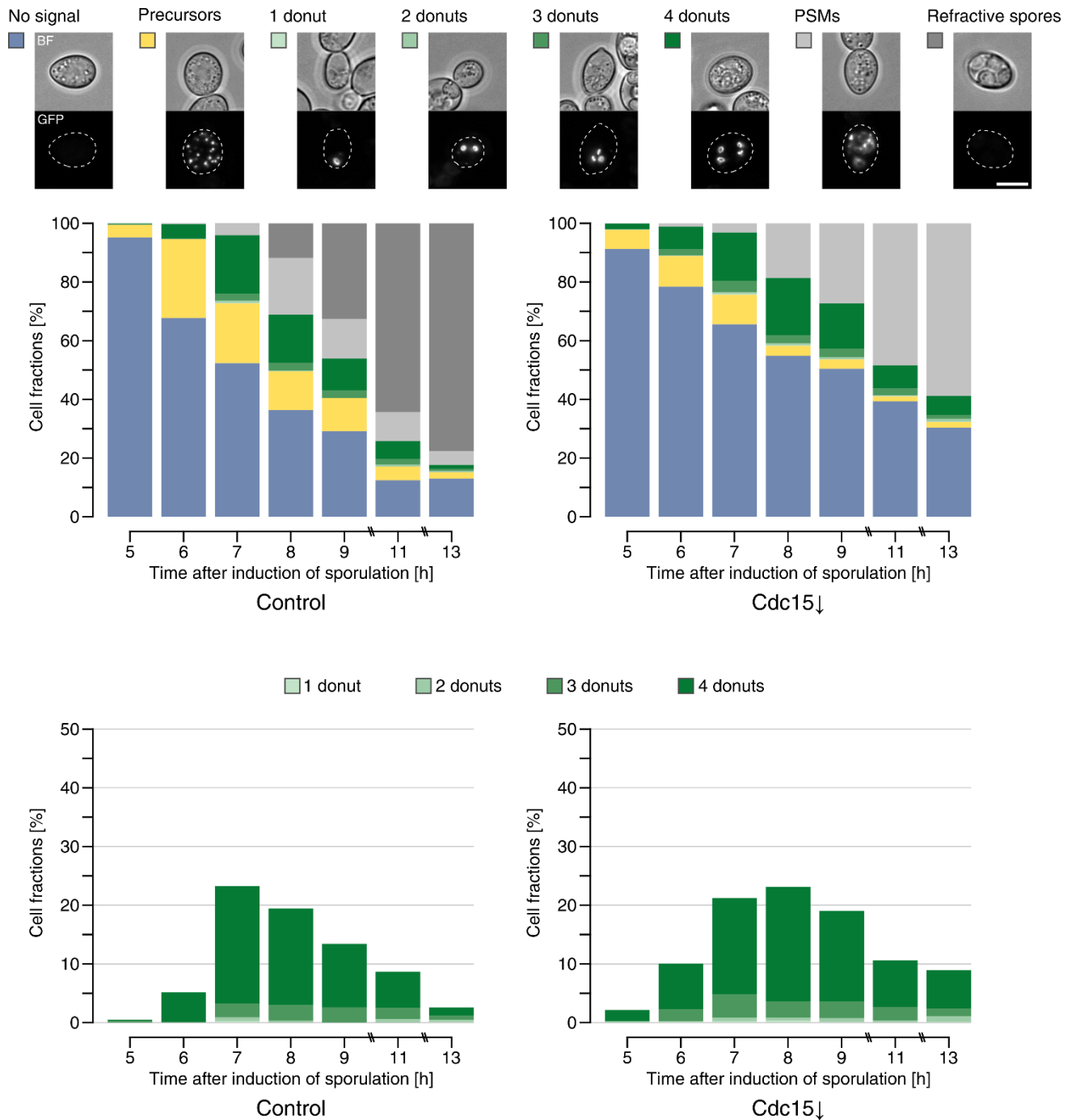
Supplementary Figure S6 – Defects of the Cdc15↓ mutant in PSM closure and spore maturation. Time course analysis of PSM formation in a Cdc15↓ and a control strain under high acetate conditions (5-13 h). Don1-GFP was used as marker for the leading edge of PSMs. By correlation of fluorescent and brightfield images cells prior to meiosis I (no Don1-GFP signals; blue), prior to meiosis II (Don1-GFP at precursor vesicles; yellow), in meiosis II with one to four donuts (Don1-GFP signals at the leading edges of PSMs; light to dark green), cells at/after closure of the PSMs (Don1-GFP signals at whole PSMs; light grey) and cells with refractive spores (dark grey) could be distinguished. Upper panel shows fractions of all cell classes, lower panel only cells with donuts (Control: n = 2, Cdc15↓: n = 3; scale bar: 5 µm). Please note that in contrast to the control the Cdc15↓ strain bore the DON1-GFP fusion only heterozygously, which hindered detection of precursor vesicles.
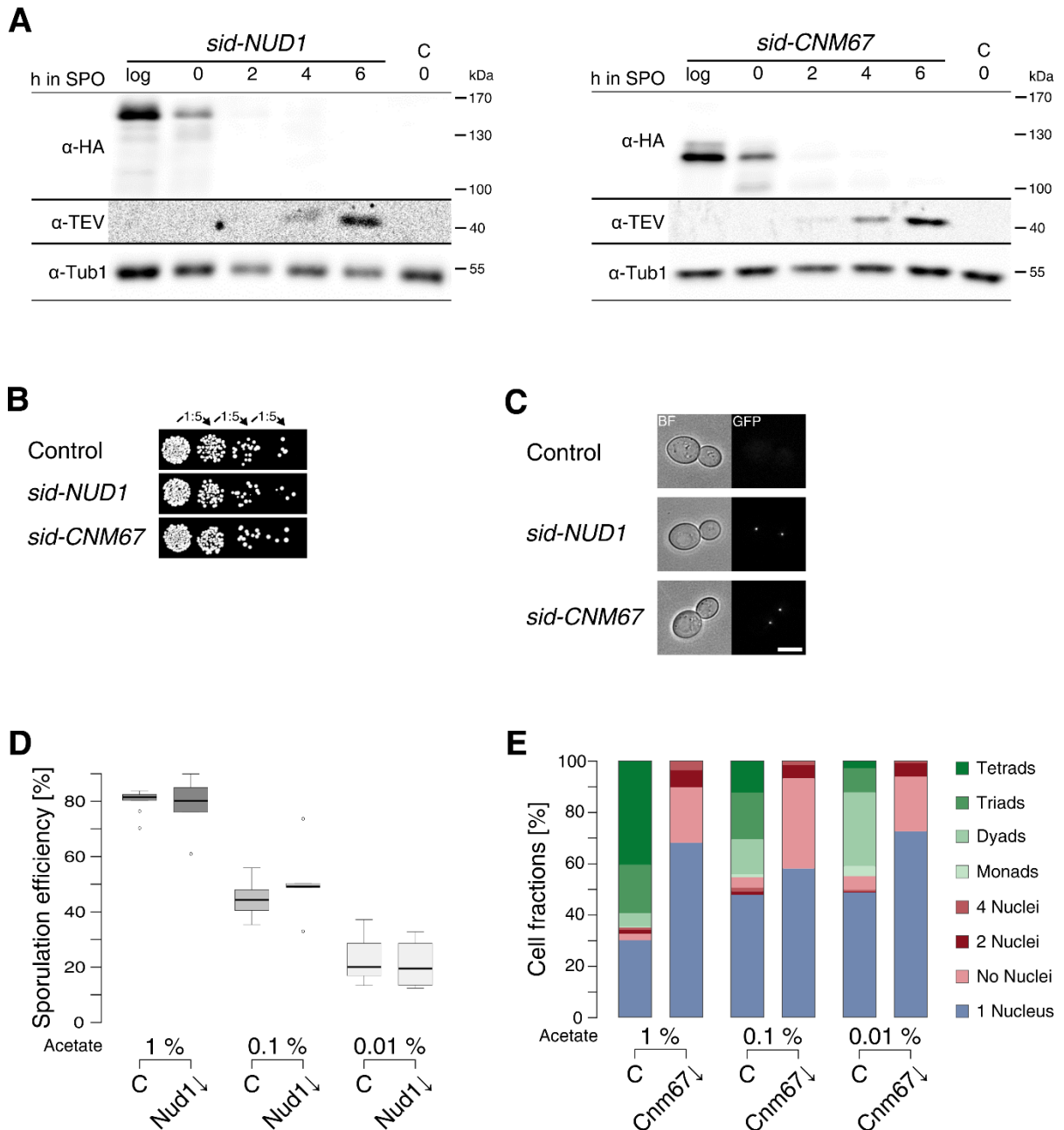
Supplementary Figure S7 – Sporulation-specific protein depletion, vegetative characterization, and sporulation of the *sid-NUD1* and *sid-CNM67* strains.

A – Sporulation-induced depletion of sid-Nud1 and sid-Cnm67. Depletion mutants of Nud1 and Cnm67 were sporulated together with a control strain (C) in liquid 1 % acetate. Samples were collected at the indicated time points. The fusion proteins were detected by anti-HA antibody, pTEV[+] production was followed with anti-TEV antibody and anti-Tub1 antibody was used for loading control.

B – Vegetative growth of the *sid-NUD1* and *sid-CNM67* strains. Serial 1:5 dilutions of the strains of **A** were spotted in on solid YPD medium and images were taken after 2 days at 30 °C.

C – Mitotic localization of sid-Nud1 and sid-Cnm67. The same strains as in **A** were grown to mid-log phase in LFM + 2 % glucose and images in brightfield (BF) and GFP channels were taken. Scale bar: 5 µm.

D – Sporulation efficiencies of the Nud1↓ strain under different acetate concentrations. Sporulation efficiencies for the experiments shown in Figure 7A were calculated as described before. No statistical significant differences to the control were found in Wilcoxon-Mann-Whitney tests (n ≥ 4; p ≥ 0.05).

E – Sporulation profiles of the Cnm67↓ mutant strain. A Cnm67↓ and control (C) strain were sporulated on solid medium with 1 %, 0.1 % and 0.01 % acetate. Cells were counted according to cell morphology and number of nuclei. Means of at least 3 biological replicates are shown.
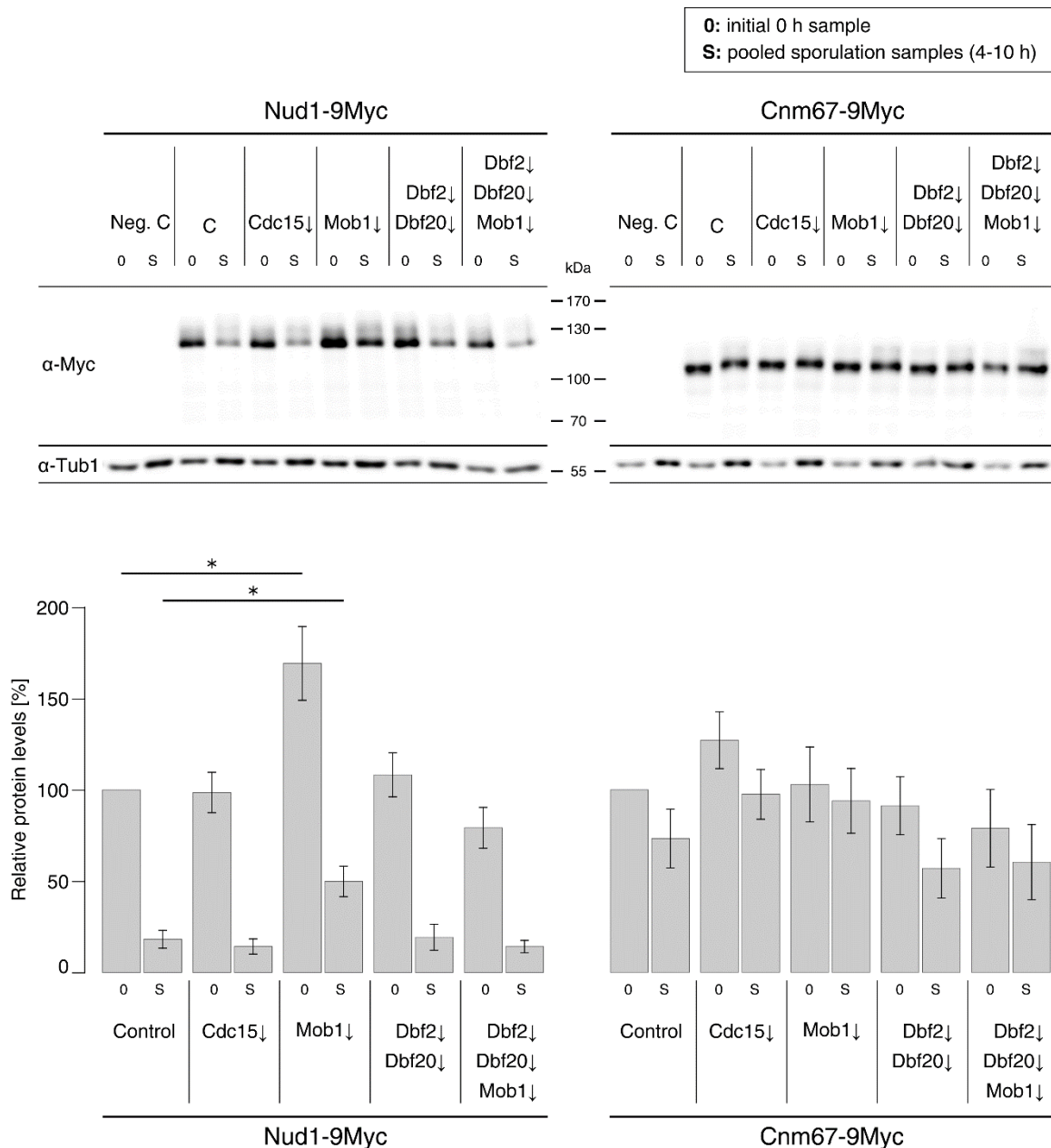
Supplementary Figure S8 – Levels of the SPB outer plaque proteins Nud1 and Cnm67 during sporulation in Cdc15↓, Mob1↓, Dbf2↓ Dbf20↓ and Dbf2↓ Dbf20↓ Mob1↓ strains. The SPB protein Nud1 and in parallel Cnm67 were fused to 9Myc in the indicated depletion mutants and a control with only P_{IME2}-$pTEV^+$-T_{DIT1} (C). Strains were sporulated in liquid 1 % acetate and samples were collected at 0 h as well as every hour from 4 h to 10 h. The initial sample and pooled 4-10 h samples were subjected to immunoblotting. Anti-Myc antibody was used for detection of Nud1-9Myc and Cnm67-9Myc, respectively, anti-Tub1 antibody served as loading control. The upper panel shows the immunoblot signals; for the graphs in the lower panel, signals were quantified, corrected for Tub1 and normalized to the 0 h control values. Bars represent the means of at least three biological replicates ± SEM, statistical significances of differences to the control were checked by either one-sample t-tests against 100 % for 0 h values or two-sample t-tests against control for values from pooled sporulation samples (∗: p ≤ 0.05).
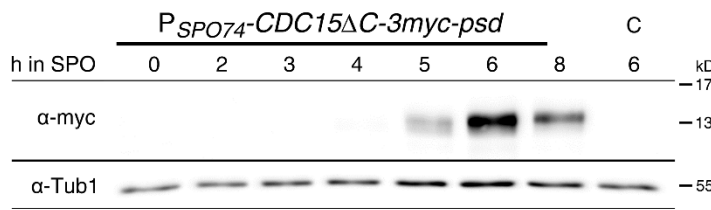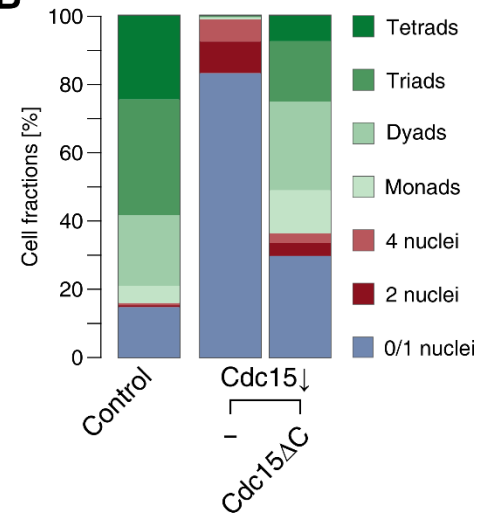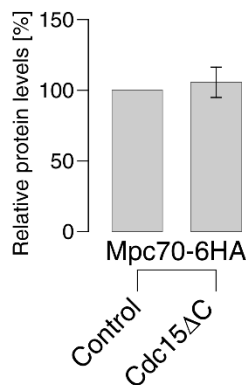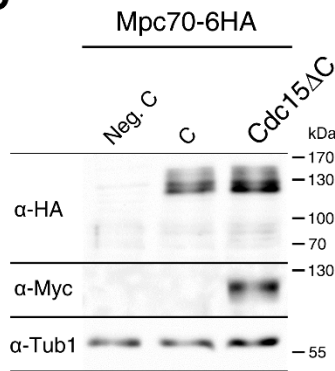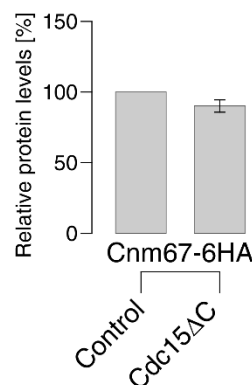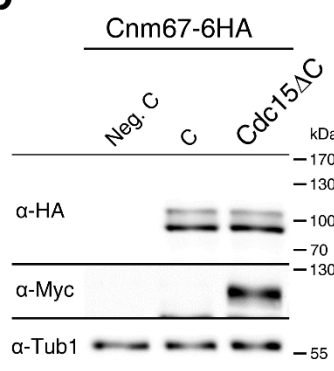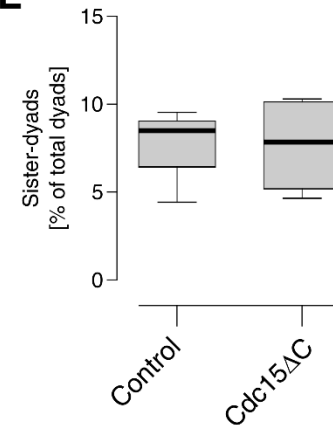
Supplementary Figure S9 – Sporulation-specific production and functional analysis of Cdc15ΔC.

A – Sporulation-specific production of Cdc15ΔC-3myc-psd. A strain with plasmid-borne *CDC15ΔC-3myc-psd* under control of the *SPO74* promoter or an empty vector (C) was subjected to sporulation in liquid 1 % acetate and darkness. Samples were collected at the indicated time points. The Cdc15-3myc-psd construct was detected using anti-Myc antibody, anti-Tub1 antibody served as loading control.

B – Complementation of the Cdc15↓ phenotype with Cdc15ΔC. A Cdc15↓ strain transformed with either an empty vector (−) or a plasmid with the P*SPO74*-*CDC15ΔC-3myc-psd* construct (Cdc15ΔC) was subjected to sporulation on solid medium with 1 % acetate. A control strain (C) with an empty vector was used as reference for wild-

131

type sporulation. Cells were counted according to their morphology and number of nuclei. The plot shows means of at least four biological replicates.

C – Mpc70 levels in the presence of Cdc15ΔC during sporulation. An *MPC70-6HA* strain carrying either an empty vector (C) or the P*SPO74*-*CDC15ΔC-3myc-psd* construct (Cdc15ΔC) was sporulated in liquid 1 % acetate. A strain without modifications was used as control for antibody specificity (Neg. C). Samples were collected at 4 h, 5 h, 6 h, 7 h, 8 h, 9 h and 10 h and pooled. Anti-HA antibody was used to detect Mpc70-6HA. Cdc15ΔC-3myc-psd levels were detected by anti-Myc antibody and anti-Tub1 antibody served as loading control. The upper panel shows the Western blot, the lower panel shows quantified protein levels of four biological replicates which were corrected for Tub1 and normalized to the control. Differences were found not to be statistical significant in an unpaired t-test ($p \geq 0.05$).

D – Cnm67 levels in the presence of Cdc15ΔC during sporulation. Experiment was performed exactly as in **C** with the exception that a CNM67-6HA strain was used. The upper panel shows the Western blot, the lower panel shows quantified protein levels of four biological replicates which were corrected for Tub1 and normalized to the control. Differences were found not to be statistical significant in an unpaired t-test ($p \geq 0.05$).

E – Sister-dyad formation in the presence of Cdc15ΔC. strains as in **A** were sporulated on solid medium with 0.1 % acetate. Heterozygous, spore-autonomous markers CENV::P*YKL050C*-*RFP* and CENV::P*YKL050C*-*GFP* allowed assessment of sister dyad formation. Dyads with one GFP-containing and one RFP-containing spore were counted as non-sister dyads; asci with two spores with identical fluorophores were classified as sister-dyads. Differences in the fraction of sister dyads were found not to be statistical significant (Wilcoxon-Mann-Whitney test; $n = 4$; $p \geq 0.05$).
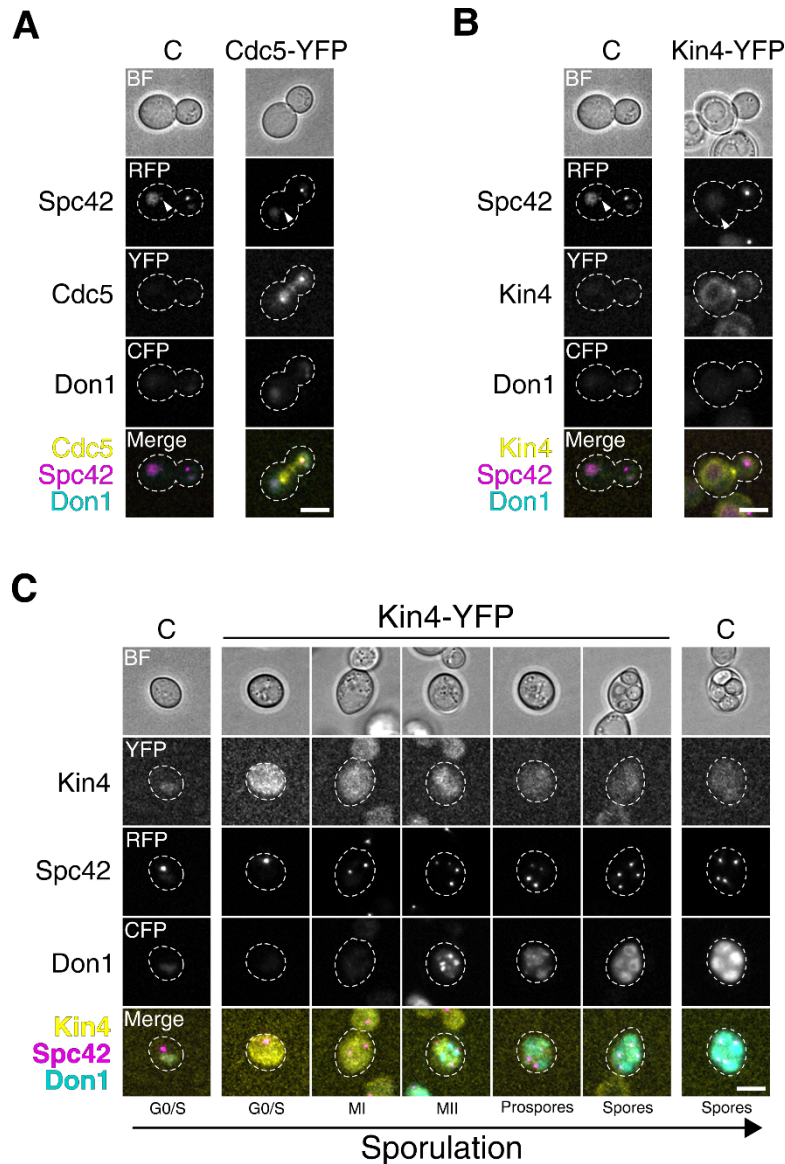
Supplementary Figure S10 – Mitotic localization of Cdc5 and localization of Kin4 during mitosis and sporulation.

A – Mitotic localization of Cdc5. Diploid strains shown in Figure 6A with either Spc42-RFP and Don1-CFP (C) or additionally Cdc5-YFP were grown to mid-log phase in LFM + 2 % glucose and subjected to fluorescence microscopy. Shown are images from brightfield (BF) and the different fluorescence channels together with a color merge of the fluorescence images. Cell outlines are marked as broken lines. Filled triangles point to the younger SPB. Scale bar: 5 µm.

B – Mitotic localization of Kin4. Kin4-YFP localization was checked in a strain with Spc42-RFP and Don1-CFP fusions, a strain without Kin4-YFP served as control (C). Cells were grown to mid-log phase in LFM + 2 % glucose and subjected to fluorescence microscopy. Images from brightfield (BF) and the different fluorescence channels are shown together with a color merge of the fluorescence images. Cell outlines are marked as broken lines. Filled triangles point to the younger SPB. Scale bar: 5 µm.

C – Localization of Kin4 during sporulation. Same strains as in **B** were subjected to sporulation conditions and images were taken at 0 h and hourly between 5 h and

10 h after induction of sporulation. Sporulation stages were assigned according to SPB signals of Spc42-RFP and Don1-CFP at the leading edge of the PSMs. For the control, cells in G0/S phase as well as with refractive spores are shown to account for spore wall autofluorescence in the CFP channel. Scale bar: 5 µm.
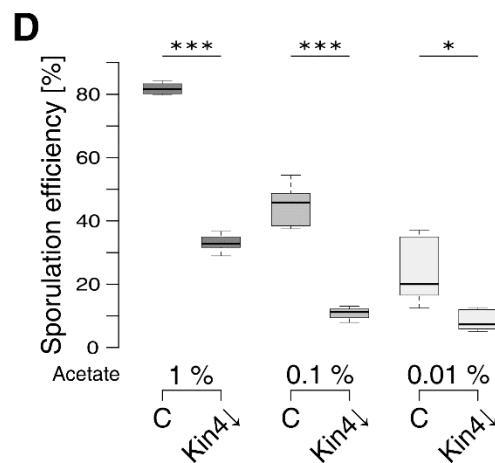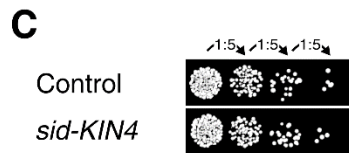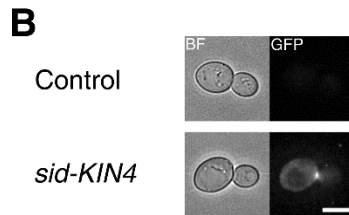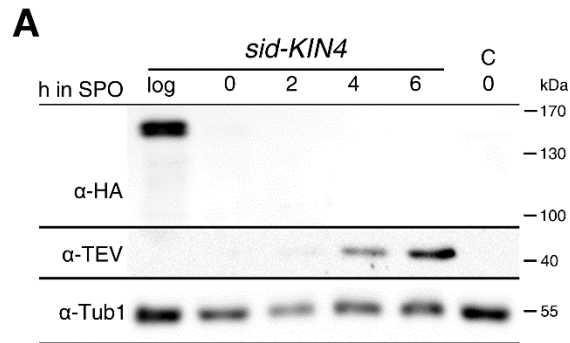
Supplementary Figure S11 – Sporulation-specific protein depletion, vegetative characterization, and sporulation efficiency of the *sid-KIN4* strain.

A – Sporulation-specific depletion of sid-Kin4. Sporulation in liquid 1 % acetate was performed with a sid-Kin4 and a control strain (C). Samples were collected at the indicated time points. Anti-HA antibody was used for detection of the fusion protein, anti-TEV antibody allowed observation of pTEV$^+$ levels and anti-Tub1 antibody served as loading control.

B – Mitotic localization of sid-Kin4. The strains of **A** were grown to mid-log phase in LFM + 2 % glucose. Images were taken in the brightfield (BF) and GFP channel. Scale bar: 5 µm.

C – Vegetative growth of the *sid-KIN4* strain. Serial 1:5 dilutions of the same strains as in **A** were spotted on YPD solid medium and images were taken after 2 days at 30 °C.

D – Sporulation efficiencies of the Kin4↓ strain under various acetate concentrations. Sporulation efficiencies of the experiment of Figure 6B were calculated as described before. Statistical significance of differences to the control strain was assessed by Wilcoxon-Mann-Whitney tests (n ≥ 6; ∗: p ≤ 0.05; ∗∗∗: p ≤ 0.001).

Supplementary Table S1 - Yeast strains used in this study.

Strain	Relevant genotype	Source
YKS32	*MATa/MATα lys2/lys2 ura3/ura3 ho::hisG/ho::LYS2 LEU2/leu2::hisG*	(Knop & Strasser, 2000)
LH177	*MATa/MATα his3/his3 ura3/ura3 leu2/leu2 trp1/trp1 lys2/lys2 ho::hisG/ho::hisG*	(Huang *et al*, 2005)
YAB12	*MATa lys2 ura3 ho::hisG MNN1::P$_{YKL050C}$-RedStar::kanMX4*	A kind gift of M. Knop
YCT716	YKS32 *MNN1/MNN1::P$_{YKL050c}$-GFP::kanMX4*	(Gordon *et al*, 2006)
YKS53	YKS32 *DON1-GFP::kanMX4/DON1-GFP::kanMX4*	(Knop & Strasser, 2000)
YCR77	*MATa/MATα his3/his3 ura3/ura3 leu2/leu2 trp1/trp1 lys2/lys2 ho::LYS2/ho::LYS2*	This work
YCR330	*MATa/MATα lys2/lys2 ura3/ura3 ho::LYS2/ho::LYS2 leu2::hisG/leu2::hisG*	This work
YAL19	YCR77 *TRP1::P$_{HIS3}$-mCherry-TUB1::trp1*	This work
YAL47	YAL19 *DBF2-yeGFP::KanMX4*	This work
YAL48	YAL19 *DBF20-yeGFP::KanMX4*	This work
YCR329	YKS32 *his3::P$_{IME2}$-pTEV$^+$-T$_{DIT1}$::kanMX4::his3/his3::P$_{IME2}$-pTEV$^+$-T$_{DIT1}$::kanMX4::his3 trp1::P$_{IME2}$-pTEV$^+$-T$_{DIT1}$::kanMX4::trp1/t trp1::P$_{IME2}$-pTEV$^+$-T$_{DIT1}$::kanMX4::trp1*	This work
YAA146	YCR329 *leu2/leu2 ho::LYS2/ho::LYS2*	This work
YCR332	YCR329 *natNT2::sid-CDC15/natNT2::sid-CDC15*	This work
YCR356	YCR329 *MPC54-yeGFP::hphNT1/MPC54*	This work
YCR357	YCR356 *natNT2::sid-CDC15/natNT2::sid-CDC15*	This work
YCR370	YCR77 *MNN1::P$_{YKL050C}$-RedStar::hphNT1/MNN1::P$_{YKL050C}$-GFP::hphNT1*	This work
YCR575	YAA146 *natNT2::sid-CDC15/natNT2::sid-CDC15*	This work
YCR358	YCR332 *DON1-yeGFP::hphNT1/DON1*	This work
YCR333	YCR329 *natNT2::sid-MOB1/natNT2::sid-MOB1*	This work
YCR359	YCR329 *natNT2::sid-DBF2/natNT2::sid-DBF2*	This work
YCR344	YCR329 *natNT2::sid-DBF20/natNT2::sid-DBF20*	This work
YCR363	YCR329 *natNT2::sid-DBF2/natNT2::sid-DBF2 natNT2::sid-DBF20/natNT2::sid-DBF20*	This work
YCR447	YCR329 *natNT2::sid-DBF2/natNT2::sid-DBF2 natNT2::sid-MOB1/natNT2::sid-MOB1*	This work
YCR450	YCR329 *natNT2::sid-DBF20/natNT2::sid-DBF20 natNT2::sid-MOB1/natNT2::sid-MOB1*	This work
YCR446	YCR329 *natNT2::sid-DBF2/natNT2::sid-DBF2 natNT2::sid-DBF20/natNT2::sid-DBF20 natNT2::sid-MOB1/natNT2::sid-MOB1*	This work
YCR481	YAA146 *MNN1::P$_{YKL050C}$-RedStar::hphNT1/MNN1::P$_{YKL050C}$::GFP::hphNT1*	This work
YCR482	YCR481 *natNT2::sid-MOB1/natNT2::sid-MOB1*	This work
YCR483	YCR481 *natNT2::sid-DBF2/natNT2::sid-DBF2 natNT2::sid-DBF20/natNT2::sid-DBF20*	This work
YCR525	YCR481 *natNT2::sid-DBF2/natNT2::sid-DBF2 natNT2::sid-DBF20/natNT2::sid-DBF20 natNT2::sid-MOB1/natNT2::sid-MOB1*	This work
YCR555	YCR329 *MPC54-myCitrine::hphNT1/MPC54 SPC42-yotagRFP-T::spHIS3MX6/SPC42*	This work
YCR556	YCR555 *natNT2::sid-MOB1/natNT2::sid-MOB1*	This work
YCR557	YCR555 *natNT2::sid-DBF2/natNT2::sid-DBF2 natNT2::sid-DBF20/natNT2::sid-DBF20*	This work

Strain	Relevant genotype		Source
YCR558	YCR555 *natNT2::sid-DBF2/natNT2::sid-DBF2 DBF20 natNT2::sid-MOB1/natNT2::sid-MOB1*	*natNT2::sid-DBF20/natNT2::sid-*	This work
YCR536	YCR329 *DON1-yeGFP::hphNT1/ DON1-yeGFP::hphNT1*		This work
YCR537	YCR537 *natNT2::sid-MOB1/natNT2::sid-MOB1*		This work
YCR538	YCR537 *natNT2::sid-DBF2/natNT2::sid-DBF2 DBF20*	*natNT2::sid-DBF20/natNT2::sid-*	This work
YCR539	YCR537 *natNT2::sid-DBF2/natNT2::sid-DBF2 DBF20 natNT2::sid-MOB1/natNT2::sid-MOB1*	*natNT2::sid-DBF20/natNT2::sid-*	This work
YCR484	YCR77 *MPC54/MPC54-6HA*::*HIS3MX6*		This work
YCR540	YCR329 *MPC54/MPC54-9MYC*::*hphNT1*		This work
YCR541	YCR540 *natNT2::sid-CDC15/natNT2::sid-CDC15*		This work
YCR542	YCR540 *natNT2::sid-MOB1/natNT2::sid-MOB1*		This work
YCR543	YCR540 *natNT2::sid-DBF2/natNT2::sid-DBF2 DBF20*	*natNT2::sid-DBF20/natNT2::sid-*	This work
YCR544	YCR540 *natNT2::sid-DBF2/natNT2::sid-DBF2 DBF20 natNT2::sid-MOB1/natNT2::sid-MOB1*	*natNT2::sid-DBF20/natNT2::sid-*	This work
YCR485	YCR77 *MPC70/MPC70-6HA*::*HIS3MX6*		This work
YCR545	YCR329 *MPC70/MPC70-9MYC*::*hphNT1*		This work
YCR546	YCR545 *natNT2::sid-CDC15/natNT2::sid-CDC15*		This work
YCR547	YCR545 *natNT2::sid-MOB1/natNT2::sid-MOB1*		This work
YCR548	YCR545 *natNT2::sid-DBF2/natNT2::sid-DBF2 DBF20*	*natNT2::sid-DBF20/natNT2::sid-*	This work
YCR549	YCR545 *natNT2::sid-DBF2/natNT2::sid-DBF2 DBF20 natNT2::sid-MOB1/natNT2::sid-MOB1*	*natNT2::sid-DBF20/natNT2::sid-*	This work
YCR486	YCR77 *SPO74/SPO74-6HA*::*HIS3MX6*		This work
YCR550	YCR329 *SPO74/SPO74-9MYC*::*hphNT1*		This work
YCR551	YCR550 *natNT2::sid-CDC15/natNT2::sid-CDC15*		This work
YCR552	YCR550 *natNT2::sid-MOB1/natNT2::sid-MOB1*		This work
YCR553	YCR550 *natNT2::sid-DBF2/natNT2::sid-DBF2 DBF20*	*natNT2::sid-DBF20/natNT2::sid-*	This work
YCR554	YCR550 *natNT2::sid-DBF2/natNT2::sid-DBF2 DBF20 natNT2::sid-MOB1/natNT2::sid-MOB1*	*natNT2::sid-DBF20/natNT2::sid-*	This work
YCR606	YCR77 *NUD1/NUD1-6HA*::*HIS3MX6*		This work
YCR607	YCR329 *NUD1/NUD1-9MYC*::*hphNT1*		This work
YCR608	YCR607 *natNT2::sid-CDC15/natNT2::sid-CDC15*		This work
YCR609	YCR607 *natNT2::sid-MOB1/natNT2::sid-MOB1*		This work
YCR610	YCR607 *natNT2::sid-DBF2/natNT2::sid-DBF2 DBF20*	*natNT2::sid-DBF20/natNT2::sid-*	This work
YCR611	YCR607 *natNT2::sid-DBF2/natNT2::sid-DBF2 DBF20 natNT2::sid-MOB1/natNT2::sid-MOB1*	*natNT2::sid-DBF20/natNT2::sid-*	This work
YCR612	YCR77 *CNM67/CNM67-6HA*::*HIS3MX6*		This work
YCR613	YCR329 *CNM67/CNM67-9MYC*::*hphNT1*		This work
YCR614	YCR613 *natNT2::sid-CDC15/natNT2::sid-CDC15*		This work
YCR615	YCR613 *natNT2::sid-MOB1/natNT2::sid-MOB1*		This work
YCR616	YCR613 *natNT2::sid-DBF2/natNT2::sid-DBF2 DBF20*	*natNT2::sid-DBF20/natNT2::sid-*	This work

Strain	Relevant genotype	Source
YCR617	YCR613 *natNT2::sid-DBF2/natNT2::sid-DBF2 natNT2::sid-DBF20/natNT2::sid-DBF20 natNT2::sid-MOB1/natNT2::sid-MOB1*	This work
YAA9	YKS32 *SPC42-tdTomato::hphNT1/SPC42-tdTomato::hphNT1 BIK1/BIK1-4yeGFP::KanMX6*	
YCR686	YCR481 *natNT2::sid-KIN4/natNT2::sid-KIN4*	This work
YCR689	YAA146 *MPC54-myCitrine::hphNT1/MPC54 SPC42-yotagRFP-T::spHIS3MX6/SPC42*	This work
YCR690	YCR689 *natNT2::sid-CDC15/natNT2::sid-CDC15*	This work
YCR699	YCR481 *natNT2::sid-NUD1/natNT2::sid-NUD1*	This work
YAA187	YAA146 *natNT2::sid-CNM67/natNT2::sid-CNM67*	This work
YAA216	YAA146 *natNT2::sid-NUD1/natNT2::sid-NUD1*	This work
YAA215	YAA146 *natNT2::sid-KIN4/natNT2::sid-KIN4*	This work
YAA249	YCR330 *DON1-3mTurquoise2::KanMX4/DON1 SPC42-yotagRFP-T::KanMX4/SPC42*	This work
YAA250	YAA249 *KIN4-yomNeonGreen::NatNT2/KIN4*	This work
YAA252	YAA249 *CDC5-yomNeonGreen::NatNT2/CDC5*	This work

Supplementary Table S2 - Plasmids used in this study.

Plasmid	Relevant genotype	Source
pRS315	OriR bla CEN6/ARS209 LEU2	(Sikorski & Hieter, 1989)
pRS426	OriR bla 2µm URA3	(Christianson et al, 1992)
pFA6a-kanMX4	OriR bla KanMX4	(Wach et al, 1994)
pFA6a-hphNT1	OriR bla hphNT1	(Janke et al, 2004)
pFA6a-NatNT2	OriR bla NatNT2	(Janke et al, 2004)
pYM12	OriR bla yeGFP::KanMX4	(Janke et al, 2004)
pYM15	OriR bla 6HA::HIS3MX6	(Janke et al, 2004)
pYM20	OriR bla 9MYC::hphNT1	(Janke et al, 2004)
pYM25	OriR bla yeGFP::hphNT1	(Janke et al, 2004)
pCM29	OriR bla myCitrine::SpHIS5	(van der Felden et al, 2014)
pCM49	OriR bla tdTomato::hphNT1	(Maeder et al, 2007)
pSM1023	OriR bla 4yeGFP::kanMX6	(Khmelinskii et al, 2007)
pAK010	OriR bla TRP1 P_{HIS3}-mCherry-TUB1	(Gibeaux et al, 2013)
pMJ11	OriR bla ura3::P_{IME2}-pTEV$^+$-T$_{CYC1}$::kanMX::ura3	(Jungbluth et al, 2010)
pCT289	OriR bla natNT2::P_{ADH1}::GFP-TDegF-3HA	(Taxis et al, 2009)
pDS37	OriR bla 2µm URA3 P_{IME2}-GFP-pTEV$^+$-T$_{CYC1}$	(Jungbluth et al, 2010)
pDS89	OriR bla CEN6/ARS209 LEU2 P_{ADH1}-3MYC-psd	(Renicke et al, 2013)
pCR6	OriR bla CEN6/ARS209 hphNT1 P_{SPO74}::GFP-pTEV$^+$	This work
pCR65	OriR bla natNT2::P_{MCD1}-GFP-TDegF-3HA	This work
pCR81	OriR bla 2µm URA3 P_{IME2}-pTEV$^+$-T$_{DIT1}$	This work
pCR87	OriR bla yomTagRFP-T::KanMX4	This work
pCR93	OriR bla 3mTurquoise2::KanMX4	This work
pCR95	OriR bla yomNeonGreen::NatNT2	This work
pCR107	OriR bla ura3::P_{IME2}-pTEV$^+$-T$_{DIT1}$::kanMX::ura3	This work
pCR118	OriR bla LEU2 P_{SPO74}-CDC15$^{1-2250}$-3MYC-psd^{E139N}	This work
pCR122	OriR bla myCitrine::hphNT1	This work
pCR124	OriR bla yomTagRFP-T::spHIS5	This work

Supplementary Table S3 - Overview of yeast strains used in experiments.

Figure	Strains
Figure 1B	YKS32 [pRS426] or [pDS37] or [pCR81]
Figure 1C, D, E	YCR329, YCR332
Figure 2	YCR329, YCR359, YCR344, YCR333, YCR363, YCR447, YCR450, YCR446
Figure 3A	YCR481, YCR482, YCR483, YCR525
Figure 3B	Controls: YCR555, YCR689; Mutants: YCR690, YCR556, YCR557, YCR558
Figure 4A	YCR689, YCR690
Figure 4B	YCR555, YCR556, YCR557, YCR558
Figure 5	YCR536, YCR537, YCR538, YCR539
Figure 6A	YAA146, YAA216
Figure 6B, C	YCR481, YCR699
Figure 6D	YAA9
Figure 7A	YCR370 [pRS315] or [pCR118]
Figure 7B	YCR77 [pRS315]; YCR484 [pRS315] or [pCR118]; YCR486 [pRS315] or [pCR118]
Figure 7C	YCR77 [pRS315], YCR606 [pRS315] or [pCR118]
Figure 8A, B	YAA249, YAA252
Figure 8C	YAA146, YAA215
Figure 8D, E	YCR481, YCR686
S. Figure 1	YAL19, YAL47, YAL48
S. Figure 2A	YCR329, YCR359, YCR344, YCR333
S. Figure 2B, C	YCR329, YCR359, YCR344, YCR333, YCR363, YCR447, YCR450, YCR446
S. Figure 3	YCR329, YCR359, YCR344, YCR333, YCR363, YCR447, YCR450, YCR446
S. Figure 4	YKS32, YCR540, YCR541, YCR542, YCR543, YCR544, YCR545, YCR546, YCR547, YCR548, YCR549, YCR550, YCR551, YCR552, YCR553, YCR554
S. Figure 5	YCR481, YCR482, YCR483, YCR525
S. Figure 6	YKS53, YCR358
S. Figure 7A, B, C	YAA146, YAA187, YAA216
S. Figure 7D	YAA146, YAA216
S: Figure 7E	YAA146, YAA187
S. Figure 8	YKS32, YCR607, YCR608, YCR609, YCR610, YCR611, YCR613, YCR614, YCR615, YCR616, YCR617
S. Figure 9A	YCR370 [pRS315] or [pCR118]
S. Figure 9B	YCR77 [pRS315], YCR575 [pRS315] or [pCR118]
S. Figure 9C	YCR77 [pRS315], YCR485 [pRS315] or [pCR118]
S. Figure 9D	YCR77, YCR612 [pRS315] or [pCR118]
S. Figure 9E	YCR370 [pRS315] or [pCR118]
S. Figure 10A	YAA249, YAA252
S. Figure 10B, C	YAA249, YAA250
S. Figure 11	YAA146, YAA215

Supplementary References:

Christianson TW, Sikorski RS, Dante M, Shero JH & Hieter P (1992) Multifunctional yeast high-copy-number shuttle vectors. *Gene* **110:** 119–122

van der Felden J, Weisser S, Bruckner S, Lenz P & Mosch H-U (2014) The Transcription Factors Tec1 and Ste12 Interact with Coregulators Msa1 and Msa2 To Activate Adhesion and Multicellular Development. *Mol Cell Biol* **34:** 2283–2293

Gibeaux R, Politi AZ, Nédélec F, Antony C & Knop M (2013) Spindle pole body-anchored Kar3 drives the nucleus along microtubules from another nucleus in preparation for nuclear fusion during yeast karyogamy. *Genes Dev* **27:** 335–49

Gordon O, Taxis C, Keller PJ, Benjak A, Stelzer EHK, Simchen G & Knop M (2006) Nud1p, the yeast homolog of Centriolin, regulates spindle pole body inheritance in meiosis. *EMBO J* **25:** 3856–68

Huang LS, Doherty HK & Herskowitz I (2005) The Smk1p MAP kinase negatively regulates Gsc2p, a 1,3-beta-glucan synthase, during spore wall morphogenesis in Saccharomyces cerevisiae. *Proc Natl Acad Sci U S A* **102:** 12431–6

Janke C, Magiera MM, Rathfelder N, Taxis C, Reber S, Maekawa H, Moreno-Borchart A, Doenges G, Schwob E, Schiebel E & Knop M (2004) A versatile toolbox for PCR-based tagging of yeast genes: new fluorescent proteins, more markers and promoter substitution cassettes. *Yeast* **21:** 947–62

Jungbluth M, Renicke C & Taxis C (2010) Targeted protein depletion in Saccharomyces cerevisiae by activation of a bidirectional degron. *BMC Syst Biol* **4:** 176

Khmelinskii A, Lawrence C, Roostalu J & Schiebel E (2007) Cdc14-regulated midzone assembly controls anaphase B. *J Cell Biol* **177:** 981–993

Knop M & Strasser K (2000) Role of the spindle pole body of yeast in mediating assembly of the prospore membrane during meiosis. *EMBO J* **19:** 3657–67

Maeder CI, Hink M a, Kinkhabwala A, Mayr R, Bastiaens PIH & Knop M (2007) Spatial regulation of Fus3 MAP kinase activity through a reaction-diffusion mechanism in yeast pheromone signalling. *Nat Cell Biol* **9:** 1319–26

Renicke C, Schuster D, Usherenko S, Essen L-O & Taxis C (2013) A LOV2 domain-based optogenetic tool to control protein degradation and cellular function. *Chem Biol* **20:** 619–26

Sikorski RS & Hieter P (1989) A system of shuttle vectors and yeast host strains designed for efficient manipulation of DNA in Saccharomyces cerevisiae. *Genetics* **122:** 19–27

Taxis C, Stier G, Spadaccini R & Knop M (2009) Efficient protein depletion by genetically controlled deprotection of a dormant N-degron. *Mol Syst Biol* **5:** 267

Wach A, Brachat A, Pöhlmann R & Philippsen P (1994) New heterologous modules for classical or PCR-based gene disruptions in Saccharomyces cerevisiae. *Yeast* **10:** 1793–808

Source Data For Figure 3A – Values for weighted changes in sporulation behavior

Differences to control:

Acetate Conc. [%]	Depleted Proteins	One Nucleus	Two Nuclei	Four Nuclei	No Nuclei	Monads	Dyads	Triads	Tetrads
1	Dbf2	0	0	1	-1	1	0	-3	-3
1	Dbf20	2	0	1	0	3	6	1	-14
1	Mob1	9	2	2	2	3	5	4	-20
1	Dbf2 Dbf20	2	1	1	2	4	6	5	-22
1	Dbf2 Mob1	15	4	2	3	5	8	-5	-25
1	Dbf20 Mob1	-5	3	2	3	10	15	2	-30
1	Dbf2 Dbf20 Mob1	4	1	1	5	11	13	0	-44
0.1	Dbf2	1	0	0	-2	0	-3	4	0
0.1	Dbf20	5	0	0	1	4	-2	-5	-1
0.1	Mob1	-1	1	2	8	7	-10	-6	-1
0.1	Dbf2 Dbf20	2	1	2	5	7	-1	-6	-9
0.1	Dbf2 Mob1	9	3	1	12	5	-11	-12	-1
0.1	Dbf20 Mob1	-13	3	1	10	11	-5	-8	-3
0.1	Dbf2 Dbf20 Mob1	1	4	1	16	12	-10	-18	-2
0.01	Dbf2	-2	0	0	-3	1	7	0	1
0.01	Dbf20	-1	1	0	3	2	-5	-1	0
0.01	Mob1	2	1	0	2	-1	-7	-1	0
0.01	Dbf2 Dbf20	1	1	0	3	4	-9	-6	-2
0.01	Dbf2 Mob1	13	4	1	15	-4	-20	-3	0
0.01	Dbf20 Mob1	-2	2	0	12	-3	-9	-2	0
0.01	Dbf2 Dbf20 Mob1	13	2	0	13	-2	-16	-1	0

log2-fold changes (compared to control):

Acetate Conc. [%]	Depleted Proteins	One Nucleus	Two Nuclei	Four Nuclei	No Nuclei	Monads	Dyads	Triads	Tetrads
1	Dbf2	-0.01	0.23	0.52	-0.40	1.54	0.00	-0.18	-0.07
1	Dbf20	0.12	-0.09	0.48	0.11	3.33	0.90	0.06	-0.60
1	Mob1	0.50	1.33	1.71	0.83	1.71	0.72	0.20	-1.61
1	Dbf2 Dbf20	0.16	0.81	0.90	0.96	2.94	0.96	0.42	-0.99
1	Dbf2 Mob1	0.73	1.78	1.81	1.05	2.33	1.17	-0.35	-1.76
1	Dbf20 Mob1	-0.29	1.25	1.62	0.93	3.18	1.60	0.11	-1.82
1	Dbf2 Dbf20 Mob1	0.40	1.07	2.34	1.31	3.28	1.79	0.01	-2.26
0.1	Dbf2	0.03	-0.35	-0.16	-0.88	0.30	-0.14	0.21	-0.09
0.1	Dbf20	0.21	0.23	-0.04	0.44	1.55	-0.11	-0.45	-0.19
0.1	Mob1	-0.06	1.05	1.82	1.41	1.58	-0.73	-1.02	-1.00
0.1	Dbf2 Dbf20	0.14	1.14	1.56	1.05	2.15	-0.07	-0.78	-1.12
0.1	Dbf2 Mob1	0.25	1.18	1.34	1.79	2.28	-0.84	-1.61	-0.87
0.1	Dbf20 Mob1	-0.41	1.55	0.90	1.52	2.62	-0.39	-1.18	-0.94
0.1	Dbf2 Dbf20 Mob1	0.06	2.27	0.82	2.21	2.11	-0.61	-2.42	-4.18
0.01	Dbf2	-0.08	-0.16	0.66	-0.72	0.14	0.33	0.05	2.52
0.01	Dbf20	-0.02	0.42	0.12	0.96	0.33	-0.57	-0.26	0.95
0.01	Mob1	0.06	1.02	0.11	0.32	-0.11	-1.39	-1.23	0.00
0.01	Dbf2 Dbf20	0.04	0.74	0.41	0.78	1.06	-0.81	-2.02	-1.45
0.01	Dbf2 Mob1	0.34	1.31	1.39	2.41	-0.76	-2.18	-2.94	0.00
0.01	Dbf20 Mob1	-0.04	1.13	0.82	2.15	-0.41	-1.22	-1.10	0.00
0.01	Dbf2 Dbf20 Mob1	0.28	1.52	0.80	1.84	-0.32	-2.25	-3.19	0.00

Weighted changes: *weighted change$_{cell\ species}$ = $log_2 \frac{cell\ fraction_{mutant}}{cell\ fraction_{control}}$ × |cell fraction$_{mutant}$− cell fraction$_{control}$|*

Acetate Conc. [%]	Depleted Proteins	One Nucleus	Two Nuclei	Four Nuclei	No Nuclei	Monads	Dyads	Triads	Tetrads
1	Dbf2	0	0	0	0	1	0	-1	0
1	Dbf20	0	0	0	0	10	6	0	-8
1	Mob1	5	2	4	2	4	3	1	-32
1	Dbf2 Dbf20	0	1	1	2	11	6	2	-21
1	Dbf2 Mob1	11	7	3	4	11	10	-2	-45
1	Dbf20 Mob1	-2	3	3	3	30	24	0	-54
1	Dbf2 Dbf20 Mob1	1	2	3	7	35	23	0	-99
0.1	Dbf2	0	0	0	-2	0	0	1	0
0.1	Dbf20	1	0	0	1	6	0	-2	0
0.1	Mob1	0	1	3	11	11	-8	-6	-1
0.1	Dbf2 Dbf20	0	2	2	5	14	0	-5	-10
0.1	Dbf2 Mob1	2	4	1	22	12	-9	-19	-1
0.1	Dbf20 Mob1	-5	4	1	15	28	-2	-9	-3
0.1	Dbf2 Dbf20 Mob1	0	8	1	35	25	-6	-44	-7
0.01	Dbf2	0	0	0	-2	0	2	0	2
0.01	Dbf20	0	0	0	3	1	-3	0	0
0.01	Mob1	0	1	0	1	0	-10	-1	0
0.01	Dbf2 Dbf20	0	1	0	2	4	-7	-12	-2
0.01	Dbf2 Mob1	4	5	1	37	-3	-44	-9	0
0.01	Dbf20 Mob1	0	3	0	25	-1	-10	-2	0
0.01	Dbf2 Dbf20 Mob1	4	3	0	24	0	-35	-3	0

6 Discussion

In this study, I used the model eukaryote *Saccharomyces cerevisiae* as a platform for development of synthetic biology tools to regulate protein abundance. These tools were used to analyze the role of a conserved signaling pathway during gametogenesis. With the photo-sensitive degron (psd) module, I expanded the optogenetics toolbox with a technique for precise regulation of protein degradation by blue light. For enhancement of a second method, the TEV protease induced protein instability (TIPI) system, I created a TEV protease variant with a high tolerance for different residues at the P1' position of its recognition sequence. Optimization of a meiosis-specific variant of this system enabled detailed characterization of the core mitotic exit network during *S. cerevisiae* sporulation; Using the latter method, I could demonstrate developmental-specific remodeling of this signal transduction pathway and function in several consecutive steps of spore formation.

6.1 Development of Synthetic Tools for Targeted Protein Depletion

Conditional mutants are of major significance for a detailed understanding of molecular and cellular biology. I worked on two different systems for construction of conditional mutants. Both strategies were aimed on regulation of protein stability by synthetic degrons and were designed to be applicable during sporulation of *S. cerevisiae.*

The photo-sensitive degron module, consisting of a fusion of the synthetic degron sequence cODC1 to the C-terminal Jα-helix of the *A. thaliana* LOV2 domain, is activated by blue light and leads to degradation of target proteins. I characterized the depletion kinetics of this degron, its spatial regulation, light-dose dependency and target spectrum in vegetative cell growth (Renicke *et al*, 2013a). Furthermore, I could demonstrate its function in sporulation by using the Polo-like kinase Cdc5, Sec62 as part of the ER translocation machinery and the phosphatase Cdc14 as proof-of-principle targets (Renicke & Taxis, 2016). However, this type of degron was not able to evoke the expected sporulation defects when applied on the MEN kinase Cdc15 (Kamieniecki *et al*, 2005; Pablo-Hernando *et al*, 2007; Diamond *et al*, 2009; Attner & Amon, 2012). Thus the strategy of constructing conditional MEN mutants with the help of this tool was rejected. Another reason for employment of a strategy, directly controlled by entry into meiosis, was that sporulation of yeast cultures is not synchronous and light-induced depletion therefore leads to a population carrying heterogeneous defects. Later a set of psd variants with

faster depletion kinetics has been created by other members of the group (Usherenko *et al*, 2014). Due to promising results with the TIPI system and the described disadvantage of the psd module, these variants were not tested with the different MEN components during meiosis. Though, a psd variant with shorter half-live was only used to minimize the levels of a hyperactive Cdc15 mutant prior to induction of sporulation.

Nevertheless, the psd-module has proven to be a useful expansion of the optogenetics toolkit. It was the first method to control protein stability by light using a genetically introduced, generic tag which did not involve generation of reactive oxygen species accompanied by unspecific negative side-effects (Liao *et al*, 1994; Bulina *et al*, 2006; Shu *et al*, 2011). It has been already applied in *S. cerevisiae* to study iron-sulfur cluster biogenesis (Paul *et al*, 2015) and to characterize a novel, atypical E3 ligase (Lutz *et al,* manuscript in preparation). In addition, the degron was used to regulate swimming locomotion of *Caenorhabditis elegans* (Hermann *et al*, 2015). However, the full potential of this degron has not been exploited yet: the high spatial precision offered by light enables manipulation of single cells side-by-side with unperturbed cells in a microscopic set up useful for tissue engineering and the study of cell-cell interactions (Kaji *et al*, 2011). Moreover, the direct connection between light intensity and depletion efficiency provides a straight-forward strategy to investigate thresholds and dosage effects within complex signaling networks. To enhance the potential of the psd system, modules, which react to longer wavelengths of light could be the engineered to enable independent destabilization of several targets. However, this will be challenging since the FMN cofactor limits the LOV2 domains to short wavelengths. Although phytochromes are available covering the whole spectrum of visible and near-infrared light, their mode of structural rearrangements does not fit to activation of degrons that have been characterized so far (Christie, 2007; Bae & Choi, 2008; Rockwell *et al*, 2015).

In contrast to the psd, the TIPI system offers higher flexibility. TEV protease production can be activated not only by extrinsic but also by intrinsic signals. Use of a meiosis-specific promoter for *pTEV⁺* expression allowed to exclusively deplete proteins in cells undergoing meiosis (Jungbluth *et al*, 2010, 2012). This prevented any misleading data from premature depletion of target proteins and was successfully employed to study effects of the cAMP/PKA pathway on spore number control (Jungbluth *et al*, 2012). However, the lower expression levels of the meiosis-specific *IME2* promoter compared to the *GAL1* promoter used for vegetatively growing

cells frequently required introduction of several gene copies of the P_{IME2}-$pTEV^+$ construct on high copy plasmids (Jungbluth *et al*, 2010, 2012). Beside the need of an additional transformation step and continuous selective pressure, the number of plasmid copies per cell varies considerably if 2µ vectors are used (Christianson *et al*, 1992). Differences in pTEV$^+$ levels can cause heterogeneous effects in the cell population thereby hindering interpretation of the data. To address these issues, I sought to improve this system by two parallel strategies; by generation of a TEV protease variant with a higher tolerance for the strongest N-degron arginine at position P1', and by elevation of TEV protease production from stable chromosomally integrated expression constructs combined with additional meiosis-specific transcriptional target gene shut-off.

For the first strategy, I combined random PCR-mutagenesis of the TEV protease encoding gene with a colony color-based screen to probe for efficient cleavage of a target sequence containing arginine at the P1' position (cODC1-TDegR; Renicke *et al*, 2013b). This led to identification of a protease variant, pTEV2, with a single point mutation (R203G) which was able to efficiently process the cODC1-TDegR construct. Additional experiments showed that this variant had almost lost its selectivity for P1' position. Structural modeling by Dr. Roberta Spadaccini revealed that the amino acid exchange occurred within a hydrophobic surface patch distant from the catalytic center, reducing the charge of this region. In the wild type protease this patch might prevent access of peptides with a positively charged amino acid at position P1' while the reduced charge could permit their access to the catalytic center. However, no pronounced impact of the expected N-degron strength on tester construct depletion was observed for the constructs efficiently cleaved by the TEV protease. Thus, the limiting step in protein depletion by the TIPI system is probably protease processivity rather than N-degron strength. Even if changes in specificity of pTEV2 had little impact on the value of the TIPI system, TEV2 may be beneficial for other applications. It offers much higher flexibility in the choice of the residue at position P1'. This protease could be used *in vivo* to regulate maturation and secretion of active proteins with native N-termini from pro-proteins or proteins fused to an inhibitory domain (Rogers & Overall, 2013; Cesaratto *et al*, 2015; Fernandez-Rodriguez & Voigt, 2016). The TEV2 protease might be also useful for affinity purification of proteins where TEV protease is routinely employed to remove affinity and solubility tags from recombinant proteins (Waugh, 2011; Pina *et al*, 2014). The complete removal of a tag and creation of proteins with native N-termini can be critical especially in the field of peptide and protein therapeutic

agents (Mooney *et al*, 2015; Panteleev & Ovchinnikova, 2015; Rodríguez *et al*, 2015; Zhang *et al*, 2015). The structural insights on substrate selectivity of the TEV protease obtained by our and other studies may also contribute to a better understanding of the molecular basis of substrate specificity and pave the way for rational design of customized protease variants (Phan *et al*, 2002; Verhoeven *et al*, 2012; Yi *et al*, 2013; Renicke *et al*, 2013b; Carrico *et al*, 2016).

Three major changes of the TIPI system finally led to significant enhancement of sporulation-specific depletion of target proteins: 1. Exchange of the constitutive promoters previously used in the N-terminal *TDegF* construct for expression of the resulting fusion gene against the promoter of *MCD1*, a gene encoding a mitosis-specific subunit of the cohesion complex. *MCD1* is not expressed during meiosis and has been employed for creation of sporulation-specific mutants before (Klein *et al*, 1999; Clyne *et al*, 2003; Jungbluth *et al*, 2010). 2. Exchange of the *CYC1* terminator in the meiosis-specific P_{IME2}-*pTEV$^+$*-T_{CYC1} expression construct against the more efficient *DIT1* terminator (Yamanishi *et al*, 2013; Ito *et al*, 2013). 3. Stable chromosomal integration of the resulting construct at two different loci (*TRP1*, *HIS3*) to further increase *pTEV$^+$* expression. This combination enabled successful creation of sporulation-specific loss-of-function mutants of the core MEN components Cdc15, Dbf2, Dbf20 and Mob1 during meiosis. In addition to its demonstrated function during sporulation, this method may provide a blue-print for adaptation of the TIPI system for different developmental programs in yeast but also other eukaryotes where transcriptomic data allow selection of appropriate promoters.

6.2 Functions of the Mitotic Exit Network During Sporulation

The improved, meiosis-specific TIPI system allowed to efficiently deplete Cdc15, which completely blocked spore formation. This resembled the previously published data obtained by mutants based on chemical inhibition or solely transcriptional repression (Kamieniecki *et al*, 2005; Pablo-Hernando *et al*, 2007; Attner & Amon, 2012). I also succeeded in generating single, double and a triple mutant for the three downstream components Dbf2, Dbf20 and Mob1. The triple mutant showed a severe sporulation defect, although less pronounced than the Cdc15 depletion phenotype. The single Dbf2 and Dbf20 mutants displayed almost no phenotype, consistent with earlier proposed redundant meiotic functions (Attner & Amon, 2012) whereas the single Mob1 and the different double mutant showed intermediate phenotypes. The Dbf2 Dbf20 depletion strain exhibited a weaker phenotype than different strains depleted for Mob1. Further experiments with the Mob1 single, the Dbf2 Dbf20 double and the Dbf2 Dbf20 Mob1

triple mutants as well as the Cdc15 single mutant revealed that the decreased spore formation was not due to reduction of meiotic plaque levels and Dbf2, Dbf20 as well as Mob1 are required for correct chromosome inheritance. Moreover, I found all core MEN components to be involved in age-based SPB selection. However, the effect of Cdc15 depletion was more severe compared to depletion of the downstream components. Additionally, Cdc15 was found to influence the meiotic plaque numbers in sporulating cells. Further functional diversification of MEN proteins was observed at the later stages of spore formation. As reported before (Kamieniecki *et al*, 2005; Pablo-Hernando *et al*, 2007; Attner & Amon, 2012), Cdc15 depleted cells arrested at the end of meiosis II before prospore membrane closure. Depletion of the downstream components blocked spore formation probably by interfering with spore wall assembly. These data demonstrate that the MEN functions in regulation of distinct steps of sporulation. *In vitro* phosphorylation experiments have shown that the kinase activities of the Dbf2-Mob1 and Dbf20-Mob1 complexes rely on Cdc15 phosphorylation (Attner & Amon, 2012). Thus, the function of these complexes at the end of sporulation in spore wall formation is probably Cdc15-dependent. The independent Cdc15 function in PSM closure is most likely regulation of Ama1-dependent removal of Ssp1 from the LEPC while a role of Cdc15 in the Sps1/Spo77 pathway for Ssp1 removal needs further investigation (Maier *et al*, 2007; Diamond *et al*, 2009; Slubowski *et al*, 2014; Paulissen *et al*, 2016). In summary, the presented results implicate that the core MEN pathway is subject of significant functional diversification during sporulation compared to its rather linear function in mitosis.

The additive phenotypes observed in spore formation and chromosome inheritance between the Dbf2 Dbf20 Mob1 triple mutant and the Dbf2 Dbf20 as well as the Mob1 mutant are still puzzling. They could be caused just by a stoichiometric effect of providing the basal levels of otherwise depleted proteins with a high concentration of complex partners. Yet, the observed phenotypes may also point to independent functions of the NDR (nuclear Dbf2-related) kinases Dbf2 and Dbf20 and their canonical coactivator Mob1. In *S. cerevisiae* beside the MEN, a second hippo-like pathway exists, the RAM (regulation of ace2 and morphogenesis) network, which is required during vegetative growth for cell morphogenesis and polarization as well as daughter cell separation after cytokinesis (Weiss, 2012). Especially the NDR kinase of this network Cbk1 and its coactivator Mob2 are similar to Dbf2/20 and Mob1, respectively. Mob1 has been found in a high-throughput yeast-2-hybrid screen to interact with Cbk1 (Ito *et al*, 2001). Furthermore, it has been shown *in vitro* and *in vivo* that Mob1 can form heterodimers with Mob2 (Mrkobrada

et al, 2006). No biological function of these interactions has been clearly identified. Yet, in *Drosophila melanogaster* and human cells some flexibility in the interactions of different NDR-kinases with different MOB coactivators has been reported suggesting overlapping functions (Devroe *et al*, 2004; He *et al*, 2005). However, in *S. cerevisiae,* depletion of the RAM-specific Ste20-like kinase Kic1, activating the Cbk1-Mob2 complex in mitosis, has not been found to significantly impair sporulation (Master thesis of Ann-Kathrin Allmann, 2015). Further studies targeting Cbk1 and Mob2 directly will be required to assess the possibility of sporulation-specific cross-talk between the two pathways.

One putative target of the MEN in regulation of age-based SPB selection may be the SPB outer plaque protein Nud1. Especially Cdc15 depletion caused a nearly identical defect in this process like the one observed for inactivation of a temperature-sensitive Nud1 mutant (Nud1-2; Gordon *et al*, 2006). Surprisingly, experiments on meiosis-specific depletion of Nud1 indicated an inhibitory function of this protein on spore formation (Master thesis of Ann-Kathrin Allmann, 2015). This was an unexpected result as the Nud1-2 mutant was reported to reduce spore numbers (Gordon *et al*, 2006). The reason for these different results could be a consequence of the different types of mutants. The temperature-sensitive mutant was shifted to the restrictive temperature already 90 minutes after induction of meiosis. Therefore, inactivation of Nud1 may have occurred already in cells prior to meiosis or in meiotic pro-phase. In contrast, sporulation-induced depletion of Nud1 only affects meiotic cells and depends on production of sufficient amounts of TEV protease and subsequent cleavage, ubiquitylation and proteasomal degradation. In contrast to the differences found in spore formation, the effects of both mutants on genome inheritance were similar. An inhibitory role of Nud1 could also explain the stronger phenotypes I found in most experiments for the Mob1 mutant compared to the Dbf2 Dbf20 double mutant. Nud1 levels in the Mob1 depletion strain were significantly elevated compared to the control and other mutant strains. Several studies have reported localization of Nud1 to meiosis II SPBs (Knop & Strasser, 2000; Nickas *et al*, 2004; Attner & Amon, 2012). However, these studies differed in the number of SPB-localized Nud1 signals. Thus, these data do neither exclude nor support an inhibitory function of Nud1 at specific SPBs.

Further investigations will be required to assess the exact role of Nud1 on age-based SPB selection and spore formation. Colocalization experiments with a fluorescent timer fused at the SPBs and an additional meiotic plaque marker could be performed to elucidate a putative

connection between SPB age, meiotic plaque formation and Nud1 localization. Furthermore, *NUD1* could be overexpressed during sporulation by an early meiosis-specific promoter (e.g. P*IME2*) or the inducible *CUP1* promoter used for meiotic overexpression before (Taxis *et al*, 2005). Another approach may be the constitutive, meiosis-specific tethering of Nud1 to the SPB by a meiosis-specific production of a Nud1-Cnm67 chimera. Constitutive targeting of proteins to the SPB by fusion to Cnm67 has been reported for vegetative cells (Park *et al*, 2004; Caydasi & Pereira, 2009; Caydasi *et al*, 2010; Valerio-Santiago & Monje-Casas, 2011; Scarfone & Piatti, 2015; Ratsima *et al*, 2016). To maximize the effect, this could be done in the sporulation-specific Cnm67 depletion mutant, which was successfully complemented by *CNM67* expressed under control of the mid-sporulation-specific *SPO74* promoter (Master thesis of Ann-Kathrin Allmann, 2015). Nud1 and Cnm67 bear several possible consensus sites for phosphorylation by Cdc15 ([ST]X[RK]) as well as Dbf2/20-Mob1 (RXXS) and it has been experimentally shown that Cdc15 directly phosphorylates Nud1 during mitotic exit (Mah *et al*, 2005; Mok *et al*, 2010; Rock *et al*, 2013). Thus, meiosis-specific expression of Cnm67 and Nud1 variants with mutated MEN kinase consensus sites in the strains depleted for the native proteins could be used to monitor directly whether the two SPB outer plaque components are targets of the different kinases. Together, these experiments would provide more detailed information about the function of Nud1 and Cnm67 in age-based SPB selection.

In mitosis, Cdc5 and Kin4 are central regulators of MEN activity (D'Aquino *et al*, 2005; Pereira & Schiebel, 2005; Maekawa *et al*, 2007; Gryaznova *et al*, 2016; Falk *et al*, 2016). Therefore, a putative role of these kinases in MEN regulation during sporulation was investigated during in the context of a master thesis (Ann-Kathrin Allmann, 2015). Kin4 depletion somewhat resembled the Dbf2 Dbf20 Mob1 triple depletion phenotype during spore formation. However, in contrast to this mutant, I observed no elevated frequency of sister dyads upon depletion of Kin4. Therefore, it is unlikely that this kinase plays a role in MEN activation during meiosis. The same might be true for Cdc5, for which no correlation between SPB localization and PSM formation has been observed.

A possibility to address the open questions of meiotic upstream regulators of the MEN as well as its downstream targets might be affinity purification of the MEN components and associated proteins followed by mass-spectrometry to identify these interaction partners. Similar approaches are commonly used to reveal protein interaction networks during vegetative

growth (Krogan *et al*, 2006; Breitkreutz *et al*, 2010; Gavin *et al*, 2011). To specifically identify interactions during sporulation, epitope-tagged Cdc15, Dbf2, Dbf20 and Mob1 can be produced under control of a meiosis-specific promoter like P$_{IME2}$ or P$_{SPO74}$. Usage of Ime2-GFP as a meiotic marker would allow fluorescence activated cell sorting (FACS) and thus, selection of only sporulating cells for downstream processing of the samples. Many interactions could only be of transient. Thus, chemical *in vivo* cross-linking may be required (Guerrero, 2005; Vasilescu & Figeys, 2006). The parallel usage of different promoters, active at different time points during sporulation may even allow rough correlation of interactions with the different steps of sporulation. In summary, this strategy could significantly contribute to an in-depth understanding of MEN signaling during sporulation and might provide a basis for detailed functional genetic studies of the identified interaction partners of the MEN.

7 References

Adames NR & Cooper J a (2000) Microtubule interactions with the cell cortex causing nuclear movements in Saccharomyces cerevisiae. *J. Cell Biol.* **149:** 863–74

Adams IR & Kilmartin J V (1999) Localization of core spindle pole body (SPB) components during SPB duplication in Saccharomyces cerevisiae. *J. Cell Biol.* **145:** 809–23

Asakawa K, Yoshida S, Otake F & Toh-e A (2001) A novel functional domain of Cdc15 kinase is required for its interaction with Tem1 GTPase in Saccharomyces cerevisiae. *Genetics* **157:** 1437–50

Attner MA & Amon A (2012) Control of the mitotic exit network during meiosis. *Mol. Biol. Cell* **23:** 3122–32

Bae G & Choi G (2008) Decoding of light signals by plant phytochromes and their interacting proteins. *Annu. Rev. Plant Biol.* **59:** 281–311

Beach DL, Thibodeaux J, Maddox P, Yeh E & Bloom K (2000) The role of the proteins Kar9 and Myo2 in orienting the mitotic spindle of budding yeast. *Curr. Biol.* **10:** 1497–506

Benjamin KR, Zhang C, Shokat KM & Herskowitz I (2003) Control of landmark events in meiosis by the CDK Cdc28 and the meiosis-specific kinase Ime2. *Genes Dev.* **17:** 1524–39

Bertazzi DT, Kurtulmus B & Pereira G (2011) The cortical protein Lte1 promotes mitotic exit by inhibiting the spindle position checkpoint kinase Kin4. *J. Cell Biol.* **193:** 1033–48

Bi E & Park H-O (2012) Cell Polarization and Cytokinesis in Budding Yeast. *Genetics* **191:** 347–387

Bienkowska D & Cowan CR (2012) Centrosomes can initiate a polarity axis from any position within one-cell C. Elegans embryos. *Curr. Biol.* **22:** 583–589

Bishop a C, Ubersax J a, Petsch DT, Matheos DP, Gray NS, Blethrow J, Shimizu E, Tsien JZ, Schultz PG, Rose MD, Wood JL, Morgan DO & Shokat KM (2000) A chemical switch for inhibitor-sensitive alleles of any protein kinase. *Nature* **407:** 395–401

Bonger KM, Rakhit R, Payumo AY, Chen JK & Wandless TJ (2014) General method for regulating protein stability with light. *ACS Chem. Biol.* **9:** 111–5

Breitkreutz A, Choi H, Sharom JR, Boucher L, Neduva V, Larsen B, Lin Z-YY, Breitkreutz B-JJ, Stark C, Liu G, Ahn J, Dewar-Darch D, Reguly T, Tang X, Almeida R, Qin ZS, Pawson T, Gingras A-CC, Nesvizhskii AI & Tyers M (2010) A global protein kinase and phosphatase interaction network in yeast. *Science* **328:** 1043–6

Bugaj LJ, Spelke DP, Mesuda CK, Varedi M, Kane RS & Schaffer D V (2015) Regulation of endogenous transmembrane receptors through optogenetic Cry2 clustering. *Nat. Commun.* **6:** 6898

Bulina ME, Chudakov DM, Britanova O V, Yanushevich YG, Staroverov DB, Chepurnykh T V, Merzlyak EM, Shkrob MA, Lukyanov S & Lukyanov KA (2006) A genetically encoded photosensitizer. *Nat Biotechnol* **24:** 95–99

Bullitt E, Rout MP, Kilmartin J V & Akey CW (1997) The yeast spindle pole body is assembled around a central crystal of Spc42p. *Cell* **89:** 1077–86

Carrico ZM, Strobel KL, Atreya ME, Clark DS & Francis MB (2016) Simultaneous selection and counter-selection for the directed evolution of proteases in E. coli using a cytoplasmic anchoring strategy. *Biotechnol. Bioeng.* **113:** 1187–1193

Carvalho P, Gupta ML, Hoyt MA & Pellman D (2004) Cell cycle control of kinesin-mediated transport of Bik1 (CLIP-170) regulates microtubule stability and dynein activation. *Dev. Cell* **6:** 815–29

Caydasi AK, Ibrahim B & Pereira G (2010) Monitoring spindle orientation: Spindle position checkpoint in charge. *Cell Div.* **5:** 28

Caydasi AK, Lohel M, Grünert G, Dittrich P, Pereira G & Ibrahim B (2012) A dynamical model of the spindle position checkpoint. *Mol. Syst. Biol.* **8:** 582

Caydasi AK & Pereira G (2009) Spindle alignment regulates the dynamic association of checkpoint proteins with yeast spindle pole bodies. *Dev. Cell* **16:** 146–56

Cesaratto F, López-Requena A, Burrone OR & Petris G (2015) Engineered tobacco etch virus (TEV) protease active in the secretory pathway of mammalian cells. *J. Biotechnol.* **212:** 159–166

Christianson TW, Sikorski RS, Dante M, Shero JH & Hieter P (1992) Multifunctional yeast high-copy-number shuttle vectors. *Gene* **110:** 119–122

Christie JM (2007) Phototropin Blue-Light Receptors.

Chu S, DeRisi J, Eisen M, Mulholland J, Botstein D, Brown PO & Herskowitz I (1998) The transcriptional program of sporulation in budding yeast. *Science* **282:** 699–705

Chu S & Herskowitz I (1998) Gametogenesis in yeast is regulated by a transcriptional cascade dependent on Ndt80. *Mol. Cell* **1:** 685–96

Clyne RK, Katis VL, Jessop L, Benjamin KR, Herskowitz I, Lichten M & Nasmyth K (2003) Polo-like kinase Cdc5 promotes chiasmata formation and cosegregation of sister centromeres at meiosis I. *Nat. Cell Biol.* **5:** 480–5

Colomina N, Garí E, Gallego C, Herrero E & Aldea M (1999) G1 cyclins block the Ime1 pathway to make mitosis and meiosis incompatible in budding yeast. *EMBO J.* **18:** 320–9

Coluccio A, Bogengruber E, Conrad MN, Dresser ME, Briza P & Neiman AM (2004) Morphogenetic pathway of spore wall assembly in Saccharomyces cerevisiae. *Eukaryot. Cell* **3:** 1464–75

D'Aquino KE, Monje-Casas F, Paulson J, Reiser V, Charles GM, Lai L, Shokat KM & Amon A (2005) The protein kinase Kin4 inhibits exit from mitosis in response to spindle position defects. *Mol. Cell* **19:** 223–34

Davidow LS, Goetsch L & Byers B (1980) Preferential Occurrence of Nonsister Spores in Two-Spored Asci of SACCHAROMYCES CEREVISIAE: Evidence for Regulation of Spore-Wall Formation by the Spindle Pole Body. *Genetics* **94:** 581–95

Deng C & Saunders WS (2001) ADY1, a novel gene required for prospore membrane formation at selected spindle poles in Saccharomyces cerevisiae. *Mol. Biol. Cell* **12:** 2646–59

Devroe E, Erdjument-Bromage H, Tempst P & Silver PA (2004) Human Mob proteins regulate the NDR1 and NDR2 serine-threonine kinases. *J. Biol. Chem.* **279:** 24444–24451

Diamond AE, Park J-S, Inoue I, Tachikawa H & Neiman AM (2009) The anaphase promoting complex targeting subunit Ama1 links meiotic exit to cytokinesis during sporulation in Saccharomyces cerevisiae. *Mol. Biol. Cell* **20:** 134–45

Dohmen RJ, Wu P & Varshavsky a (1994) Heat-inducible degron: a method for constructing temperature-sensitive mutants. *Science* **263:** 1273–6

Duina AA, Miller ME & Keeney JB (2014) Budding yeast for budding geneticists: A primer on the Saccharomyces cerevisiae model system. *Genetics* **197:** 33–48

Eastwood MD, Cheung SWT, Lee KY, Moffat J & Meneghini MD (2012) Developmentally programmed nuclear destruction during yeast gametogenesis. *Dev. Cell* **23:** 35–44

Elliott S, Knop M, Schlenstedt G & Schiebel E (1999) Spc29p is a component of the Spc110p subcomplex and is essential for spindle pole body duplication. *Proc. Natl. Acad. Sci. U. S. A.* **96:** 6205–6210

Falk JE, Tsuchiya D, Verdaasdonk J, Lacefield S, Bloom K & Amon A (2016) Spatial signals link exit from mitosis to spindle position. *Elife* **5:** e14036

Fernandez-Rodriguez J & Voigt CA (2016) Post-translational control of genetic circuits using *Potyvirus* proteases. *Nucleic Acids Res.* **44:** gkw537

Fraschini R, D'Ambrosio C, Venturetti M, Lucchini G & Piatti S (2006) Disappearance of the budding yeast Bub2-Bfa1 complex from the mother-bound spindle pole contributes to mitotic exit. *J. Cell Biol.* **172:** 335–46

Gavin AC, Maeda K & Kühner S (2011) Recent advances in charting protein-protein interaction: Mass spectrometry-based approaches. *Curr. Opin. Biotechnol.* **22:** 42–49

Geymonat M, Spanos A, Smith SJM, Wheatley E, Rittinger K, Johnston LH & Sedgwick SG (2002) Control of mitotic exit in budding yeast. In vitro regulation of Tem1 GTPase by Bub2 and Bfa1. *J. Biol. Chem.* **277:** 28439–45

Goldstein B & Hird SN (1996) Specification of the anteroposterior axis in Caenorhabditis elegans. *Development* **122:** 1467–1474

Goldstein B & Macara IG (2007) The PAR Proteins: Fundamental Players in Animal Cell Polarization. *Dev. Cell* **13:** 609–622

Gordon O, Taxis C, Keller PJ, Benjak A, Stelzer EHK, Simchen G & Knop M (2006) Nud1p, the yeast homolog of Centriolin, regulates spindle pole body inheritance in meiosis. *EMBO J.* **25:** 3856–68

Gossen M & Bujard H (1992) Tight control of gene expression in mammalian cells by tetracycline-responsive promoters. *Proc. Natl. Acad. Sci. U. S. A.* **89:** 5547–51

Gotta M, Abraham MC & Ahringer J (2001) CDC-42 controls early cell polarity and spindle orientation in C. elegans. *Curr. Biol.* **11:** 482–488

Gryaznova Y, Koca Caydasi A, Malengo G, Sourjik V & Pereira G (2016) A FRET-based study reveals site-specific regulation of spindle position checkpoint proteins at yeast centrosomes. *Elife* **5:** e14029

Guerrero C (2005) An Integrated Mass Spectrometry-based Proteomic Approach: Quantitative Analysis of Tandem Affinity-purified in vivo Cross-linked Protein Complexes (qtax) to Decipher the 26 s Proteasome-interacting Network. *Mol. Cell. Proteomics* **5:** 366–378

Harper SM, Neil LC & Gardner KH (2003) Structural basis of a phototropin light switch. *Science* **301:** 1541–1544

Hartwell LH, Mortimer RK, Culotti J & Culotti M (1973) Genetic Control of the Cell Division Cycle in Yeast: V. Genetic Analysis of cdc Mutants. *Genetics* **74:** 267–86

He Y, Emoto K, Fang X, Ren N, Tian X, Jan Y-N & Adler PN (2005) Drosophila Mob family proteins interact with the related tricornered (Trc) and warts (Wts) kinases. *Mol. Biol. Cell* **16:** 4139–52

Heil-Chapdelaine R a, Oberle JR & Cooper J a (2000) The cortical protein Num1p is essential for dynein-dependent interactions of microtubules with the cortex. *J. Cell Biol.* **151:** 1337–44

Hermann A, Liewald JF & Gottschalk A (2015) A photosensitive degron enables acute light-induced protein degradation in the nervous system. *Curr. Biol.* **25:** R749–R750

Hotz M, Leisner C, Chen D, Manatschal C, Wegleiter T, Ouellet J, Lindstrom D, Gottschling DE, Vogel J & Barral Y (2012a) Spindle Pole Bodies Exploit the Mitotic Exit Network in Metaphase to Drive Their Age-Dependent Segregation. *Cell* **148:** 958–972

Hotz M, Lengefeld J & Barral Y (2012b) The MEN mediates the effects of the spindle assembly checkpoint on Kar9-dependent spindle pole body inheritance in budding yeast. *Cell Cycle* **11:** 3109–16

Hüls D, Storchova Z & Niessing D (2012) Post-translational modifications regulate assembly of early spindle orientation complex in yeast. *J. Biol. Chem.* **287:** 16238–45

Hwang E, Kusch J, Barral Y & Huffaker TC (2003) Spindle orientation in Saccharomyces cerevisiae depends on the transport of microtubule ends along polarized actin cables. *J. Cell Biol.* **161:** 483–8

Ito T, Chiba T, Ozawa R, Yoshida M, Hattori M & Sakaki Y (2001) A comprehensive two-hybrid analysis to explore the yeast protein interactome. *Proc. Natl. Acad. Sci. U. S. A.* **98:** 4569–74

Ito Y, Yamanishi M, Ikeuchi A, Imamura C, Tokuhiro K, Kitagawa T & Matsuyama T (2013) Characterization of five terminator regions that increase the protein yield of a transgene in Saccharomyces cerevisiae. *J. Biotechnol.* **168:** 486–92

Juanes MA, Twyman H, Tunnacliffe E, Guo Z, ten Hoopen R & Segal M (2013) Spindle pole body history intrinsically links pole identity with asymmetric fate in budding yeast. *Curr. Biol.* **23:** 1310–9

Jungbluth M, Mösch H-U & Taxis C (2012) Acetate regulation of spore formation is under the control of the Ras/cyclic AMP/protein kinase A pathway and carbon dioxide in Saccharomyces cerevisiae. *Eukaryot. Cell* **11:** 1021–32

Jungbluth M, Renicke C & Taxis C (2010) Targeted protein depletion in Saccharomyces cerevisiae by activation of a bidirectional degron. *BMC Syst. Biol.* **4:** 176

Kaji H, Camci-Unal G, Langer R & Khademhosseini A (2011) Engineering systems for the generation of patterned co-cultures for controlling cell-cell interactions. *Biochim. Biophys. Acta - Gen. Subj.* **1810:** 239–250

Kamieniecki RJ, Liu L & Dawson DS (2005) FEAR but not MEN genes are required for exit from meiosis I. *Cell Cycle* **4:** 1093–8

Klein F, Mahr P, Galova M, Buonomo SB, Michaelis C, Nairz K & Nasmyth K (1999) A central role for cohesins in sister chromatid cohesion, formation of axial elements, and recombination during yeast meiosis. *Cell* **98:** 91–103

Knop M & Schiebel E (1998) Receptors determine the cellular localization of a gamma-tubulin complex and thereby the site of microtubule formation. *EMBO J.* **17:** 3952–67

Knop M & Strasser K (2000) Role of the spindle pole body of yeast in mediating assembly of the prospore membrane during meiosis. *EMBO J.* **19:** 3657–67

Krogan NJ, Cagney G, Yu H, Zhong G, Guo X, Ignatchenko A, Li J, Pu S, Datta N, Tikuisis AP, Punna T, Peregrín-Alvarez JM, Shales M, Zhang X, Davey M, Robinson MD, Paccanaro A, Bray JE, Sheung A, Beattie B, et al (2006) Global landscape of protein complexes in the yeast Saccharomyces cerevisiae. *Nature* **440:** 637–643

Lam C, Santore E, Lavoie E, Needleman L, Fiacco N, Kim C & Neiman AM (2014) A visual screen of protein localization during sporulation identifies new components of prospore membrane-associated complexes in budding yeast. *Eukaryot. Cell* **13:** 383–91

Lee W-L, Oberle JR & Cooper J a (2003) The role of the lissencephaly protein Pac1 during nuclear migration in budding yeast. *J. Cell Biol.* **160:** 355–64

Leisner C, Kammerer D, Denoth A, Britschi M, Barral Y & Liakopoulos D (2008) Regulation of Mitotic Spindle Asymmetry by SUMO and the Spindle-Assembly Checkpoint in Yeast. *Curr. Biol.* **18:** 1249–1255

Li R (2013) The art of choreographing asymmetric cell division. *Dev. Cell* **25:** 439–450

Liakopoulos D, Kusch J, Grava S, Vogel J & Barral Y (2003) Asymmetric loading of Kar9 onto spindle poles and microtubules ensures proper spindle alignment. *Cell* **112:** 561–74

Liao JC, Roider J & Jay DG (1994) Chromophore-assisted laser inactivation of proteins is mediated by the photogeneration of free radicals. *Proc Natl Acad Sci U S A* **91:** 2659–2663

Lutz AP, Schladebeck S, Renicke C, Spadaccini R, Mösch H-U & Taxis C Budding yeast HECT_2 protein

Utd1 is a ubiquitin-protein ligase important for proteasome activity.

Macara IG & Mili S (2008) Polarity and Differential Inheritance—Universal Attributes of Life? *Cell* **135:** 801–812

Maekawa H, Priest C, Lechner J, Pereira G & Schiebel E (2007) The yeast centrosome translates the positional information of the anaphase spindle into a cell cycle signal. *J. Cell Biol.* **179:** 423–36

Mager WH & Winderickx J (2005) Yeast as a model for medical and medicinal research. *Trends Pharmacol. Sci.* **26:** 265–73

Mah AS, Elia AEH, Devgan G, Ptacek J, Schutkowski M, Snyder M, Yaffe MB & Deshaies RJ (2005) Substrate specificity analysis of protein kinase complex Dbf2-Mob1 by peptide library and proteome array screening. *BMC Biochem.* **6:** 22

Maier P, Rathfelder N, Finkbeiner MG, Taxis C, Mazza M, Le Panse S, Haguenauer-Tsapis R & Knop M (2007) Cytokinesis in yeast meiosis depends on the regulated removal of Ssp1p from the prospore membrane. *EMBO J.* **26:** 1843–52

Meitinger F, Palani S, Hub B & Pereira G (2013) Dual function of the NDR-kinase Dbf2 in the regulation of the F-BAR protein Hof1 during cytokinesis. *Mol. Biol. Cell* **24:** 1290–304

Meitinger F, Petrova B, Lombardi IM, Bertazzi DT, Hub B, Zentgraf H & Pereira G (2010) Targeted localization of Inn1, Cyk3 and Chs2 by the mitotic-exit network regulates cytokinesis in budding yeast. *J. Cell Sci.* **123:** 1851–61

Menendez-Benito V, van Deventer SJ, Jimenez-Garcia V, Roy-Luzarraga M, van Leeuwen F & Neefjes J (2013) Spatiotemporal analysis of organelle and macromolecular complex inheritance. *Proc. Natl. Acad. Sci. U. S. A.* **110:** 175–80

Möglich A & Moffat K (2010) Engineered photoreceptors as novel optogenetic tools. *Photochem. Photobiol. Sci.* **9:** 1286–300

Mohl DA, Huddleston MJ, Collingwood TS, Annan RS & Deshaies RJ (2009) Dbf2-Mob1 drives relocalization of protein phosphatase Cdc14 to the cytoplasm during exit from mitosis. *J. Cell Biol.* **184:** 527–39

Mok J, Kim PM, Lam HYK, Piccirillo S, Zhou X, Jeschke GR, Sheridan DL, Parker SA, Desai V, Jwa M, Cameroni E, Niu H, Good M, Remenyi A, Ma J-LN, Sheu Y-J, Sassi HE, Sopko R, Chan CSM, De Virgilio C, et al (2010) Deciphering protein kinase specificity through large-scale analysis of yeast phosphorylation site motifs. *Sci. Signal.* **3:** ra12

Mooney JT, Fredericks DP, Christensen T, Bruun Schiødt C & Hearn MTW (2015) N-terminal processing of affinity-tagged recombinant proteins purified by IMAC procedures. *J. Mol. Recognit.* **28:** 401–412

Moreno-Borchart AC, Strasser K, Finkbeiner MG, Shevchenko A, Shevchenko A & Knop M (2001) Prospore membrane formation linked to the leading edge protein (LEP) coat assembly. *EMBO J.* **20:** 6946–57

Mrkobrada S, Boucher L, Ceccarelli DFJ, Tyers M & Sicheri F (2006) Structural and Functional Analysis of Saccharomyces cerevisiae Mob1. *J. Mol. Biol.* **362:** 430–440

Mumberg D, Müller R & Funk M (1994) Regulatable promoters of Saccharomyces cerevisiae: comparison of transcriptional activity and their use for heterologous expression. *Nucleic Acids Res.* **22:** 5767–8

Munro E, Nance J & Priess JR (2004) Cortical flows powered by asymmetrical contraction transport PAR proteins to establish and maintain anterior-posterior polarity in the early C. elegans embryo. *Dev. Cell* **7:** 413–424

Nakanishi H, Morishita M, Schwartz CL, Coluccio A, Engebrecht J & Neiman AM (2006) Phospholipase D and the SNARE Sso1p are necessary for vesicle fusion during sporulation in yeast. *J. Cell Sci.*

119: 1406–15

Neiman AM (1998) Prospore membrane formation defines a developmentally regulated branch of the secretory pathway in yeast. *J. Cell Biol.* **140:** 29–37

Neiman AM (2011) Sporulation in the Budding Yeast Saccharomyces cerevisiae. *Genetics* **189:** 737–65

Nickas ME, Diamond AE, Yang M-J & Neiman AM (2004) Regulation of spindle pole function by an intermediary metabolite. *Mol. Biol. Cell* **15:** 2606–16

Nickas ME & Neiman AM (2002) Ady3p links spindle pole body function to spore wall synthesis in Saccharomyces cerevisiae. *Genetics* **160:** 1439–50

Nickas ME, Schwartz C & Neiman AM (2003) Ady4p and Spo74p are components of the meiotic spindle pole body that promote growth of the prospore membrane in Saccharomyces cerevisiae. *Eukaryot. Cell* **2:** 431–45

Nishimura K, Fukagawa T, Takisawa H, Kakimoto T & Kanemaki M (2009) An auxin-based degron system for the rapid depletion of proteins in nonplant cells. **6:** 917–922

O'Toole ET, Winey M & McIntosh JR (1999) High-voltage electron tomography of spindle pole bodies and early mitotic spindles in the yeast Saccharomyces cerevisiae. *Mol. Biol. Cell* **10:** 2017–2031

Oh Y, Chang K-J, Orlean P, Wloka C, Deshaies R & Bi E (2012) Mitotic exit kinase Dbf2 directly phosphorylates chitin synthase Chs2 to regulate cytokinesis in budding yeast. *Mol. Biol. Cell* **23:** 2445–56

Pablo-Hernando ME, Arnaiz-Pita Y, Nakanishi H, Dawson D, del Rey F, Neiman AM & Vázquez de Aldana CR (2007) Cdc15 is required for spore morphogenesis independently of Cdc14 in Saccharomyces cerevisiae. *Genetics* **177:** 281–93

Panteleev P V. & Ovchinnikova T V. (2015) Improved strategy for recombinant production and purification of antimicrobial peptide tachyplesin I and its analogs with high cell selectivity. *Biotechnol. Appl. Biochem.:* n/a-n/a

Park J-E, Park CJ, Sakchaisri K, Karpova T, Asano S, McNally J, Sunwoo Y, Leem S-H & Lee KS (2004) Novel functional dissection of the localization-specific roles of budding yeast polo kinase Cdc5p. *Mol. Cell. Biol.* **24:** 9873–9886

Paul VD, Mühlenhoff U, Stümpfig M, Seebacher J, Kugler KG, Renicke C, Taxis C, Gavin A-C, Pierik AJ & Lill R (2015) The deca-GX3 proteins Yae1-Lto1 function as adaptors recruiting the ABC protein Rli1 for iron-sulfur cluster insertion. *Elife* **4:** e08231

Paulissen SM, Slubowski CJ, Roesner JM & Huang LS (2016) Timely closure of the prospore membrane requires SPS1 and SPO77 in Saccharomyces cerevisiae. *Genetics:* 143–148

Pereira G & Schiebel E (2005) Kin4 kinase delays mitotic exit in response to spindle alignment defects. *Mol. Cell* **19:** 209–21

Phan J, Zdanov A, Evdokimov AG, Tropea JE, Peters HK, Kapust RB, Li M, Wlodawer A & Waugh DS (2002) Structural basis for the substrate specificity of tobacco etch virus protease. *J. Biol. Chem.* **277:** 50564–72

Piatti S, Venturetti M, Chiroli E & Fraschini R (2006) The spindle position checkpoint in budding yeast: the motherly care of MEN. *Cell Div.* **1:** 2

Pina AS, Lowe CR & Roque ACA (2014) Challenges and opportunities in the purification of recombinant tagged proteins. *Biotechnol. Adv.* **32:** 366–381

Ratsima H, Serrano D, Pascariu M & D'Amours D (2016) Centrosome-Dependent Bypass of the DNA Damage Checkpoint by the Polo Kinase Cdc5. *Cell Rep.:* 1–13

Ravid T & Hochstrasser M (2008) Diversity of degradation signals in the ubiquitin-proteasome system. *Nat. Rev. Mol. Cell Biol.* **9:** 679–90

Renicke C, Schuster D, Usherenko S, Essen L-O & Taxis C (2013a) A LOV2 domain-based optogenetic tool to control protein degradation and cellular function. *Chem. Biol.* **20:** 619–26

Renicke C, Spadaccini R & Taxis C (2013b) A Tobacco Etch Virus Protease with Increased Substrate Tolerance at the P1' position. *PLoS One* **8:** e67915

Renicke C & Taxis C (2016) Development of an optogenetic tool to regulate protein stability in vivo. In *OPTOGENETICS: From Neuronal Function to Mapping & Disease Biology*, Appasani K (ed) p in press. Cambridge, UK: Cambridge University Press

Rock JM & Amon A (2011) Cdc15 integrates Tem1 GTPase-mediated spatial signals with Polo kinase-mediated temporal cues to activate mitotic exit. *Genes Dev.* **25:** 1943–54

Rock JM, Lim D, Stach L, Ogrodowicz RW, Keck JM, Jones MH, Wong CCL, Yates JR, Winey M, Smerdon SJ, Yaffe MB & Amon A (2013) Activation of the yeast Hippo pathway by phosphorylation-dependent assembly of signaling complexes. *Science* **340:** 871–5

Rockwell NC, Duanmu D, Shelley S, Bachy C, Price DC, Bhattacharya D, Worden AZ, Lagarias JC, Rockwell NC, Duanmu D, Martin SS, Bachy C, Price DC & Bhattacharya D (2015) Eukaryotic algal phytochromes span the visible spectrum. *Proc. Natl. Acad. Sci.* **112:** E1051–E1051

Rodríguez V, Lascani J, Asenjo JA & Andrews BA (2015) Production of Cell-Penetrating Peptides in Escherichia coli Using an Intein-Mediated System. *Appl. Biochem. Biotechnol.* **175:** 3025–3037

Rogers LD & Overall CM (2013) Proteolytic post-translational modification of proteins: proteomic tools and methodology. *Mol. Cell. Proteomics* **12:** 3532–42

Rose L & Gönczy P (2014) Polarity establishment, asymmetric division and segregation of fate determinants in early C. elegans embryos. *WormBook***:** 1–43

Roubinet C & Cabernard C (2014) Control of asymmetric cell division. *Curr. Opin. Cell Biol.* **31:** 84–91

Sagee S, Sherman A, Shenhar G, Robzyk K, Ben-Doy N, Simchen G & Kassir Y (1998) Multiple and distinct activation and repression sequences mediate the regulated transcription of IME1, a transcriptional activator of meiosis-specific genes in Saccharomyces cerevisiae. *Mol. Cell. Biol.* **18:** 1985–95

Scarfone I & Piatti S (2015) Coupling spindle position with mitotic exit in budding yeast: the multifaceted role of the small GTPase Tem1. *Small GTPases* **1248:**

Schaerer F, Morgan G, Winey M & Philippsen P (2001) Cnm67p is a spacer protein of the Saccharomyces cerevisiae spindle pole body outer plaque. *Mol. Biol. Cell* **12:** 2519–33

Schneekloth JS, Fonseca FN, Koldobskiy M, Mandal A, Deshaies R, Sakamoto K & Crews CM (2004) Chemical genetic control of protein levels: selective in vivo targeted degradation. *J. Am. Chem. Soc.* **126:** 3748–54

Shcherbakova DM, Shemetov AA, Kaberniuk AA & Verkhusha V V (2015) Natural photoreceptors as a source of fluorescent proteins, biosensors, and optogenetic tools.

Shefer-Vaida M, Sherman a, Ashkenazi T, Robzyk K & Kassir Y (1995) Positive and negative feedback loops affect the transcription of IME1, a positive regulator of meiosis in Saccharomyces cerevisiae. *Dev. Genet.* **16:** 219–28

Sherman a, Shefer M, Sagee S & Kassir Y (1993) Post-transcriptional regulation of IME1 determines initiation of meiosis in Saccharomyces cerevisiae. *Mol. Gen. Genet.* **237:** 375–84

Shimizu-Sato S, Huq E, Tepperman JM & Quail PH (2002) A light-switchable gene promoter system. *Nat. Biotechnol.* **20:** 1041–4

Shu X, Lev-Ram V, Deerinck TJ, Qi Y, Ramko EB, Davidson MW, Jin Y, Ellisman MH & Tsien RY (2011) A genetically encoded tag for correlated light and electron microscopy of intact cells, tissues, and organisms. *PLoS Biol.* **9:**

Simchen G (2009) Commitment to meiosis: what determines the mode of division in budding yeast? *Bioessays* **31:** 169–77

Slubowski CJ, Paulissen SM & Huang LS (2014) The GCKIII Kinase Sps1 and the 14-3-3 Isoforms, Bmh1 and Bmh2, Cooperate to Ensure Proper Sporulation in Saccharomyces cerevisiae. *PLoS One* **9:** e113528

Strickland D, Lin Y, Wagner E & Hope C (2012) TULIPs: tunable, light-controlled interacting protein tags for cell biology. *Nat. Methods* **9:**

Takeuchi J, Chen H, Hoyt M a & Coffino P (2008) Structural elements of the ubiquitin-independent proteasome degron of ornithine decarboxylase. *Biochem. J.* **410:** 401–7

Taxis C, Keller P, Kavagiou Z, Jensen LJ, Colombelli J, Bork P, Stelzer EHK & Knop M (2005) Spore number control and breeding in Saccharomyces cerevisiae: a key role for a self-organizing system. *J. Cell Biol.* **171:** 627–40

Taxis C, Stier G, Spadaccini R & Knop M (2009) Efficient protein depletion by genetically controlled deprotection of a dormant N-degron. *Mol. Syst. Biol.* **5:** 267

Toyn JH, Araki H, Sugino a & Johnston LH (1991) The cell-cycle-regulated budding yeast gene DBF2, encoding a putative protein kinase, has a homologue that is not under cell-cycle control. *Gene* **104:** 63–70

Tsokos CG & Laub MT (2012) Polarity and cell fate asymmetry in Caulobacter crescentus. *Curr. Opin. Microbiol.* **15:** 744–750

Usherenko S, Stibbe H, Muscò M, Essen L-O, Kostina EA & Taxis C (2014) Photo-sensitive degron variants for tuning protein stability by light. *BMC Syst. Biol.* **8:** 128

Valerio-Santiago M & Monje-Casas F (2011) Tem1 localization to the spindle pole bodies is essential for mitotic exit and impairs spindle checkpoint function. *J. Cell Biol.* **192:** 599–614

Varshavsky A (2011) The N-end rule pathway and regulation by proteolysis. *Protein Sci.* **20:** 1298–1345

Vasilescu J & Figeys D (2006) Mapping protein-protein interactions by mass spectrometry. *Curr. Opin. Biotechnol.* **17:** 394–399

Verhoeven KD, Altstadt OC & Savinov SN (2012) Intracellular detection and evolution of site-specific proteases using a genetic selection system. *Appl. Biochem. Biotechnol.* **166:** 1340–1354

Visintin R & Amon A (2001) Regulation of the mitotic exit protein kinases Cdc15 and Dbf2. *Mol. Biol. Cell* **12:** 2961–74

Visintin R, Craig K, Hwang ES, Prinz S, Tyers M & Amon A (1998) The phosphatase Cdc14 triggers mitotic exit by reversal of Cdk-dependent phosphorylation. *Mol. Cell* **2:** 709–18

Visintin R, Hwang ES & Amon A (1999) Cfi1 prevents premature exit from mitosis by anchoring Cdc14 phosphatase in the nucleolus. *Nature* **398:** 818–23

Wallenfang MR & Seydoux G (2000) Polarization of the anterior-posterior axis of C. elegans is a microtubule-directed process. *Nature* **408:** 89–92

Waugh DS (2011) An overview of enzymatic reagents for the removal of affinity tags. *Protein Expr. Purif.* **80:** 283–293

Weiss EL (2012) Mitotic exit and separation of mother and daughter cells. *Genetics* **192:** 1165–202

Wigge PA, Jensen ON, Holmes S, Souès S, Mann M & Kilmartin J V (1998) Analysis of the

Saccharomyces spindle pole by matrix-assisted laser desorption/ionization (MALDI) mass spectrometry. *J. Cell Biol.* **141:** 967–77

Wu YI, Frey D, Lungu OI, Jaehrig A, Schlichting I, Kuhlman B & Hahn KM (2009) A genetically encoded photoactivatable Rac controls the motility of living cells. *Nature* **461:** 104–8

Xu L, Ajimura M, Padmore R, Klein C & Kleckner N (1995) NDT80, a meiosis-specific gene required for exit from pachytene in Saccharomyces cerevisiae. *Mol. Cell. Biol.* **15:** 6572

Yamanishi M, Ito Y, Kintaka R, Imamura C, Katahira S, Ikeuchi A, Moriya H & Matsuyama T (2013) A genome-wide activity assessment of terminator regions in Saccharomyces cerevisiae provides a "terminatome" toolbox. *ACS Synth. Biol.* **2:** 337–47

Yi L, Gebhard MC, Li Q, Taft JM, Georgiou G & Iverson BL (2013) Engineering of TEV protease variants by yeast ER sequestration screening (YESS) of combinatorial libraries. *Proc. Natl. Acad. Sci. U. S. A.* **110:** 7229–7234

Yin H, Pruyne D, Huffaker TC & Bretscher a (2000) Myosin V orientates the mitotic spindle in yeast. *Nature* **406:** 1013–5

Yin T & Wu YI (2013) Guiding lights: recent developments in optogenetic control of biochemical signals. *Pflugers Arch.* **465:** 397–408

Zhang Y, Teng D, Wang X, Mao R, Cao X, Hu X, Zong L & Wang J (2015) In vitro and in vivo characterization of a new recombinant antimicrobial peptide, MP1102, against methicillin-resistant Staphylococcus aureus. *Appl. Microbiol. Biotechnol.* **99:** 6255–6266

Appendix

List of Abbreviations

Curriculum vitae

Danksagung

Eidesstattliche Erklärung

Erklärung der Eigenanteile1

List of abbreviations

AIR	5'-phosphoribosyl-5-aminoimidazole
aMT	astral microtubule
BF	brightfield
BLUF	blue-light-utilizing flavin adenine dinucleotide
CFP	cyan fluorescent protein
dCTP	deoxycytosine triphosphate
DIC	differential interference contrast
dTTP	deoxythymidine triphosphate
E1	ubiquitin-activating enzyme
E2	ubiquitin-conjugating enzyme
E3	ubiquitin-protein ligase
ER	endoplasmatic reticulum
FACS	fluorescence-activated cell sorting
FACS	fluorescence-activated cell sorting
FMN	flavin mono nucleotide
GAP	GTPase activating protein
GDP	guanosine triphosphate
GFP	green fluorescent protein
GTP	guanosine diphosphate
HRPO	horseradish peroxidase
KOAc	potassium acetate
LED	light-emitting diode
LEPC	leading edge protein coat
LFM	low fluorescence medium

LOV	light oxygen voltage
MEN	mitotic exit network
MP	meiotic plaque
NDR	nuclear Dbf2-related
ODC	ornithine decarboxylase
PCR	polymerase chain reaction
Protein↓	protein depletion
psd	photo-sensitive degron
PSM	prospore membrane
RAM	regulation of ace2 and morphogenesis
RFP	red fluorescent protein
SDS-PAGE	sodium dodecyl sulfate
SEM	standard error of the mean
sid	sporulation-induced protein depletion
SPB	spindle pole body
SPOC	spindle position checkpoint
TCA	trichloroacetic acid
TDegX	TEV protease dependent degron with residue X at position P1'
TEV	tobacco etch virus
TIPI	tobacco etch virus protease induced protein instability
YFP	yellow fluorescent protein

Curriculum vitae

Personal Information

Name	**Christian Renicke**
Address	Peter-Götz-Straße 11 D-36277 Schenklengsfeld
Date of birth	November 29, 1984
Place of birth	Bad Hersfeld, Germany
Nationality	German
Languages	German (first language), English

Education

July 2001 – June 2004

University entrance qualification at Modellschule Obersberg, Bad Hersfeld, Germany (2.2)
    Main subjects: Biology and Chemistry

October 2005 – July 2008

Bachelor of Science in Biology at Philipps-Universität Marburg, Germany (2.2)
Bachelor thesis in the laboratory of Prof. Dr. Hans-Ulrich Mösch:
> *Meiose- und sporulationsspezifische Expression der Tabak-Ätz-Virus-Protease (tobacco etch virus protease) in der Hefe Saccharomyces cerevisiae*

October 2008 – October 2010

Master of Science in Molecular and Cellular Biology at Philipps-Universität Marburg, Germany (1.3)
Master thesis in the laboratory of Prof. Dr. Hans-Ulrich Mösch:
> *Erweiterung eines Systems zur gezielten Proteindestabilisierung durch Degronaktivierung mittels Tabak-Ätz-Virus-Protease in Saccharomyces cerevisiae*

since January 2011

Doctoral research studies at Philipps-Universität Marburg, Germany
Department of Biology – Molecular Genetics
Group of Dr. Christof Taxis
PhD Project:
> *Conditional Degrons to Study Gene Functions During Saccharomyces cerevisiae Gametogenesis and Proliferation*

Member of the DFG Research Training Group *Intra- and Intercellular Transport and Communication IITC* (January 2011 – October 2011: PhD scholarship; November 2011 – March 2015: associated PhD student)

Visited Workshops

September 2012	**IITC workshop** in Kleinwalsertal, Germany
February 2015	**BioVoxxel Workshop** *Scientific Image Processing and Analysis* in Marburg, Germany
July 2015	**Workshop on** *Statistical programming with R in the life sciences* in Marburg, Germany

Visited Conferences

July 2011	**25th International Conference on** *Yeast genetics and Molecular Biology*, July 11-16, 2011 in Olsztyn-Kortowo, Poland
September 2011	**10th VAAM Symposium** *Molecular Biology of Fungi*, September 11-14, 2011 in Marburg, Germany
September 2011	**Student-organized International Symposium** *Intra- and Intercellular Transport and Communication*, September 21 – 23, 2011 in Marburg, Germany
July/August 2012	***2012 Yeast Genetics & Molecular Biology Meeting***, July 31 – August 5, 2012 in Princeton, USA
September 2014	**Joint International Symposium of SFB 593 and GRK 1216** *Mechanisms of cellular compartmentalization*, September 24 – 26, 2014 in Marburg, Germany
June 2016	**13th** *International Coral Reef Symposium*, June 19 – 24, 2016 in Honolulu, Hawai'i, USA

Meinen Freunden und Verwandten danke ich für die angediehene Unterstützung auch in schwierigen Zeiten und trotz meiner persönlichen Schwächen. Das gilt ganz besonders für meine Mutter, die immer für mich da war, wenn ich eine Stütze oder helfende Hände brauchte und wesentlich dazu beigetragen hat, dass ich auch persönliche oder wissenschaftliche Durststrecken überwinden konnte. Außerdem möchte ich mich bei meinem Opa danken für das Interesse und die schöne, miteinander verbrachte Zeit.

Danke.

Eidesstattliche Erklärung

Hiermit erkläre ich, dass ich meine Dissertation mit dem Titel: "Conditional Degrons to Study Gene Functions During *Saccharomyces cerevisiae* Gametogenesis and Proliferation " selbständig, ohne unerlaubte Hilfsmittel angefertigt und ich mich keiner anderen als der von mir ausdrücklich bezeichneten Quellen und Hilfen bedient habe.

Die Dissertation wurde weder in der vorliegenden noch in einer ähnlichen Form bei einer anderen Hochschule eingereicht und hat noch keinen sonstigen Prüfungszwecken gedient.

Marburg, den 16.09.2016   Christian Renicke

Erklärung der Eigenanteile

Renicke C, Schuster D, Usherenko S, Essen L-O & Taxis C (2013) A LOV2 Domain-Based Optogenetic Tool to Control Protein Degradation and Cellular Function. *Chem. Biol.* **20:** 619–26

Christian Renicke führte die Experimente zu den Abbildungen 2 C und D, 3 A, 5 A und 6 sowie den ergänzenden Abbildungen S3 C und D als auch S5 B und D durch. Das Manuskript wurde von Dr. Christof Taxis, Christian Renicke, Svetlana Usherenko und Dr. Lars-Oliver Essen geschrieben.

Renicke C, Taxis C (2016) Development of an optogenetic tool to regulate protein stability in vivo. Manuskript auf Einladung, im Druck (Buchkapitel in „ OPTOGENETICS: From Neuronal Function to Mapping & Disease Biology". Appasani K (ed). Cambridge, UK: Cambridge University Press).

Christian Renicke trug die Experimente für Abbildung 3 bei. Die Publikation wurde von Dr. Christof Taxis und Christian Renicke geschrieben.

Renicke C, Spadaccini R & Taxis C (2013) A Tobacco Etch Virus Protease with Increased Substrate Tolerance at the P1' position. *PLoS One* **8:** e67915

Die Experimente zu Abbildung 1 wurden von Dr. Christof Taxis durchgeführt, die Immunodetektion für diese Abbildung wurde während dieser Arbeit von Christian Renicke durchgeführt. Die erste Runde aus *pTEV⁺* Mutagenese und Durchmustern der Mutanten waren Teil der Masterarbeit von Christian Renicke, die folgenden Runden (Abbildung 2) sowie die genaue Charakterisierung der TEV2 Variante (Abbildung 3) und die Versuche zum Einfluss der Aminosäure an Position P2' (Abbildung 4) wurden im Rahmen der vorliegenden Arbeit vollzogen. Das Manuskript wurde von Dr. Christof Taxis, Christian Renicke und Dr. Roberta Spadaccini geschrieben.

Renicke C, Allmann AK, Lutz A and Taxis C. The mitotic exit network regulates spindle pole body inheritance during sporulation of budding yeast. (Manuskript eingereicht im August 2016; unter Begutachtung)

Christian Renicke führte im Rahmen dieser Arbeit die Experimente zu den Abbildungen 1 bis 5 und 8, den ergänzenden Abbildungen 2 bis 7 und 11, sowie die Analyse der Chromosomenverteilung der Kin4 und Nud1 Mutanten (Abbildung 6C und D, Abbildung 7B und C) durch. Ann-Katrin Allmann trug im Rahmen einer Masterarbeit Daten zur Lokalisation von Cdc5 und Kin4 (Abbildung 6A und ergänzende Abbildung 8) sowie zur Sporulation der Kin4, Nud1 und Cnm67 Depletions-Stämme (Abbildungen 6B und 7A, sowie ergänzende Abbildungen S9A und D und S10A, D und E) bei. Das Wachstum dieser Stämme und die mitotische Lokalisierung der Fusionsproteine wurden von Christian Renicke überprüft (ergänzende Abbildungen S9B und C, S10B und C). Darüber hinaus führte Ann-Katrin Allmann die Experimente zu Abbildung 6D durch, welche anschließend von Christian Renicke analysiert wurden. Anne Lutz untersuchte während ihrer Bachelorarbeit die Meiose-spezifischen Lokalisationen von Dbf2 und Dbf20 (ergänzende Abbildung 1). Christian Renicke führte Datenanalyse und −Visualisierung aller Experimente durch. Die Publikation wurde von Christian Renicke und Dr. Christof Taxis verfasst.

Marburg, den 16.09.2016   Christian Renicke

                                                                Dr. Christof Taxis